TESIS DOCTORAL

UCAM
UNIVERSIDAD CATÓLICA DE MURCIA

ESCUELA INTERNACIONAL DE DOCTORADO

Programa de Doctorado en Ciencias de la Salud

Oleanolic Acid Improves Different Aspects of Wound Healing

Autor/a:

Javier Stelling Férez

Directores/as:

Dr. D. Francisco José Nicolás Villaescusa

Dr. D. José Antonio Gabaldón Hernández

Murcia, diciembre de 2023

TESIS DOCTORAL

UCAM
UNIVERSIDAD CATÓLICA DE MURCIA

ESCUELA INTERNACIONAL DE DOCTORADO

Programa de Doctorado en Ciencias de la Salud

Oleanolic Acid Improves Different Aspects of Wound Healing

Autor/a:

Javier Stelling Férez

Directores/as:

Dr. D. Francisco José Nicolás Villaescusa

Dr. D. José Antonio Gabaldón Hernández

Murcia, diciembre de 2023

UCAM
UNIVERSIDAD CATÓLICA DE MURCIA

EIDUCAM
Escuela Internacional de Doctorado

AUTORIZACIÓN DEL DIRECTOR DE LA TESIS PARA SU PRESENTACIÓN

El Dr. D. Francisco José Nicolás Villaescusa y el Dr. D. José Antonio Gabaldón Hernández como Directores de la Tesis Doctoral titulada "Oleanolic acid improves different aspects of wound healing" realizada por D. Javier Stelling Férez en el Programa de Doctorado Ciencias de la Salud, **autoriza su presentación a trámite** dado que reúne las condiciones necesarias para su defensa.

Lo que firmo, para dar cumplimiento al Real Decreto 99/2011 de 28 de enero, en Murcia a 11 de Diciembre de 2023.

NICOLAS VILLAESCUSA FRANCISCO JOSE - 27467061R

Firmado digitalmente por NICOLAS VILLAESCUSA FRANCISCO JOSE - 27467061R
Fecha: 2023.12.12 11:08:32 +01'00'

Francisco J. Nicolás Villaescusa

JOSE ANTONIO| GABALDON| HERNANDEZ

Firmado digitalmente por JOSE ANTONIO|GABALDON|HERNANDEZ
Nombre de reconocimiento (DN): cn=JOSE ANTONIO|GABALDON|HERNANDEZ, serialNumber=29040687J, givenName=JOSE ANTONIO, sn=GABALDON HERNANDEZ, ou=CIUDADANOS, o=ACCV, c=ES
Fecha: 2023.12.12 08:00:12 +01'00'

José A. Gabaldón Hernández

UCAM
EIDUCAM
Escuela Internacional de Doctorado

RESUMEN

Entre los compuestos naturales bioactivos, los triterpenoides pentacíclicos son conocidos por sus efectos farmacológicos y gran versatilidad, entre los cuales, el ácido oleanólico (AO), es conocido por sus propiedades antitumorales, antiinflamatorias, antioxidantes o hepatoprotectoras. La distribución de este compuesto es amplia entre especies vegetales, especialmente en el olivo, una planta muy utilizada en el Mediterráneo por su alto valor nutricional. Normalmente, el aceite de oliva se obtiene del prensado de las aceitunas, mientras que los subproductos resultantes de las aceitunas se desechan. Sin embargo, estos subproductos contienen altos niveles de AO y pueden aprovecharse para extraer este compuesto. En cuanto a sus propiedades, el AO posee efectos sobre la cicatrización de heridas, aunque en la actualidad no están estudiados completamente. La cicatrización es un proceso fisiológico necesario para la restauración del tejido después del daño en la piel. Es un proceso finamente regulado que depende de la secuencia correcta de varias fases, con el objetivo de regenerar el tejido y cerrar la herida. Diferentes tipos celulares desempeñan un papel fundamental en este proceso: las células epiteliales proliferan y migran para cerrar la herida, las células inmunitarias controlan el entorno inflamatorio causado por la lesión junto con las células endoteliales, que proliferan, migran y forman nuevos vasos sanguíneos para la regeneración del tejido. Curiosamente, se ha demostrado que el AO promueve la migración celular desde los bordes de la herida. Lamentablemente, se necesita estudiar en profundidad los efectos moleculares subyacentes a este fenómeno. Es más, la naturaleza lipofílica del AO dificulta su aplicabilidad en soluciones acuosas debido a su baja solubilidad en agua, lo que da como resultado efectos limitados del AO, presentando una baja biodisponibilidad. La presente tesis doctoral se ha centrado en el estudio de estos aspectos y características de la cicatrización de heridas bajo los efectos del AO, para desentrañar sus mecanismos moleculares en la biología celular. Al mismo tiempo, este estudio ha recurrido a nuevos agentes encapsulantes, las ciclodextrinas, como candidatos adecuados para la administración de AO y para mejorar así su manipulación, conservación y aplicabilidad en modelos celulares in vitro. Para estos fines, los modelos de células epiteliales Mv1Lu y MDA MB 231 se trataron

con AO en ensayos de scratch, para imitar lo que sucede en un epitelio después de una lesión. Este enfoque se complementó con el estudio de proteínas clave relacionadas con la migración celular EGFR, MAP quinasas ERK y JNK, y c-Jun. Además, también se estudiaron proteínas de la arquitectura celular: actina, paxilina y FAK; las cuales se observaron en la migración del frente celular. Además, el AO se estudió también en células endoteliales, mediante el uso del modelo de células humanas endoteliales de la vena de cordón umbilical (HUVEC). Además, se utilizaron HUVEC, afectadas por hiperglucemia (GD-HUVEC) o no (C-HUVEC), para observar los efectos promotores del AO sobre la angiogénesis. Además, con el objetivo de imitar lo que sucede en el tejido de la herida bajo inflamación, estas células fueron sometidas a un estímulo pro-inflamatorio mediante la citoquina TNF-α, después del pretratamiento con AO, para estudiar la expresión de las moléculas de adhesión E-selectina, I-CAM1 y V-CAM1, un análisis complementado con el ensayo de adhesión de monocitos. Paralelamente, para desarrollar una nueva formulación para el AO, éste se complejó con hidroxipropil beta y gamma ciclodextrinas (HP-β- y HP-γ-CDs). La adición de un paso de deshidratación por liofilización fue crítica para permitir la aplicación de los complejos de AO resultantes (AO/HP-β-CD, AO/HP-γ-CD) en los ensayos in vitro. Más adelante, se testó la actividad biológica de estos complejos en células Mv1Lu y MDA MB 231, ya que son buenos biosensores de la actividad del AO. Todos estos estudios alcanzaron numerosos y prometedores resultados sobre el uso de AO en cicatrización. Las células epiteliales mostraron una sobreexpresión y fosforilación de c-Jun en las células del borde de la herida en respuesta a AO en ensayos de scratch. Sorprendentemente, las proteínas clave en migración celular EGFR, ERK, JNK y c-Jun, bajo el tratamiento conjunto con AO e inhibidores farmacológicos revelaron una activación temprana de c-Jun independiente de EGFR. El estudio de las proteínas de señalización nos ayudó a observar que la migración celular desencadenada por AO es impulsada por un mecanismo bifásico con la participación del eje JNK/c-Jun y, posteriormente, el eje EGFR/MEK/ERK/c-Jun. Ambos ejes parecían contribuir a la migración celular inducida por AO y podrían estar intercomunicados por receptores GPCR. Además, los ensayos de migración del frente celular revelaron cambios en la arquitectura de las células epiteliales por AO, al observar modificaciones en la F-actina, la distribución de la paxilina, el número y tamaño de las adhesiones focales, la activación de FAK y la colocalización

de FAK/paxilina. Todos estos efectos fueron coherentes con el mecanismo bifásico de señalización inducido por AO. Respecto a las células endoteliales, el pretratamiento con AO mostró la atenuación de los efectos pro-inflamatorios de TNF-α, al provocar la reducción en la expresión de V-CAM1, I-CAM y E-selectina. Esto correlacionó positivamente con la reducción de la adhesión de monocitos a las HUVECs por AO. Sorprendentemente, el AO también rescató varias características afectadas de la angiogénesis de GD-HUVEC. Por otra parte, el AO indujo la migración de C- y GD-HUVEC en ensayos de scratch, un efecto promotor que se correlacionó con el aumento en el número de adhesiones focales revelado por la paxilina. Finalmente, la complejación de AO en ciclodextrinas, mostró altas tasas de encapsulación y mejor solubilidad en agua en medios de cultivo celular. Cabe destacar que la nueva formulación de los complejos de AO mantuvo la actividad y la conservación del AO durante largos períodos de tiempo. Además, la actividad de los complejos se testó en células Mv1Lu y MDA-MB-231, mostrando una migración celular mejorada al exhibir el reclutamiento de un alto número de células, en las que también fue patente la sobreexpresión de c-Jun a lo largo del borde de la herida. Asimismo, los complejos de AO desencadenaron una migración compatible con la observada con AO libre, ya que indujeron la activación de EGFR, MAP quinasas y c-Jun. Estos efectos también mostraron la dinamización de paxilina y actina, junto con el aumento del número de adhesiones focales. Notablemente, los complejos de AO impidieron que las células epiteliales sufrieran efectos los citotóxicos leves del AO. En resumen, esta tesis doctoral muestra un gran potencial del AO para la cicatrización de heridas debido a la mejora de varios aspectos de la cicatrización por sus efectos positivos sobre las células epiteliales y endoteliales. De hecho, el AO desencadena un fino mecanismo molecular que actúa en estas células y que vale la pena descifrar en su totalidad. Además, su nueva formulación mejorada con ciclodextrinas impulsa al AO como un agente cicatrizante para tratar heridas agudas y crónicas en el futuro, una afección que normalmente requiere mucho tiempo y conlleva tratamientos costosos. Por estos motivos, la formulación de AO podría utilizarse como un tratamiento alternativo para evitar estos problemas y mejorar la regeneración de la piel y, en definitiva, la vida de los pacientes.

PALABRAS CLAVE

Ácido oleanólico, cicatrización de heridas, ciclodextrinas, liofilización, migración celular, MAP quinasas, receptor del factor de crecimiento epidérmico, arquitectura celular, inflamación, moléculas de adhesión, hiperglicemia, angiogénesis, bioquímica molecular, biología celular, farmacología, piel.

ABSTRACT

Among natural bioactive compounds, pentacyclic triterpenoids are known for their pharmacological effects and their chemical versatility, among which, oleanolic acid (OA) is known for its antitumoral, anti-inflammatory, antioxidant, or hepatoprotective properties. Of relevant significance is the widespread distribution of this bioactive compound among plant species, especially in the olive tree, an edible plant very commonly-used in the Mediterranean. Usually, olive oil is obtained from pressing olives, and the resulting by-products of olives are discarded. However, these by-products contain high OA levels and can be exploited. Among OA's properties, its effects on wound healing are important, although they are not yet fully understood. In case of injury, wound healing is the physiological process needed for skin restoration. It is a tightly regulated process that depends on the correct sequence of several phases to finally reach skin-tissue integrity. Relevant cell types play a pivotal role in this process: epithelial cells proliferate and migrate to close the wound, immune cells manage the inflammation milieu caused by injury together with endothelial cells, which proliferate, migrate, and form new blood vessels for tissue regeneration. Interestingly, it has been shown that OA promotes cell migration from wound edges. Regrettably, the molecular effects underlying this phenomenon have not been fully deciphered yet. Furthermore, OA's lipophilic nature hampers its applicability in aqueous solutions due to its poor water-solubility, resulting in limited OA effects with low bioavailability. The present doctoral thesis focused on the study of these wound-healing aspects and features under the effects of OA, to unravel its molecular impact on cell biology. Simultaneously, this study has resorted to novel microcarriers, cyclodextrins, as suitable candidates for the delivery of OA and for

improving its handling, conservation, and applicability on in vitro cell models. For these purposes, epithelial cell models Mv1Lu and MDA-MB-231 were treated with OA in scratch assays in order to mimic what happens in an epithelium after injury. This approach was complemented with the study of key proteins related to cell migration, EGFR, MAP kinases ERK and JNK, and c-Jun. Additionally, cell architecture proteins, namely actin, paxillin, and FAK, were studied on the migration cell front. Furthermore, OA was also studied in endothelial cells, by using the human umbilical vein endothelial cell (HUVEC) model. Moreover, HUVECs, affected by hyperglycemia (GD-HUVECs) or not (C-HUVECs), were used to observe OA promoting effects on angiogenesis. Moreover, with the objective of mimicking what happens in the wound tissue under inflammation, C- and GD-HUVECs were subjected to a pro-inflammatory stimulus by cytokine TNF-α, after OA pre-treatment, to study the expression of adhesion molecules E-selectin, I-CAM1 and V-CAM1, an analysis which was complemented with monocyte adhesion assays. To set a new formulation for OA, the triterpenoid was complexed in modified hydroxypropyl beta and gamma cyclodextrins (HP-β and HP- γ-CDs). Interestingly, the addition of a dehydration step by freeze drying was essential to allow for OA complexes (OA/HP-β-CD, OA/HP-γ-CD) application on in vitro assays. Then, the biological activity of these OA complexes was tested in Mv1Lu and MDA-MB-231 cells, as they are good biosensors for OA activity. All these studies yielded numerous and promising results of OA in wound healing. Epithelial cells responded to OA by showing c-Jun overexpression and phosphorylation in cells at wound edge in scratch assays. Strikingly, key cell migration proteins EGFR, ERK, JNK, and c-Jun, under co-treatment with OA and pharmacological inhibitors, revealed an early activation of c-Jun that was independent of EGFR. The study of signaling proteins helped us to observe that OA-triggered cell migration is driven by a biphasic mechanism with the participation of the JNK/c-Jun axis and, later, the EGFR/MEK/ERK/c-Jun axis. Both axes seemed to be contributing to OA-triggered cell migration and might be intercommunicated by GPCR receptors. Additionally, cell front migration assays revealed changes on the architecture of epithelial cells induced by OA, such as modifications in F-actin, paxillin distribution, focal adhesion number and size, FAK activation, and FAK/paxillin colocalization. All these effects were coherent with the OA-induced signaling biphasic mechanism. Regarding endothelial cells, the OA

pre-treatment showed the attenuation of TNF-α pro-inflammatory effects, by reducing the expression of V-CAM1, I-CAM and E-selectin. Coherently with this, monocyte adhesion was reduced by OA. Strikingly, OA rescued several affected features of angiogenesis in GD-HUVEC. Additionally, OA induced the migration of C- and GD-HUVECs in scratch assays, a promoting effect that correlated with the increase in the number of focal adhesions revealed by paxillin. Finally, OA complexation with HP-β and HP-γ-CDs, followed by a dehydration step, showed high-efficiency encapsulation rates and better water solubility in cell culture media. Moreover, the new formulation preserved OA stability and activity for long-term storages. Surprisingly, OA complexes' activity tested in Mv1Lu and MDA-MB-231 showed improved cell migration by exhibiting the recruitment of a large number of cells, which was also patent with the overexpression of c-Jun across the wound edge. Furthermore, OA complexes triggered a migration that was compatible with the one seen with free OA, since they induced the activation of EGFR, MAP kinases, and c-Jun. These effects also modified the architecture of the cells by showing paxillin and actin dynamization and an increased number of focal adhesions. In addition to these effects, OA complexes protected epithelial cells from OA mild cytotoxic effects. In summary, this doctoral thesis shows great OA potential for wound healing because of its improvement of several aspects of wound healing and its positive effects on epithelial and endothelial cells. Indeed, OA triggers a fine molecular mechanism that acts on these cells and is worth deciphering in its entirety. Furthermore, its improved application with cyclodextrins prompted OA as a wound healing agent to treat acute and chronic wounds in the future, a condition that is time-consuming and entails expensive treatments. For these reasons, OA formulation could be used as an alternative treatment to avoid these issues and improve skin regeneration.

KEYWORDS

Oleanolic acid, wound healing, cyclodextrins, water solubility, freeze drying, cell migration, MAP kinases, epidermal growth factor receptor, cell architecture, inflammation, adhesion molecules, hyperglycemia, angiogenesis, molecular biochemistry, cell biology, pharmacology, skin.

AGRADECIMIENTOS

En este apartado tan especial, quería agradecer a todas aquellas personas que han formado parte de este recorrido profesional y también personal que ha sido para mí la tesis doctoral, la cual ha concluido en mi desarrollo como investigador.

En primer lugar, agradecer a mis directores de tesis Franjo y José Antonio, por haberme brindado esta gran oportunidad y haber depositado su confianza en mí, por permitirme iniciar un proyecto que nació de la colaboración y el conocimiento de dos grupos de investigación pertenecientes al IMIB y la UCAM. Habéis sido fundamentales en este proyecto tan importante para mí y para el inicio de mi carrera como científico. A ti José Antonio, por brindarme siempre tu ayuda, los medios, las ideas y consejos para el desarrollo de la tesis. A ti Franjo, por enseñarme a exprimir todo el potencial que requiere la investigación, por enseñarme que cada error es sólo un paso más para llegar a un resultado gratificante, por esa gran inquietud y cuestionamiento científicos que posees y que me has inculcado; por enseñarme que, incluso en los momentos en los que la investigación de la tesis parece un callejón sin salida, siempre hay respuestas si sabes encontrarlas. Por otro lado, no puedo concluir este apartado sin antes agradecer a Ángel Bernabé y Sergio Liarte, antiguos compañeros que también han sido claves en los primeros años de desarrollo de mi tesis, junto con David Armero, ya que todos ellos iniciaron esta línea del ácido oleanólico sobre la que he trabajado.

También debo agradecer a los siguientes profesores e investigadores UCAM que también han sido clave en esta tesis doctoral. A Santiago López, porque sin ese gran conocimiento sobre ciclodextrinas, sin habernos peleado codo con codo con los complejos de oleanólico, sin tu gran ayuda y disposición, gran parte de esta tesis no sería la que es hoy. A ti, Begoña Alburquerque, por haberme aconsejado y ayudado tanto sobre divulgación científica y por haberme dirigido tan bien la tesis en tres minutos. Por último, a Silvia Montoro, por la colaboración tan fructífera que hemos desarrollado ambos grupos de investigación, y, sobre todo, por estar siempre dispuesta a ayudarme y resolver todas mis dudas con los trámites del doctorado.

Quiero agradecer también al extraordinario grupo de investigación que me acogió durante mi estancia internacional en Chieti (Italia), el cual también ha sido esencial para la producción científica de esta tesis. Gracias a la profesora Assunta Pandolfi, por brindarme la oportunidad de investigar en su grupo, por su gran amabilidad y por acogerme tan bien. Por supuesto, con mucho cariño agradezco a la gran investigadora y amiga Caterina Pipino, por trabajar conmigo y sacar todos los experimentos que hicieran falta, peleando por ese artículo conjunto. Gracias a Caterina, junto con las compañeras Ilaria, Letizia y Pamela, hicieron que me sintiera en su grupo en Italia como en casa. Con vosotras he descubierto muchas cosas de vuestro precioso país además de aprender cómo es trabajar en equipo.

A mis compañeros de laboratorio Isabel, Silvia y José María, por ese gran equipo que formamos, por esa ayuda que siempre nos damos, por las risas y los almuerzos, que hacen que cada día duro de trabajo sea más llevadero. Por vuestra disposición a ayudarme siempre que podéis y los ánimos que me dais. Por supuesto, también debo agradecer a las personas que fueron mis compañeros en otras etapas de la tesis, compañeros de penurias y de éxitos, con las que al mismo tiempo he aprendido y también he enseñado: Juanjo, Pilar, Irene, Adela, Andrea y Carlos. Por otro lado, a mis compañeros de la UCAM Clara, Ramiro, David, Cindy e Iván, por haber compartido con ellos el viaje de la tesis doctoral y el apoyo mutuo que nos hemos dado.

Por último, en este ámbito profesional, también quiero agradecer a dos personas que me ayudaron a iniciarme en la investigación y con las que también aprendí muchísimo, de Microbiología y de Bioquímica, a mis tutores de TFG y TFM Francisco Torrella y Encarna Muñoz.

Seguidamente quiero seguir este bloque de agradecimientos centrándome en todas aquellas personas que me han acompañado durante el doctorado. A todas aquellas personas con las que me siento enormemente afortunado por formar parte de su vida y ellas de la mía, a todos aquellos y aquellas que son mi red de apoyo y que a día de hoy vertebran mi vida, con las que siento que llevo un pedacito de cada una de ellas, haciéndome sentir mejor persona cada día.

Quiero empezar agradeciendo a mis padres, Pilar y Erich, por siempre haberse esforzado enormemente, aportar todos los medios que hicieran falta, y haberme animado, no sólo en mi actual desarrollo académico y profesional, sino también desde bien pequeño avivando esa inquietud que poseía por descubrir y

cuestionarme todo lo que me rodeaba. También por inculcarme siempre unos valores centrados en el respeto, en la igualdad y en el esfuerzo. A mí hermano Miguel, por haber sido y ser siempre más que un hermano, también un amigo. A mi segunda familia, mis tíos Margarita y Arturo, a mis primos Ángela y Adri.

Por otra parte, con especial cariño, a mi compañero de vida, a mi mejor amigo, a mi pareja Jaime. Has sido la persona en primera línea de fuego en todo este proceso, has ido de la mano conmigo, en las buenas y en las malas, mi confidente, la persona que me ha escuchado y me ha apoyado enormemente en mis inquietudes y deseos. Por haber iniciado esta etapa juntos y cerrarla juntos, sumando experiencias a las todas las que ya tenemos. Juntos podemos con todo y tú lo eres todo para mí.

Por supuesto, a mis amigas y amigos, porque todas ellas y ellos son mi familia elegida y han supuesto también un apoyo fundamental en todo este proceso.

A mis amigas Esperanza, Lola y Marta. Porque desde el máster iniciamos juntos nuestras carreras, y al mismo tiempo forjamos una amistad enorme. Gracias por vuestra complicidad, por ser como sois, por hacer la vida tan fácil, por los viajes y las escapadas, por apoyarnos en los momentos más críticos y por hacer que cualquier problema se diluyera simplemente saliendo a tomar algo y riéndonos de cualquier cosa. Aprovecho también para mencionar a Nora e Irene, por habernos conocido también en el máster y sentirme también afortunado por teneros como amigas.

A mis amigos de Alicante, Miriam y Dylan. A ti Miriam por todos los años que llevamos juntos desde el instituto, por las incontables experiencias, por ser mi mejor amiga, por el cariño y aprecio mutuos que nos tenemos, por reírnos de la vida. A ti Dylan por tu cariño y apoyo, por reencontrarnos y haber forjado esta amistad de nuevo.

A mis amigos Elena y Pablo, por ser unas personas enormes, por escucharme, por hacerme sentir como un niño con todas nuestras tonterías y por compartir nuestras aficiones juntos, como la que más nos gusta, cocinar y comer.

A mis amigas Marian y Ainhoa, por haber conservado una amistad a la que tengo especial cariño desde el instituto, por ser un gran apoyo en los momentos más críticos, por tenernos siempre.

Por último, no puedo concluir los agradecimientos sin mencionar a un grupo de amigos que he conocido casi al final de este viaje, pero que también significan muchísimo a día de hoy. A mis amigos Miki, Ro, Javi, Pepe, Fran, Juan, Diego, Alberto, Curro. Gracias por haberme arropado tan bien desde el primer momento, por todas esas salidas juntos que me han recargado las pilas, por todo ese gran apoyo que habéis sabido darme. A todos vosotros, gracias.

"Self-assertion, even when it is incomprehensible to others, can be a step toward career advancement."
Audre Lorde (1934-1992).

TABLE OF CONTENTS

ABBREVIATIONS

Akt, protein kinase B

α-CD, alpha cyclodextrin

AP-1, activating protein 1 transcription complex

BA, betulinic acid

BAS, beta amyrin synthase

β-CD, beta cyclodextrin

BMAL1, Basic Helix-Loop-Helix ARNT Like 1 gene

c-Fos, c-Fos transcription factor AP-1 subunit

C-HUVEC, control human umbilical cord vein endothelial cells

c-Jun, c-Jun transcription factor AP-1 subunit

CAT, catalase

CCL2, chemokine (C-C motif) ligand 2

CD, cyclodextrin

γ-CD, gamma cyclodextrin

CGTas, glycosyltransferase

CLOCK, circadian locomotor output cycles kaput gene

DL, drug load

DMEM, Dulbecco modified eagle medium

DW, dry weight

ECM, extracellular matrix

EE, encapsulation efficiency

EGF, epidermal growth factor

EGFR, epidermal growth factor receptor

EMEM, Eagle's minimum essential medium

EMT, epithelial mesenchymal transition

eNOS, endothelial nitric oxide synthase

ERK1/2, extracellular signal-regulated kinase 1,2

FA, focal adhesion

FAK, focal adhesion kinase

FDA, U.S Food and Drug Administration

GD-HUVEC, gestational diabetes human umbilical cord vein endothelial cells

GDP, guanosine diphosphate

GLUT4, glucose transporter 4

GRAS, generally regarded as safe

Grb2, growth factor binding protein 2

GTP, guanosine triphosphate

GTPase, guanosine triphosphate hydrolases

HCT-116, human colon carcinoma cell line

HeLa, cervical carcinoma cells

HepG2, human liver cancer cells

HIV, human immunodeficiency virus

HP-α-CD, hydroxypropyl alpha cyclodextrin

HP-β-CD, hydroxypropyl beta cyclodextrin

HP-γ-CD, hydroxypropyl gamma cyclodextrin

HPLC, high-performance liquid chromatography

HUVEC, human umbilical cord vein endothelial cells

I-CAM1, intracellular adhesion molecule 1

IκBα, inhibitor of nuclear factor kappa b

IKK, IκB kinase

IL-1β, interleukin 1 beta

IL-6, interleukin 6

iNOS, inducible nitric oxide synthase

IPP, isopentenyl pyrophosphate

IRS1, insulin receptor substrate 1

JNK1/2, c-Jun N-terminal protein kinase 1,2

K_c, complexation constant

LDL, low-density lipoprotein

LPS, lipopolysaccharide

MA, maslinic acid

MALDI-TOF, matrix-assisted laser desorption/ionization coupled to time-of-flight mass spectrometry

MAPK, mitogen-activated protein kinase

MAPKK, mitogen-activated protein kinase kinase

MAPKKK, mitogen-activated protein kinase kinase kinase

MDA-MB-231, human mammary gland epithelial cells

MDCK, Madin-Darby canine kidney cells

MEK, mitogen-activated protein kinase kinase

miR, micro-RNA

MoA, morolic acid

mRNA, messenger RNA

Mv1Lu, non-malignant mink lung epithelial cells

NF-κB, nuclear factor kappa b

NFR2, nuclear factor erythroid 2 related factor

NO, nitric oxide

NS5B, non-structural protein 5B, RNA polimerase

OA, oleanolic acid

PI3K, phosphoinositide 3-kinase

PTK, protein tyrosine kinase

qPCR, quantitative polymerase chain reaction

QZG, human hepatic cell line

RAF, Rapidly accelerated fibrosarcoma

RAS, rat sarcoma virus

ROS, radical oxygen species

RTK, receptor tyrosin kinase

SELE, E-selectin gene

Ser, serine

SOD1, super oxide dismutase 1

SOS, son of sevenless protein

TGF-α, transforming growth factor α

TGF-β, transforming growth factor β

TGs, triglycerides

TNF-α, tumor necrosis factor α

Tyr, tyrosine

UA, ursolic acid

V-CAM1, vascular cell adhesion molecule 1

VEGF, vascular endothelial growth factor

VEGFR, vascular endothelial growth factor receptor

LIST OF FIGURES, TABLES AND ANNEXES

LIST OF FIGURES

LIST OF TABLES

LIST OF ANNEXES

I – INTRODUCTION

I - INTRODUCTION

In recent years, there has been widespread interest on new active compounds with health benefits for treating several pathologies. Numerous studies have demonstrated the feasibility of isolating and characterizing plant-derived compounds that possess biological activities, thus facilitating the development of novel pharmaceuticals (1-5). The characterization of these bioactive compounds has revealed different health properties, such as antimicrobial, antitumoral, antiaging, anti-inflammatory, or antioxidant effects (6-9). The use of these molecules as therapeutic agents is a noteworthy option to enhance human health since they can avoid expensive and time-consuming conventional treatments, ultimately improving the quality of life (10). Moreover, many of these bioactive compounds possess not only a single activity, but multiple activities. Additionally, they can be chemically modified to enhance their effects. An interesting group of bioactive compounds is the pentacyclic triterpenes, which are synthesized by secondary metabolism of a wide variety of plant species. These compounds have shown promising effects on human health (4, 6, 8-10). Among them, the most remarkable and attainable pentacyclic triterpenoid is oleanolic acid (OA), known for its multiple biological activities, which have been shown in numerous in vitro and in vivo studies (11, 12). Among them, one of its most remarkable activities is wound healing promotion, a crucial process to restore skin integrity and homeostasis after skin injury (13). However, the cellular and biomolecular mechanisms underlying this phenomenon are far from being understood. Furthermore, OA's high insolubility may compromise its activity in wound healing due to its poor delivery to biological systems.

This research aims to comprehend the molecular mechanisms behind OA activities on wound healing, study its effects on cellular types involved in wound healing, and, finally, focus on how to improve OA for better water solubility and delivery, in order to maximize its foreseeable biological effects.

1.1. OLEANOLIC ACID

Oleanolic acid (OA), a pentacyclic triterpenoid, has emerged as a subject of profound scientific interest due to its versatile pharmacological properties and abundance in plants (11, 14). OA is classified as triterpenoid, a subclass of terpenes characterized by their intricate structure composed of 6 isoprene units (15). Plant cells synthesize pentacyclic triterpenes in the cytosol from isopentenyl pyrophosphate (IPP), which is the precursor produced in the mevalonate pathway and is subsequently converted to 2,3-oxidosqualene (Figure I-1) (16, 17). Then, cyclase enzyme β-amyrin synthase (BAS) and oxidase CYP716A transform 2,3-oxidosqualene to produce five rings leading to oleanolic acid (16-18). This molecule, 3β-hydroxyolean-12-en-28-oic acid ($C_{30}H_{48}O_3$), has a complex chemical structure, with five fused rings (A, B, C, D, and E), a β-hydroxy group at C-3, and a carboxyl group (-COOH) linked to the C-17 position between rings D and E (Figure I-2) (16). This structure provides OA with diverse chemical interactions and also constitutes a scaffold molecule for the development of novel pharmaceutical agents (19).

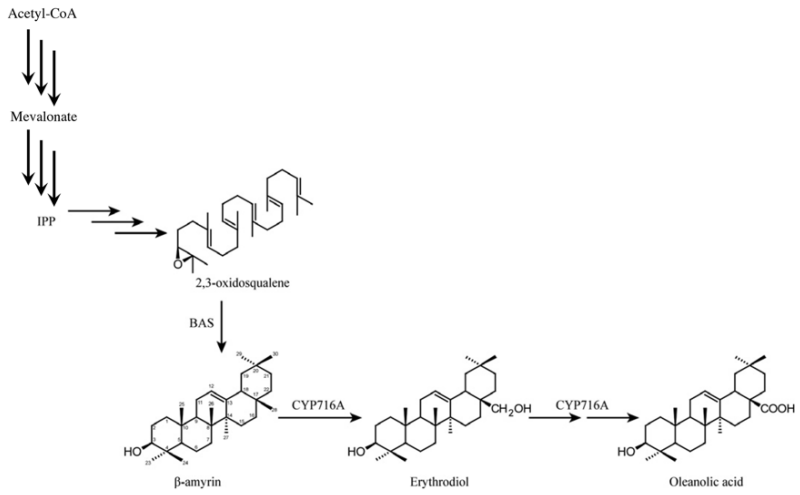

Figure I-1. Oleanolic acid biosynthesis in plants. *This pentacyclic triterpene is produced in cell cytosol via mevalonate pathway from isopentenyl pyrophosphate (IPP). IPP is converted with cyclase β-amyrin synthase (BAS) and oxidase enzyme CYP716A resulting in oleanolic acid. Multiple arrows indicate multiple biochemical steps in the pathway. — Modified figure from Pollier et al. (2012) (16).*

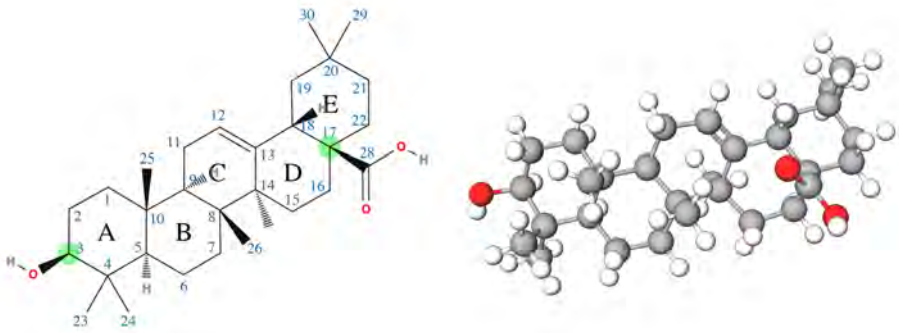

Figure I-2. Oleanolic acid 2D and 3D chemical structures. *2D structure shows the five cyclic rings of oleanolic acid (A, B, C, D, and E) and the number of carbon atoms in blue. Green dots indicate the position of the functional chemical groups -OH and -COOH at C3 and C17, respectively. Balls and sticks represent the 3D structure of oleanolic acid. — Modified figures from MolView.*

1.1.1. Oleanolic acid sources

OA has a widespread distribution in the plant kingdom (20). This compound can be found in nature as a free acid or as an aglycone, which in this case, can be linked to one or more monosaccharide units (16, 21). In plant cells, it is distributed either inside the vacuoles with other secondary metabolites or outside the cells in cell walls, acting as a barrier agent (22).

OA exists in numerous aromatic, edible, and medicinal plant species. Regarding plant organs, OA can be found in the flowers, sprouts, bark, and especially the leaves (23). In particular, OA is found crystalized in the epicuticular wax of leaves to protect them from water loss or pathogens, forming a true physical barrier (24, 25). Furthermore, OA is found in the seeds and pericarp of several plant fruits (23). Among plant species, OA is abundant in *Calendula officinalis* (pot marigold flowers), *Viscum album* (mistletoe sprouts), *Rosmarinus officinalis* (rosemary leaves), *Salvia officinalis* (sage leaves) or *Syzygium aromaticum* (clove flowers) (26). The name "oleanolic acid" derives from the name of the plant species *Olea europaea*, and this plant is currently the main source of commercial OA preparations (27). This is because OA is quite abundant in the leaves of *Olea*

europaea, containing 31 mg per g of dry weight (DW), and also in the bark of the tree, which contains a substantial amount of 9.8 mg/g DW (26).

1.1.1.1. ***Olive tree (Olea europaea)***

The Olive tree is widespread within southern Spain, being one of the most consumed edible plants in our region because of its interest as a producer of olives and extra virgin olive oil (28). It is noteworthy that Spanish olive oil production represents 70% of the European production and 45% of the production worldwide (29). Extra virgin olive oil is a precious food product in the Mediterranean diet and has numerous health benefits due to its high content of bioactive polyphenols (30-32). However, this product is not rich in triterpenes like OA. The obtaining of oleanolic acid depends on the fruit (olives) processing, since several by-products are formed during this process (30). Olive by-products are obtained from solid matter fruits, pericarps, and olive shells, which are discarded during olive oil extraction and processing (Figure I-3). One of these by-products is pomace oil, known for its properties and with a high content of OA triterpenes (33). Indeed, the olive oil industry can be very efficient and environmentally friendly because it uses products that are often discarded, such as olive leaves, shells, or seeds, which are rich in OA and other compounds with therapeutic interest (34). Furthermore, there are specific methods to extract OA. It can be obtained by conventional techniques, such as stirring or maceration, or even by innovative techniques, such as microwave-assisted extraction or ultrasound-assisted extraction (35, 36). The most common extraction method of pentacyclic triterpenes is by using organic solvents, such as ethanol or acetone, since they are hydrophobic compounds (37).

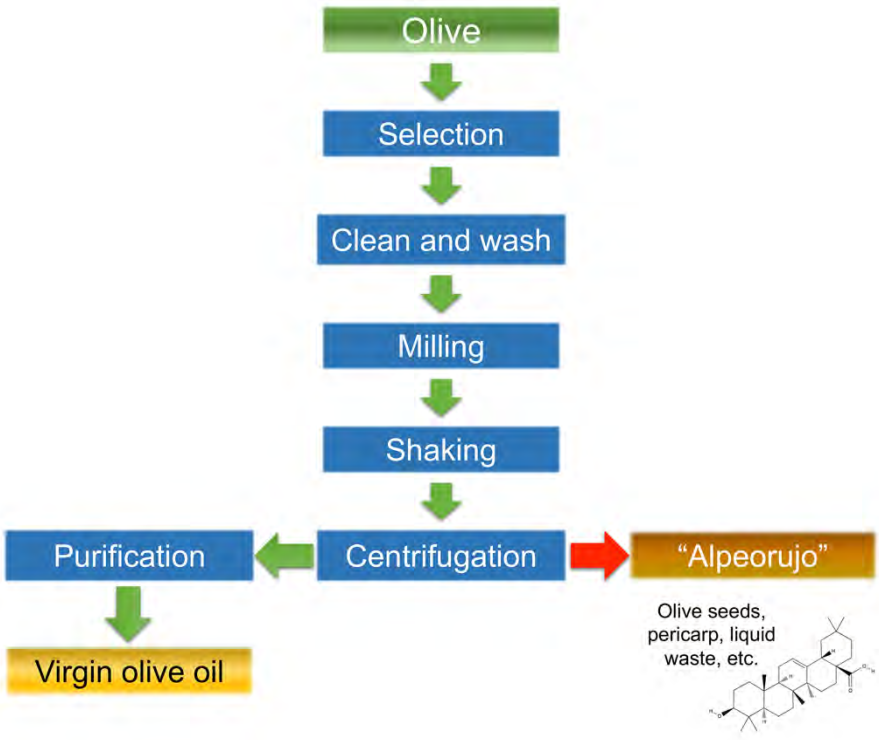

Figure I-3. Olive oil process and extraction. *In the final steps of olive processing, the olive mixture is centrifuged to separate all the solid matter from the oil. This solid matter is called "alpeorujo" and it contains all the seeds, pericarp, and shells from the olive that are discarded. However, they have high oleanolic acid content and it can be extracted by several methods. — Own elaboration.*

1.1.2. Oleanolic acid isomers

In many plant species, OA is present along with other triterpenes. Ursolic acid (UA), a triterpenoid, is a geometric isomer of OA, differing only in the position of one methyl group on ring E (Figure I-4A) (38). Both isomers have similar physiochemical properties and biological effects and both can be found in olive tree leaves (20, 39). It has been shown that ursolic acid has anti-inflammatory, antitumoral, and hepatoprotective effects (39-41).

In addition, several structural OA isomers that differ in the position of the chemical groups within the pentacyclic ring have been identified. Maslinic acid (MA) (Figure I-4B) can be found in olive oil and leaves. It has neuroprotective, antioxidant, anti-inflammatory, and antitumoral properties (42). Betulinic acid (BA) (Figure I-4C), another isomer found in birch bark, has antiviral, antitumoral, and anti-melanoma effects (43). Lastly, morolic acid (MoA) (Figure I-4D) has a widespread presence in plants, especially in the *Morus* genus, with antidiabetic, antimicrobial, and antitumoral properties (44, 45).

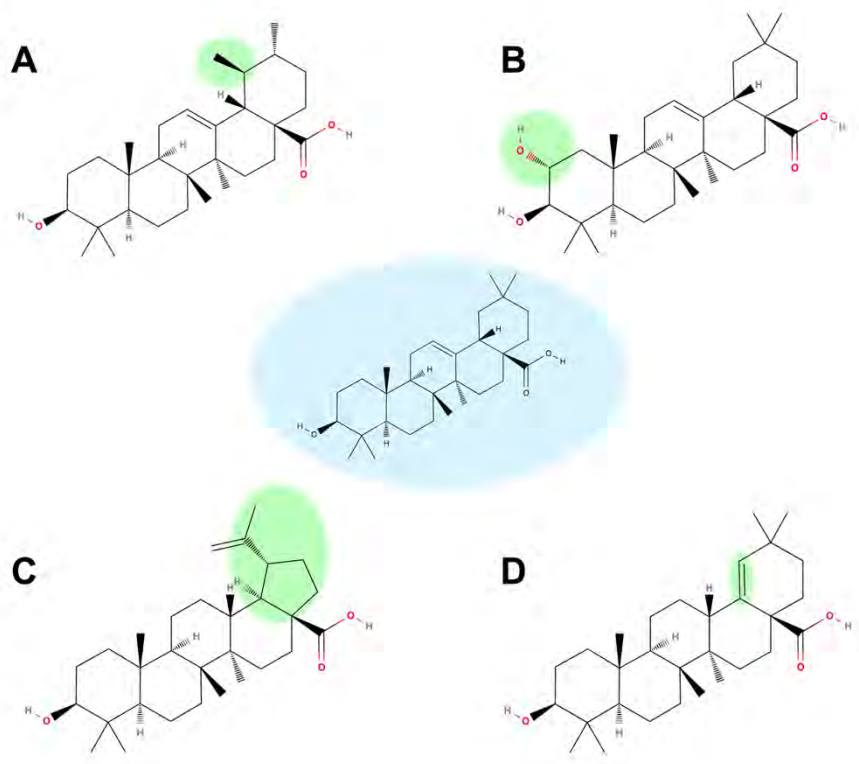

Figure I-4. Oleanolic acid structural isomers. ***A.*** *Ursolic acid.* ***B.*** *Maslinic acid.* ***C.*** *Betulinic acid.* ***D.*** *Morolic acid. Green circles indicate the chemical groups that differ from oleanolic acid (center of the figure). — Modified pictures from MolView.*

1.1.3. Pharmacological properties

As previously mentioned, the particular structure and chemistry of OA provides this molecule with a significant spectrum of pharmacological properties against pathological conditions (12).

An important use of OA comes from its anticancer effect (4, 46). OA inhibits cell growth and proliferation, and produces apoptosis at high doses (47, 48). OA has been shown to have antitumoral effects on in vitro cell lines, such as HeLa cells, liver cells, HepG2, or colorectal cancer cells, HCT-116 (12, 34, 49, 50). Some of the molecular mechanisms of action behind these effects have been deciphered. For instance, high concentrations of OA enhance apoptosis by the inhibition of protein kinase B (Akt) and extracellular signal-regulated kinases 1, 2 (ERK1/2), which are regulatory proteins needed for cell growth and survival (48). Moreover, OA overexpresses a microRNA, miR-122, involved in the tumor suppression of some types of cancer (51, 52). Furthermore, OA antitumor activity has been assayed in vivo with mice with cervical cancer, the results showing that the increase in the volume and the weight of the tumors was inhibited by OA after 15 days of daily intraperitoneal injections of 80 mg/kg of OA (53). Additionally, several synthetic analogs obtained from oleanolic acid have also shown antitumoral effects and are being studied in clinical trials (54, 55).

Moreover, OA has emergent effects on the regulation of glucose metabolism, as it shows antihyperglycemic properties (56). Strikingly, *in vitro* assays treating HepG2 cells with OA revealed that the triterpenoid attenuated insulin resistance, one of the main conditions that produce diabetes (57). HepG2 treated to develop insulin resistance show a decrease of insulin resistance when treated with OA by upregulating the expression of insulin receptor substrate 1 (IRS1) and glucose transporter 4 (GLUT4) and also by reducing the content of pro-inflammatory cytokines (58). Indeed, OA can enhance GLUT4 translocation to the cell membrane (59). These findings correlate positively with in vivo assays, since it has been shown that rats with a diet with OA induce the attenuation of insulin resistance by modulating IRS1 expression (60). Moreover, pomace oil, a high-content OA olive by-product, reduces body weight, insulin resistance, and adipose tissue inflammation in obese mice (33).

Regarding metabolism, several studies unraveled OA hepatoprotective and gastroprotective activity. Interestingly, OA's chemical structure is very similar to that of bile acids (61). Indeed, cholestasis in vivo models are used by chemically injuring the liver to study whether OA can rescue this condition. In this sense, it is known that OA alleviates liver injury in rats, since it accelerates bile acid metabolism and reduces its accumulation in the liver by the overexpression of bile acid transporters (62). Furthermore, OA in injured rats upregulates the expression of nuclear factor erythroid 2-related factor (NFR2), a key transcription factor that intervenes in the defensive response against toxic and oxidative stress (62-64). Remarkably, OA influences liver function since it has been demonstrated that a daily diet with OA changes the expression of *CLOCK* and *BMAL1* circadian liver genes in rats and mice (65). Most notably, in humans, a preliminary clinical trial with hyperlipidemic patients revealed that a four-week intake of OA produced a decrease in triglycerides (TGs), cholesterol, glucose, insulin, and low-density lipoproteins (LDL) blood serum levels (66). Moreover, OA can heal in vivo chronic lesions on the stomach, as demonstrated with gastric acetic acid-induced lesions in rats (67).

Regarding OA antimicrobial activities, there is evidence that OA and its derivatives act against common human pathogens such as mycobacteria, fungi, or even viruses. In vitro assays have shown that OA and its derivatives can inhibit human immunodeficiency virus (HIV) replication and proteases activity, both needed for the formation of new viral particles (68). Similarly, OA is capable of inhibiting NS5B protein, an RNA polymerase needed for the replication of the hepatitis C virus (69). Other OA derivatives could also be used as drug candidates against respiratory viruses that cause high mortality in the population (70). However, the mechanisms of action of OA in these studies are not fully deciphered, and need to be extrapolated to in vivo assays to ensure its therapeutic effect (71). In the case of OA antibacterial activity, this molecule and its derivatives can penetrate and damage the bacterial cell membrane. Remarkably, they can reduce *Staphylococcus aureus* biofilm formation on hospital instruments (72).

Finally, OA has modulating effects on oxidative stress and inflammation, two physiological processes that are closely related. It should be noted that behind OA hepatoprotective ability, attenuation of oxidative stress injury is produced by the upregulation of transcription factor NFR2 by OA, which activates a gene

expression profile that involves antioxidant enzymes glutathione peroxidase, superoxide dismutase 1 (SOD1) and catalase (CAT) (62, 64). Indeed, in vitro assays inducing oxidative stress in human liver cell line QZG showed that OA protects cells from radical oxygen species (ROS) toxicity, by increasing NFR2 expression and activating MAP kinases, together with the ROS scavenging of OA molecule (73). In addition, OA antioxidant chemical and biological effects have been tested on microglial cell models to study brain dysfunctions caused by ROS and inflammation, where OA was able to decrease the release and the expression of pro-inflammatory cytokines IL-1β and IL-6 (74). Moreover, OA can reduce ROS levels of microglia cells in rats, enhancing better behavior in rats predisposed to Parkinson's disease or even in rats with cerebral ischemic injury (75, 76). Besides, OA has the potential to mitigate lipopolysaccharide (LPS) induced-inflammation in in vitro models, thus decreasing tumor necrosis factor α (TNF-α) production and nuclear factor κB (NF-κB) activation (77). The anti-inflammatory potential of OA has been observed in vivo in mice with autoimmune myocarditis, where OA reduced the inflammatory milieu by decreasing the production of pro-inflammatory cytokines (78).

Overall, OA is an active triterpenoid with diverse chemical and biological effects that can promote, attenuate, or restore several physiological and molecular processes in vitro or in vivo (Table I-1). Nonetheless, more research is needed to unravel the molecular mechanisms behind some of the properties of OA. In addition, more studies are needed to translate this OA potential for human health with clinical trials, in combination with improved OA administration.

Table I-1. Summary of the oleanolic acid's most relevant properties found in the literature. *Inf: inflammation. Pro-inf: pro-inflammatory. (-): no evidence.*

OA properties	In vitro	In vivo	Molecular mechanism of action	Clinical trial
Antitumoral	HeLa, HepG2, HCT-116 cell lines	Mice with cervical cancer, rats with glioblastoma cancer	MAP kinases inhibition, miR-122 tumor suppressor expression	Under research (first clinical phase)
Antihyperglycemic	HepG2 cell line	Insulin-resistant mice, obese mice	IRS1 and GLUT4 expression increase, pro-inf. cytokines reduction	–
Hepatoprotective **Gastroprotective**	Primary rat hepatocytes, HepG2 HSCs and cells	Rats with cholestasis, mice and rats with gastric lesions	Bile acid transporters expression, NFR2 factor upregulation, circadian liver genes regulation	Hyperlipidemic patients (low cholesterol, TGs, and LDL levels)

OA properties	In vitro	In vivo	Molecular mechanism of action	Clinical trial
Antibacterial	Assays with nosocomial infections pathogens like *S. aureus*	Invertebrate model of infection *Galleria mellonella*	Biofilm formation reduction, bacterial membrane disruption	–
Antiviral	Assays with isolated viral enzymes	–	Hepatitis C RNA polymerase inhibition, HIV proteases inhibition	–
Antioxidant	QZG cells, microglia cells	Rats with Parkinson predisposition, rats' cerebral ischemia	NFR2 factor upregulation, SOD1 and CAT enzymes production, ROS scavenging, MAP kinases activation, lower pro-inf. cytokines levels	–
Anti-inflammatory	Primary endothelial cells	Mice with autoimmune myocarditis, mice with LPS-induced infl.	TNF-α levels decrease, NF-κB attenuation, lower production of pro-inf. cytokines-	–

1.2. WOUND HEALING

Despite all the above-mentioned pharmacological properties of oleanolic acid, there is one that is not yet fully understood: its effect on wound healing. Wound healing is a complex physiological process that requires the participation of various cell types to restore the skin barrier (13). Effective wound healing relies on efficient cell coordination among growth factors, cytokines, and second messengers that regulate the process (79, 80). However, when this repair mechanism is compromised, an acute wound may turn into a chronic wound, a condition with a sustained high inflammation and incomplete wound closure (81). For this reason, the discovery of new therapies and drugs is pertinent to address this problem, since the skin is a fundamental organ that protects us from dehydration, pathogens, irritants, allergens, mechanical injury or ultraviolet light (76, 82).

1.2.1. Human skin structure

The human skin is the largest organ of the organism. It is biologically complex and has multiple functions such as physic protection, sensory perception, immune defense, and thermoregulation (83-85). To secure these properties, the skin is a multilayered structure composed of three differentiated components: epidermis, dermis, and subcutaneous tissue (Figure I-5A) (86).

The epidermis is the outer layer of the skin (87). It is made up of several sublayers that are the result of different phases of keratinocyte growth, differentiation, and death (88, 89). They are, from inside to outside: stratum basale, stratum spinosum, stratum granulosum, and stratum corneum (Figure I-5B) (90). The epidermis exists thanks to the continuous renewal of those layers by keratinocyte proliferation and differentiation (91).

Below the epidermis lies the dermis, which is the inner layer containing blood vessels, nerve endings, and mostly extracellular matrix (ECM), with dermal fibroblasts as the main cellular type (Figure I-5B) (92). The dermis is crucial to bringing structural support and elasticity to the skin (93). This is because of the synthesis of collagen and elastin fibers by dermal fibroblasts, which confers tensile strength and resilience to the skin (92, 94, 95). In addition, the dermis is highly

vascularized with the networks of blood vessels lined with endothelial cells, that allow for oxygen and nutrient supply, thermoregulation, and wound healing (13).

Finally, the hypodermis is the deepest skin layer (Figure I-5B). It is a subcutaneous coating composed of adipose and connective tissue (96). Adipocytes are the main constituent cell type with energy storage and insulation functions (97). This innermost layer already contains the circulatory and nervous system, connecting with deeper anatomical structures (84).

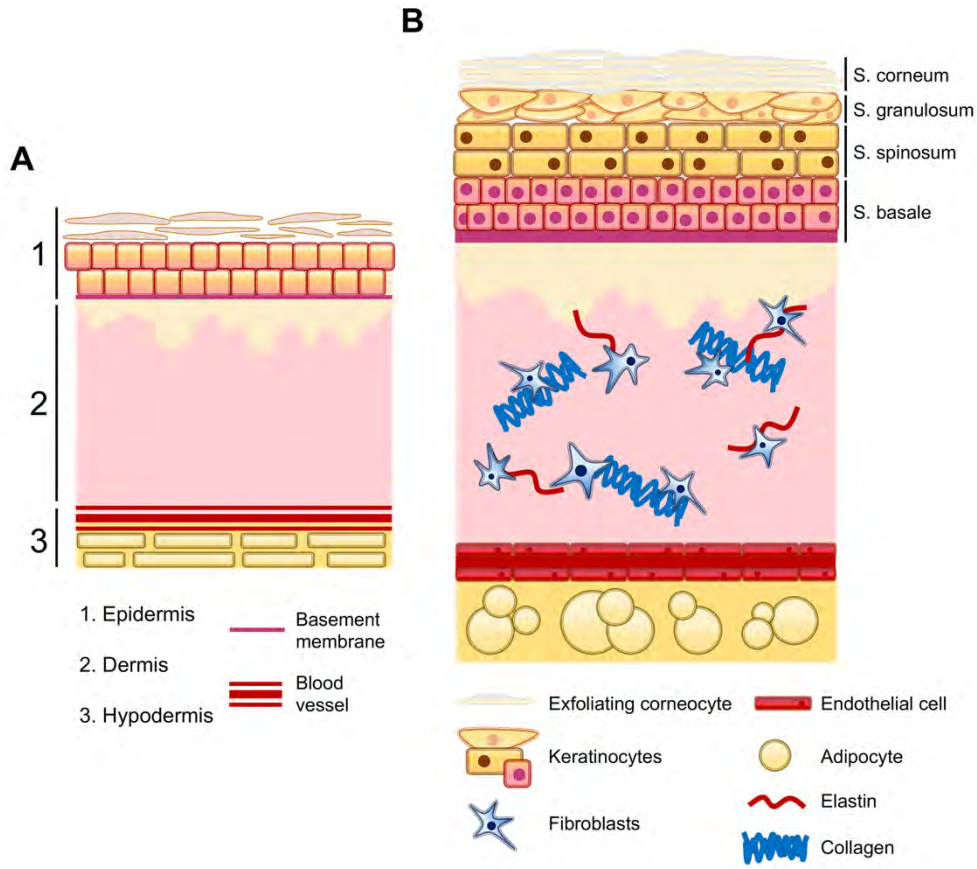

Figure I-5. Human skin structure. ***A.*** *The three layers of the skin are epidermis, dermis, and hypodermis.* ***B.*** *Detailed view of the skin at the cellular level, indicating the main cell types and the four strata of the epidermis: basale, spinosum, granulosum, and corneum. Epidermis renewal is produced by the keratinocyte's proliferation from the basement membrane. — Own elaboration.*

1.2.2. Wound healing

Wound healing is the process by which skin integrity is restored after an injury and it can be divided into sequential phases (13, 98-102). Hemostasis (Figure I-6A) is the first phase to occur in a deep wound. In the newly open wound, fibrin and blood platelets form a loose blood plug to stop the bleeding (102, 103). The plug provides a temporary seal, creating a scaffold for further tissue repair. Platelets produce chemokines to recruit immune system cells to the wound (104). The damage also induces the vasoconstriction of the blood vessels of the dermis to avoid blood loss (102).

In the inflammatory phase (Figure I-6B), neutrophils and macrophages intervene to remove microbes and other antigens by neutrophil extracellular traps, cytotoxic molecules, and phagocytosis (101, 102, 105). Simultaneously, macrophages prompt inflammatory mediators IL-1β, IL-6, and TNF-α to communicate with the rest of the cell types in the wound and manage the inflammatory milieu (80, 100, 102). This phase is very critical because of the effective defense against infections.

The resolution of the inflammation allows for tissue repair and progression into the proliferation phase (Figure I-6C). In this phase, endothelial cells, fibroblasts, and keratinocytes are recruited to proliferate and migrate onto the damaged tissue of the wound (106). Therefore, the wound ends up surrounded by these cell types with the production of cytokines and growth factors that are known to play important roles in them: IL-1, epidermal growth factor (EGF), vascular endothelial growth factor (VEGF), transforming growth factor α (TGF-α), and transforming growth factor β (TGF-β) (79, 80, 107). Fibroblasts synthesize extracellular matrix (ECM) proteins, such as collagen, enabling wound contraction (94). Endothelial cells proliferate, migrate, and produce angiogenesis providing the wound with new blood capillaries, mainly by the effect of VEGF (80, 108). On the other hand, keratinocytes proliferate and migrate from the wound edges over the newly constituted dermis, separating it from the crust, to finally close the wound in response to the release of EGF and TGF-α (13, 107, 109).

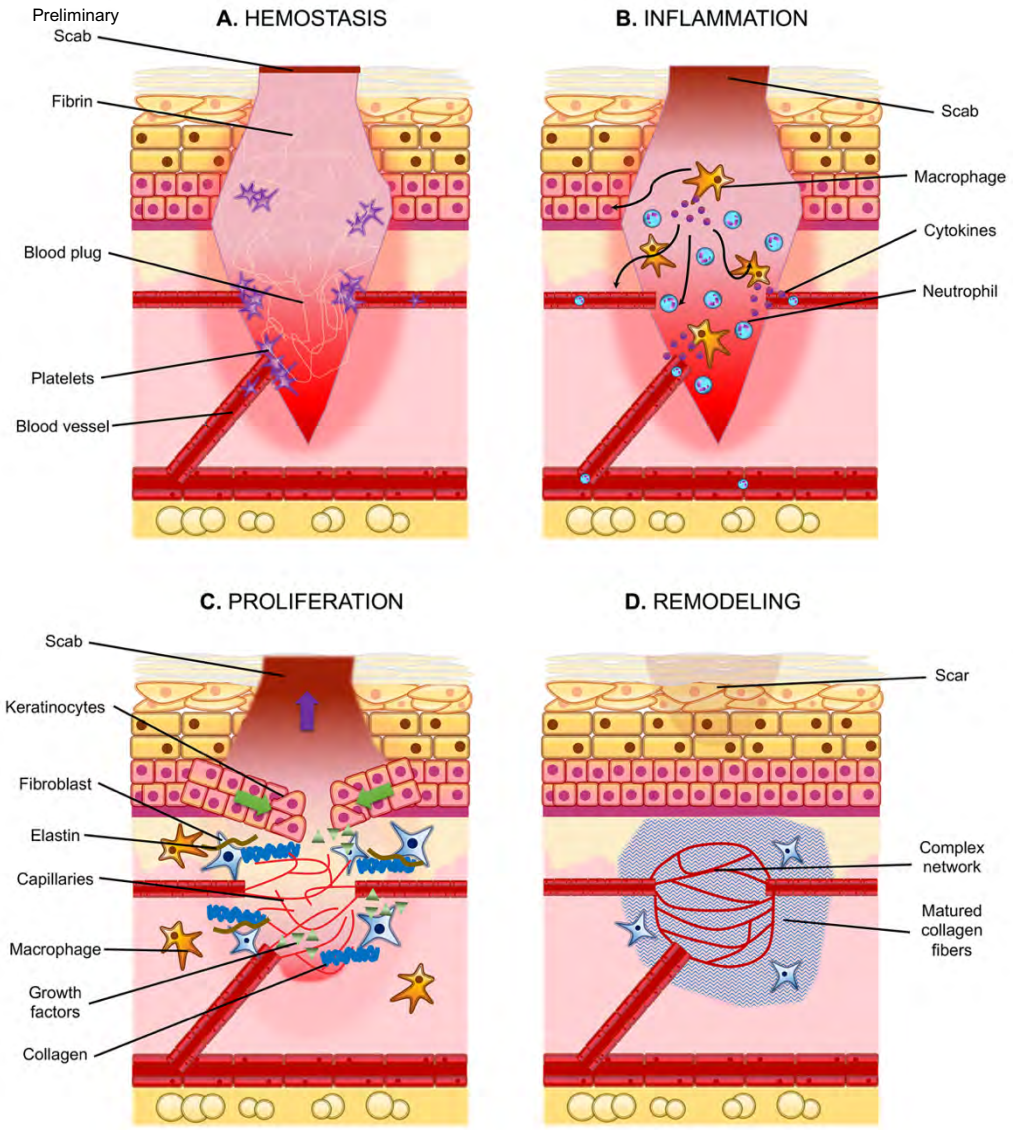

Figure I-6. The wound healing phases. ***A.*** *In the hemostasis phase, platelets invade the newly produced wound, together with fibrin, to stop the bleeding.* ***B.*** *During the inflammatory phase, monocytes and neutrophils are recruited to the wound. Within the wound, monocytes differentiate into pro-inflammatory macrophages (M1). Both neutrophils and macrophages initiate a cascade of cytokines and chemokines to clear pathogens and manage the inflammatory milieu.* ***C.*** *The proliferation phase is characterized by the participation of epithelial cells, fibroblasts, and endothelial cells that invade the wound and secrete various growth factors. Epithelial cells proliferate, migrate, and close the wound by pushing up the superficial scab upwards. Fibroblasts synthesize new ECM proteins collagen and elastin. Endothelial cells proliferate, migrate, and form new tubes to supply the wound with oxygen, cells, and growth factors. M1 macrophages switch their phenotype to M2 tissue-repair macrophages.* ***D.*** *Finally, the remodeling phase, the longest of the phases, occurs by increasing tissue complexity through ECM deposition and organization by fibroblasts and the maturation of new blood vessels by endothelial cells. The newly formed tissue is re-epithelialized and appears as a scar. — Own elaboration.*

Lastly, in the remodeling phase (Figure I-6D), all these cells form a mesh known as granulation tissue. This phase is the longest one, characterized mainly by fibroblast collagen deposition and remodeling. In this way, the ECM becomes more complex and organized, in terms of strengthening the tissue followed by wound contraction (110). Lastly, scar tissue is formed, which has a higher density of collagen fibers than normal skin with a complete epithelization of keratinocytes (102).

1.2.3. Epithelial cell migration

During wound healing, cell migration is a crucial process to allow for tissue remodeling and wound closure, which is carried out by either fibroblasts, endothelial cells or epithelial cells (109, 111, 112). Precisely, epithelial cells are required to restore the epidermal barrier, by a process called re-epithelialization (109). Re-epithelialization is a type of epithelial-mesenchymal transition (EMT), in which cells change their morphology and migrate due to the communication with other cell types and the interaction with ECM proteins collagen, elastin, and laminin (113). Cells communicate by the release of growth factors and cytokines, which establish exogenous, paracrine, and autocrine loops (114). All these stimuli set off a whole regulatory system on epithelial cells, with multiple signaling networks involved, which will be explained below.

1.2.3.1. Epidermal growth factor and MAP kinase signaling pathways

One of the most important signaling pathways involved in epithelial cell migration starts with receptor tyrosine kinases (RTKs) on the cell surface. These receptors embedded in the plasma membrane transduce the extracellular signals given by growth factors and cytokines to intracellular signals, in order to drive essential processes for the cell (115).

In this line, epidermal growth factor receptor (EGFR) has a wide range of effects on the cells. For instance, it is related to cell proliferation, growth, and differentiation (116). Indeed, the overexpression of EGFR causes uncontrolled cell growth and invasiveness, thus resulting in the development of numerous tumors such as breast cancer (117). EGFR plays a key role in cell migration regulation, as it activates epithelial regeneration by EGF binding. Indeed, EGFR pharmacological

inhibitors block cell migration (118-120). This receptor, like many other RTKs, has three main domains: an extracellular domain where ligands bind, a transmembrane domain, and a cytosolic domain with tyrosine kinase activity (115, 121). Inactive EGFR is located on the cell surface as a monomer (122). Therefore, when extracellular ligands like EGF bind to each EGFR monomer, the two EGFR monomers interact, dimerize, and self-phosphorylate on several tyrosine residues (Figure I-7A) (117, 122, 123). When tyrosine residues are phosphorylated in the cytosolic domain, the recruitment of several adaptor proteins is produced, thus communicating EGFR activation to cytosolic protein kinases in order to trigger multiple signaling pathways (Figure I-7B) (124). Concretely, EGFR's phospho tyrosine 1068 and 1086 residues recruit growth factor receptor binding protein 2 (Grb2) and subsequently son of sevenless 1 (SOS1) protein (123). Indeed, phosphorylation at Tyr 1068 is required for cell repair and migration processes (125, 126). SOS is a guanine nucleotide exchange protein that binds to RAS, thus activating RAS by exchanging its linked GDP to GTP (127, 128). Likewise, RAS-GTP interacts with RAF, which is the entry point to mitogen-activated protein kinases (MAP kinases) module (129). RAF is a serine-threonine kinase that directly switches on MEK1/2 by the phosphorylation at its serine residues 217 and 221 (123).

Mitogen-activated protein kinase kinase 1/2 (MEK1/2, MEKK1/2, MKK1/2 or MAPKK) is a particular kinase due to its dual phosphorylation activity on tyrosine and serine/threonine residues (130). This regulatory protein controls cell proliferation and survival, and is also a key point on the EGFR pathway in epithelial cells (123, 131). MEK1/2 phosphorylates its direct substrate, ERK1/2, on threonine 202 and tyrosine 204 residues following the MAP kinases module (132). Interestingly, extracellular signal-regulated kinase 1/2 (ERK1/2), a MAPK, is essential for epithelial cell migration during wound healing (133, 134). Indeed, both MEK and ERK expression and activation are required for cell migration (135). ERK has a high number of downstream substrates (134). Finally, ERK can translocate to the cell nucleus and activate several transcription factors, including c-Fos and c-Jun (136, 137).

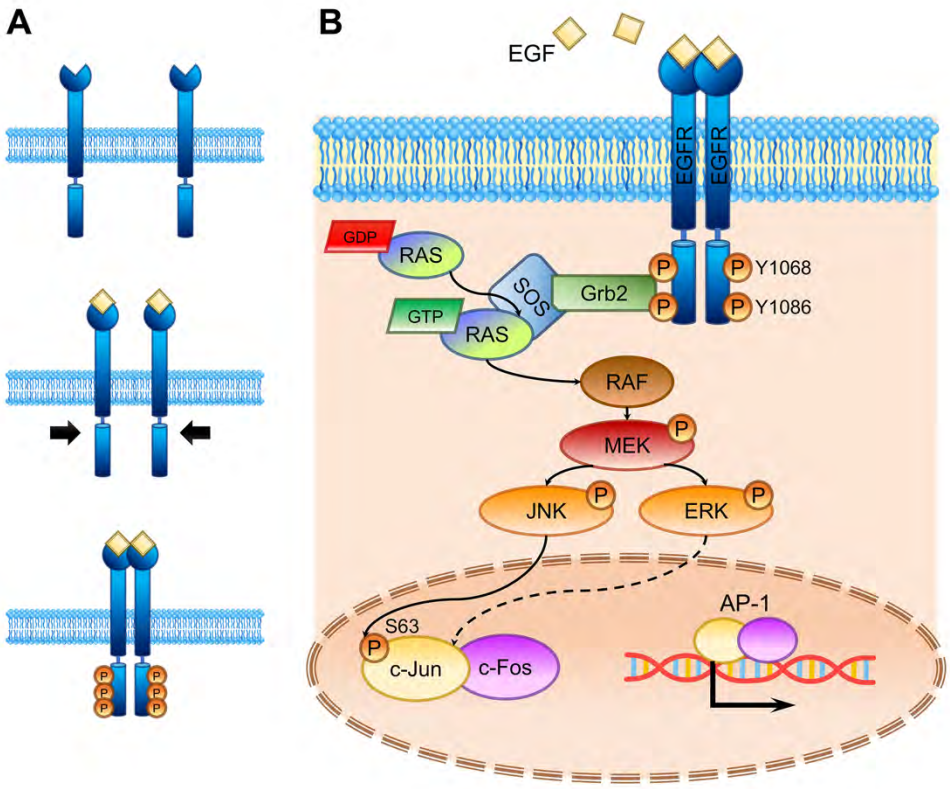

Figure I-7. EGFR activation and signaling. A. *EGFR remains inactive on the cell surface as a monomer. When this monomer binds its ligand EGF, EGFR dimerizes and self-phosphorylates its tyrosine residues at the cytosolic domain.* ***B.*** *The EGFR phosphorylation is an event that recruits adaptor proteins Grb2 and SOS in the cell cytosol. SOS allows the nucleotide exchange of RAS-GDP to RAS-GTP, thus activating RAS, which in turn activates RAF, a MAPKKK. Then the MAP kinases module is activated by the sequential phosphorylation of MEK (MAPKK) followed by ERK and JNK (MAPKs). Both kinases' function is to phosphorylate c-Jun transcription factor in the cell nucleus to finally form AP-1 complex with c-Fos and upregulate the expression of genes involved in cell proliferation, growth, and migration. — Own elaboration.*

Furthermore, similarly to ERK, other regulatory proteins intervene in these pathways and have c-Jun transcription factor as their substrate. One of these proteins is c-Jun N-terminal kinase (JNK), which belongs to the MAPKs family with ERK (137). JNK is a serine/threonine kinase that responds to growth factors, cytokines, and cellular stress (138). Remarkably, MEK1 is required for JNK activation and subsequently c-Jun overexpression in order to trigger cell migration (139, 140). JNK has transcription factor c-Jun as a direct substrate, among many

others, driving multiple actions on cell motility including cytoskeletal dynamics and directional migration (141). In addition, JNK is needed for keratinocyte migration, critical for re-epithelization during wound healing (142). Downstream ERK and JNK, in the cell nucleus, the transcription factor complex called activator protein 1 (AP-1) is made up of c-Fos and c-Jun protein subunits (Figure I-7B) (143-145). AP-1 activation upregulates the expression of cell cycle genes such as cyclin D1, promoting cell proliferation, survival, and tissue regeneration (146-148). It should be emphasized that c-Jun is considered a master regulator of cutaneous wound healing that has an important role when skin integrity is altered by injury (149). In fact, c-Jun expression is increased in keratinocytes at the wound edge in human wounded skin (150). Additionally, overexpressed c-Jun, in diabetic rat models, accelerates the healing when a wound is produced on them. (151). As mentioned above, activation of c-Jun is produced by ERK and JNK through the phosphorylation of its serine 63 and 73 residues, thus interconnecting both MAP kinases pathways (144, 145, 152). Epithelial cells expressing EGFR subsequently trigger c-Jun expression and activation, implying the role of c-Jun as a true organizing center for epidermal organization and eventually re-epithelization (153).

Additionally, there are other pathways in the cells that contribute to migration. The phosphoinositide 3-kinase (PI3K), which starts AKT/mTOR pathway, has a remarkable role in this process by influencing cell survival, polarity, and motility (154). Indeed, it has a crosstalk with the MAPK pathways mentioned above (155). Furthermore, the Wnt signaling pathway modulates cell polarity, directional movement, and cytoskeleton rearrangement by β-catenin protein stabilization and nuclear translocation (156).

*1.2.3.2. **Cell motility by focal adhesions and cytoskeleton***

When epithelial cells start to migrate along the wound, the movement is driven by changes in the cell morphology and architecture (157). Behind these changes, there are protein complexes regulated by an intricate signaling network that allows the necessary mechanical forces to produce cell motility (158, 159).

Cells under dynamization show a strong polarization and restructure the architecture to direct the movement (157, 159, 160). Therefore, microscopic

distinguishable shapes are produced: leading edge, lamellipodia, and filopodia (Figure I-8) (160). Lamellipodia and filipodia are structures that produce cell protrusion, and both are enriched with actin filaments (F-actin) (161-163). Actin is a ubiquitous protein of the cytoskeleton that polymerizes to form lamellipodia and filopodia, which also serves as a scaffold for the generation of mechanical forces to trigger cell migration (164, 165). Indeed, during cell migration, actin is on a constant assemble-disassemble loop necessary for the high dynamization of the cell (Figure I-8) (162, 166). Other proteins from the cytoskeleton are microtubules and intermediate filaments, which are involved in intracellular transport and mechanical stability respectively (167, 168).

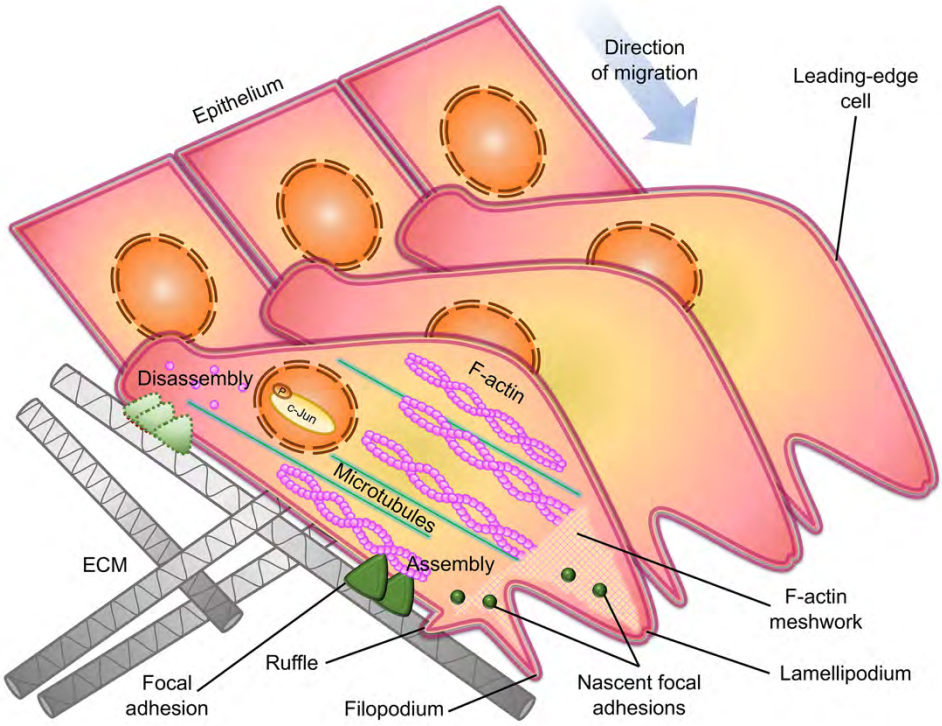

Figure I-8. Cell architecture during migration. *At the wound edge, epithelial cells change their morphology and gain polarity to move over the extracellular matrix (ECM) and invade the wound area. Then, dynamic structures, namely lamellipodia, filopodia, and ruffles, appear by actin dynamization to move through the substrate, where polymerized actin is present to form and hold these structures (F-actin). In addition, focal adhesions, multiprotein complexes, are associated with F-actin and provide the necessary forces and interactions with the ECM for migration. Actin and focal adhesions are in constant flux in leading-edge cells to maintain a highly dynamic state. — Own elaboration.*

These changes in cell morphology and actin reorganization are the result of cells' dynamic interactions with ECM components, like collagen (158, 169, 170). In this sense, integrins are the fundamental receptors of ECM, since they act as true mechanosensory proteins due to their lack of intrinsic catalytic activity (Figure I-9) (171-173). However, their role is recruiting adaptor and catalytic proteins, giving rise to focal adhesion (FA) complexes, the central players of this interaction (167, 174). FAs are multiprotein complexes that connect the actin cytoskeleton to the ECM (Figures I-8 and I-9) (170, 175). These complexes afford signal transduction sites where multiple signaling pathways converge, resulting in the cells' movement through the substratum (175). Among these, small G proteins, Rho GTPases, modulate cytoskeleton dynamics by promoting actin polymerization and myosin contraction (Figure I-9) (176). Moreover, PI3K/AKT/mTOR axis and MAPKs like ERK1/2 assume a critical role in regulating cell motility and polarity through the dynamization of the actin cytoskeleton (154, 177, 178).

Alternatively, in this intricate network, focal adhesion kinase (FAK), is the key recruitment in response to integrin-ECM binding and RTKs activation by growth factors (Figure I-9) (172, 179). Together with actin, FAs are in continuous turnover to modulate cell adhesion and migration due to FAK activation (180). FAK is a protein tyrosine kinase (PTK) that connects integrins with intracellular signaling pathways (181, 182). FAK has numerous substrates to phosphorylate; however, paxillin is one of the most critical ones. Paxillin is an adaptor protein with multiple protein interactions and phosphorylation sites to manage FA remodeling (183, 184). This protein localizes with FAK at FAs, thus, both proteins act as key regulators of FA dynamization during cell migration (185). It is known that alterations in paxillin/FAK interaction reduce cell migration (186, 187). Furthermore, the use of various functional mutants of FAK has unveiled the significance of FAK localization to focal adhesions in regulating their dynamism (188). Paxillin is another key driver of cell migration because of its importance in lamellipodia positioning and directional motility (189). Besides, recent evidence attributes to paxillin additional functions as a transcription factor involved in the expression of migration and survival genes (190). Finally, JNK is another protein kinase that phosphorylates paxillin, therefore influencing key processes such as cytoskeletal dynamics and focal adhesion turnover (191, 192). Interestingly, it has

been shown that JNK is required for lamellipodia formation and cell protrusion in Madin-Darby canine kidney cells (MDCK) (193).

In summary, cell motility requires the fine-tuned regulation of a signaling network composed of protein kinases, adaptor proteins, and mechanosensitive proteins, to promote the turnover of both actin and FAs, a condition that triggers lamellipodia and filopodia formation, cell adhesion, and directional movement.

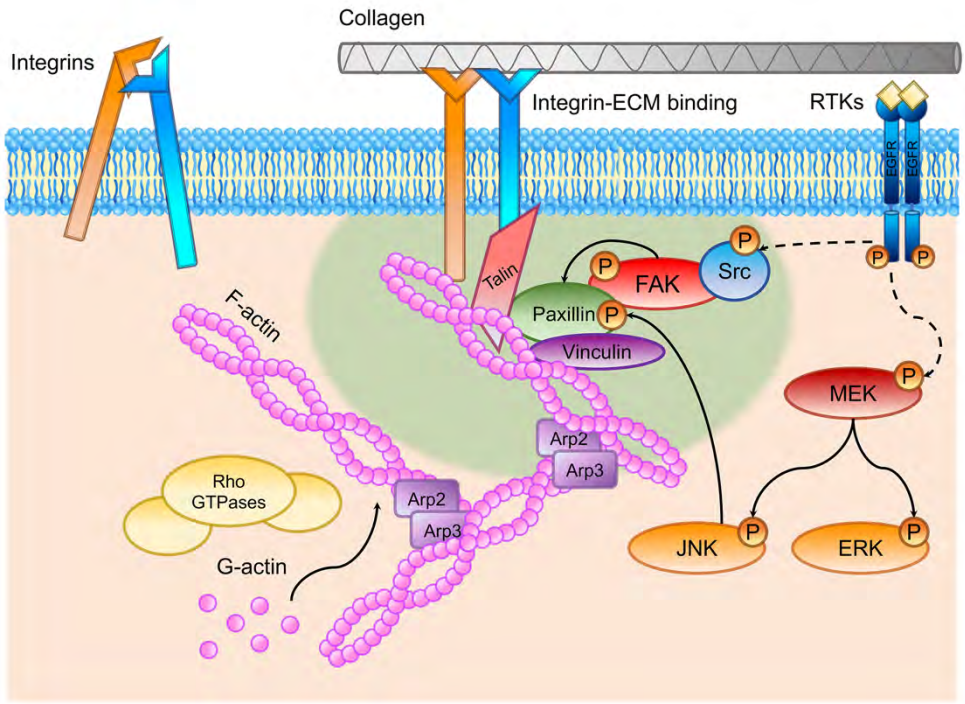

Figure I-9. Focal adhesion signaling. *Integrins on the cell surface are initially in an off-conformation. When these molecules interact with ECM components like collagen, they switch to an on-conformation. This triggers talin recruitment, which links integrins to the F actin cytoskeleton. Following this, multiple adaptor proteins are recruited, leading to the formation of the focal adhesion (FA) complex (marked as green shaded area in the figure): paxillin and vinculin. This event results in the targeting of FAK to the FA, a regulatory kinase that integrates and manages the FA function to activate this complex for cell movement. The activation of RTKs, such as EGFR, activates FAK by Src kinases, thus linking both pathways. Consequently, Rho GTPases act to polymerize globular actin (G actin) into actin filaments (F actin). The Arp2/3 complex then links to F actin to produce its branching. In addition, activation of receptor tyrosine kinases (RTKs) like EGFR induces the activation of the MAP kinase module MEK, JNK, and ERK, which regulate the cytoskeleton adaptor proteins. — Own elaboration.*

1.2.4. Endothelial cell functions

Endothelial cells play a critical role during the wound healing course due to their participation in the inflammatory and proliferation phases (101). These cells play a pivotal role in inflammation management and the formation of new blood vessels that will supply the wound with oxygen, nutrients, and growth factors (100, 101, 194, 195).

1.2.4.1. Inflammation regulation

During inflammation, the extravasation of neutrophils, lymphocytes, and monocytes into the damaged tissue is produced from the lumen of blood vessels through endothelial cells, thus allowing the migration of these immune cells to the wound (195). Extravasation is mediated by adhesion molecule expression at the endothelium surface, which produces circulating cells to tether to endothelial cells (195-197). During wound healing, TNF-α is the key inducer to expose adhesion molecules onto endothelial cells. TNF-α is a pro-inflammatory cytokine mainly released by wound resident macrophages during the inflammation phase (79, 102). TNF-α binds to TNF-α receptors 1 and 2 on the endothelial cell surface (198). These receptors recruit several regulatory proteins to trigger the nuclear factor kappa B (NF-κB) signaling pathway. NF-κB is a transcription factor that remains inactive by the inhibitor of NF-κB, IκBα (Figure I-10A). When TNF-α receptors are activated, the phosphorylation of IκB is produced by IKK (IκB kinase), and releases NF-κB in the cytosol to translocate to the cell nucleus, thus promoting the expression of inflammatory genes, especially cytokines and adhesion molecules (Figure I-10A) (199, 200). This augments the production of the adhesion molecules that are exposed to the cell membrane: P-selectin, E-selectin, vascular cell adhesion molecule (V-CAM1), and intracellular adhesion molecule (I-CAM1) (201-203). E-selectin plays a crucial role in the initial stages of monocyte recruitment, facilitating their tethering and rolling (201). Subsequently, integrins I-CAM1 and V-CAM1 secure the adhesion of leukocytes and monocytes, allowing their extravasation into the wounded area (204-207). Monocytes recruitment and differentiation into macrophages within the wound are essential processes to resolve inflammation and prompt tissue reparation mechanisms (Figure I-10B) (204, 208, 209).

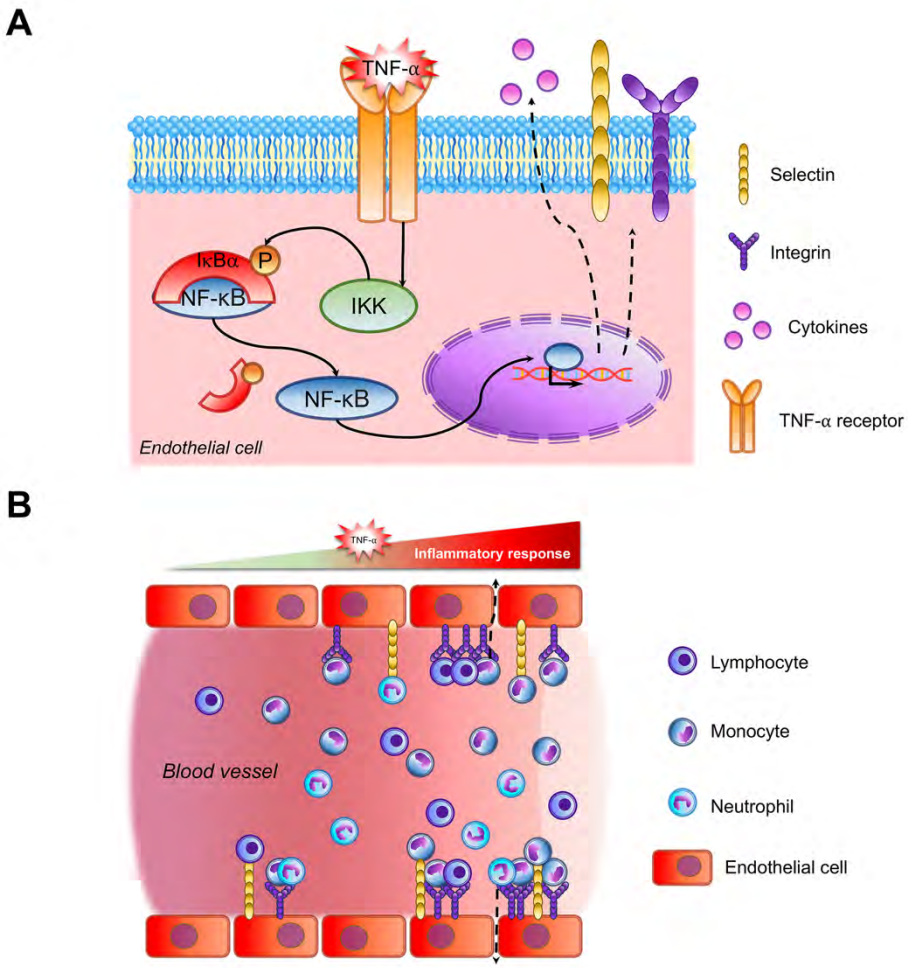

Figure I-10. NF-κB signaling and adhesion molecule expression. A. *After tissue damage, pro-inflammatory mediators are released. TNF-α targets endothelial cells by binding its receptors on the endothelium surface. The activation of these receptors leads to IKK activity, thus phosphorylating IκBα inhibitor. Finally, IκBα is removed and NF-κB translocates to the nucleus to promote a gene expression profile that results in pro-inflammatory responses. Subsequently, endothelial cells release pro-inflammatory cytokines and expose adhesion molecules selectins P-selectin, E-selectin, and integrins I-CAM1, and V-CAM1.* ***B.*** *As a consequence of TNF-α stimulation, the endothelium of blood vessels expresses adhesion molecules, resulting in recruitment and extravasation of lymphocytes, neutrophils, and monocytes (indicated by dashed black arrows). — Own elaboration.*

*1.2.4.2. **Angiogenesis***

New blood vessel formation, called neo-angiogenesis, is a process that restores dermal microvasculature, which is crucial for wound tissue restoration (194, 210, 211). This process occurs when the inflammation phase is about to finish, starting the proliferation and remodeling phases (13, 102, 106). It should be noted that angiogenesis is different from vasculogenesis, mainly because the latter is produced from blood islands, where no preexistent blood vessels are present, being more common during embryonal development (212).

Hypoxia is the strongest stimulus that triggers angiogenesis by the release of VEGF (13, 211). VEGF is released by subcutaneous cells, epithelial cells, and, mostly, macrophages (Figure 11) (79, 102). VEGF-activated endothelial cells degrade ECM, proliferate, migrate, modify their cell-cell junctions, and branch out from the preexistent vessels to form new capillaries (102, 213). Moreover, during inflammation resolution, the macrophages switch from the pro-inflammatory (M1 macrophages) to the anti-inflammatory (M2 macrophages) phenotype, acting as a pro-angiogenic stimulus for endothelial cells to increase vessel formation and vasculature density (Figure 11) (214-216). Therefore, VEGF is the key factor in promoting neo-angiogenesis. Thus, it has been shown that its topical application accelerates wound healing in diabetic mice (108). VEGF receptors (VEGFR) belong to the receptor tyrosine kinases (RTKs) family and are very similar to EGF receptors (217-219). Signaling mechanisms involved in neo-angiogenesis are shared with those involved in epithelial cell migration, since endothelial cells need to proliferate and migrate to form new blood vessels from preexistent ones (220). Receptors VEGFR1 and VEGFR2 are the ones that intervene in vasculogenesis and angiogenesis (218, 221). Indeed, these receptors have been deeply studied for their implication in cancer, since the formation of new vessels is essential for tumor cell growth and survival (222).

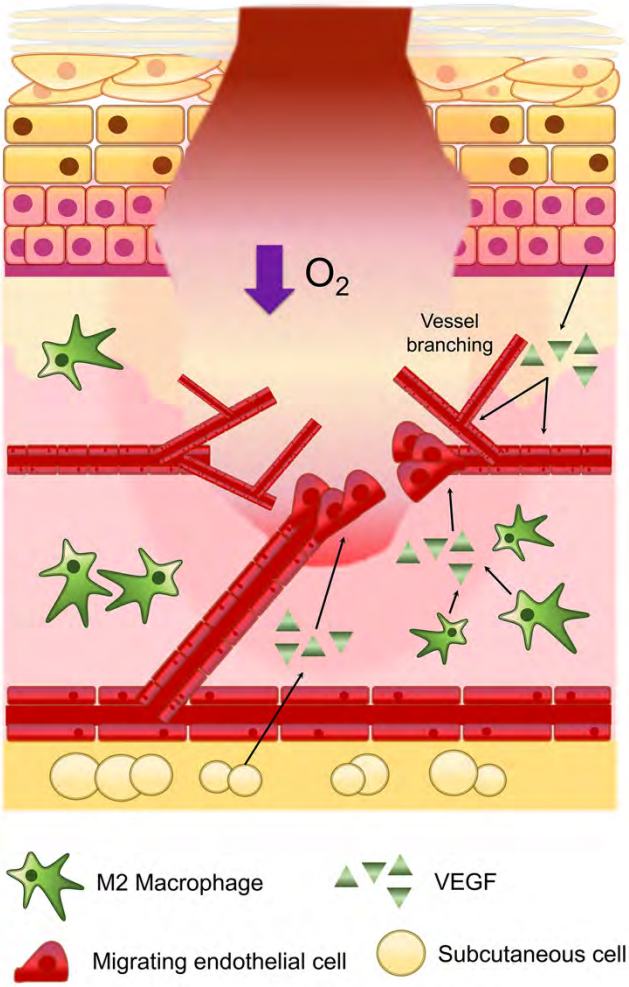

Figure I-11. Angiogenesis in the wound. *Hypoxia in the injured tissue initiates VEGF secretion by macrophages, subcutaneous cells, and epithelial cells at the wound site. The VEGF levels promote endothelial cell proliferation, migration, and tube formation. Subsequently, new tubes sprout and branch, resulting in the development of a complex vascular network through continuous elongation and cutting of the capillaries. — Own elaboration.*

1.2.5. Oleanolic acid on wound healing

Among its properties, some evidence has proved that OA has positive effects on wound healing, because it improves various wound features (3, 223-225). For

instance, rabbits treated with OA-enriched plant extracts show accelerated wound healing with better aesthetic results (3). Moreover, OA application increases the tensile strength in mice wounds (223). However, the molecular mechanisms underlying these processes are not fully understood.

One of the most significant effects of OA on wound healing is its positive impact on cell migration (126, 225). However, in recent years, several authors have shown a negative effect of OA on cell migration deducing an antitumoral activity of this molecule. By using tumor cell lines, OA proved to inhibit migration and invasiveness (52, 226-228). Although this effect could seem negative for regular cells, OA activity is cell-type-specific and depends on the concentrations used. This will be discussed in the next sections. Nonetheless, it has been shown that OA can promote cell migration in mouse fibroblasts and epithelial-cell models: non-malignant mink lung epithelial cells (Mv1Lu) and human mammary gland epithelial cells (MDA-MB-231) (126, 225).

Indeed, a first study was conducted in our lab to understand which molecular mechanisms are stimulated by OA to enhance cell migration (126). In this study, in vitro Mv1Lu and MDA-MB-231 epithelial cell lines were used (229-234). In both cell lines mentioned, OA significantly stimulated cell migration on in vitro scratch assays (126). These results were accompanied by key migration proteins MAP kinases ERK1/2 and JNK1/2 activation, together with c-Jun activation in protein cell lysates treated with OA (126, 153). It is noteworthy that OA also stimulated EGFR phosphorylation and EGFR levels by endocytosis, in a similar fashion to its ligand EGF (117, 126, 235). These findings suggest that OA-powered cell migration is produced by an undetermined OA interaction with EGFR, which produces MAPK activation and subsequent c-Jun activation (126). Strikingly, the addition of pharmacological inhibitors against EGFR, MEK, and JNK upon OA stimulation reduces migration by 80%, 50%, and 50%, respectively (126). These data suggest that ERK and JNK pathways, which seem intimately related, both contribute to migration triggered by OA and are completely dependent on EGFR to c-Jun signaling.

1.3. CYCLODEXTRINS

Numerous novel bioactive compounds can be easily obtained from nature and can be applied to therapy (7, 9, 10). However, some of them have a hydrophobic chemical nature, as is the case of OA, with poor water solubility (5-0.02 μg/ml) (49, 236). This feature involves the need for novel microcarriers to improve the harmless delivery and application of these compounds to biological systems. Several studies have explored the vehiculation of OA through diverse microcarriers (237, 238). For instance, nanoparticles made from polymers such as polyethylene glycol, cellulose, or silicone have been synthesized to improve OA solubility (238-241). Nonetheless, these nanoparticles need to be synthesized from scratch and have time-consuming chemical processes.

Luckily, cyclodextrins (CDs) can be easily obtained and emerge as a favorable alternative to OA encapsulation. These macromolecules, present in nature, are known for their unique tridimensional structure, characterized by a truncated cone structure (Figure I-12) (242-244). These nanostructures are cyclic oligosaccharides composed of glucose units linked with α(1→4) glycosidic bonds, where the cavity of the cone is hydrophobic, whereas the surface of the cone is hydrophilic (243, 245, 246). This amphiphilic nature gives CDs a double property (247). On the one hand, they can encapsulate or complex a wide range of hydrophobic poor water-soluble or unstable compounds. On the other hand, they have high solubility in aqueous solutions (245, 248, 249). Complexation with CDs has been extensively applied to increase the water-solubility of many compounds, and also to enhance the extraction of poor-concentrated (247) water-soluble compounds from some dietary by-products (247, 250-252). Considering a pharmacological approach, several authors have shown the power of CDs to deliver drugs because they can reinforce the solubility, stability, activity, and bioavailability of molecules of interest (253-255).

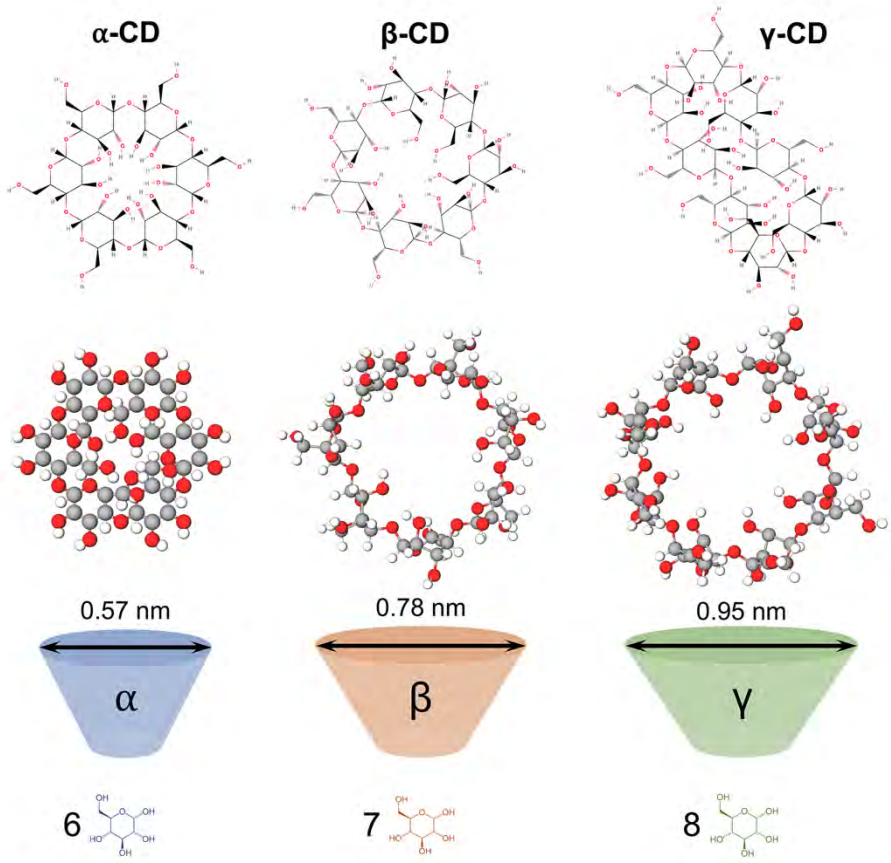

Figure I-12. The three native cyclodextrins. *The size of the hydrophobic cavity is determined by the number of glucose units within the cyclic structure. — Modified figures from MolView.*

1.3.1. Cyclodextrins synthesis and types

CDs are synthesized from starch by glycosyltransferase (CGTase), an enzyme produced by microorganism species from the genus *Bacillus* (256-258). The enzyme catalyzes the formation of cyclodextrins by cleaving the glucose units from the linear starch chain and reassembling them into cyclic nanostructures (256, 257). In nature, there are three types of CDs, called natural or native CDs: α-, β-, and γ-CDs, depending on the number of D-glucose units that compose the oligosaccharide, 6, 7, or 8, respectively (Figure I-12). The size of the hydrophobic cavity of the three

CD types is progressively increased by the number of glucose units (243, 259, 260). Moreover, the hydrophilic nature of the surface of the truncated cone is given by the hydroxyl groups of the glucose units. Interestingly, apart from native cyclodextrins, there are other cyclodextrins with additional chemical groups added to the cone surface, to give CDs extra properties. This is the case of modified cyclodextrins with hydroxypropyl groups (HP-α-, HP-β-, and HP-γ-CDs), which have a high hydrophilic nature, thus providing these CDs with extra water-solubility (Figure I-13) (261-263).

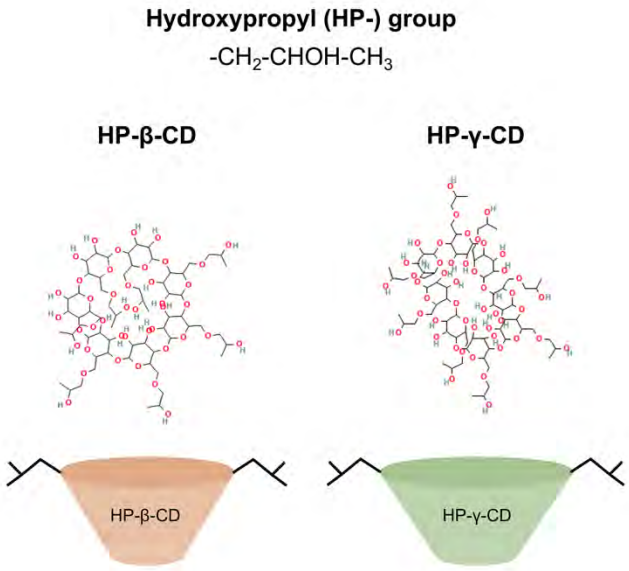

Figure I-13. 2-Hydroxypropyl beta and 2-hydroxypropyl gamma-cyclodextrins. *By introducing hydroxypropyl groups to glucose hydroxyl (-OH) groups located externally to the cyclic structure, native beta and gamma cyclodextrins aqueous solubility can be enhanced. — Modified figures from PubChem.*

1.3.2. Cyclodextrins inclusion complexes and properties

CDs have numerous and interesting properties that reinforce their use in the pharmaceutical, food, and cosmetic industries (246). The complexation of a particular compound depends on the size of the CD hydrophobic cavity, together with the molecular weight and structure of the host compound (259, 261).

The most significant properties of CDs are their encapsulation dynamic and inclusion complex formation (242, 246, 264). Usually, CDs come into contact with the host molecule in an aqueous solution, a polar solution (265). When the host molecule enters the hydrophobic cavity, it displaces all the water molecules due to its higher affinity for the CD chemical groups (Figure I-14A) (242, 246, 248). This structure is the inclusion complex, which is stabilized by non-covalent interactions: hydrophobic interactions, van der Waals forces, and hydrogen bonds (263, 266, 267). The size and shape of the guest molecule in the CD cavity, as well as the nature of the functional groups that are present, determine the strength and specificity of these interactions (268).

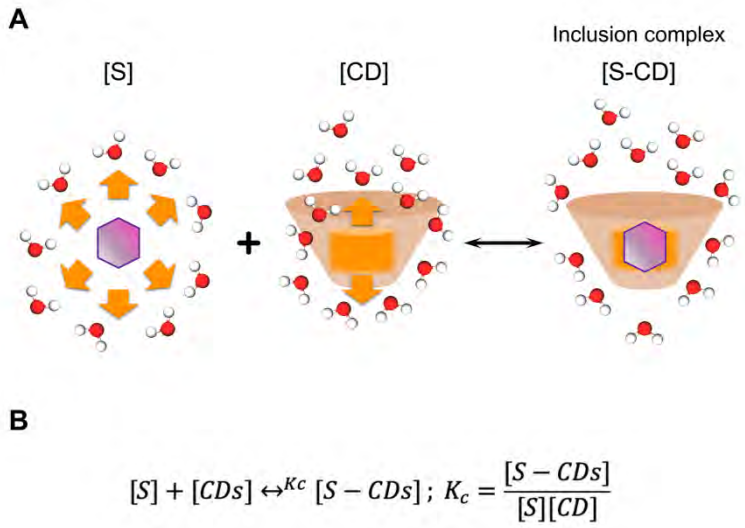

Figure I-14. Formation and kinetics of inclusion complexes. A. *A hydrophobic substrate [S] repels water molecules in an aqueous solution. When combined with cyclodextrin [CD], the substrate enters the inner cavity of the cyclodextrin and displaces the water molecules to the exterior of the cone. Following this, coupling occurs between the substrate and the cyclodextrin, thus creating the inclusion complex [S-CD]. The shaded orange area designates the hydrophobic cavity of the cyclodextrin.* ***B.*** *Inclusion complex formation is governed by complexation constant (K_c), which indicates the substrate's affinity to the cyclodextrin's inner cavity. This property establishes a dynamic equilibrium that can be shifted towards substrate release, or inclusion complex formation — Own elaboration.*

The interactions formed at the inclusion complexes are established by a dynamic equilibrium governed by a complexation constant (K_c). This K_c is quantified by an equation that relates inclusion complex concentration in the solution [S-CD] with cyclodextrin concentration [CD] and free compound or

substrate concentration in the solution [S] (Figure I-14B) (242, 245). The higher the K_c, the higher the complexation (262, 266, 269). In other words, the higher the K_c, the higher the amount of compound linked to the CD, which, in turn, provides inclusion complexes with more stability (262).

Besides the thermodynamic interactions between cyclodextrin and compound, chemical factors, pH, temperature, and the chosen solvent also affect the stability of the inclusion complex (270, 271). There are several methods to calculate K_c (272). One of them is the solubility method, in which different measures are performed with increasing CD concentrations and a compound fixed concentration, which is in excess (273, 274). Then, serial solutions are formed with the CDs, and later, mixed CDs and compound solutions are filtered to remove the excess of the non-complexed compound, and finally, the complexed compound is quantified by high-performance liquid chromatography (HPLC) (270). As a result, phase diagrams are obtained, which are useful for interpreting the dynamics and the type of complexation between the CDs and the substrate of interest (273, 275). Depending on the solubility of inclusion complexes, two types of phase diagrams can be obtained: a high solubility level without precipitation in the solution (type A), or a low solubility level with precipitation (type B) (Figure I-15) (276). Regarding type A, complexes can display different subtypes: one CD molecule encapsulates one substrate molecule, A_L; two CDs encapsulate one substrate, A_P; or two substrates are complexed by one CD, A_N (Figure I-15) (276-278). The type A_L or 1:1 are the most common complexes and the CD concentration and dissolved substrate are positively linearly related (265, 274, 278).

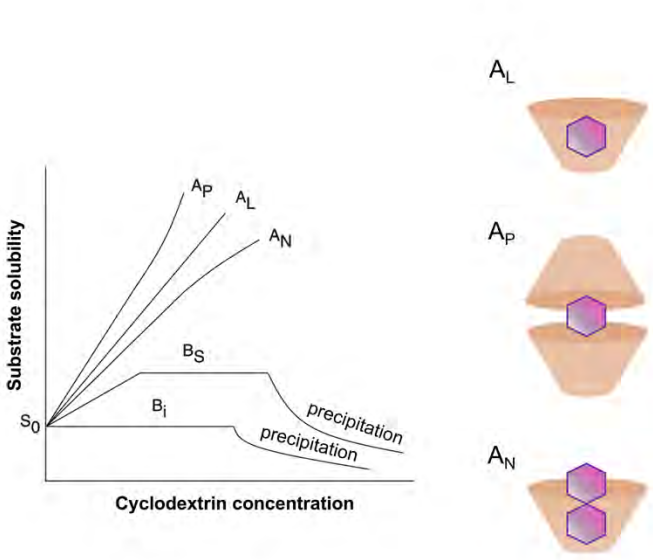

Figure I-15. Phase solubility diagram and inclusion complexes types. *These diagrams are essential for interpreting the nature of the inclusion complexes. Type A diagrams display a positive correlation between the solubility of the substrate and the concentration of cyclodextrin. As the concentration of the cyclodextrin increases, the substrate solubility also increases. In contrast, type B diagrams eventually reach a point where the substrate no longer dissolves despite the increase in cyclodextrin, resulting in the precipitation of the inclusion complex. Type A diagrams, allow for substrate linkage to one cyclodextrin (A_L), two cyclodextrins (A_P), or even one cyclodextrin linking two substrates (A_N). — Modified figures from Loftsson et al. (2005) (245).*

1.3.3. Cyclodextrin properties for the pharmaceutical industry

CDs display intrinsic properties that reinforce their application in the pharmaceutical industry. It has been shown that these macromolecules have low toxicity in biological systems, which provides them with high biocompatibility (245, 249, 279, 280). Indeed, native CDs are recognized by the FDA as "Generally Regarded as Safe" (GRAS), making them suitable for pharmaceutical, cosmetic, or food applications (281). When administered orally, they are not absorbed by the gut but they are metabolized by gut microbiota (244). Additionally, some studies have shown that even γ-CDs can be administered parenterally. However, that is not the case of β-CDs, since they cause renal toxicity (244, 249). Therefore, the data safety of CDs must be carefully managed, as the toxicity depends on the type of CD

used, whether it is a native or derivative CD, and on the route of administration (244, 249, 281, 282).

Furthermore, due to the formation of inclusion complexes, CDs stabilize a large number of drugs, even in extreme pH and temperature conditions, contributing to their versatility as encapsulating agents and allowing for long-term storages (269, 272, 283). Moreover, encapsulated compounds are protected from the degradation that is produced by light exposure or oxidation, thus enhancing their stability and shelf life (284-286). Because of the dynamics of the inclusion complexes provided by K_c, the addition of complexes ([S-CD]) to a new solution ([S] = 0) shifts the equilibrium of the substrate release ([S] + [CD]), which determines the continuous release of the substrate (287). This release, as indicated above, can be controlled and is a clear advantage in drug delivery systems, since many drugs are more effective in low doses and continuous application (265). Interestingly, CDs can be chemically modified to improve their water solubility, increase the size of their cavity, or form complex structures to remove toxic compounds from aqueous solutions (255, 263, 280). For instance, these properties have given rise to various studies that have achieved the encapsulation of bioactive flavonols, essential oils, or antimicrobial agents (247, 253, 278, 288). Finally, CDs have allowed for the complexation of drugs with antitumoral or anti-inflammatory effects for the development of new therapies, which have been translated into in vivo studies using mice models (289-291).

1.3.4. Oleanolic acid complexation with cyclodextrins

Due to the interest in obtaining OA-enriched by-products from olive oil extraction and in finding efficient microcarriers to improve OA effects, CDs have arisen as interesting candidates for OA complexation. Remarkably, a recent study conducted by Lopez-Miranda et al. (2018) performed an optimization to complex oleanolic and maslinic acids by using native and modified CDs (270). In this line, the complexation constant (K_c) and encapsulation efficiency (EE) were measured to evaluate which CD type had the best performance with OA and MA. Regarding OA, the study revealed that the highest K_c, namely the highest affinity with OA achieved, was for β-, and γ-CDs, followed by their modified homologs HP-β-, and HP-γ-CDs (Table I-2) (270). Interestingly, although β-CD had a higher K_c than

HP-β-CD, the modified CD was able to complex a higher amount of OA than native β-CD (270). This result could be explained by the higher water solubility of HP-β-CD (Table I-2), since there were more HP-β-CD molecules in the aqueous solution, thus complexing more OA molecules (270). This study also determined that the higher the pH in the solution, the higher the complexation carried out by CDs. Unfortunately, high pH can modify OA chemical structure and activity, so the complexation may be carried out with lower pH (270). Additionally, the efficacy of the OA complexation was reinforced by the study of phase solubility diagrams, which indicated that β-, γ-, HP-β-, and HP-γ-CDs formed 1:1 (type A_L) inclusion complexes (270). Given the relevance of this optimization on OA encapsulation, it should be noted that more studies must be carried out to unravel the biological activities behind these OA/CD complexes.

Table I-2. Physicochemical properties of beta and gamma cyclodextrins and 2-hydroxypropyl beta and gamma cyclodextrins. *MW: molecular weight of CD. The hydroxypropyl groups (substituents) are added by reacting with the primary or secondary -OH groups of the cyclodextrin. The aqueous solubility parameter is indicated in pure water at 25ºC. The complexation constant (Kc) for oleanolic acid was determined for the different types of CD used in pure water at 25ºC. — Data obtained from Lopez-Miranda et al. (2018), Saokham et al. (2018), Armstrong et al. (1988), and Jansook et al. (2018) (270, 277, 292, 293).*

CD type	MW (g/mol)	Substituent	Aqueous solubility (mg/mL)	K_c for OA (M^{-1})
β-CD	1135	-H	18.5	825
2-HP-β-CD	1400	$-CH_2$ -CHOH-CH_3	>1200	201
γ-CD	1297	-H	249	4895
2-HP-γ-CD	1576	$-CH_2$ -CHOH-CH_3	800	645

II – JUSTIFICATION

II - JUSTIFICATION

OA, a pentacyclic triterpenoid widely present in plants, represents a bioactive molecule with growing interest due to its multiple valuable effects on human health (4, 11, 12, 47). Among these, the wound-healing properties of OA are the least studied because of the lack of sufficient in vitro and in vivo assays that have approached this aspect (223, 225). Although preliminary positive effects enhancing wound healing have been attributed to OA (223), the need to decipher OA molecular mechanisms related to one of the most critical processes behind healing, cell migration, justifies the search for novel OA molecular targets inside epithelial cells. In this sense, a previous study set the first hypothesis by studying the role of EGFR and MAP kinase pathways triggered by OA during cell migration, in which OA might be interacting with EGFR (126). The results of this thesis will prove that this concept is no longer sustainable.

The healing of an acute wound is of particular significance, since after injury, this highly coordinated process must manage the inflammatory environment produced in the tissue to allow for both the restoration of homeostasis and subsequent integrity of the skin (13, 98, 99, 103). However, if the inflammation does not resolve, the wound does not re-epithelize and turns into a chronic, non-healing wound, thus resulting in the impossibility to close the wound (81, 294-296). Chronic or complex wounds are a serious problem for healthcare systems, as they can take more than six weeks to heal and can persist for months after injury, requiring time-consuming and expensive treatments (297, 298). Although complex wounds appear in the population, independent of age or gender, they are more common in old age (299). Occasionally, these wounds result as complications of chronic diseases, for instance, ulcers from diabetes (81, 300, 301). Indeed, one of the worst consequences of diabetes in the elderly is diabetic foot ulcer, with complications in the healing process that frequently cause the amputation of the limb (302). Apart from this, other causes for non-healing chronic wounds can be either severe infections, hypoxia in the wound bed, or increased levels of inflammatory mediators (294). For these reasons, the search for new alternative treatments must

be a priority to solve this problem. The application of OA to the wound may be one of the solutions.

Besides a future clinical approach to the use of OA on wounds, OA could be also conceived as a cosmetic agent in healthy skin. The skin is usually affected by pollutants, oxidative stress, light exposure, and mostly, aging (303). Therefore, the research on OA effects and its application improvement could be very profitable for its use on healthy skin, to improve its moisturizing, maintain its integrity, elongate its firmness, and prevent wrinkles. Hence, it is pertinent to focus on the potential of OA to repair and recondition human skin, by studying OA's contribution to the cell types that constitute the skin tissue and are its key players during wound healing and repair processes (13, 210, 304, 305).

Regrettably, one of the downsides of OA is its lipophilic nature, a property that hampers its application in hydrophilic contexts, such as in vitro cell culturing (16, 126, 225). For this reason, OA needs to be delivered with dimethyl sulfoxide (DMSO) to aqueous solutions, an organic solvent with mild cytotoxic effects that compromise cell viability (306, 307). In addition, meticulous management of the OA/DMSO formulation is required, as OA can precipitate and crystalize, making it difficult to handle, and losing any positive effects on the cells (126). As a result, the development of a new formulation is required to improve OA handling, applicability, and bioavailability. To address all these issues, cyclodextrins (CDs) emerge as suitable candidates to deliver OA, as it has been shown that OA can be complexed with either native or modified cyclodextrins (244, 253, 270, 283). Remarkably, complexation with cyclodextrins could provide OA with a slow-release dynamic that might be positive for its bioavailability in vitro, since this molecule has a limited concentration range of beneficial effects on cell culture. Unfortunately, OA complexation with CDs is performed on water solutions, which are not compatible with in vitro applicability. Therefore, additional steps after OA complexation with CDs must be considered to make a suitable formulation for in vitro cell culture, these steps are dehydration methods (254, 255, 308). This improvement in formulation is particularly significant, because it could allow future OA long-term preservation, as well as an improved handling for its topical administration for wound healing.

III – OBJECTIVES

III - OBJECTIVES

The research carried out in this doctoral thesis revolves around the potentiality of oleanolic acid as a wound healing agent. Therefore, in approaching the goal, the research has been divided into three main areas of work, each of them with their specific objectives:

I. To elucidate of the mechanism of action of oleanolic acid underlying the enhancement of cell migration using epithelial cell lines Mv1Lu and MDA-MB-231:
   - To analyze c-Jun subcellular localization and actin cytoskeleton structure under OA treatment in cell front migration assays.
   - To analyze the focal adhesion regulatory proteins paxillin and FAK during OA-induced cell migration.
   - To study the effects of OA on EGFR, MAP kinases and c-Jun.

II. To study the effects of oleanolic acid in endothelial cell C-HUVEC model and hyperglycemia affected GD-HUVEC model:
   - To study the effects of OA in adhesion molecule expression under a pro-inflammatory stimulus.
   - To study the effects of OA in monocyte-endothelial cell interaction under a pro-inflammatory stimulus.
   - To conduct Matrigel tube formation assays for the study of angiogenic features under OA treatment.
   - To test the effects of OA on cell migration and focal adhesions.

III. To improve oleanolic acid in vitro application with modified cyclodextrins:
   - To use complexation of OA in modified cyclodextrins HP-β-CD and HP-γ-CD, dehydration of the complexes.

- To measure the stability of OA in the dehydrated complexes.
- To test OA/cyclodextrin complexes on Mv1Lu and MDA-MB-231 to measure cell viability.
- To test OA/cyclodextrin complexes on Mv1Lu and MDA-MB-231 to measure their activity on cell migration and c-Jun.
- To quantify focal adhesion structures in Mv1Lu and MDA-MB-231 under OA/cyclodextrin complexes treatment.
- To study EGFR, MAP kinases, and c-Jun contribution in Mv1Lu and MDA-MB-231 under OA/cyclodextrin complexes treatment.

IV – COMPENDIUM OF SCIENTIFIC ARTICLES

IV -COMPENDIUM OF SCIENTIFIC ARTICLES

4.1. ARTICLE 1: OLEANOLIC ACID STIMULATION OF CELL MIGRATION INVOLVES A BIPHASIC SIGNALING MECHANISM

Stelling-Férez J, Gabaldón JA, Nicolás FJ. (2022) **Oleanolic acid stimulation of cell migration involves a biphasic signaling mechanism.** *Scientific Reports*, 5;12(1):15065. PMID: 36064555 doi: 10.1038/s41598-022-17553-w

scientific reports

Check for updates

OPEN

Oleanolic acid stimulation of cell migration involves a biphasic signaling mechanism

Javier Stelling-Férez[1,2], José Antonio Gabaldón[1] & Francisco José Nicolás[2]✉

Cell migration is a critical process for wound healing, a physiological phenomenon needed for proper skin restoration after injury. Wound healing can be compromised under pathological conditions. Natural bioactive terpenoids have shown promising therapeutic properties in wound healing. Oleanolic acid (OA), a triterpenoid, enhances in vitro and in vivo cell migration. However, the underlying signaling mechanisms and pathways triggered by OA are poorly understood. We have previously shown that OA activates epidermal growth factor receptor (EGFR) and downstream effectors such as mitogen-activated protein (MAP) kinase cascade and c-Jun N-terminal kinase (JNK), leading to c-Jun transcription factor phosphorylation, all of which are involved in migration. We performed protein expression or migration front protein subcellular localization assays, which showed that OA induces c-Jun activation and its nuclear translocation, which precisely overlaps at wound-edge cells. Furthermore, c-Jun phosphorylation was independent of EGFR activation. Additionally, OA promoted actin cytoskeleton and focal adhesion (FA) dynamization. In fact, OA induced the recruitment of regulator proteins to FAs to dynamize these structures during migration. Moreover, OA changed paxillin distribution and activated focal adhesion kinase (FAK) at focal adhesions (FAs). The molecular implications of these observations are discussed.

Wound healing is a physiological phenomenon that involves different cell types, which mainly carry out proliferation, differentiation and migration. These processes are tightly regulated for proper wound closure and skin barrier restoration. Taking this into account, wound healing is a process that is often compromised under pathological conditions associated with aging and illness, thus resulting in an incomplete wound closure, and frequently turning into a chronic wound[1]. Therefore, the search for active natural compounds capable of enhancing cell migration, and consequently wound healing, must be considered an alternative interesting option to solve this problem. Oleanolic acid (OA), a natural triterpenoid found in a large number of plants[2], is known for its beneficial properties in wound healing: it accelerates wound healing with better aesthetic results[3], it increases the tensile strength of wounds[4], and it also has ulcer healing properties[4–7]. Recently, several authors have reported a negative effect of OA on cell migration[8–11], see "Discussion" for further details. Nevertheless, we and others have shown that OA is able to promote cell migration in Mv1Lu and MDA-MB-231 cell lines[12] and in mouse fibroblasts[6]. However, the molecular mechanisms behind this process are not yet fully understood.

Cell migration is important during wound closure to reshape the skin epithelium and restore its integrity[13,14]. Cell migration is the cells' response to a variety of cytokines and other molecular messengers through proteins responsible for integrating these signals: mitogen-activated protein (MAP) kinases[14]. Recently, Bernabé et al.[12] showed that OA triggers different cell-migration-related molecular mechanisms by using Mv1Lu and MDA-MB-231 cells. Thus, in both mentioned cell lines, OA induces the activation of extracellular signal-regulated kinases (ERK1/2) and c-Jun N-terminal kinases (JNK1/2), with c-Jun overexpression and activation by phosphorylation as a consequence[12]. JNK[15,16] and MAP kinase /ERK kinase, kinase 1[17,18], have been shown to be essential for cell migration. Indeed, MEK1 (ERK1/2 kinase) and JNK1/2 specific inhibitors prevent OA-stimulated cell migration in both Mv1Lu and MDA-MB-231 cells[12]. On the other hand, OA also stimulates Epidermal growth factor receptor (EGFR) phosphorylation in a protein-synthesis independent fashion[12] in MDA-MB-231 cells. Actually, in this later cell line, specific inhibition of EGFR by PD153035 produces a severe halt of OA-stimulated cell migration and so does an EGFR blocking antibody[12]. Moreover, OA treatment causes the cell internalization of EGFR similarly to its ligand, EGF[12].

[1]Department of Nutrition and Food Technology, Health Sciences PhD Program, Universidad Católica de Murcia (UCAM), Campus de los Jerónimos nº135, Guadalupe, 30107 Murcia, Spain. [2]Regeneration, Molecular Oncology and TGF-ß, Instituto Murciano de Investigación Biosanitaria (IMIB)-Arrixaca, Hospital Clínico Universitario Virgen de la Arrixaca, El Palmar, Murcia, Spain. ✉email: franciscoj.nicolas2@carm.es

Cell migration[13,14] is a very well-coordinated process that requires a directional organized movement of cells[19]. Besides the rapid change of actin filaments[20], the formation and disassembly of cell adhesion sites are required[21,22]. Therefore, it is observed in actively migrating cells at the leading edge of epithelia[19]. Cytoskeleton and focal adhesions (FAs) are integrated into a dynamic machinery in continuous change, with many actin-cytoskeleton interacting proteins involved[20,22,23]. One of them is paxillin, a cytosolic adaptor protein that coordinates the process[24] and binds to other proteins that constitute FAs[25]. FAs are macromolecular complexes which interact with the extracellular matrix (ECM) through integrins[26]. FAs integrate multiple regulation pathways, detecting mechanical signals that allow cells to migrate[27]. In these multiprotein complexes, paxillin is essential to integrate all these signals and is found bound to regulatory kinases that are necessary to manage actin dynamics. Paxillin Ser 178 is phosphorylated by c-Jun N-terminal kinase (JNK) and this residue is critical for paxillin regulation of cell migration[28].

Focal adhesion kinase (FAK) is another important paxillin regulator. FAK is a non-receptor tyrosine kinase combining both integrin and growth-factor signals on cell migration[29], and it plays a key role in cell migration dynamics[22,30–33]. FAK operates as the cell master controller for FAs remodeling at the migration leading edge, consequently driving directional cell movement[22,34]. There is evidence that FAK stimulation occurs when growth factors bind to tyrosine kinase receptors, especially EGFR[35]. Indeed, activation of EGFR has been linked to phosphorylation of different residues at FAK with the phosphorylation of Tyr 925 as the final consequence[35]. FAK Tyr 925 phosphorylation is critical for its activating function, and it is induced by cell integrin assembling and growth factor stimulation[31,36]. FAK also modulates focal adhesion assembly and disassembly by the phosphorylation of different proteins, including paxillin[22,33,37].

In this paper, we narrowed down the molecular and subcellular events that happen in the cell in the presence of OA. By using differential time read-out and specific inhibitors, we came across a complex and interesting molecular mechanism, involving EGFR and possibly receptors lacking intrinsic tyrosine-kinase activity. We also studied the effect of OA on cytoskeleton reorganization and focal adhesion dynamics at the wound-edge of the healing scratch.

Results

Oleanolic acid over-expresses c-Jun and promotes its activation at the wound edge during migration. C-Jun is overexpressed in response to OA stimulation[12] in non-malignant mink lung epithelial cells, Mv1Lu. This cell line is recognized as a good epithelial model for the study of cell motility due to its ability to migrate and also to stop proliferation when the cells reach confluence[38–40]. Mv1Lu cells were stimulated with OA during a wound healing scratch assay. The evolution of the migration front was monitored and the expression of c-Jun was studied by immunostaining. The advantage of this approach is to directly study proteins involved in OA enhanced migration, focusing on its topographic and subcellular localization along the wound edge. The presence of OA produced a neat overexpression of c-Jun at the wound edge, which was significantly high after 6 h (Fig. 1a; Supplemental Fig. 1a).

Also, upon OA treatment (6 h), levels of phospho-c-Jun, regarded as phospho-Ser 63, were significantly high at the wound edge (Fig. 1b; Supplemental Fig. 1b). Remarkably, c-Jun and p-c-Jun overexpression occurred at the nucleus of actively migrating cells. Although c-Jun and p-c-Jun levels were enhanced at the migration edge of Mv1Lu, there was a clear decrease in the c-Jun protein expression and its active form as cells were further away from the wound edge. The visualization of actin, by using phalloidin staining (Supplemental Fig. 2), revealed critical changes in the intensity of the cytoskeleton, which were very evident after OA stimulation.

All these data suggest that the effect of OA is especially powerful at wound-edge cells, activating and overexpressing c-Jun protein there, which correlates well with the improvement of cell migration exhibited by OA[12].

Activation of different OA targets exhibits different timing. Previously, it has been shown that OA produces an activation of EGFR in MDA-MB-231 cells that is independent of protein translation[12]. MDA-MB-231 cells are a good model for cell migration[41–43] and exhibit a good expression of EGFR[44]. Indeed, EGFR inhibitor (EGFRi), PD153035, was capable of completely reducing OA-stimulated migration of MDA-MB-231 (Fig. 2a,b)[12]. It is important to measure the effect of OA at the protein signaling level. By using sub-confluent cells, we can interpret what the effect of OA might be on the wound edge[12,45]. To gain further knowledge of the activation of EGFR by OA and its involvement in the activation of previously described protein targets[12], we conducted an OA-induction and monitored it at different times. Immediately after stimulation with OA (1 h), the activation by phosphorylation of JNK1/2 and c-Jun was detected together with the total level increase of both proteins (Fig. 2c,d). Strikingly, when looking at EGFR, we could detect its OA activation at three hours, but no sign of activation was seen at earlier time points. So, compared with c-Jun or JNK1/2, activation of EGFR showed a delayed stimulation by OA (Fig. 2c,d). Moreover, c-Jun phosphorylation experienced a further increase at three hours, which may suggest a double response and different phosphorylation dynamics for both proteins, c-Jun and EGFR. Coherently with this, the activation of JNK kinase seemed to be also biphasic, showing an early activation and a later (6 h) higher activation.

Activation of EGFR has been linked to phosphorylation of different residues at the Focal Adhesion Kinase (FAK), which leads to the Tyr 925 phosphorylation[35]. Tyr 925 phosphorylation of FAK is a key event on the management of cell migration[46]. Interestingly, OA produced the phosphorylation of FAK with a time dynamic parallel to the phosphorylation of EGFR (Fig. 2c,d).

Altogether, these results suggest that OA stimulates different targets to activate several key elements related to cell migration showing a clear time-uncoupling for different proteins.

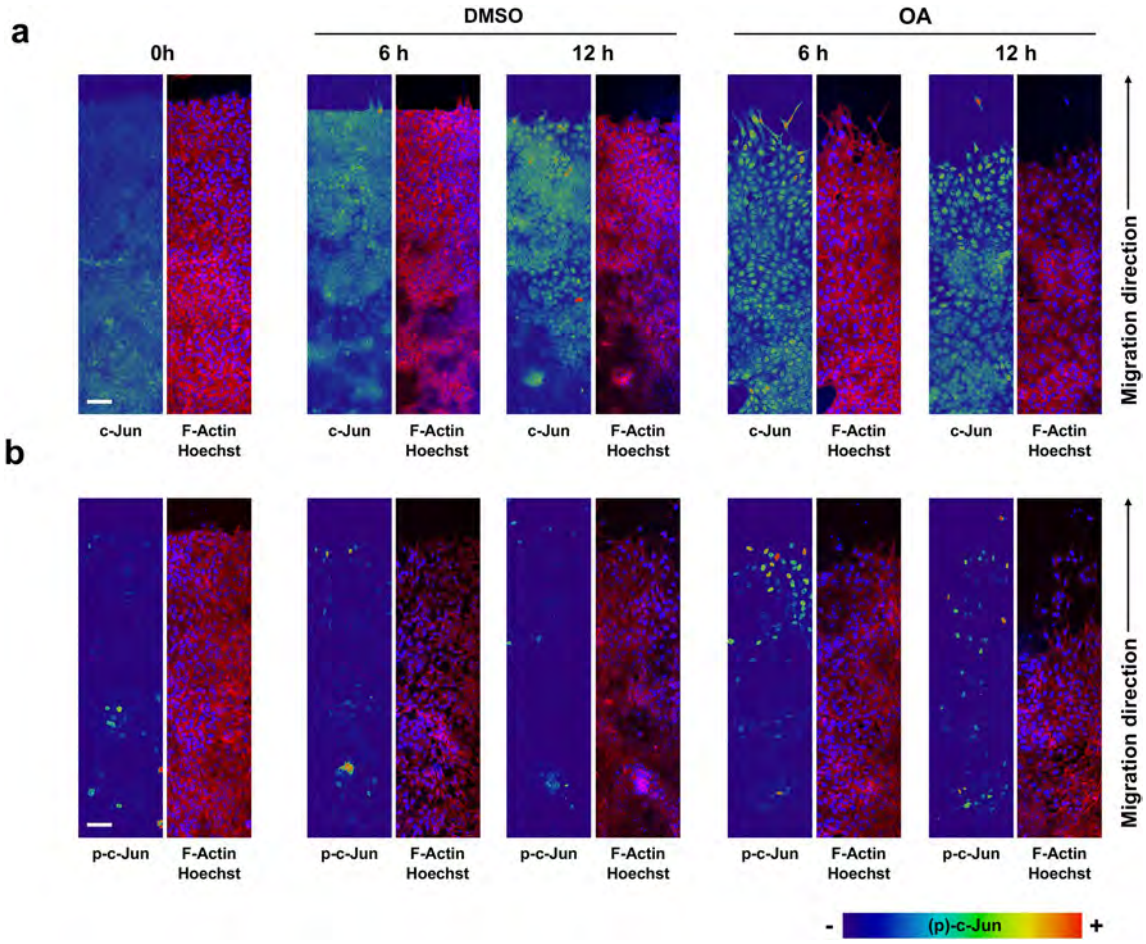

Figure 1. Oleanolic acid induces the expression of c-Jun and promotes its phosphorylation at the edge of wound-scratched Mv1Lu cells. Confluent Mv1Lu cells were scratched and allowed to migrate for the indicated times. Cells were treated with 5 μM OA or DMSO equivalent volume (control). Cells were immunostained with specific antibodies against c-Jun (**a**) and its active phosphorylated form, p-c-Jun (**b**). Co-staining with phalloidin and Hoechst-33258 was used to show actin cytoskeleton and nuclei, respectively. Images of c-Jun/p-c-Jun fluorescence were converted into pseudo-color with ImageJ software to show the intensity of c-Jun staining. Color rainbow scale represents fluorescence intensity for either c-Jun or phospho-c-Jun. Actin fibers (F-actin): red. Nuclei: blue. Images were obtained with a confocal microscope. This experiment was repeated at least three times. Representative images are shown. Scale bar indicates 50 μm.

Uncoupled timing activation of c-Jun and EGFR can also be seen in Mv1Lu cells. Mv1Lu cells were also stimulated to migrate by OA[12]. Moreover, Mv1Lu OA stimulated migration was severely inhibited by EGFRi (Fig. 3a,b)[12]. A time course experiment was conducted to investigate the sequence of events. In this case, and similarly to MDA-MB-231 cells, we observed an early (1 h) c-Jun phosphorylation and total protein level increase compared with a later activation of EGFR (2 h) (Fig. 3c,d). Likewise, JNK1/2 phosphorylation could be detected 1 h after OA activation, being enhanced from 2 h onwards. In a similar trend, we could observe that ERK was phosphorylated by OA not earlier than 2 h following the same dynamics than EGFR phosphorylation, and therefore suggesting that ERK OA activation could be dependent on EGFR OA activation.

These data support the evidence that, upon OA treatment, c-Jun is activated before EGFR, thus suggesting a primary induction triggered by OA on this transcription factor through an alternative pathway different from the one activating EGFR. Also, these data, together with MDA-MB-231 data, support the possibility that, at least, two independent OA stimulated pathways converge on the activation of c-Jun and therefore are involved in OA-stimulated cell migration.

The use of specific inhibitors against EGFR, MEK and JNK confirms an EGFR independent OA-induced pathway in MDA-MB-231 cells. The study of OA-activation of different proteins showed time uncoupling between c-Jun phosphorylation and EGFR activation. To assess whether there was an effective independence of both phenomena, cells were stimulated with OA in the presence of a specific inhibitor for EGFR, PD153035 (EGFRi). Although EGFRi importantly reduced OA-stimulated phosphorylation of EGFR, a minute effect was perceived on c-Jun phosphorylation or JNK1/2 phosphorylation. However, the presence of JNK1/2 inhibitor SP600125 (JNKi) caused a drastic negative effect on c-Jun phosphorylation (Fig. 4a,b). When

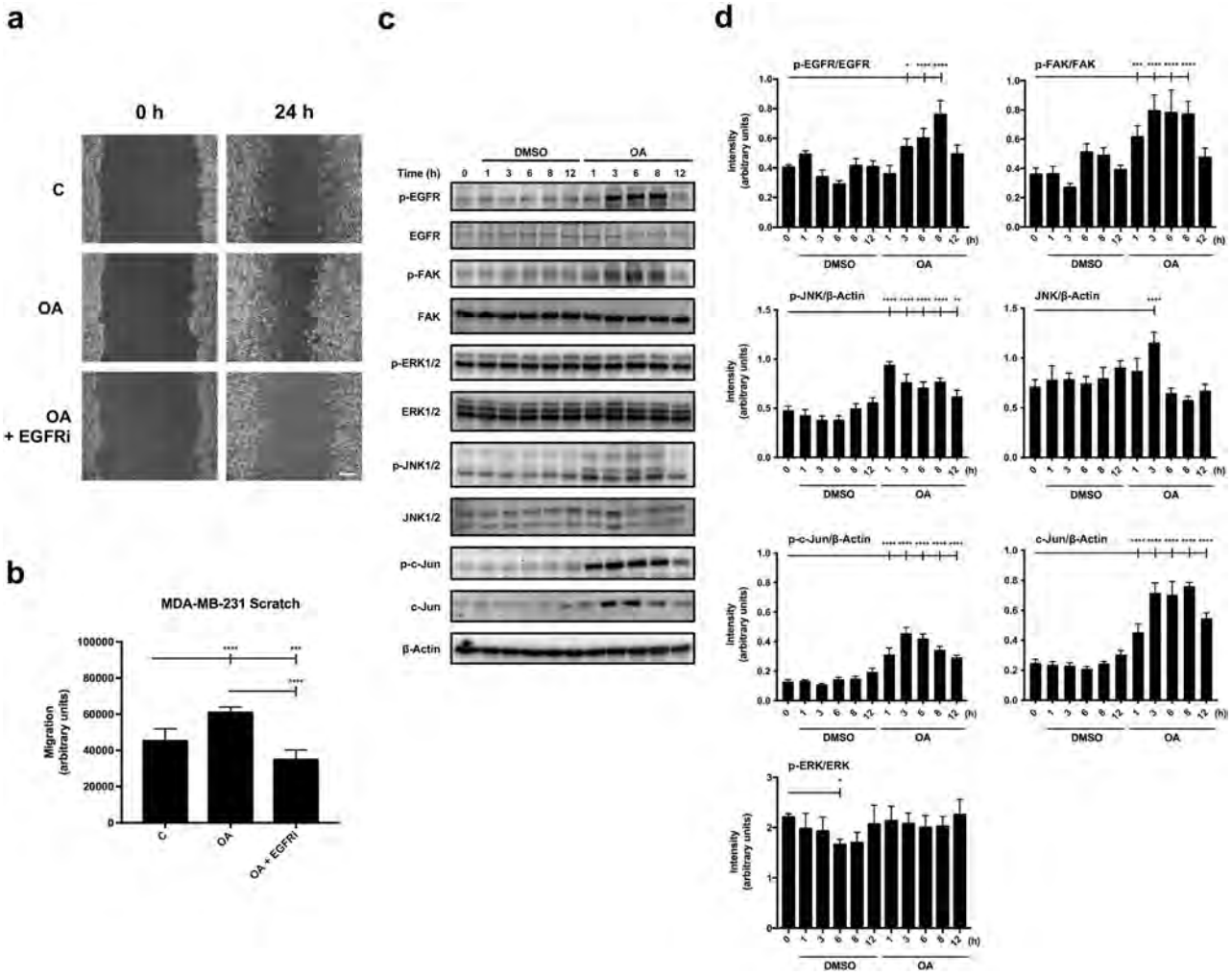

Figure 2. C-Jun and EGFR OA activation, necessary for OA-cell migration, are decoupled in MDA-MB-231 cells. (**a**) The figure shows representative images of cell migration obtained under control conditions compared to those with 10 μM OA and OA plus 2,5 μM EGFRi after 24 h treatment. Scale bar 200 μm. (**b**) Plot represents cell migration as the difference obtained between the quantified areas at time 0 h and time 24 h in each condition. Asterisks indicate statistically significant differences between the selected conditions according to a one-way ANOVA statistical analysis: (*$p < 0.05$, **$p < 0.005$, ***$p < 0.001$ and ****$p < 0.0001$). (**c**) Total protein extracts from serum-starved sub-confluent MDA-MB-231 cells treated with 10 μM OA, EGF or DMSO equivalent volume as vehicle control. Different proteins were assayed at the indicated times (h) targeting phospho-FAK (Tyr 925), phospho-EGFR (Tyr 1068), phospho-ERK1/2 (Thr 202/Tyr 204), phospho-JNK1/2 (Thr 183/Tyr 185), phospho-c-Jun (Ser 63). Additionally, total protein expression was assayed: EGFR, FAK, ERK1/2, JNK1/2 and c-Jun. β-Actin was used as a loading control. A representative experiment is shown. (**d**) Plots with intensity values of each protein assayed by Western-blot, by gathering the data of three independent experiments. Intensity values were quantified and collected by ImageJ software. Asterisks indicate statistically significant differences between the selected conditions according to a one-way ANOVA statistical analysis: (*$p < 0.05$, **$p < 0.005$, ***$p < 0.001$ and ****$p < 0.0001$).

the phosphorylation of FAK was measured in these conditions, the clear activation by OA was inhibited by the presence of EGFRi, drastically reducing the phosphorylation of FAK. The use of PD98059, a MAPK inhibitor (MEKi), produced a clear abrogation of both c-Jun and FAK phosphorylation (Fig. 4a,b). All these data suggest a complex and intricate signaling network that is interconnected to activate several proteins in response to OA. Nevertheless, a clear independence of c-Jun phosphorylation could be seen in the activation of EGFR phosphorylation upon OA stimulation, while FAK activation was dependent on EGFR activity.

We wanted to assess the effect of the different inhibitors previously used on the activation of the same proteins upon OA stimulation at Mv1Lu cells. In this scenario, the stimulation with OA produced a late activation of ERK that was inhibited with EGFRi or MEKi but not with JNKi. The activation of c-Jun, however, was not prevented by EGFRi (Supplemental Fig. 3a,b). The activation (phosphorylation) of c-Jun after OA stimulation overlapped with migrating cells at the wound-healing scratch assay front (Fig. 5a,b). Strikingly, both JNKi and MEKi prevented the phosphorylation of c-Jun. On the other hand, the presence of EGFRi enabled the activation

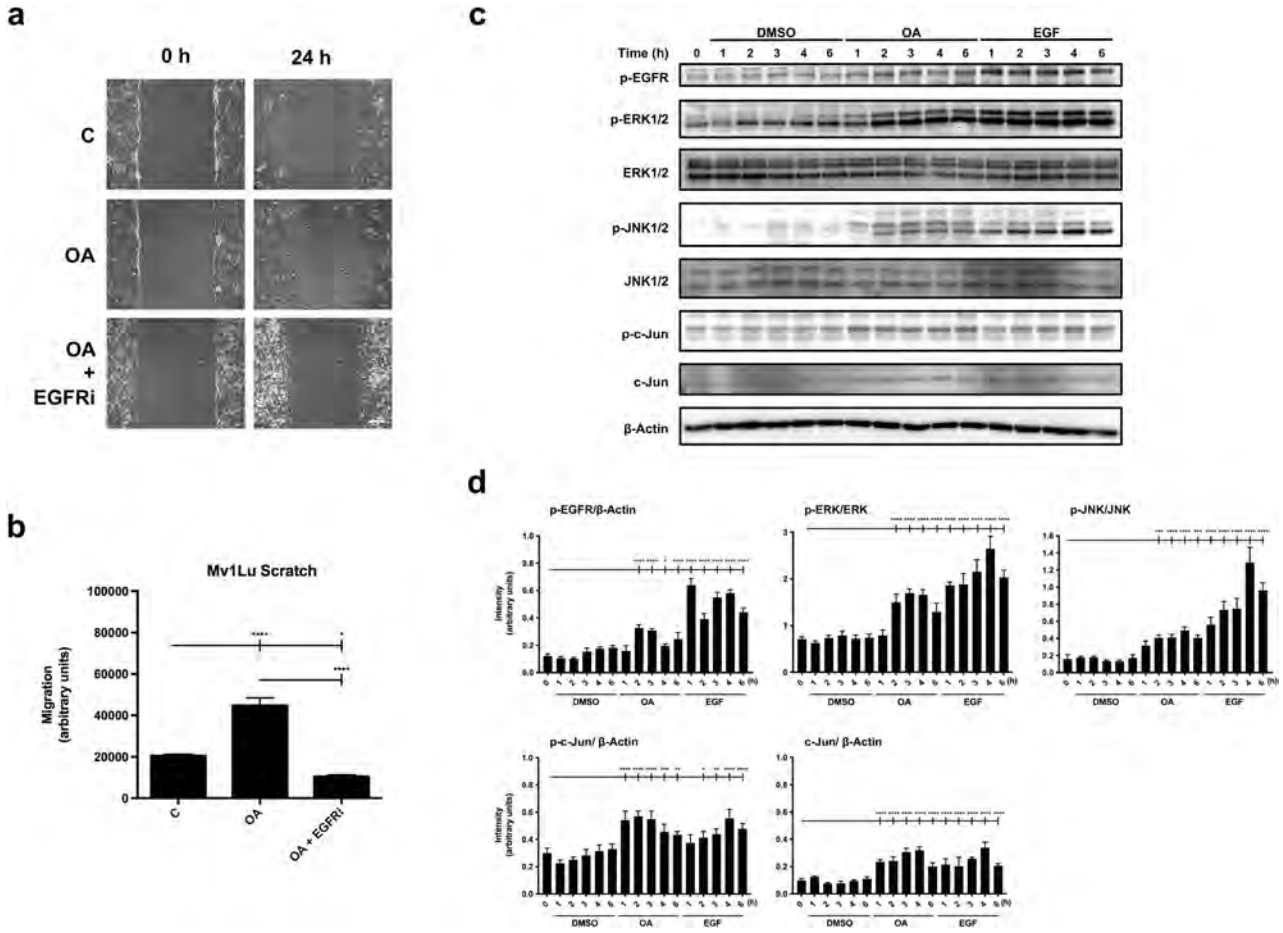

Figure 3. C-Jun and EGFR OA activation, necessary for OA-cell migration, are decoupled in Mv1Lu cells. (**a**) The figure shows representative images of cell migration obtained under control conditions compared to those with 5 µM OA and OA plus 2,5 µM EGFRi after 24 h treatment. Scale bar 200 µm. (**b**) Plot represents cell migration as the difference obtained between the quantified areas at time 0 h and time 24 h in each condition. Asterisks indicate statistically significant differences between the selected conditions according to a one-way ANOVA statistical analysis: (*$p < 0.05$, **$p < 0.005$, ***$p < 0.001$ and ****$p < 0.0001$). (**c**) Total protein extracts from serum-starved sub-confluent Mv1Lu cells treated with 5 µM OA, EGF or DMSO equivalent volume as vehicle control. Different protein phosphorylation was assayed at the indicated times (h) targeting phospho-EGFR (Tyr 1068), phospho-ERK1/2 (Thr 202/Tyr 204), phospho-JNK1/2 (Thr 183/Tyr 185) and phospho-c-Jun (Ser 63). Additionally, total protein expression was assayed: ERK1/2, JNK1/2 and c-Jun. β-Actin was used as a loading control. A representative experiment is shown. (**d**) Plots with intensity values of each protein assayed by Western-blot, by gathering the data of three independent experiments. Asterisks indicate statistically significant differences between the selected conditions according to a one-way ANOVA statistical analysis: (*$p < 0.05$, **$p < 0.005$, ***$p < 0.001$ and ****$p < 0.0001$).

of c-Jun further supporting the fact that c-Jun activation by OA was not dependent on EGFR activation. All these data reinforced the notion that the activation of c-Jun by OA in different cell lines has, at least, two distinct non-related mechanisms, one of which does not require EGFR activation.

OA promotes changes in actin fibers and paxillin distribution. In cell migration, actin protein is essential for building a suitable dynamic architecture that allows cells to migrate[23,47,48]. As shown before, actin varies in response to OA in the migrating cells (see Supplemental Fig. 2). Actin interacts, among others, with paxillin, which is an adaptor protein, playing a role in cytoskeleton anchoring to focal adhesion (FA) and its remodeling during cell migration[24,27,37,49]. One of the consequences of OA stimulation was the phosphorylation of paxillin at Ser 178 (Supplemental Fig. 4a,b). JNK regulates cell migration through the phosphorylation of paxillin at Ser 178[50], and indeed JNK is activated in response to OA (see Fig. 2c,d). Both phosphorylation of JNK and phosphorylation of paxillin were coincidental in time, thus suggesting a correlation between both phenomena and the activation by OA.

To further understand the effect of OA on cell migration, we immunostained paxillin in wound-healing scratched Mv1Lu cells. When immediately-scratched cells were observed, paxillin was distributed as compacted focal adhesions (Fig. 6). As soon as 6 h after stimulation with OA, paxillin staining pattern changed to display smaller FA and denser distribution. This was especially noticeable at places where the cells were forming

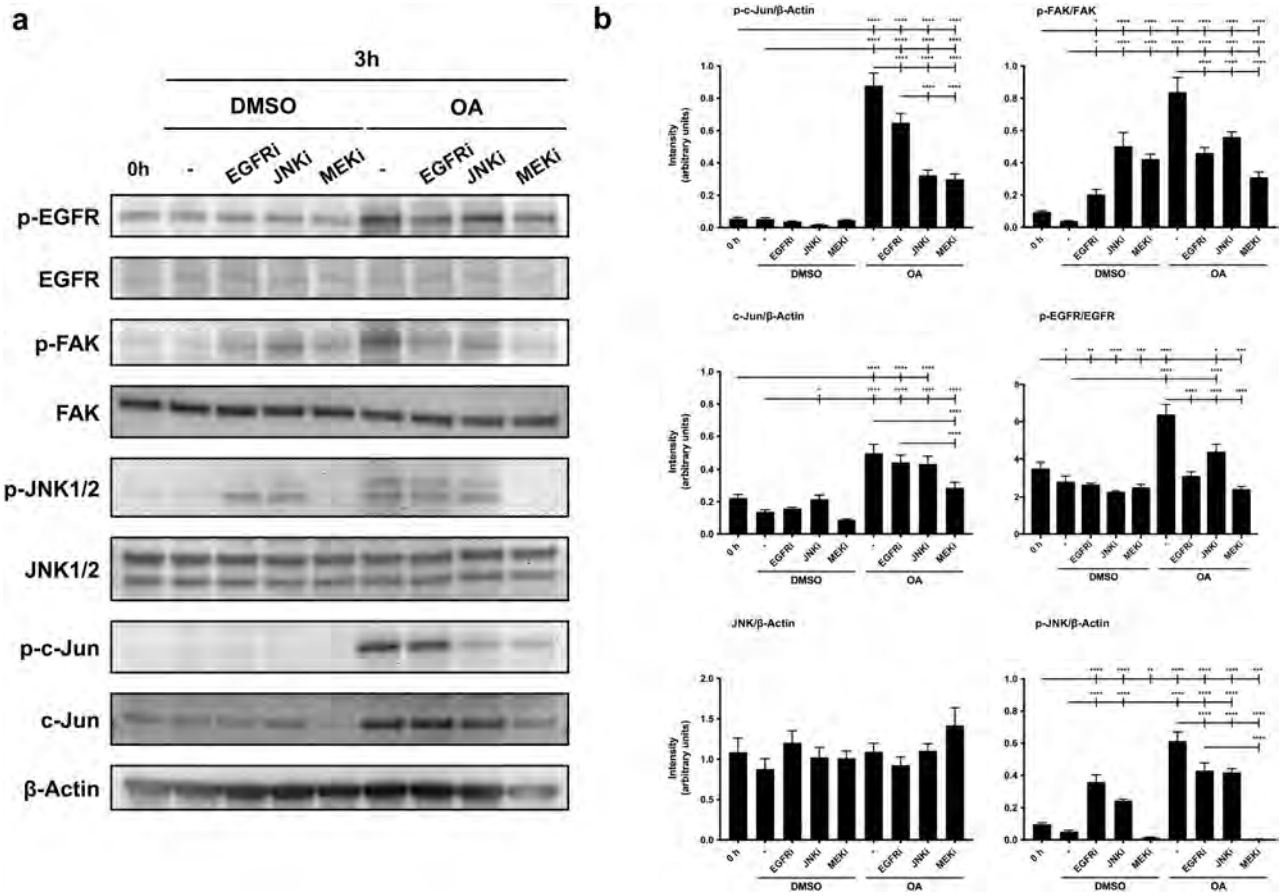

Figure 4. The use of specific inhibitors against EGFR, MEK and JNK upon OA treatment reveals a new OA-induced pathway in MDA-MB-231 cells. (**a**) Total protein extracts from serum-starved sub-confluent MDA-MB-231 cells, treated with 10 μM OA, EGF or DMSO. Besides, cells were treated 30 min before with the following inhibitors in the absence or presence of OA: 2.5 μM EGFRi, 50 μM MEKi and 15 μM JNKi. Different proteins' phosphorylation was assayed at the indicated times (h): phospho-FAK (Tyr 925), phospho-EGFR (Tyr 1068), phospho-ERK1/2 (Thr 202/Tyr 204), phospho-JNK1/2 (Thr 183/Tyr 185) and phospho-c-Jun (Ser 63). Additionally, total protein expression was assayed: EGFR, FAK, JNK1/2 and c-Jun. β-Actin was used as a loading control. A representative experiment is shown. (**b**) Plots with intensity values of each protein assayed by Western-blot, by gathering the data of three independent experiments. Intensity values were quantified and collected by ImageJ software. Asterisks indicate statistically significant differences between the selected conditions according to a one-way ANOVA statistical analysis: (*$p < 0.05$, **$p < 0.005$, ***$p < 0.001$ and ****$p < 0.0001$).

lamellipodia or filopodia (Fig. 6; Supplemental Fig. 5). Again, as seen before (see Supplemental Fig. 1), changes in actin intensity were very evident 6 h after OA stimulation (Fig. 6; Supplemental Fig. 5), became more apparent after 12 h after OA treatment. This correlated well with the fact that OA enhances cell migration[12]. All these observations suggest that OA produces high dynamization of cytoskeleton and FA compatible with a higher migration rate.

In a previous publication, we showed that EGFRi, JNKi or MEKi had an inhibitory effect on OA-stimulated cell migration[12]. To further comprehend the consequences of using these inhibitors, we studied the subcellular actin architecture of the cells upon OA stimulation in the presence of these inhibitors. Both OA and EGF produced clear changes in cell architecture losing actin stress fibers, which were still evident with JNKi and MEKi but not with EGFRi (Supplemental Fig. 6a). Concerning FAs, the use of MEKi and EGFRi decreased their density and increased their size, although the effect of EGFRi was milder size-wise (Supplemental Fig. 6b,c). In contrast, in response to OA, neither the size nor the density of FA seemed to be affected by the presence of JNKi.

OA treatment produces FAK activation and promotes focal adhesion remodeling in scratched Mv1Lu cells. Analyses of various FAK mutants have revealed that FAK targeting to FA is important in the regulation of its activity[51]. Previously, we showed that OA produced an activation of FAK at residue Tyr 925 (see Figs. 2, 4) in MDA-MB-231 cells. Western blot results in Mv1Lu cells confirmed that OA caused a strong FAK phosphorylation on Tyr 925, similarly to EGF, but at a different timing (Fig. 7a). Thus, we decided to study the OA effect on phospho-Tyr 925 FAK subcellular localization at wound-edge migrating cells. As a consequence of wounding, in control cells, we observed a p-FAK sharp and pointed pattern located at FA 6 h after wound scratch

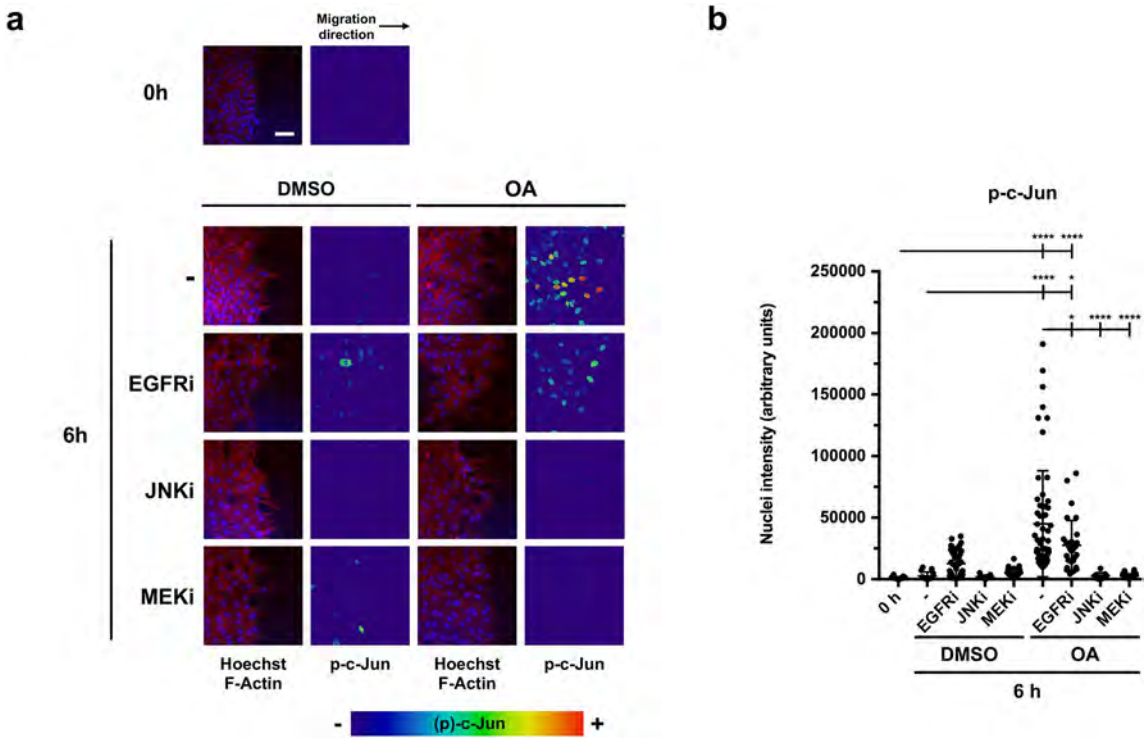

Figure 5. Specific inhibitors against EGFR, MEK and JNK, upon OA treatment, show the independent OA-activation on c-Jun at the edge of wound-scratched Mv1Lu cells at wound edge. (**a**) Confluent Mv1Lu cells were scratched and allowed to migrate for 6 h. Cells treated with 5 μM OA or DMSO equivalent volume were immunostained with specific antibodies against c-Jun transcription factor. Additionally, cells were treated 30 min before with the following inhibitors: 2.5 μM EGFRi, 50 μM MEKi and 15 μM JNKi. Co-staining with phalloidin and Hoechst-33258 was used to show actin cytoskeleton and nuclei, respectively. Images of p-c-Jun fluorescence were converted into pseudo-color with ImageJ software to show the intensity of c-Jun staining. Color rainbow scale represents fluorescence intensity for phospho-c-Jun. Actin fibers (F-actin): red. Nuclei: blue. Images were obtained with a confocal microscope. This experiment was repeated at least three times. Representative images are shown. Scale bar indicates 10 μm. (**b**) Plot represents the data obtained by p-c-Jun intensity at cell nuclei. In every condition, each point on the plot represents p-c-Jun intensity at the nucleus of one cell, quantified by ImageJ software. With the collected data of p-c-Jun intensity, a one-way ANOVA statistical analysis was performed (*$p < 0.05$, **$p < 0.005$, ***$p < 0.001$ and ****$p < 0.0001$).

(Fig. 7b). Strikingly, upon OA treatment (6 h), the signal increased both at FA and cytosol, thus suggesting the mobilization of the active (phospho-Tyr 925) form of the protein (Fig. 7b). The treatment with EGF produced a similar effect on the increased signal of activated FAK to FA with much less presence to the cytosol. Additionally, the stimulation with OA induced the phosphorylation of paxillin on Ser 178 by JNK (see Supplemental Fig. 4a,b). This phosphorylation supports the association of paxillin with FAK[50]. Strikingly, we noticed a strong merge of p-FAK (Tyr 925) and paxillin in OA-stimulated cells, indicating the localization of active FAK at FAs (Fig. 7c; Supplemental Fig. 7). Pearson´s correlation showed significant values between paxillin and p-FAK (Tyr 925) upon OA treatment that were not noticeable immediately after wounded cells or control (DMSO-treated) cells (Fig. 7d). OA-like results were obtained upon EGF treatment.

Similarly, in MDA-MB-231, we observed that OA produced the phosphorylation of the FAK that was overlapping with the focal structures revealed by paxillin staining. Pearson's correlation of the staining of both proteins confirmed that phospho-Tyr 925 activated FAK was localized at the focal structures upon OA stimulation (Supplemental Fig. 8a–c).

Therefore, all these results suggest that OA treatment induces an activation of FAK that occurs mainly at the FAs.

Effect of inhibitors on the OA activation of FAK. In culture cells, the treatment with OA produced the phosphorylation of FAK at Tyr 925. The use of different inhibitors (EGFRi and MEKi) proved the dependence of this phosphorylation on EGFR and MAPK signaling pathways (see Fig. 4). In fact, the size and the density of FA were affected by EGFRi and MEKi (see Supplemental Fig. 6). To investigate further, we tested the effect of the aforementioned inhibitors on the OA activation of FAK at the wound-edge migrating cells and studied its colocalization with paxillin. Again, the stimulation with OA caused a general phosphorylation at Tyr 925 of FAK, which was evident due to a higher increase in the signal at the FA (Fig. 8a) and its evident colocalization with paxillin (Supplemental Fig. 9). Coherently, this effect was suppressed by the presence of EGFRi and MEKi. However, the presence of JNKi did not affect the activation of FAK measured as localization of phospho-Tyr 925 at the

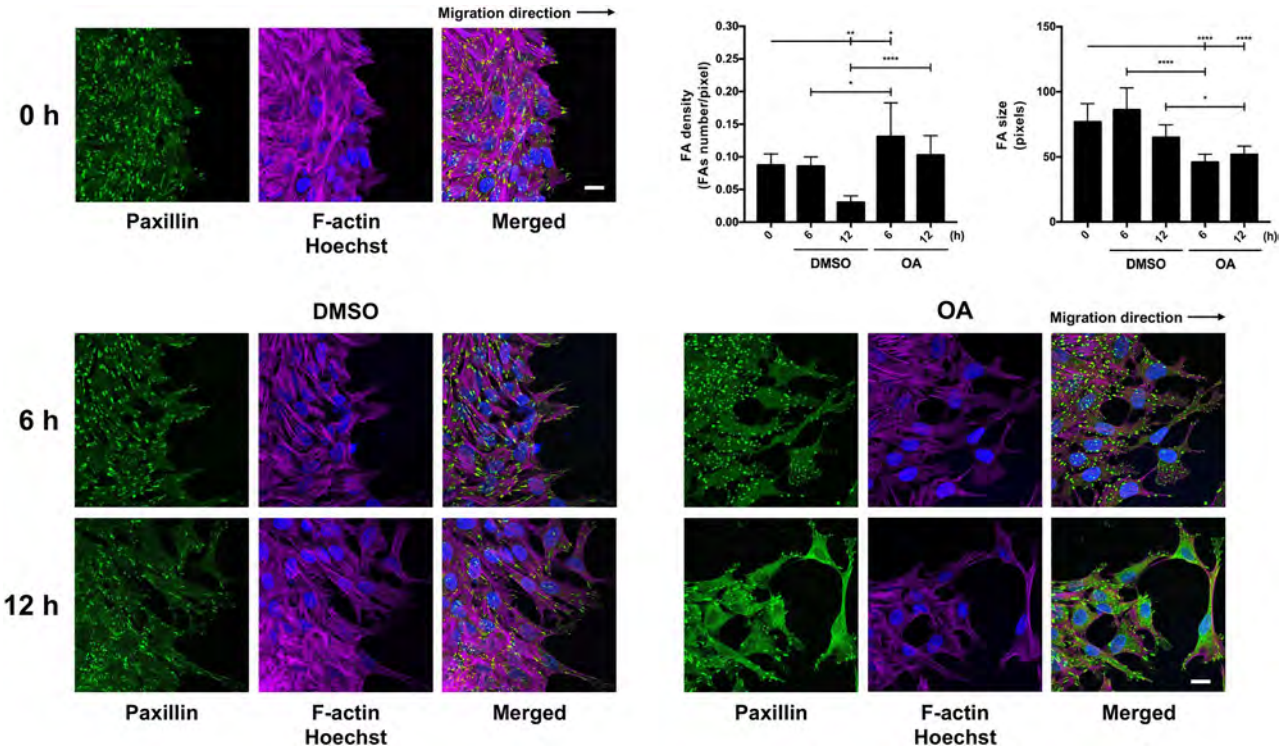

Figure 6. OA promotes changes in FAs and actin cytoskeleton. Confluent Mv1Lu cells were scratched and allowed to migrate for 6 and 12 h. Cells treated with 5 µM OA or DMSO equivalent volume (vehicle control) were immunostained with specific antibodies against paxillin (green). Co-staining with phalloidin and Hoechst-33258 was used to show actin cytoskeleton (magenta) and nuclei (blue), respectively. This experiment was repeated at least three times. Representative images are shown. Scale bar indicates 10 µm. Quantification of the density of FA as FA number per filopodia area. Quantification of FA size (average size) at the filopodia area. One-way ANOVA statistical analysis was performed (*$p < 0.05$, **$p < 0.005$, ***$p < 0.001$ and ****$p < 0.0001$).

FA as well as a general mobilization of it to the cytosol (Fig. 8a). Pearson´s coefficient, calculated for all samples, clearly indicated the localization of active phosphorylated (Tyr 925) FAK at the FA structures in response to OA, independently of the activation of JNK kinase (Fig. 8b).

All these data suggest a clear OA-stimulated FAK-dependent remodeling of FA in which EGFR and MEK, but not JNK, are involved.

Discussion

In this paper, we have disclosed more molecular details of OA mode of action on epithelial cells to produce migration and we have studied in depth the effect of OA on critical components of the cell migration machinery. Regarding OA effect on cell migration, it has been reported to inhibit migration on a laryngeal squamous carcinoma cell line (Hep-2) at 30 µM OA concentration in serum-free medium with an additional negative effect on proliferation[11]. Also, on a hepatocellular carcinoma (HepG2) cell line, concentrations of 25 and 50 µM[10] or 30 µM in the same cell line[9] have a clear migration inhibitory action. Finally, in HeLa cells, 50 µM of OA has a negative effect on migration and induces apoptosis[8]. However, we previously published that there is a narrow interval of OA concentrations in serum-free medium, 5 µM and 10 µM for Mv1Lu or MDA-MB-231, respectively, that stimulates migration[12]. Above these concentrations, OA inhibits migration in these cell lines[12]. Similarly, the same range of OA concentration for migration stimulation was reported on mouse fibroblasts, 20 µM in serum-free medium, with a migration inhibitory effect above that concentration[6]. This apparent discrepancy could be attributed to the use of different concentrations of OA, although further research should be conducted to possibly stablish differences between the cell lines that may explain the divergence in the results.

Previously, we showed that OA activates c-Jun by phosphorylation in Mv1Lu and MDA-MB-231 cells[12]. C-Jun is a key transcription factor involved in cell migration[52,53]. Active c-Jun plays an important role in the signaling of different growth factors, indeed, conditional mutations of this transcription factor at the epidermis are known to delay wound closure[54]. Our study confirmed that phosphorylation of c-Jun at the wound scratch edge is crucial for the induction of migration of epithelial cells by OA. Remarkably, OA-stimulated c-Jun overexpression and activation only occurred at the nucleus of actively migrating cells, which is consistent with the c-Jun function to promote migration[52,53] upon OA stimulation. EGF stimulation of cells produces a very extensive c-Jun overexpression and phosphorylation[45,55]. In contrast, the effect of OA was specific to the wound edge of the scratch assay, thus being more precise and avoiding the stimulation of cell migration beyond necessary.

The blockage of upstream molecular signaling by selectively inhibiting MAPKs (MEK1-ERK1/2) or JNK pathways partially inhibited OA-induced migration in Mv1Lu or MDA-MB-231 cells[12]. Moreover, inhibition of

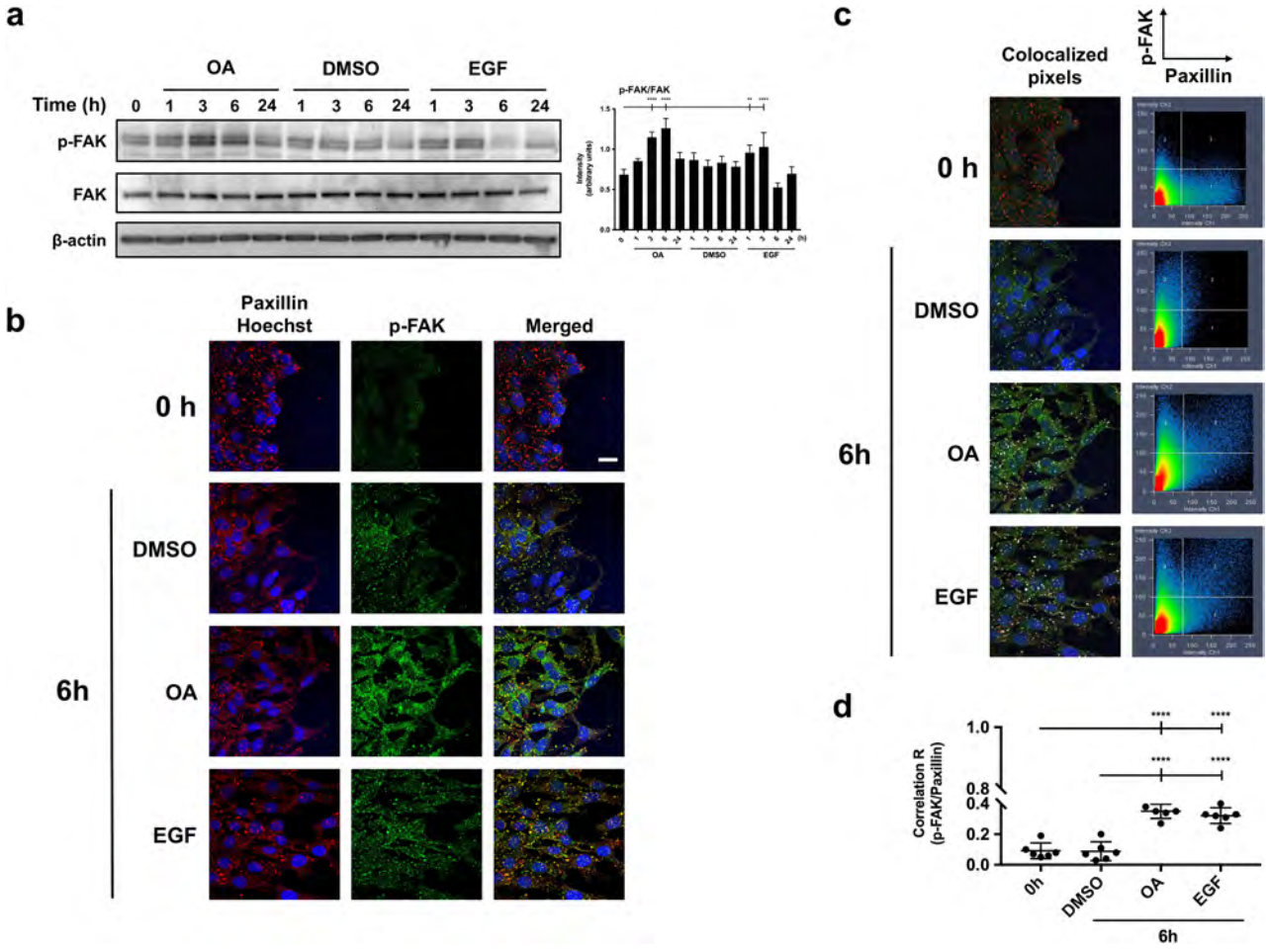

Figure 7. OA induces FAK phosphorylation and promotes its localization in focal adhesion with paxillin in Mv1Lu cells. (**a**) The activation of FAK was assessed by Western Blot at Tyr 925, at the indicated times in the presence of 5 μM OA, DMSO equivalent volume or EGF. Additionally, total protein expression was assayed: FAK. β-Actin was used as a loading control. Phospho-FAK intensity values in Western-blot were quantified by ImageJ to conduct a one-way ANOVA analysis showed on the plot (*$p < 0.05$, **$p < 0.005$, ***$p < 0.001$ and ****$p < 0.0001$). (**b**) Confluent Mv1Lu cells were scratched and allowed to migrate for 6 h. Pictures show the immunostaining with specific antibodies against phospho-FAK (Tyr 925) and paxillin. Co-staining with Hoechst-33258 was used to reveal nuclei. P-FAK: green. Paxillin: red. Nuclei: blue. (**c**) Pictures and graphs represent a colocalization analysis performed by Zeiss Efficient Navigation (ZEN) software. Colocalized pixels are highlighted in white at the immunostaining images. Graphs are dot plots representing both p-FAK and paxillin intensities in terms of number of pixels: p-FAK pixels on Y axis and paxillin pixels on X axis. The 3 quadrant (upper right) represents overlapped (common) pixels between both proteins. (**d**) Pictures of each condition (two) were divided in three horizontally distributed sectors. Pearson's correlation coefficient in each sector of each condition was calculated by the average pixel intensity of p-FAK and paxillin overlapped pixels. The plot represents Pearson's correlation values for each condition, each dot representing the value obtained in one sector. Asterisks indicate statistically significant differences between conditions according to one-way ANOVA statistical analysis: (*$p < 0.05$, **$p < 0.005$, ***$p < 0.001$ and ****$p < 0.0001$). This experiment was repeated at least three times. Representative images are shown. Scale bar indicates 10 μm.

EGFR produced a complete inhibitory effect on OA stimulation of migration, suggesting a complete dependence on the activation of EGFR for OA-induced migration[12]. Interestingly enough, the use of EGFRi did not completely suppress phosphorylation of c-Jun at the wound edge. Moreover, OA stimulation of c-Jun phosphorylation measured by western blot was not suppressed by the use of EGFRi. In a previous paper, we focused on the activation of EGFR by OA as the main event inducing migration in both Mv1Lu and MDA-MB-231 cells[12]. However, the evidence presented in this paper suggests a very early stimulation of c-Jun phosphorylation that is independent of the activation of EGFR in both Mv1Lu and MDA-MB-231 cells. Additional pathways converge into c-Jun activation[56,57]; nevertheless, all the c-Jun activation we saw, independent of or dependent on EGFR was mediated by JNK1/2. JNK has been shown to be required for Drosophila dorsal closure[15,16]. Certainly, the use of JNKi completely blocked the phosphorylation of c-Jun. In any case, further research must be carried out in order to reveal the possible pathway that specifically produces the activation of c-Jun, independently of EGFR activation.

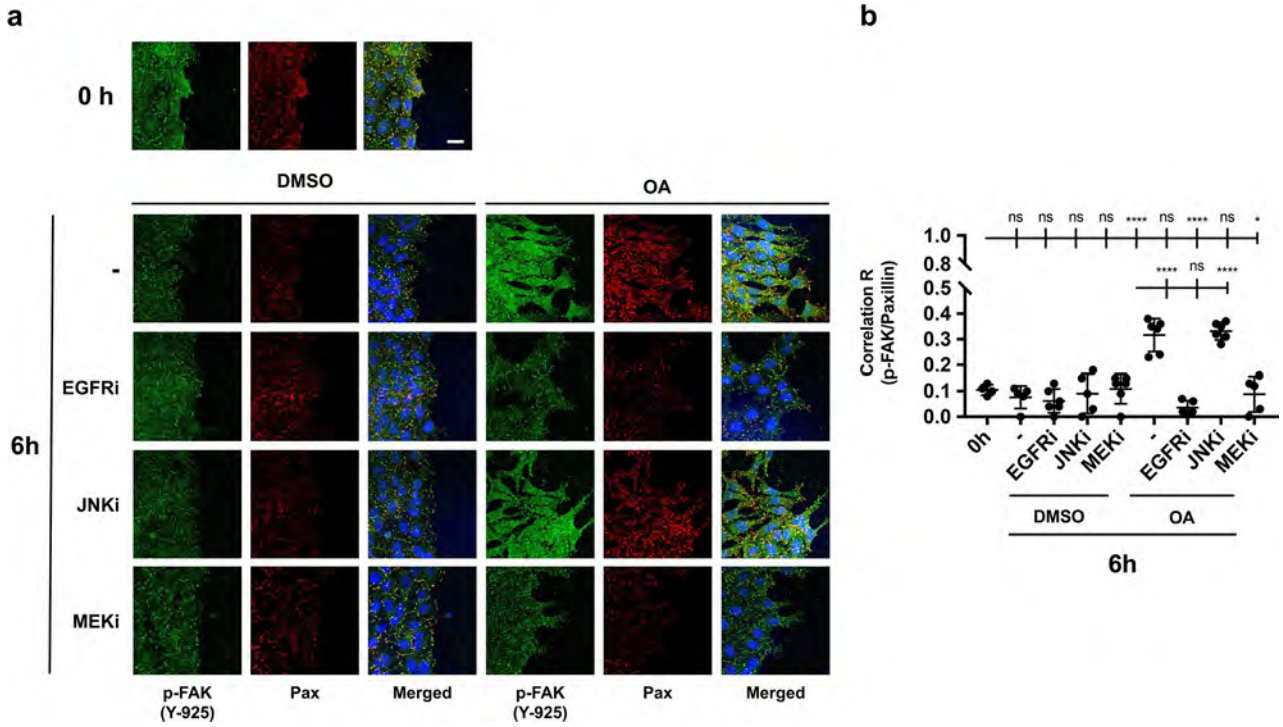

Figure 8. EGFR and MEK inhibitors prevent OA-induced FAK localization at FA in Mv1Lu cells. (**a**) Confluent Mv1Lu cells were scratched and allowed to migrate for 6 h. Cells were treated 30 min before scratch and subsequent OA treatment with specific inhibitors 2,5 μM EGFRi, 50 μM MEKi and 15 μM JNKi. Pictures show the immunostaining with specific antibodies against phospho-FAK (Tyr 925) and paxillin. Co-staining with Hoechst-33258 was used to reveal nuclei. (**b**) The plot represents a colocalization analysis performed by Zeiss Efficient Navigation (ZEN) software. Pictures of each condition (two) were divided in three horizontally distributed sectors. Pearson's correlation coefficient in each sector of each condition was calculated by the average pixel intensity of p-FAK and paxillin overlapped pixels. The plot represents Pearson's correlation values for each condition, each dot representing the value obtained in one sector. Asterisks indicate statistically significant differences between conditions according to a one-way ANOVA statistical analysis: (*$p < 0.05$, **$p < 0.005$, ***$p < 0.001$ and ****$p < 0.0001$). This experiment was repeated at least three times. Representative images are shown. Scale bar indicates 10 μm.

C-Jun, the founding member of the AP-1 family, contributes to its own transcriptional upregulation when it is activated by phosphorylation, producing a self-regulating positive feed-back[56]. OA phosphorylation/protein total level increment of c-Jun and phosphorylation of EGFR showed different time dynamics, with EGFR having a later activation compared to c-Jun activation, which suggests a complex or multiple step mechanism for OA activation of EGFR. In this context, transactivation of EGFR is a phenomenon that activates this receptor in the absence of canonical EGFR external stimuli[58]. EGFR transactivation is triggered by G-protein-coupled receptors (GPCRs) and is now recognized as a key mechanism that couples distinct signal transduction pathways to diverse cellular stimuli[58]. It is plausible that EGFR stimulation by OA could be due to receptor transactivation. Indeed, a clue comes from the fact that OA has been identified as a weak agonist for some GPCR receptors[59], which in turn would activate EGFR[60] and could also have a direct stimulatory effect on the MAPK signaling pathway[61]. Besides, as shown by Bernabé et al.[12], the stimulation of EGFR phosphorylation by OA is independent of protein synthesis. Despite all of this, activation of EGFR is clearly a key point in the process of migration induced by OA, because the inhibition of the receptor by PD153035 completely suppresses OA stimulation of migration[12].

In Mv1Lu cells, the OA-induced phosphorylation of ERK experienced a delay in comparison to c-Jun phosphorylation, and it is in synchrony with the activation of EGFR. This fact suggests that MAPK signaling pathway mainly depends on the OA-activation of EGFR. Unfortunately, in MDA-MB-231, the high overexpression of EGFR[44], causes a high level of ERK phosphorylation making it impossible to clearly distinguish ERK activation in response to OA.

So far, our results show that, in Mv1Lu and MDA-MB-231 cell lines, JNK and c-Jun OA-activation are independent of EGFR. On the other hand, our results for ERK phosphorylation support an EGFR delayed activation mechanism independent of the mechanism early activating JNK/c-Jun. In any case, MAP kinases seem to be involved in both mechanisms, early and late, because PD98059 (MEK) inhibitor blocks the activation of both EGFR and JNK/c-Jun. This way of behaving would suggest a possible feedback mechanism between the MAPK pathway and the activation mechanism that implicates both EGFR and putative GPCR. This crosstalk mechanism between both receptors has been associated with the activation of Src[61], but it is worth exploring whether there could be a similar crosstalk for other kinases such as ERK1/2. In the wounding of corneal cells, the activation of

EGFR is mediated by a shedding mechanism related to GPCR receptors[62]. Strikingly, in this system, the inhibition of ERK1/2 phosphorylation by the use of PD98059 caused a halt in the activation of EGFR, thus suggesting that, in addition to functioning as an EGFR downstream effector, ERK1/2 also mediates EGFR transactivation to a variety of stimuli[62]. Similarly, in both MDA-MB-231 and Mv1Lu cells, the use of PD98059 upon OA stimulation caused a strong inhibitory effect on EGFR activation and c-Jun phosphorylation. This suggests that, upon stimulation with OA, a similar MEK-involved crosstalk mechanism could be at work for the transactivation of EGFR. In fact, in Mv1Lu cells, a minute stimulation of ERK could be seen 1 h after OA stimulation (see Fig. 3).

At in vitro wound assays, a close look at the wound migrating edge showed morphological variations in migrating cells at the wound edge compared to cells placed in the rear. These morphological differences consist in the development of cytoplasmic protrusions such as lamellipodia and ruffles[19]. Indeed, the presence of OA increased the number of lamellipodia and ruffles at the cells at the edge of the wound. In our case, the stimulation with OA also modified the intensity and definition of actin microfilaments there. In fact, actin depolymerization and debranching happens during migration facilitating the dynamic remodeling of the actin network and the cyclic extension and retraction of lamellipodia[20]. So, the observed changes were suggestive of an active migratory status of the cells[19,20]. Cell migration, a very well-coordinated process, requires the continuous formation of focal complexes (FC) that mature into FAs[19,20]. Paxillin is a fundamental component for FA functioning because it is able to integrate multiple signaling inputs[24]. By providing a structural scaffold, paxillin facilitates the synchronized binding of different protein components, particularly signaling molecules[63]. Our results showed a differential organization of FA, revealed by paxillin staining, in response to OA. Certainly, OA caused an increased density but a decreased size of the foci. The phosphorylation of paxillin Ser 178 by JNK produced FA increased dynamics and cell motility[28]. OA stimulation produced a time phosphorylation on this residue that correlated well with JNK activation. However, in response to OA, neither the size nor the density of FA were affected by the presence of this inhibitor (JNKi), which suggests that there might be other means of focal adhesion arrangements in response to OA, independently of JNK activation. Further research is needed to stablish the particular contribution of paxillin Ser 178 phosphorylation to the migration induced by OA.

Coordination and integration of growth-factor signaling and FA remodeling is facilitated by the close physical proximity of key signaling molecules. This is the case for EGFR and FAK[64]. FAK Tyr 925 can be phosphorylated as a consequence of cell integrin assembling or growth factor stimulation[31,36]. Interestingly, OA treatment produced the phosphorylation of EGFR and thus of FAK with a very similar timing outcome. Indeed, FAK activation was completely suppressed by EGFRi. Additionally, FAK Tyr 925 phosphorylation was also suppressed by MEKi, indicating the direct involvement of EGFR via MEK in the activation of FAK in response to OA. So, regarding FA remodeling and in contrast to JNKi, the presence of EGFRi or MEKi produced bigger and consolidated FAs, thus supporting previous findings indicating the need of an EGFR/MEK active signaling for a successful OA-driven migration[12].

The use of different functional mutants of FAK has revealed that FAK localization to FAs is important for the regulation of FA dynamization[51]. Hence, increased FAK localization to FAs raises its turnover at the protrusion front[34]. Our results show that active FAK co-localized with paxillin in response to OA, thus indicating that an active remodeling of FAs was taking place in response to the triterpenoid. Active FAK localization at FAs was dependent on the activation of EGFR because it was inhibited by EGFRi. Also, the participation of active MEK was required as the use of MEKi also prevented Tyr 925 phosphorylated FAK localization at FAs. These data confirmed an OA responsive axis EGFR/MEK/ERK/FAK as a motor for FA dynamization[49]. Additionally, mobilization of phospho-Tyr 925 FAK to the cytosol indicates an intense remodeling of FAs. Certainly, active migration requires a continuous remodeling of FAs[27]. The absence of inhibitory activity on the FA localization of active FAK in the presence of JNK reinforces the idea of an independent but complementary promigratory event. Such promigratory event, although not required for FA managing, may be involved in other aspects of cell migration. So, even though active FAK mobilization to FAs did not seem to be affected by JNKi, OA-stimulated cell migration is partially inhibited[12].

In this paper, we have further dissected the molecular mechanisms underlying the effect of OA on cell migration. Our results showed that OA induces different and interconnected signaling pathways. Given the powerful effect of OA on cell-migration, the need for additional understanding of those mechanisms seems relevant and very pertinent. Finally, these findings could provide an interesting mode of action for OA that is worth investigating in other related molecules.

Materials and methods

Preparation of oleanolic acid. Oleanolic acid (purity > 97%) (Merck, Darmstadt, Germany) was dissolved in dimethyl sulfoxide (DMSO) to a 25 mM concentration. Final assay concentrations are indicated in each experiment. DMSO concentration in all assays never exceeded 1% to avoid cytotoxic effects. A DMSO control condition was performed in each experiment.

Cell culture. Mink Lung Epithelial (Mv1Lu)[38,40,65] cells were grown in Eagle's Minimum Essential Medium (EMEM) (Biowest, Nuaillé, France). Human Mammary Gland cells (MDA-MB-231)[41–43] were grown in Dulbecco's Modified Eagle Medium (DMEM) (Biowest, Nuaillé, France). Both mediums were supplemented with 10% Fetal Bovine Serum (FBS, Gibco, Thermo Fisher Scientific, Rockford, IL, USA), 1% Penicillin/Streptomycin and 1% L Glutamine (both from Biowest, Nuaillé, France). Mv1Lu and MDA-MB-231 cells were incubated in a humidified atmosphere at 37 °C, with 5% CO_2 and 7.5% CO_2, respectively.

Wound healing scratch assay. Mv1Lu or MDA-MB-231 cells were seeded in 24-well plates until they reached 100% confluence, using the appropriate medium for each line with all supplements. At that time,

medium was changed to FBS-free medium for 24 h. At the initial time (T0), a cross-shaped scratch was made on the cell monolayer using a sterile p-200 µl pipette tip. After replacing FBS-free culture medium to wash out released cells, OA (indicated concentration at each experiment) or an equivalent volume of DMSO was added. Additionally, EGFR pharmacological inhibitor PD153035 (EGFRi) 2.5 µM, was added to OA sample. After a 24-h incubation period, cells were fixed with 4% formaldehyde (Applichem GmbH, Darmstadt, Germany) in PBS (Biowest, Nuaillé, France) for 10 min. Finally, well plates were washed twice with PBS. Pictures were taken at 10× magnification using an optical microscope equipped with a digital camera (Motic Optic AE31, Motic Spain, Barcelona, Spain). To quantify cell migration, the areas of the gaps in the wounds were measured by ImageJ software. The initial cell-free surface was subtracted from the endpoint cell-free surface and plotted in a graph[66].

Cell-front migration assay, subcellular localization assay. Mv1Lu or MDA-MB-231 cells were grown until they reached confluence on round glass-coverslips using appropriate medium with 10% FBS. At that point, cells were washed and the medium was replaced by FBS-free medium for 24 h. After this, the established epithelium was scratched using a razor blade, making an artificial wound with enough space to allow cells to migrate. The new wound was set as time 0 of the experiment and then OA, DMSO or 10 ng/ml epidermal growth factor (EGF, Sigma-Aldrich, St Louis, MO, USA) was added to the medium. When using specific inhibitors, cells were treated 30 min before OA stimulation with the following pharmacological inhibitors: 2.5 µM PD153035 (Epidermal Growth Factor inhibitor, EGFRi)[68], 50 µM PD098059 (Mitogen-activated protein kinase kinase inhibitor, MEKi)[69] and 15 µM SP600125 (c-Jun N-terminal kinase inhibitor, JNKi)[70]. After the indicated times of incubation, coverslips were fixed with 4% formaldehyde (Applichem GmbH, Darmstadt, Germany) in PBS (Biowest, Nuaillé, France) for 10 min. After two washes with PBS, cells were permeabilized with 0.3% Triton X-100 (Sigma-Aldrich, St Louis, MO, USA) in PBS for 10 min. Immunostaining was performed first by blocking cells for 30 min at room temperature in PBS solution with 10% FBS, 5% skim milk (Beckton Dickinson, Franklin Lakes, NJ, USA), 0.3% bovine serum albumin (BSA, Sigma-Aldrich, St Louis, MO, USA) and 0.1% Triton X-100. After blocking the cells, they were incubated for 1 h at room temperature with anti-paxillin, anti-c-Jun or anti-phospho-FAK antibodies diluted in blocking solution, without skim milk. Appropriate fluorescent-labelled secondary antibodies were co-incubated for 30 min with Alexa Fluor 594 conjugated phalloidin (Molecular Probes, Thermo Fisher Scientific, Waltham, MA, USA) and Hoechst-33258 (Fluka, Biochemika, Sigma-Aldrich, St Louis, MO, USA) to reveal actin cytoskeleton and nuclei, respectively. Finally, samples were examined and representative images were taken with a confocal microscope (LSM 510 META from ZEISS, Jena, Germany). Images were obtained by using Zeiss Efficient Navigation (ZEN) interface software (ZEISS, Jena, Germany). When a wider view of the migration front was required, especially in c-Jun staining (indicated in figures), four linked fields were acquired by the "Tile scan" ZEN tool. Subsequently, tile scans fluorescent signals were converted to a linear mode and covered with a full data range using the Rainbow look up table (Rainbow LUT) in ImageJ software. In order to quantify c-Jun and phospho-c-Jun levels in immunofluorescence pictures, the image was analyzed and quantified by ImageJ software. For this purpose, pictures in 8-bit three-channel format (Red, Green, Blue, RGB) were divided into three separate color channels (three pictures). By using blue channel picture (Hoechst staining), regions of interest (ROIs) were stablished to define each nucleus, creating as many ROIs masks as nuclei in the image. Then, by overlapping these masks onto the corresponding green channel picture (c-Jun/p-c-Jun staining), we calculated the green intensity value of each nucleus (ROI). The quantified signal of each nucleus was used as a replicate to obtain c-Jun/p-c-Jun intensity data in each of the conditions performed. On the other hand, "Z stack" ZEN feature was used when deep cytoskeleton structure observance was required, taking a proper number of pictures along the Z axis. Focal adhesion (FA) quantifications were performed as described in Horzum et al.[67] by using CLAHE and Log3D macros for ImageJ. Briefly, focal adhesions were quantified from paxillin stained acquired pictures. We used three different images for each condition. Specifically, cell filopodia were selected as regions of interest (ROIs) and the resulting areas (containing FAs) were considered for further analysis. A number of five filopodia were taken into account from each picture. Then, the number of FAs were calculated in each filopodia by using the previously mentioned macros. The obtained number was divided by the total filopodia area to determine FA density. In parallel, the size of each FA was measured using the macros mentioned above. Finally, FA average size was calculated for each treatment. For colocalization determination of paxillin and p-FAK, ZEN interface software was used. The analysis was performed by dividing two pictures (replicates) of each experimental condition into three equal regions of interest (ROIs) including front and back of the edge. Then, overlapped pixels between channel 1 signal (paxillin) and channel 2 signal (p-FAK) were marked for a Pearson's correlation coefficient determination included in ZEN software (ZEISS, Jena, Germany).

Western blot. Mv1Lu or MDA-MB-231 cells were seeded and allowed to reach 60% confluence in 10-cm diameter plates. At that time, culture medium containing 10% FBS was replaced by an FBS-free medium, incubating the cells for a 24-h period. Serum-deprived cells were treated with OA, DMSO or 10 ng/ml EGF. When using specific inhibitors, cells were treated 30 min before OA stimulation with the following pharmacological inhibitors: 2.5 µM PD153035 (Epidermal Growth Factor inhibitor, EGFRi)[68], 50 µM PD098059 (Mitogen-activated protein kinase kinase inhibitor, MEKi)[69] and 15 µM SP600125 (c-Jun N-terminal kinase inhibitor, JNKi)[70]. After time incubations, cells were harvested, washed twice with ice cold PBS and lysed with 20 mM TRIS pH 7.5, 150 mM NaCl, 1 mM EDTA, 1.2 mM $MgCl_2$, 0.5% Nonidet p40, 1 mM DTT, 25 mM NaF and 25 mM beta-glycerophosphate supplemented with phosphatase inhibitors (I and II) and protease inhibitors (all from Sigma-Aldrich, St Louis, MO, USA). Total protein amount of all extracts was measured and normalized by Bradford assay[71] (Sigma-Aldrich, St Louis, MO, USA). The extracts were analyzed by SDS-PAGE followed by Western blot (WB) using the indicated antibodies, revealed by using Horseradish peroxidase substrate (ECL) (GE Healthcare, GE, Little Chalfont, United Kingdom) and images were taken with a Chemidoc XRS1 (Bio-Rad, Hercules, CA,

USA). For protein quantification, western pictures in 8-bit format were processed in ImageJ software. Subsequently, in all western-blot pictures, a lane was stablished for each of the samples. In each lane, the band was selected according to the appropriate size (kDa) of the protein of interest. In general, and for the phosphorylated version of each interest protein, each band's intensity peak was plotted and the area under the plot was measured using "Wand (tracing) tool" of ImageJ to obtain the intensity value. To normalize the data, obtained intensity values were referred to obtained intensity values of either the unphosphorylated form of the protein or a loading control protein such as β-actin if the unphosphorylated form was undetectable (non-available antibody for detecting the unphosphorylated form).

Antibodies. The following commercial primary antibodies were used: anti-phospho-ERK1/2, anti-ERK, anti-JNK1/2, anti-phospho-JNK1/2, and anti-phospho-c-Jun (all from Cell Signaling Technology, Danvers, MA, USA); anti-phospho-EGFR, anti-EGFR, anti-FAK (all from Thermo Fisher Scientific, Rockford, IL, USA); anti-phospho-FAK (Abcam, Cambridge, MA, USA); anti-paxillin and anti-c-Jun (Santa Cruz Biotechnology, Heidelberg, Germany); anti-phospho-paxillin Ser 178 (Antibodies-online GmbH, Aachen, Germany); and anti-β-actin (Sigma-Aldrich, St Louis, MO, USA). Secondary antibodies were anti-rabbit IgG Horseradish peroxidase linked F(ab')2 I fragment (from donkey) (GE Healthcare, GE, Little Chalfont, United Kingdom), anti-mouse IgG_1 (BD Pharmingen, Beckton Dickinson, Franklin Lakes, NJ, USA); Alexa Fluor 488 conjugated anti-rabbit (from donkey), Alexa Fluor 488 conjugated anti-mouse (from donkey) and Alexa Fluor 594 conjugated anti-mouse (from donkey) (all from Thermo Fisher Scientific, Rockford, IL, USA).

Statistical analysis. All the collected data were analyzed using Graph Pad Prism 7 software. In every analysis, classic statistical parameters were calculated and statistical tests were performed with a 95% confidence interval, consequently, p values lower than 0.05 were considered to be statistically significant. At the figure legends, the asterisks denote statistically significant difference between treatments ($^{*}p < 0.05$, $^{**}p < 0.005$, $^{***}p < 0.001$ and $^{****}p < 0.0001$). Data of intensity values, collected from Western-blots, were analyzed by a one-way ANOVA test, comparing the mean of each condition with the mean of every other condition. Then, a Tukey's multiple comparisons test was performed. Data of intensity values obtained from c-Jun and p-c-Jun nuclei quantifications were analyzed by a two-way ANOVA test. Specifically, a Tukey's multiple comparisons test was performed, comparing the mean of each condition with the mean of every other condition; however, each comparison was made within each picture sector. In this way, same picture sectors were compared (for example, sector 1, S1) between different conditions. On the other hand, to see differences between sectors from the same condition a one-way ANOVA was performed, as described elsewhere. Data of colocalization Pearson's coefficient in the immunocytochemistry assays were analyzed with a one-way ANOVA test, comparing the mean of each condition with the mean of every other condition. Then, a Tukey's multiple comparisons test was performed.

Data availability

In order to clarify Western-blot data, we displayed cropped blots of each Figure in the paper as Supplementary Figures (from Supp. Figures 10–15). These Figures contain original blots of each protein assayed with molecular weight markers for a better identification.

Received: 15 October 2021; Accepted: 27 July 2022
Published online: 05 September 2022

References

1. Qing, C. The molecular biology in wound healing & non-healing wound. *Chin. J. Traumatol.* **20**, 189–193. https://doi.org/10.1016/j.cjtee.2017.06.001 (2017).
2. Pollier, J. & Goossens, A. Oleanolic acid. *Phytochemistry* **77**, 10–15. https://doi.org/10.1016/j.phytochem.2011.12.022 (2012).
3. Metelmann, H. R. *et al.* Accelerating the aesthetic benefit of wound healing by triterpene. *J. Craniomaxillofac. Surg.* **40**, e150-154. https://doi.org/10.1016/j.jcms.2011.07.020 (2012).
4. Moura-Letts, G., Villegas, L. F., Marçalo, A., Vaisberg, A. J. & Hammond, G. B. In vivo wound-healing activity of oleanolic acid derived from the acid hydrolysis of Anredera diffusa. *J. Nat. Prod.* **69**, 978–979. https://doi.org/10.1021/np0601152 (2006).
5. Sánchez, M. *et al.* Gastroprotective and ulcer-healing activity of oleanolic acid derivatives: In vitro-in vivo relationships. *Life Sci.* **79**, 1349–1356. https://doi.org/10.1016/j.lfs.2006.03.044 (2006).
6. Kuonen, R. *et al.* Effects of lipophilic extract of *Viscum album* L. and oleanolic acid on migratory activity of NIH/3T3 fibroblasts and on HaCat keratinocytes. *Evid. Based Complement Alter. Med.* **2013**, 718105. https://doi.org/10.1155/2013/718105 (2013).
7. Ayeleso, T. B., Matumba, M. G. & Mukwevho, E. Oleanolic acid and its derivatives: Biological activities and therapeutic potential in chronic diseases. *Molecules* https://doi.org/10.3390/molecules22111915 (2017).
8. Edathara, P. M. *et al.* Inhibitory role of oleanolic acid and esculetin in HeLa cells involve multiple signaling pathways. *Gene* **771**, 145370. https://doi.org/10.1016/j.gene.2020.145370 (2021).
9. Gao, C., Li, X., Yu, S. & Liang, L. Inhibition of cancer cell growth by oleanolic acid in multidrug resistant liver carcinoma is mediated via suppression of cancer cell migration and invasion, mitochondrial apoptosis, G2/M cell cycle arrest and deactivation of JNK/p38 signalling pathway. *J. BUON* **24**, 1964–1969 (2019).
10. He, Y. *et al.* Oleanolic acid inhibits the migration and invasion of hepatocellular carcinoma cells by promoting microRNA-122 expression. *Pharmazie* **76**, 422–427. https://doi.org/10.1691/ph.2021.1366 (2021).
11. Liu, J., Ban, H., Liu, Y. & Ni, J. The expression and significance of AKR1B10 in laryngeal squamous cell carcinoma. *Sci. Rep.* **11**, 18228. https://doi.org/10.1038/s41598-021-97648-y (2021).
12. Bernabe-Garcia, A. *et al.* Oleanolic acid induces migration in Mv1Lu and MDA-MB-231 epithelial cells involving EGF receptor and MAP kinases activation. *PLoS One* **12**, e0172574. https://doi.org/10.1371/journal.pone.0172574 (2017).
13. Singer, A. J. & Clark, R. A. Cutaneous wound healing. *N. Engl. J. Med.* **341**, 738–746. https://doi.org/10.1056/NEJM199909023411006 (1999).
14. Barrientos, S., Stojadinovic, O., Golinko, M. S., Brem, H. & Tomic-Canic, M. Growth factors and cytokines in wound healing. *Wound Repair Regener.* **16**, 585–601. https://doi.org/10.1111/j.1524-475X.2008.00410.x (2008).

15. Riesgo-Escovar, J. R., Jenni, M., Fritz, A. & Hafen, E. The Drosophila Jun-N-terminal kinase is required for cell morphogenesis but not for DJun-dependent cell fate specification in the eye. *Genes Dev.* **10**, 2759–2768 (1996).
16. Sluss, H. K. *et al.* A JNK signal transduction pathway that mediates morphogenesis and an immune response in Drosophila. *Genes Dev.* **10**, 2745–2758. https://doi.org/10.1101/gad.10.21.2745 (1996).
17. Xia, Y. *et al.* MEK kinase 1 is critically required for c-Jun N-terminal kinase activation by proinflammatory stimuli and growth factor-induced cell migration. *Proc. Natl. Acad. Sci. USA* **97**, 5243–5248. https://doi.org/10.1073/pnas.97.10.5243 (2000).
18. Yujiri, T. *et al.* MEK kinase 1 gene disruption alters cell migration and c-Jun NH2-terminal kinase regulation but does not cause a measurable defect in NF-kappa B activation. *Proc. Natl. Acad. Sci. USA* **97**, 7272–7277. https://doi.org/10.1073/pnas.130176697 (2000).
19. Mayor, R. & Etienne-Manneville, S. The front and rear of collective cell migration. *Nat. Rev. Mol. Cell Biol.* **17**, 97–109. https://doi.org/10.1038/nrm.2015.14 (2016).
20. Tang, D. D. & Gerlach, B. D. The roles and regulation of the actin cytoskeleton, intermediate filaments and microtubules in smooth muscle cell migration. *Respir. Res.* **18**, 54. https://doi.org/10.1186/s12931-017-0544-7 (2017).
21. Brakebusch, C. & Fassler, R. The integrin-actin connection, an eternal love affair. *EMBO J.* **22**, 2324–2333. https://doi.org/10.1093/emboj/cdg245 (2003).
22. Mitra, S. K., Hanson, D. A. & Schlaepfer, D. D. Focal adhesion kinase: In command and control of cell motility. *Nat. Rev. Mol. Cell Biol.* **6**, 56–68. https://doi.org/10.1038/nrm1549 (2005).
23. Parsons, J. T., Horwitz, A. R. & Schwartz, M. A. Cell adhesion: Integrating cytoskeletal dynamics and cellular tension. *Nat. Rev. Mol. Cell Biol.* **11**, 633–643. https://doi.org/10.1038/nrm2957 (2010).
24. Lopez-Colome, A. M., Lee-Rivera, I., Benavides-Hidalgo, R. & Lopez, E. Paxillin: A crossroad in pathological cell migration. *J. Hematol. Oncol.* **10**, 50. https://doi.org/10.1186/s13045-017-0418-y (2017).
25. Schaller, M. D. Paxillin: A focal adhesion-associated adaptor protein. *Oncogene* **20**, 6459–6472. https://doi.org/10.1038/sj.onc.1204786 (2001).
26. Huttenlocher, A. & Horwitz, A. R. Integrins in cell migration. *Cold Spring Harb. Perspect Biol.* **3**, a005074. https://doi.org/10.1101/cshperspect.a005074 (2011).
27. Webb, D. J., Parsons, J. T. & Horwitz, A. F. Adhesion assembly, disassembly and turnover in migrating cells—over and over and over again. *Nat. Cell Biol.* **4**, 97–100. https://doi.org/10.1038/ncb0402-e97 (2002).
28. Huang, C., Rajfur, Z., Borchers, C., Schaller, M. D. & Jacobson, K. JNK phosphorylates paxillin and regulates cell migration. *Nature* **424**, 219–223. https://doi.org/10.1038/nature01745 (2003).
29. Hanks, S. K. & Polte, T. R. Signaling through focal adhesion kinase. *BioEssays* **19**, 137–145. https://doi.org/10.1002/bies.950190208 (1997).
30. Schlaepfer, D. D., Mitra, S. K. & Ilic, D. Control of motile and invasive cell phenotypes by focal adhesion kinase. *Biochim. Biophys. Acta Mol. Cell Res.* **1692**, 77–102. https://doi.org/10.1016/j.bbamcr.2004.04.008 (2004).
31. Deramaudt, T. B. *et al.* FAK phosphorylation at Tyr-925 regulates cross-talk between focal adhesion turnover and cell protrusion. *Mol. Biol. Cell* **22**, 964–975. https://doi.org/10.1091/mbc.E10-08-0725 (2011).
32. Schlaepfer, D. D., Hauck, C. R. & Sieg, D. J. Signaling through focal adhesion kinase. *Mol. Biol.* **44**, 25 (1999).
33. Sieg, D. J., Hauck, C. R. & Schlaepfer, D. D. Required role of focal adhesion kinase (FAK) for integrin-stimulated cell migration. *J. Cell Sci.* **112**(Pt 16), 2677–2691 (1999).
34. Hu, Y. L. *et al.* FAK and paxillin dynamics at focal adhesions in the protrusions of migrating cells. *Sci. Rep.* **4**, 6024. https://doi.org/10.1038/srep06024 (2014).
35. Tomar, A. & Schlaepfer, D. D. A PAK-activated linker for EGFR and FAK. *Dev. Cell* **18**, 170–172. https://doi.org/10.1016/j.devcel.2010.01.013 (2010).
36. Sieg, D. J. *et al.* FAK integrates growth-factor and integrin signals to promote cell migration. *Nat. Cell Biol.* **2**, 249–256. https://doi.org/10.1038/35010517 (2000).
37. Brown, M. C. & Turner, C. E. Paxillin: Adapting to change. *Physiol. Rev.* **84**, 1315–1339. https://doi.org/10.1152/physrev.00002.2004 (2004).
38. Demetriou, M., Nabi, I. R., Coppolino, M., Dedhar, S. & Dennis, J. W. Reduced contact-inhibition and substratum adhesion in epithelial cells expressing GlcNAc-transferase V. *J. Cell Biol.* **130**, 383–392 (1995).
39. Wu, F. *et al.* Cell cycle arrest in G0/G1 phase by contact inhibition and TGF-beta 1 in mink Mv1Lu lung epithelial cells. *Am. J. Physiol.* **270**, L879-888 (1996).
40. Rahimi, N., Hung, W., Tremblay, E., Saulnier, R. & Elliott, B. c-Src kinase activity is required for hepatocyte growth factor-induced motility and anchorage-independent growth of mammary carcinoma cells. *J. Biol. Chem.* **273**, 33714–33721 (1998).
41. Pontillo, C. A. *et al.* Activation of c-Src/HER1/STAT5b and HER1/ERK1/2 signaling pathways and cell migration by hexachlorobenzene in MDA-MB-231 human breast cancer cell line. *Toxicol. Sci.* **120**, 284–296. https://doi.org/10.1093/toxsci/kfq390 (2011).
42. McInroy, L. & Määttä, A. Down-regulation of vimentin expression inhibits carcinoma cell migration and adhesion. *Biochem. Biophys. Res. Commun.* **360**, 109–114. https://doi.org/10.1016/j.bbrc.2007.06.036 (2007).
43. Zhang, N., Kong, X., Yan, S., Yuan, C. & Yang, Q. Huaier aqueous extract inhibits proliferation of breast cancer cells by inducing apoptosis. *Cancer Sci.* **101**, 2375–2383. https://doi.org/10.1111/j.1349-7006.2010.01680.x (2010).
44. Li, R. H., Huang, W. H., Wu, J. D., Du, C. W. & Zhang, G. J. EGFR expression is associated with cytoplasmic staining of CXCR4 and predicts poor prognosis in triple-negative breast carcinomas. *Oncol. Lett.* **13**, 695–703. https://doi.org/10.3892/ol.2016.5489 (2017).
45. Ruiz-Canada, C. *et al.* Amniotic membrane stimulates cell migration by modulating Transforming Growth Factor-beta signaling. *J. Tissue Eng. Regen. Med.* https://doi.org/10.1002/term.2501 (2017).
46. Deramaudt, T. B. *et al.* Altering FAK-paxillin interactions reduces adhesion. Migration and invasion processes. *PLoS One* **9**, e92059. https://doi.org/10.1371/journal.pone.0092059 (2014).
47. Svitkina, T. The actin cytoskeleton and actin-based motility. *Cold Spring Harbor Perspect. Biol.* https://doi.org/10.1101/cshperspect.a018267 (2018).
48. Merino, F., Pospich, S. & Raunser, S. Towards a structural understanding of the remodeling of the actin cytoskeleton. *Semin. Cell Dev. Biol.* **102**, 51–64. https://doi.org/10.1016/j.semcdb.2019.11.018 (2020).
49. Teranishi, S., Kimura, K. & Nishida, T. Role of formation of an ERK-FAK-paxillin complex in migration of human corneal epithelial cells during wound closure in vitro. *Invest. Ophthalmol. Vis. Sci.* **50**, 5646. https://doi.org/10.1167/iovs.08-2534 (2009).
50. Huang, Z., Yan, D. P. & Ge, B. X. JNK regulates cell migration through promotion of tyrosine phosphorylation of paxillin. *Cell Signal* **20**, 2002–2012. https://doi.org/10.1016/j.cellsig.2008.07.014 (2008).
51. Shen, Y. & Schaller, M. D. Focal adhesion targeting: The critical determinant of FAK regulation and substrate phosphorylation. *Mol. Biol. Cell* **10**, 2507–2518. https://doi.org/10.1091/mbc.10.8.2507 (1999).
52. Yue, C. *et al.* c-Jun overexpression accelerates wound healing in diabetic rats by human umbilical cord-derived mesenchymal stem cells. *Stem Cells Int.* **2020**, 7430968. https://doi.org/10.1155/2020/7430968 (2020).
53. Nakano, T. *et al.* Promotion of wound healing by acetate in murine colonic epithelial cell via c-Jun N-terminal kinase activation. *J. Gastroenterol. Hepatol.* **35**, 1171–1179. https://doi.org/10.1111/jgh.14987 (2020).
54. Li, G. *et al.* c-Jun is essential for organization of the epidermal leading edge. *Dev. Cell.* **4**, 865–877 (2003).

55. Alcaraz, A. *et al.* Amniotic membrane modifies the genetic program induced by TGFss, stimulating keratinocyte proliferation and migration in chronic wounds. *PLoS One* **10**, e0135324. https://doi.org/10.1371/journal.pone.0135324 (2015).
56. Meng, Q. & Xia, Y. c-Jun, at the crossroad of the signaling network. *Protein Cell* **2**, 889–898. https://doi.org/10.1007/s13238-011-1113-3 (2011).
57. Bogoyevitch, M. A. & Kobe, B. Uses for JNK: The many and varied substrates of the c-Jun N-terminal kinases. *Microbiol. Mol. Biol. Rev.* **70**, 1061–1095. https://doi.org/10.1128/MMBR.00025-06 (2006).
58. Leserer, M., Gschwind, A. & Ullrich, A. Epidermal growth factor receptor signal transactivation. *IUBMB Life* **49**, 405–409. https://doi.org/10.1080/152165400410254 (2000).
59. Sato, H. *et al.* Anti-hyperglycemic activity of a TGR5 agonist isolated from *Olea europaea*. *Biochem. Biophys. Res. Commun.* **362**, 793–798. https://doi.org/10.1016/j.bbrc.2007.06.130 (2007).
60. Yasuda, H. *et al.* Involvement of membrane-type bile acid receptor M-BAR/TGR5 in bile acid-induced activation of epidermal growth factor receptor and mitogen-activated protein kinases in gastric carcinoma cells. *Biochem. Biophys. Res. Commun.* **354**, 154–159. https://doi.org/10.1016/j.bbrc.2006.12.168 (2007).
61. Cattaneo, F. *et al.* Cell-surface receptors transactivation mediated by g protein-coupled receptors. *Int. J. Mol. Sci.* **15**, 19700–19728. https://doi.org/10.3390/ijms151119700 (2014).
62. Yin, J. & Yu, F. S. ERK1/2 mediate wounding- and G-protein-coupled receptor ligands-induced EGFR activation via regulating ADAM17 and HB-EGF shedding. *Invest. Ophthalmol. Vis. Sci.* **50**, 132–139. https://doi.org/10.1167/iovs.08-2246 (2009).
63. Petit, V. *et al.* Phosphorylation of tyrosine residues 31 and 118 on paxillin regulates cell migration through an association with CRK in NBT-II cells. *J. Cell Biol.* **148**, 957–970 (2000).
64. Turner, C. E. Paxillin and focal adhesion signalling. *Nat. Cell Biol.* **2**, E231-236. https://doi.org/10.1038/35046659 (2000).
65. Zou, Y., Lim, S., Lee, K., Deng, X. & Friedman, E. Serine/threonine kinase Mirk/Dyrk1B is an inhibitor of epithelial cell migration and is negatively regulated by the Met adaptor Ran-binding protein M. *J. Biol. Chem.* **278**, 49573–49581. https://doi.org/10.1074/jbc.M307556200 (2003).
66. Liarte, S., Bernabe-Garcia, A., Armero-Barranco, D. & Nicolas, F. J. Microscopy based methods for the assessment of epithelial cell migration during in vitro wound healing. *J. Vis. Exp.* https://doi.org/10.3791/56799 (2018).
67. Horzum, U., Ozdil, B. & Pesen-Okvur, D. Step-by-step quantitative analysis of focal adhesions. *MethodsX* **1**, 56–59. https://doi.org/10.1016/j.mex.2014.06.004 (2014).
68. Bos, M. *et al.* PD153035, a tyrosine kinase inhibitor, prevents epidermal growth factor receptor activation and inhibits growth of cancer cells in a receptor number-dependent manner. *Clin. Cancer Res.* **3**, 2099–2106 (1997).
69. Shang, J., Lu, S., Jiang, Y. & Zhang, J. Allosteric modulators of MEK1: Drug design and discovery. *Chem. Biol. Drug Des.* **88**, 485–497. https://doi.org/10.1111/cbdd.12780 (2016).
70. Bennett, B. L. *et al.* SP600125, an anthrapyrazolone inhibitor of Jun N-terminal kinase. *Proc. Natl. Acad. Sci. USA* **98**, 13681–13686. https://doi.org/10.1073/pnas.251194298 (2001).
71. Ernst, O. & Zor, T. Linearization of the Bradford protein assay. *J. Vis. Exp.* https://doi.org/10.3791/1918 (2010).

Acknowledgements

At the beginning of this project, Oleanolic acid was kindly provided by Dr. Julian Castillo of Nutrafur, Murcia, Spain; nutrafur@nutrafur.com. We thank Dr. Gareth J. Inman for Mv1Lu cells and Dr. Ander Izeta for MDA-MB-231 cells. We are grateful to Marta Agudo and Caterina Pipino for their critical reading of the manuscript. JSF was supported with a "Contrato Predoctoral para la Formación de Personal Investigador" from Universidad Católica San Antonio de Murcia (UCAM). We are indebted to the Hospital Clínico Universitario Virgen de la Arrixaca for strongly supporting and providing funding to conduct this research. Also, research was funded by Instituto de Salud Carlos III, Fondo de Investigaciones Sanitarias. Plan Estatal I + D + I and Instituto de Salud Carlos III, Subdirección General de Evaluación y Fomento de la Investigación (Grants no.: PI17/02164; PI21/01339). http://www.isciii.es/. Fondos FEDER (EDRF) "Una manera de hacer Europa" A way of making Europe. Also, we thank IMIB-Arrixaca and FFIS for technical support and assistance.

Author contributions

J.S.F. conceived and prepared the experiments, gathered the data, analyzed the data, drew the figures and wrote the manuscript, J.A.G. supervised the experiments and supervised the writing of the manuscript and F.J.N. conceived the experiments, discussed the data, gathered funding, supervised the writing of the manuscript and wrote the final version of the manuscript.

Competing interests

The authors declare no competing interests.

Additional information

Supplementary Information The online version contains supplementary material available at https://doi.org/10.1038/s41598-022-17553-w.

Correspondence and requests for materials should be addressed to F.J.N.

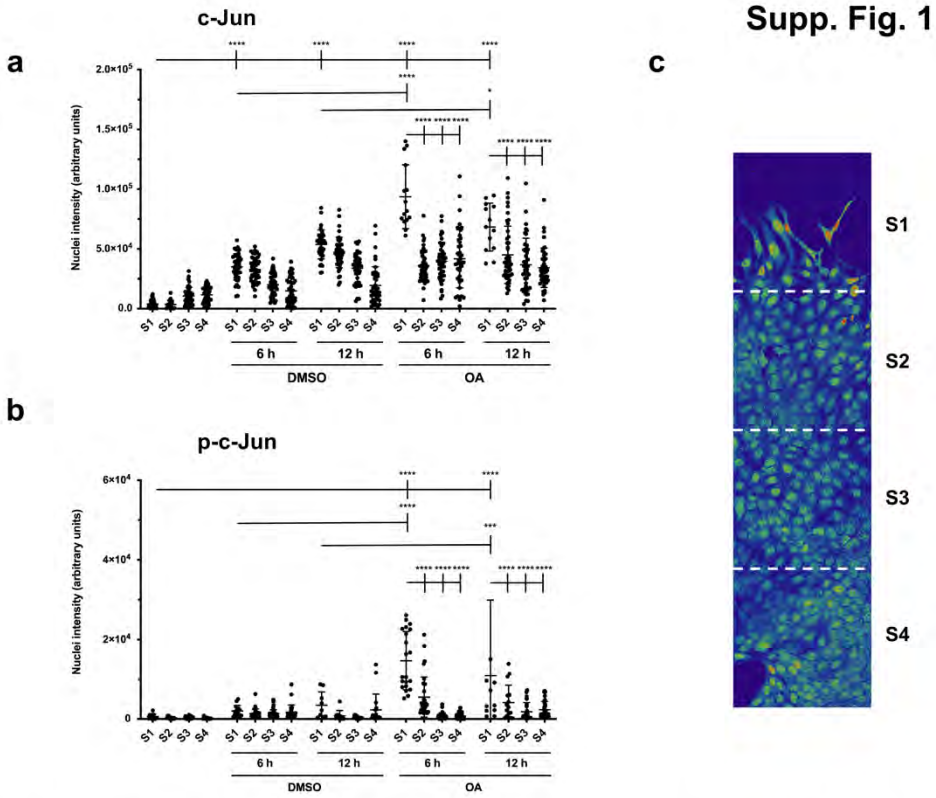

Supplemental figure 1. Oleanolic acid significantly increases c-Jun expression and its phosphorylation at the edge of wound-scratched cells. Plots represent c-Jun (a) and p-c-Jun (b) intensities at cell nuclei. In both cases, each point on the plot represents the intensity of the stained protein at the nucleus of one cell, quantified by Image J software. (c) tile scan images were divided in four equal sectors to considering wound border as the first sector (S1), followed by the rest (S2, S3 and S4). Furthermore, plots show a Two-way ANOVA statistical analysis, with asterisks indicating *p<0.05, **p<0.005, ***p<0.001 and ****p<0.0001.

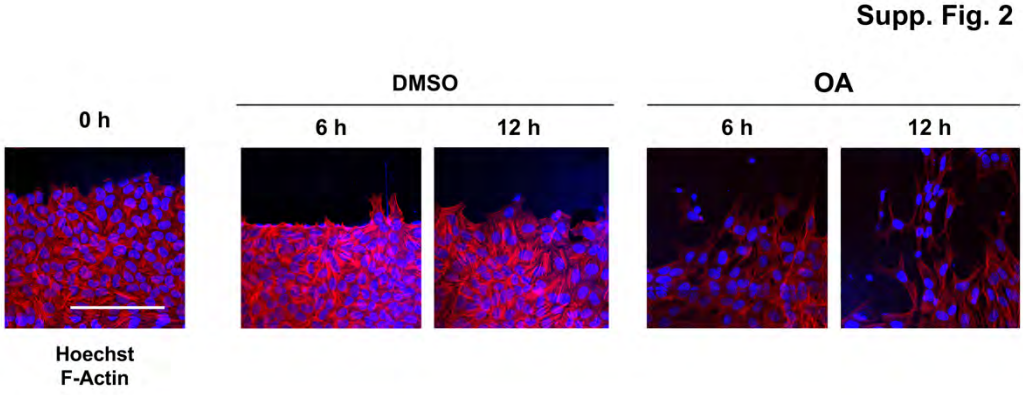

Supplemental figure 2. Oleanolic acid changes actin cytoskeleton at wound edge Mv1Lu cells. Wound edge details of Tile Scan pictures of Figure 1. Scratched Mv1Lu cells were immunostained with phalloidin and Hoechst-33258 to show actin cytoskeleton and nuclei, respectively. Actin fibers (F-actin): red. Nuclei: blue. Note that OA treatment changes actin cytoskeleton reorganization at wound edge, especially in migrating cells. Representative images are shown. Scale bar indicates 50 μm.

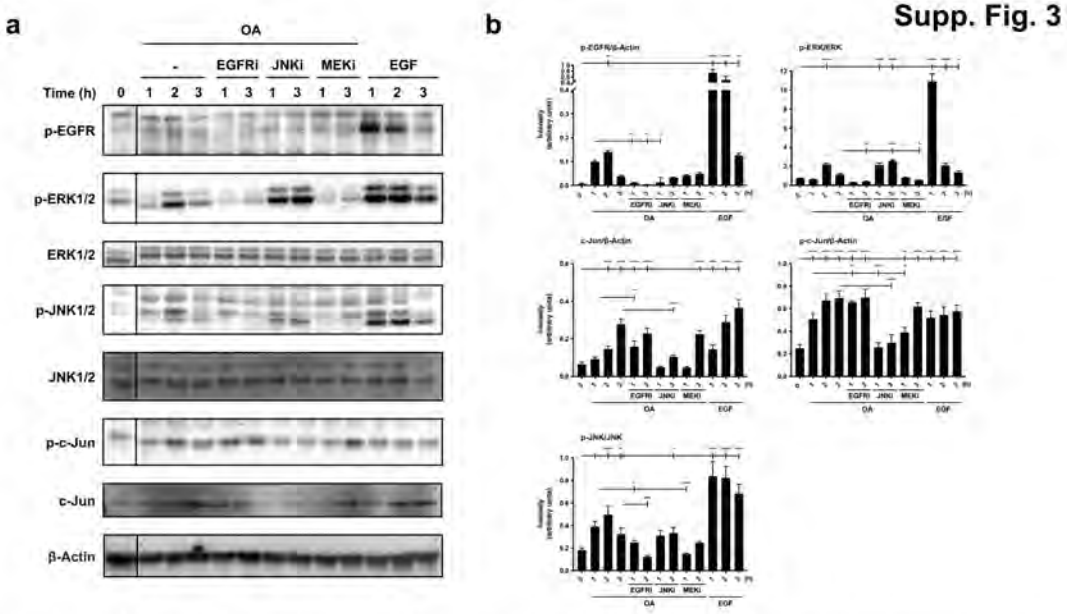

Supplemental figure 3. The use of specific inhibitors against EGFR, MEK and JNK upon OA treatment reveals a new OA-induced pathway in Mv1Lu cells. (a) Total protein extracts from serum-starved sub-confluent Mv1Lu cells, treated with 5 μM OA, EGF or DMSO. Besides that, cells were treated 30 minutes before with the following inhibitors in the absence or presence of OA: 2,5 μM EGFRi, 50 μM MEKi and 15 μM JNK. Different protein's phosphorylation were assayed at the indicated times (hours): phospho-EGFR (Tyrosine 1068), phospho-ERK1/2 (Thr 202/Tyr 204), phospho-JNK1/2 (Thr 183/Tyr 185) and phospho-c-Jun (Ser 63). Additionally, total protein expression was assayed: ERK1/2, JNK1/2 and c-Jun. β-Actin was used as a loading control. A representative experiment is shown. (b) Plots with intensity values of each protein assayed by Western-blot, by gathering the data of three independent experiments. Intensity values were quantified and collected by Image J software. Asterisks indicate statistically significant differences between the selected conditions according to a One-way ANOVA statistical analysis: (*p<0.05, **p<0.005, ***p<0.001 and ****p<0.0001).

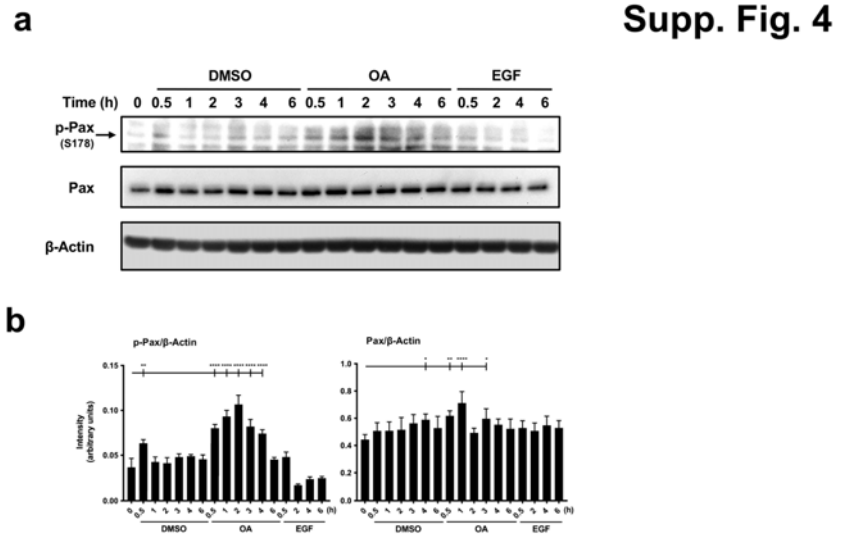

Supplemental figure 4. Oleanolic acid triggers paxillin activation by the phosphorylation on its Ser 178 residue. (a) Total protein extracts from serum-starved sub-confluent MDA-MB 231 cells treated with 10 μM OA, EGF or DMSO equivalent volume as vehicle control. Paxillin's phosphorylation was assayed at the indicated times (hours) targeting phospho-Ser 178 residue. Additionally, total paxillin expression was assayed. β-Actin was used as a loading control. A representative experiment is shown. (b) Plots with intensity values of each protein assayed by Western-blot, by gathering the data of three independent experiments. Intensity values were quantified and collected by Image J software Asterisks indicate statistically significant differences between the selected conditions according to a One-way ANOVA statistical analysis: (*p<0.05, **p<0.005, ***p<0.001 and ****p<0.0001).

Supp. Fig. 5

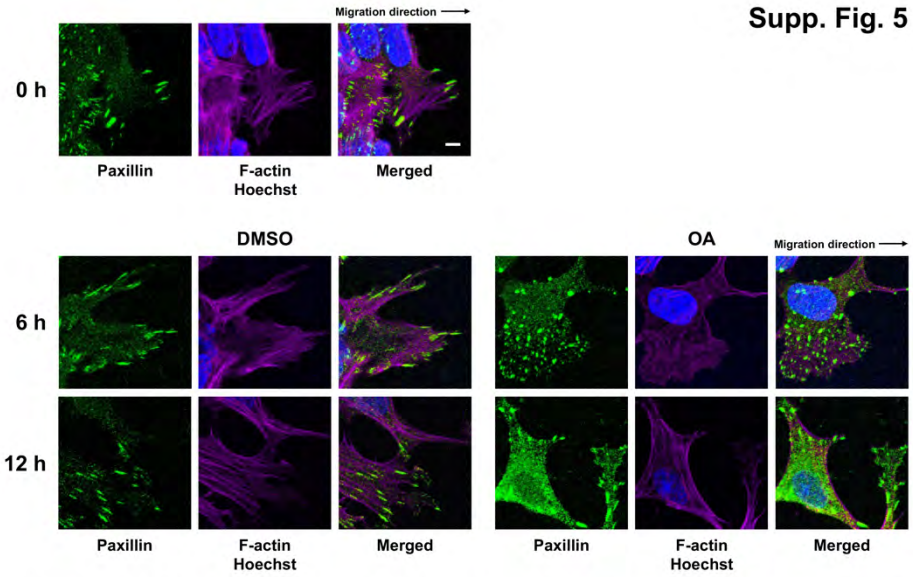

Supplemental figure 5. Oleanolic acid promotes changes in focal adhesions and actin cytoskeleton. Figure 6 insets. Confluent Mv1Lu cells were scratched and allowed to migrate for 6 and 12 hours. Cells treated with 5 µM OA or DMSO equivalent volume (vehicle control) were immunostained with specific antibodies against paxillin. Co-staining with phalloidin and Hoechst-33258 was used to show actin cytoskeleton and nuclei, respectively. Paxillin: green. Actin fibers (F-actin): magenta. Nuclei: blue. This experiment was repeated at least three times. Representative images are shown. Scale bar indicates 5 µm.

Supp. Fig. 6

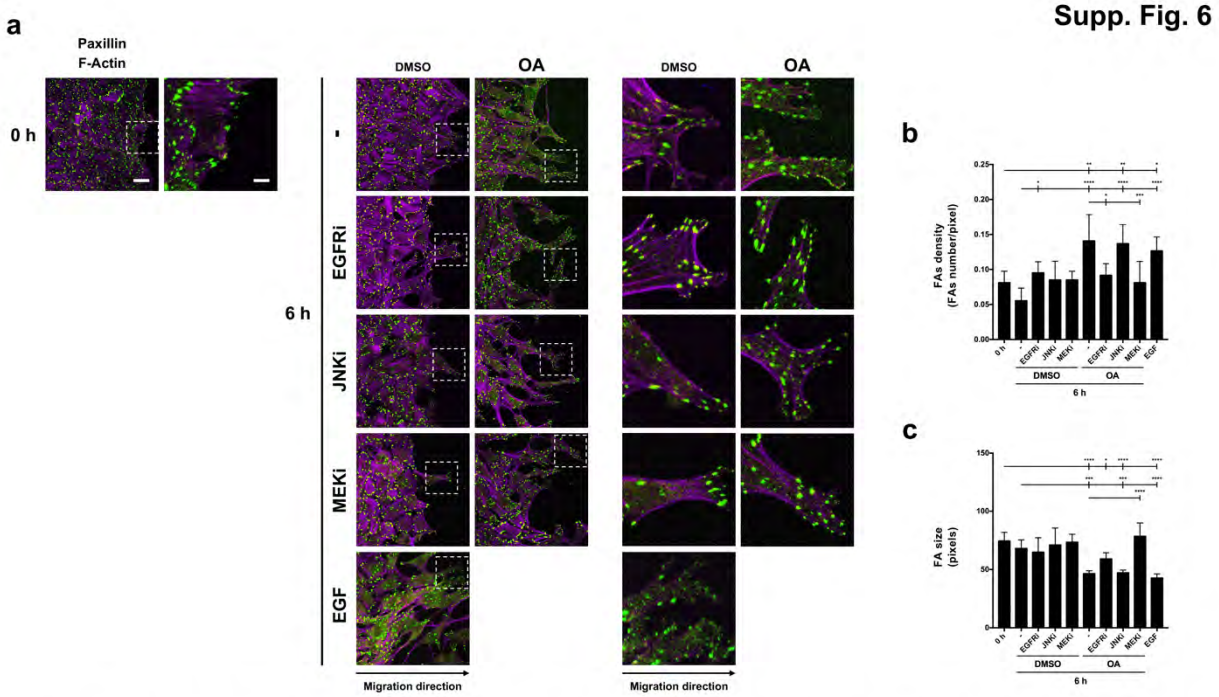

Supplemental figure 6. Specific inhibitors against EGFR, MEK and JNK, upon OA treatment, abolish OA-triggered actin and paxillin distribution in wound-scratched Mv1Lu cells. (a) Confluent Mv1Lu cells were scratched and treated 30 minutes with the following inhibitors: 2,5 µM EGFRi, 50 µM MEKi and 15 µM JNKi. Then cells were stimulated with 5 µM OA, DMSO (equivalent volume) or 10 ng/ml EGF and they were allowed to migrate for 6 h. Note that EGF treatment does not contain DMSO. For the immunostaining a specific antibody against paxillin was used. Co-staining with phalloidin and Hoechst-33258 was used to show actin cytoskeleton and nuclei, respectively. Paxillin: green. Actin fibers (F-actin): magenta. Images were acquired by a confocal microscope. This experiment was repeated at least three times. Representative images are shown. Scale bar indicates 10 µm. Insets scale bar indicates 2.8 µm. . (b) Quantification of the density of FA as FA number per filopodia area. (c) Quantification of FA size (average size) at the filopodia area. One-way ANOVA statistical analysis was performed (*p<0.05, **p<0.005, ***p<0.001 and ****p<0.0001).

Supp. Fig. 7

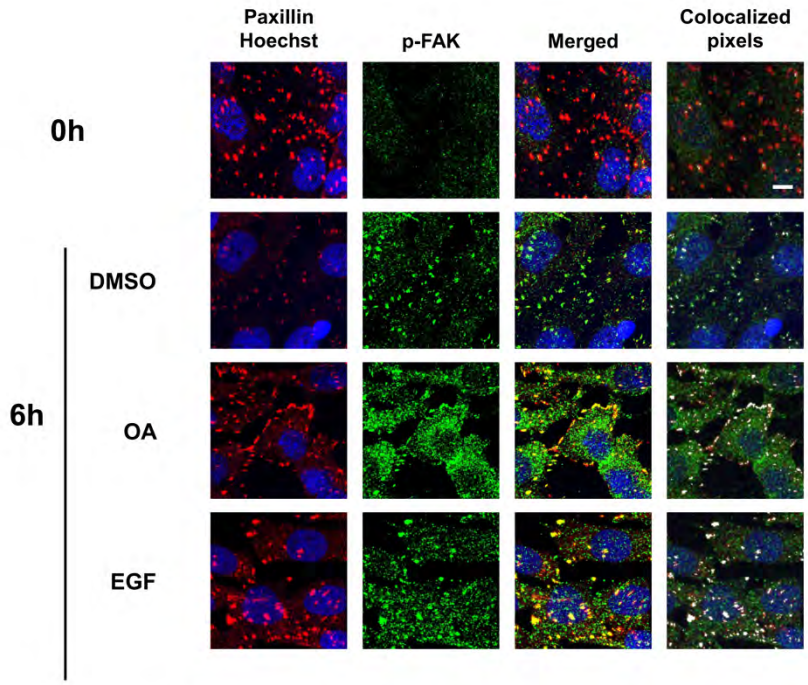

Supplemental figure 7. Oleanolic acid localizes active FAK at focal adhesions. Mv1Lu cells at wound edge showing phospho-FAK (Tyr 925) and paxillin staining. Details of Figure 7 pictures. Note that OA and EGF conditions show the overlapping of p-FAK and paxillin signals. Representative images are shown. Scale bar indicates 5 µM.

Supp. Fig. 8

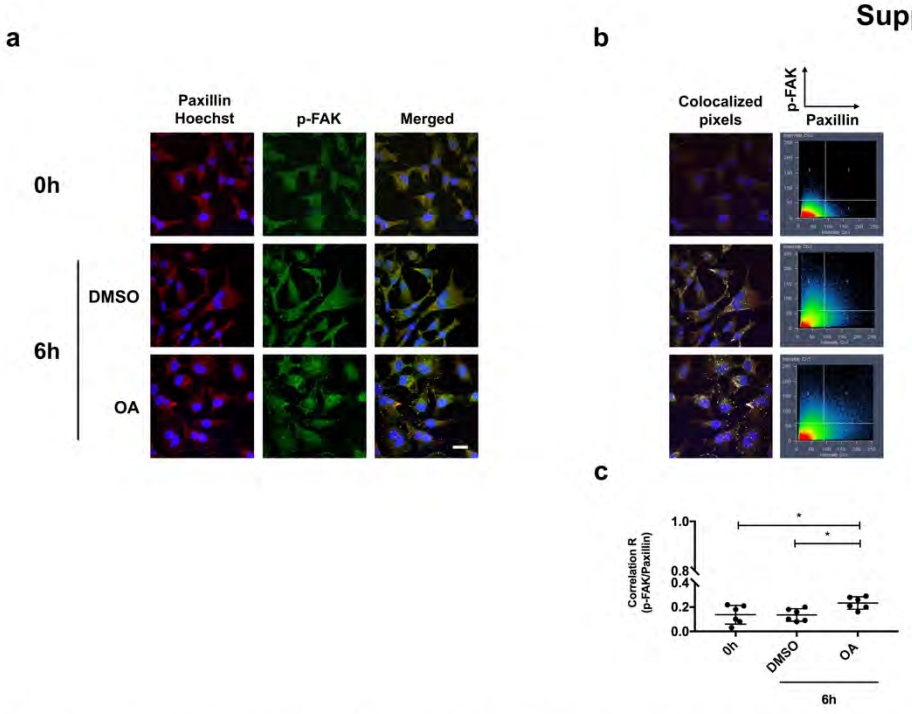

Supplemental figure 8. Oleanolic acid induces FAK phosphorylation and promotes its localization in focal adhesion with paxillin in MDA-MB 231 cells at wound edge. (a) Confluent MDA-MB 231 cells were scratched and allowed to migrate for 6 hours. Cells were treated with 5 µM OA or DMSO equivalent volume. Pictures show the immunostaining with specific antibodies against phospho-FAK (Tyr 925) and paxillin. Additional staining with Hoechst-33258 was used to reveal nuclei. (b) Pictures and graphs represent a colocalization analysis performed by Zeiss Efficient Navigation (ZEN) software. Colocalized pixels are highlighted in white color at immunostaining images. Graphs are dot plots representing both p-FAK and Paxillin intensities in terms of number of pixels: p-FAK pixels on Y axis and paxillin pixels on X axis. The 3 quadrant represents overlapped (common) pixels between both proteins. (c) Pearson's correlation coefficient of each condition was calculated by the average pixel intensity of p-FAK and paxillin overlapped pixels, representing the similarity between the two signals. The plot represents Pearson's correlation values for each condition. Asterisks indicate statistically significant differences between conditions according to a One-way ANOVA statistical analysis: (*) $p < 0.05$. This experiment was repeated at least three times. Representative images are shown. Scale bar indicates 10 µM.

Supp. Fig. 9

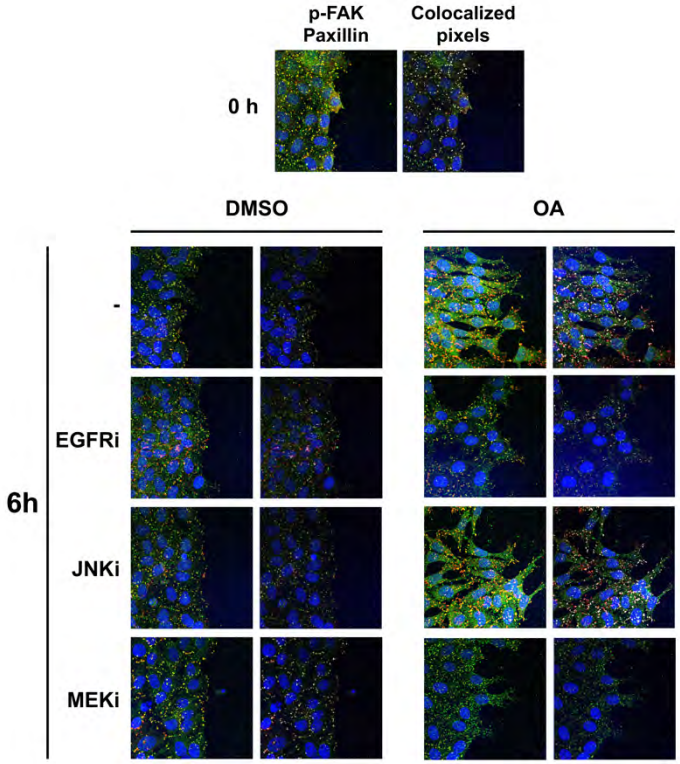

Supplemental figure 9. EGFR and MEK inhibitors prevent oleanolic acid-induced FAK localization at focal adhesion in Mv1Lu cells. Mv1Lu cells at wound edge showing phospho-FAK (Tyr 925) and paxillin staining. Colocalized analysis of Figure 8 pictures. The images represent colocalized pixels highlighted in white color, where the p-FAK and paxillin signals overlapping occurred. Representative images are shown. Phospho-FAK (p-FAK): green. Paxillin: red. Nuclei: blue. Scale bar indicates 10 μm.

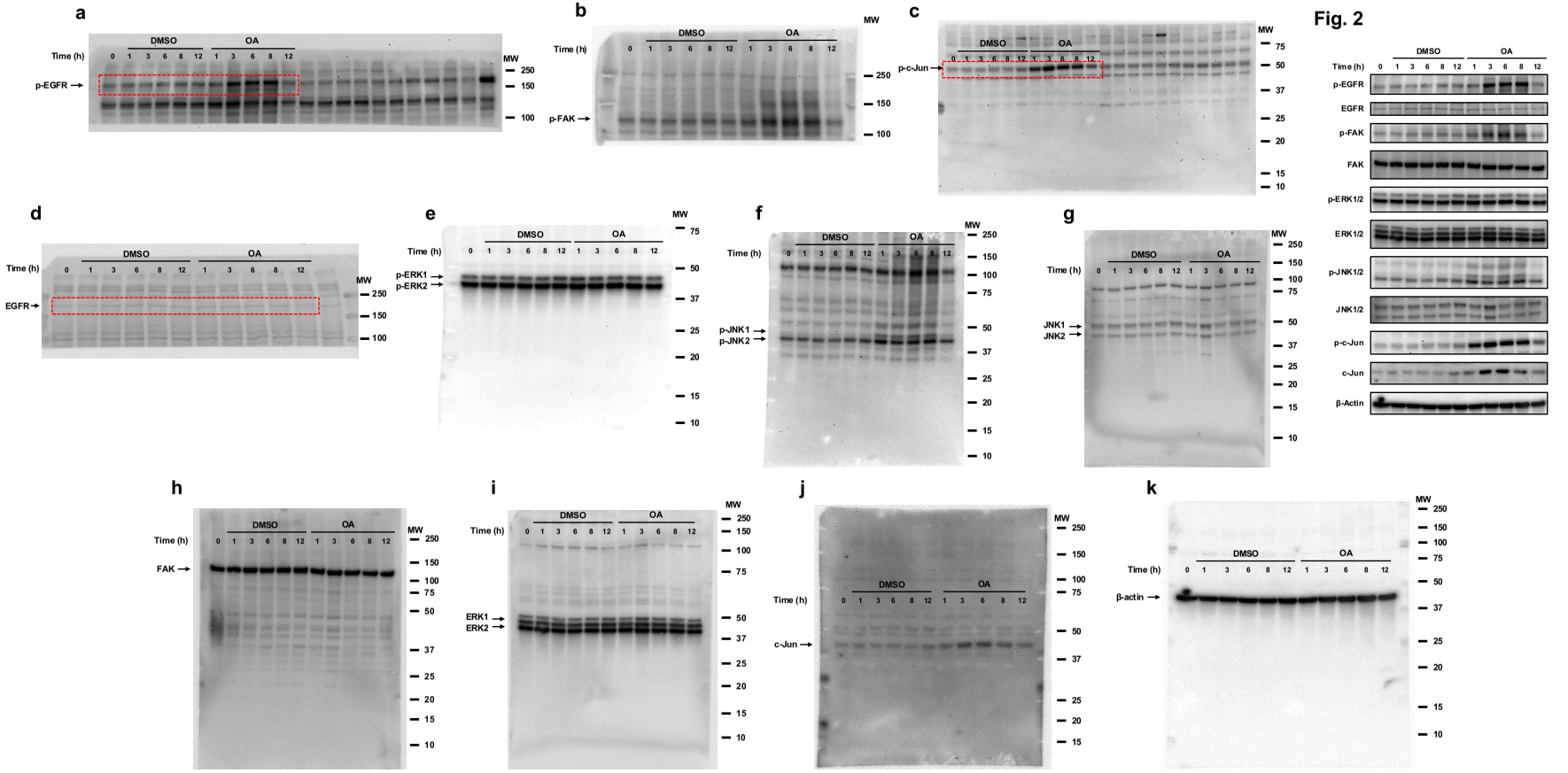

Supplemental Figure 10. Full-length blots corresponding to crops showed in Fig 2. (a) Tyr 1068 Phosphorylated-EGFR. (b) Tyr 925 Phosphorylated-FAK. (c) Ser 63 Phosphorylated c-Jun. (d) EGFR. (e) Thr 202/Tyr 204 Phosphorylated ERK. (f) Thr 183/Tyr 185 Phosphorylated JNK. (g) JNK1/2. (h) FAK. (i) ERK1/2. (j) c-Jun. (k) Beta-actin loading. Dashed red rectangle indicates the portion of the blot that was used in the figure.

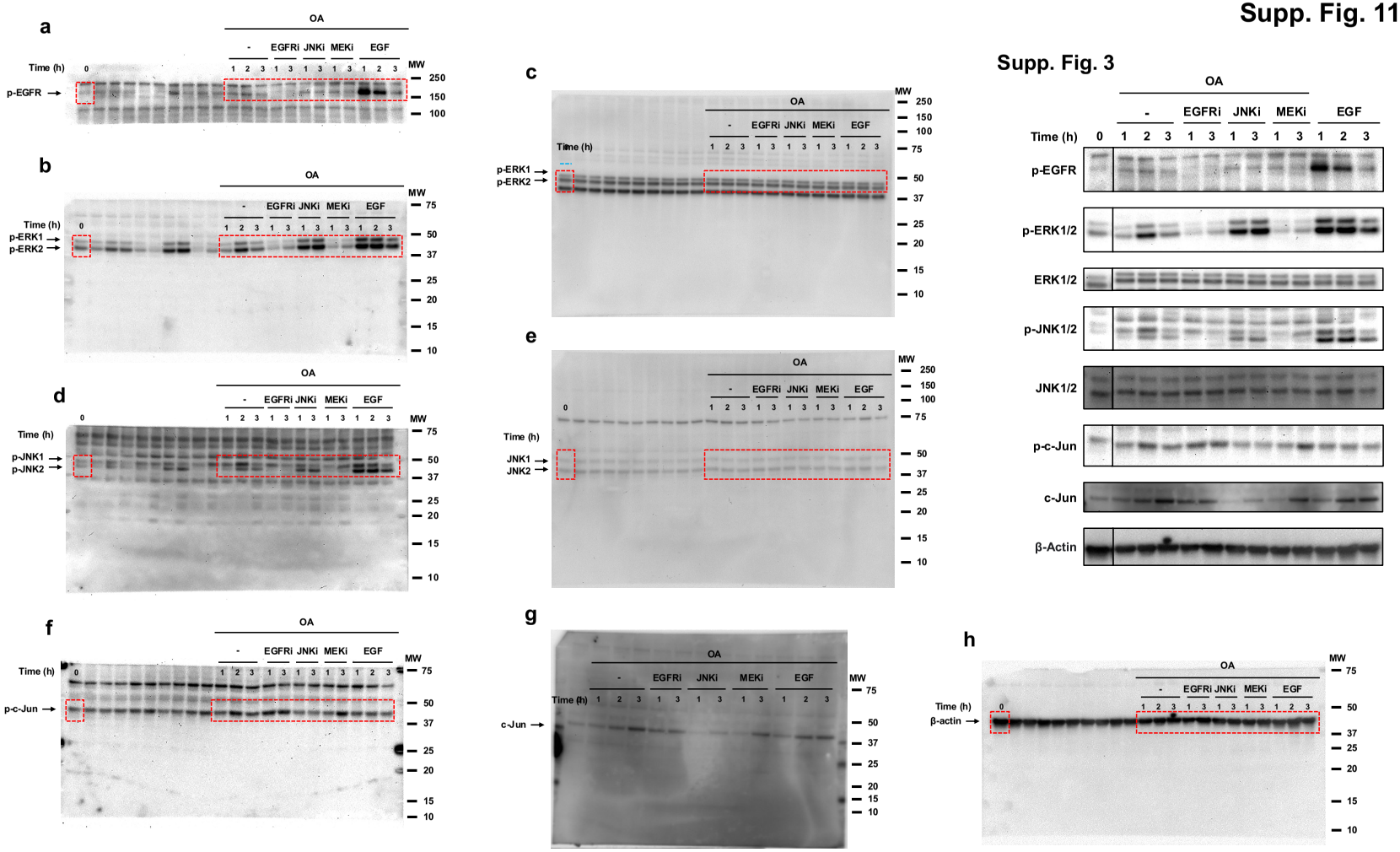

Supplemental Figure 11. Full-length blots corresponding to crops showed in Supplemental Figure 3. (a) Tyr 1068 Phosphorylated-EGFR. (b) Thr 202/Tyr 204 Phosphorylated ERK. (c) ERK1/2. (d) Thr 183/Tyr 185 Phosphorylated JNK. (e) JNK1/2. ((f) Ser 63 Phosphorylated c-Jun. (g) c-Jun. (h) Beta-actin loading. Dashed red rectangle indicates the portion of the blot that was used in the figure.

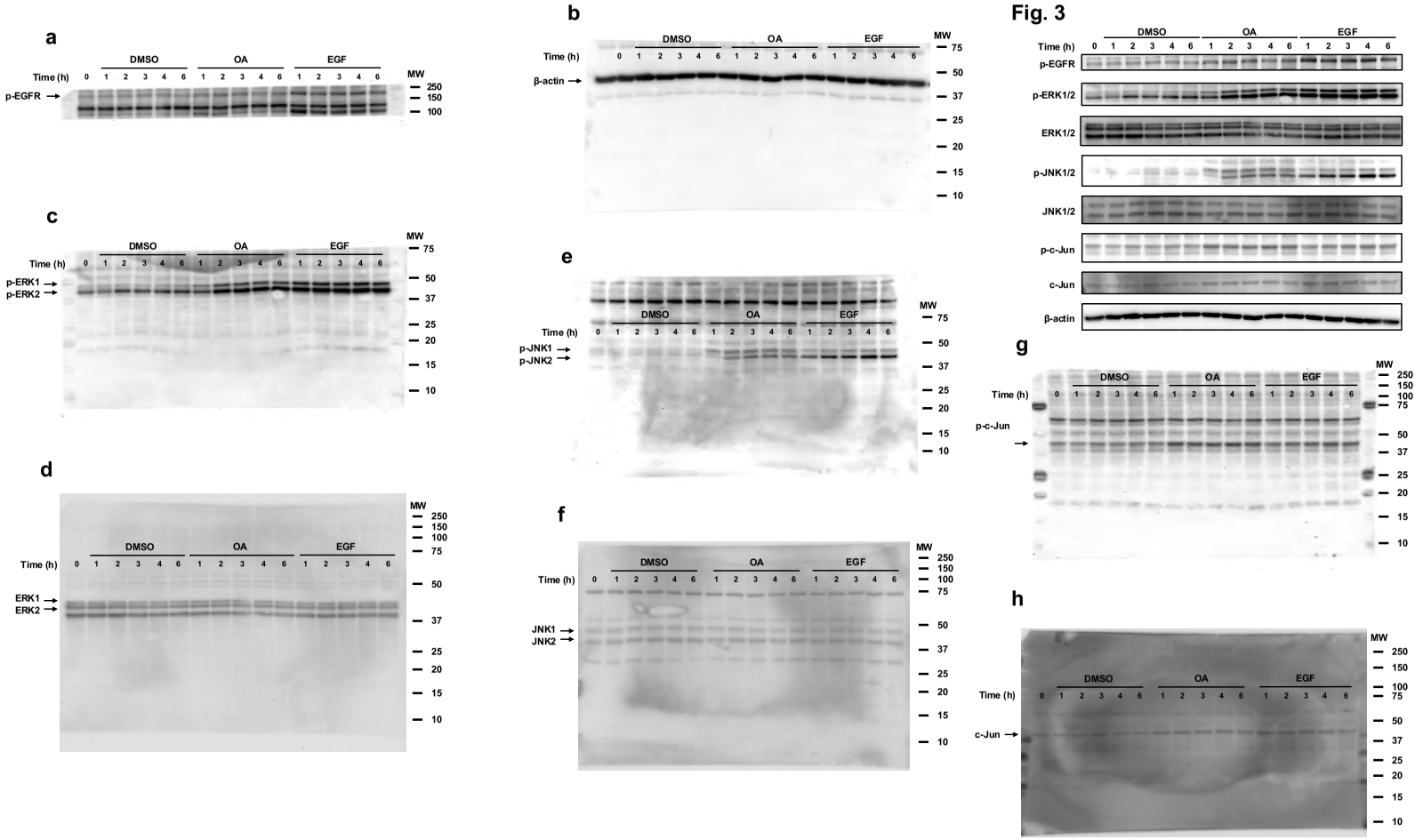

Supplemental Figure 12. Full-length blots corresponding to crops showed in Fig 3. (a) Tyr 1068 Phosphorylated-EGFR. (b) Beta-actin loading. (c) Thr 202/Tyr 204 Phosphorylated ERK. (d) ERK1/2. (e) Thr 183/Tyr 185 Phosphorylated JNK. (f) JNK1/2. (g) Ser 63 Phosphorylated c-Jun. (h) c-Jun.

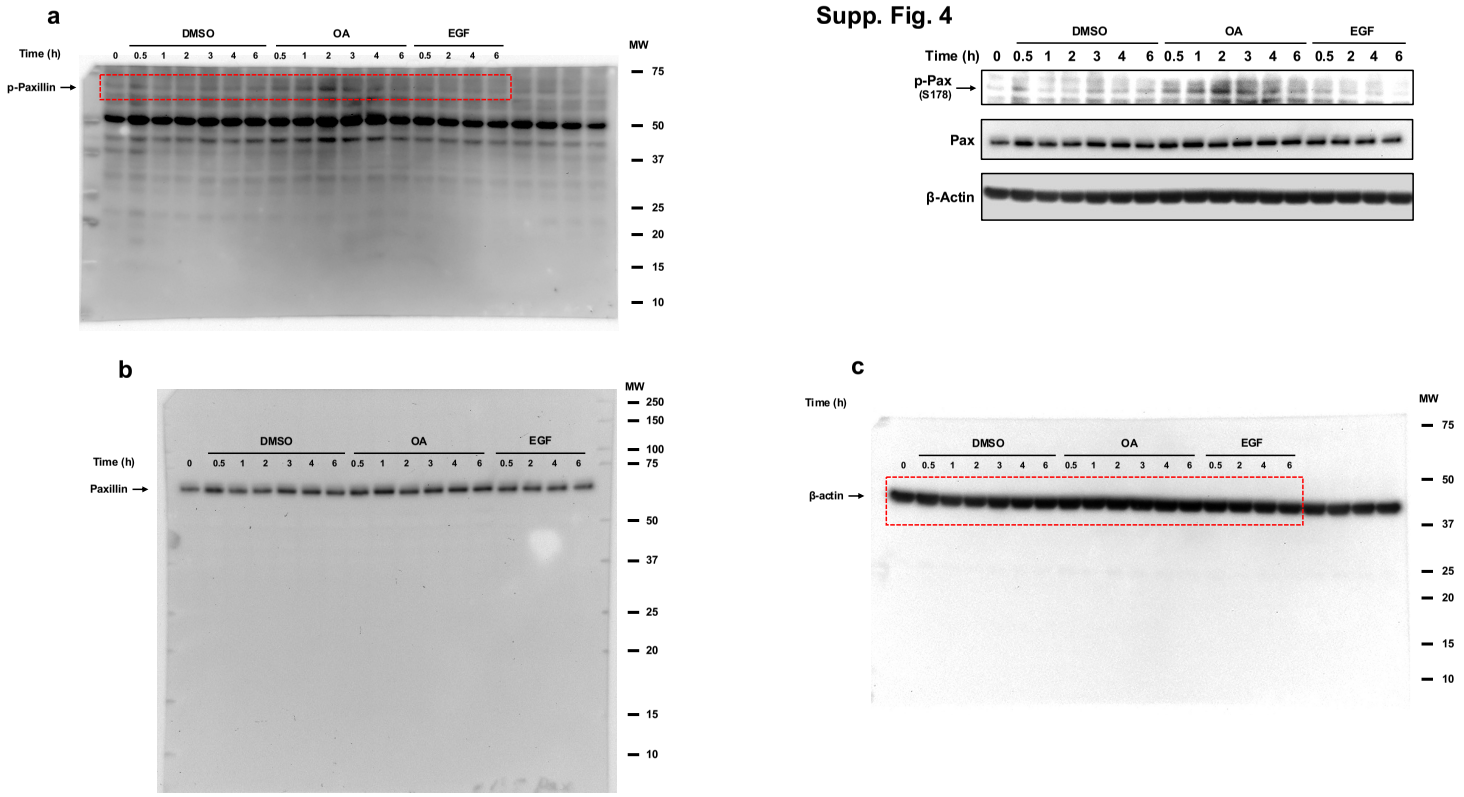

Supplemental Figure 13. Full-length blots corresponding to crops showed in Supplemental Figure 4. (a) Ser 170 Phosphorylated-Paxillin. (b) Paxillin. (c) Beta-actin loading. Dashed red rectangle indicates the portion of the blot that was used in the figure.

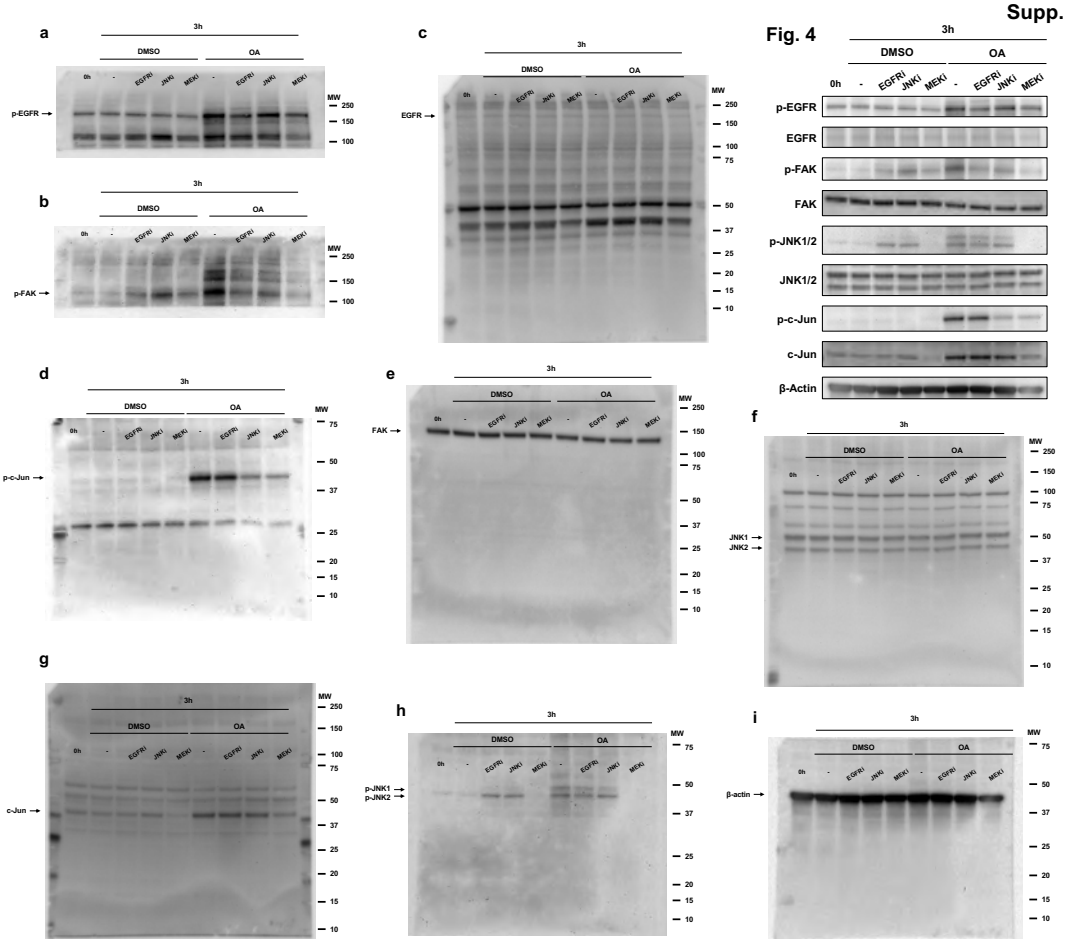

Supplemental Figure 14. Full-length blots corresponding to crops showed in Fig 4. (a) Tyr 1068 Phosphorylated-EGFR. (b) Tyr 925 Phosphorylated-FAK. (c) EGFR. (d) Ser 63 Phosphorylated c-Jun. (e) FAK. (f) JNK. (g) c-Jun. (h) Thr 183/Tyr 185 Phosphorylated JNK. (i) Beta-actin loading.

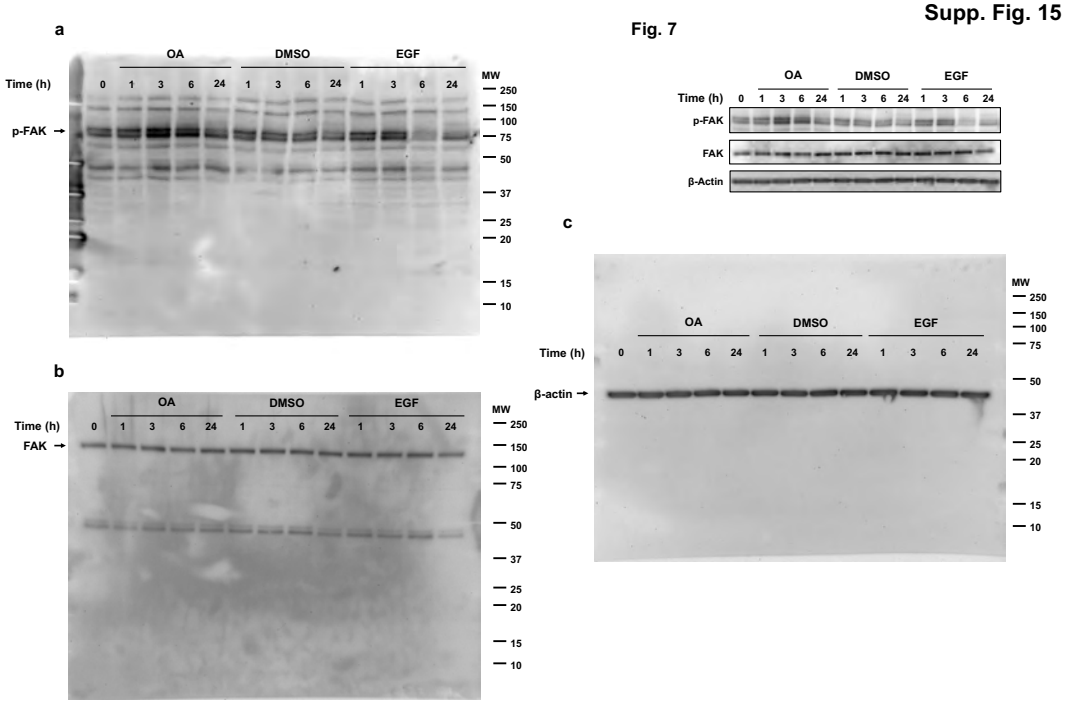

Supplemental Figure 15. Full-length blots corresponding to crops showed in Fig 7. (a) Tyr 925 Phosphorylated-FAK. (b) FAK. (c) Beta-actin loading.

4.2. ARTICLE 2: OLEANOLIC ACID RESCUES CRITICAL FEATURES OF UMBILICAL VEIN ENDOTHELIAL CELLS PERMANENTLY AFFECTED BY HYPERGLYCEMIA

Stelling-Férez J, Cappellacci I, Assunta P, Gabaldón JA, Pipino C, Nicolás FJ. (2023). **Oleanolic acid recues critical features of umbilical vein endothelial cells permanently affected by hyperglycemia**. *Frontiers in Endocrinology*, 14:1308606. doi: 10.3389/fendo.2023.1308606

frontiers | Frontiers in Endocrinology

TYPE Original Research
PUBLISHED 13 December 2023
DOI 10.3389/fendo.2023.1308606

OPEN ACCESS

EDITED BY
Pasquale Mone,
University of Molise, Italy

REVIEWED BY
Fahimeh Varzideh,
Albert Einstein College of Medicine, United States
Urna Kansakar,
Albert Einstein College of Medicine, United States
Antonio de Donato,
BioGeM Institute, Italy

*CORRESPONDENCE
Caterina Pipino
caterina.pipino@unich.it
Francisco José Nicolás
franciscoj.nicolas2@carm.es

RECEIVED 06 October 2023
ACCEPTED 23 November 2023
PUBLISHED 13 December 2023

CITATION
Stelling-Férez J, Cappellacci I, Pandolfi A, Gabaldón JA, Pipino C and Nicolás FJ (2023) Oleanolic acid rescues critical features of umbilical vein endothelial cells permanently affected by hyperglycemia. *Front. Endocrinol.* 14:1308606. doi: 10.3389/fendo.2023.1308606

Oleanolic acid rescues critical features of umbilical vein endothelial cells permanently affected by hyperglycemia

Javier Stelling-Férez[1,2], Ilaria Cappellacci[3], Assunta Pandolfi[3], José Antonio Gabaldón[1], Caterina Pipino[3]* and Francisco José Nicolás[2]*

[1]Department of Nutrition and Food Technology, Health Sciences PhD Program, Universidad Católica de Murcia (UCAM), Murcia, Spain, [2]Regeneration, Molecular Oncology, and TGF-β, IMIB-Pascual Parrilla, Hospital Clínico Universitario Virgen de la Arrixaca, Murcia, Spain, [3]Department of Medical, Oral and Biotechnological Sciences, StemTeCh Group, Center for Advanced Studies and Technology-CAST (ex CeSI-MeT), University G. D'Annunzio Chieti-Pescara, Chieti, Italy

Skin wound healing is a physiological process that involves several cell types. Among them, endothelial cells are required for inflammation resolution and neo-angiogenesis, both necessary for tissue restoration after injury. Primary human umbilical vein endothelial cells (C-HUVECs) are derived from the umbilical cord. When women develop gestational diabetes, chronic exposure to hyperglycemia induces epigenetic modifications in these cells (GD-HUVECs), leading to a permanent pro-inflammatory phenotype and impaired angiogenesis in contrast to control cells. Oleanolic acid (OA) is a bioactive triterpenoid known for its epithelial cell migration promotion stimulation and higher tensile strength of wounds. However, the potentially anti-inflammatory and pro-angiogenic properties of OA are still under investigation. We tested OA on C- and GD-HUVECs under inflammatory conditions induced by low levels of the inflammatory cytokine TNF-α. Reduced expression of adhesion molecules *VCAM1*, *ICAM1*, and *SELE* was obtained in OA-pre-treated C- and GD-HUVECs. Additionally, protein VCAM1 levels were also decreased by OA. Coherently, monocyte adhesion assays showed that a lower number of monocytes adhered to GD-HUVEC endothelium under OA pre-treatment when compared to untreated ones. It is noteworthy that OA improved angiogenesis parameters in both phenotypes, being especially remarkable in the case of GD-HUVECs, since OA strongly rescued their poor tube formation behavior. Moreover, endothelial cell migration was improved in C- and GD-HUVECs in scratch assays, an effect that was further confirmed by focal adhesion (FA) remodeling, revealed by paxillin staining on immunocytochemistry assays. Altogether, these results suggest that OA could be an emergent wound healing agent due to its capacity to rescue endothelial malfunction caused by hyperglycemia.

KEYWORDS

oleanolic acid, endothelial cells, angiogenesis, inflammation, chronic hyperglycemia, adhesion molecules

Introduction

During wound healing, epithelial cell migration is a crucial process to close and repair the skin barrier (1, 2). In pathological conditions, a physiologic impairment that halts wound healing may occur. Therefore, new treatments that could enhance or accelerate cell migration are currently of great interest. Oleanolic acid (OA), a bioactive triterpenoid present in a wide variety of plants, has shown promising effects on wound healing due to its cell migration activity on epithelial cells (3–7). Thus, OA activates epidermal growth factor receptor (EGFR), enabling a complex MAP kinase system, which in turn triggers c-Jun phosphorylation and overexpression, a key transcription factor that enhances a gene expression cell migration program (7, 8). Besides these molecular effects, OA also changes elements of the epithelial cell architecture. OA promotes the assemble–disassemble turnover of focal adhesions (FAs) together with the actin and paxillin remodeling, a dynamic state that is evidence of cell migration (7, 9–11).

The findings of effects of OA on epithelial cells encouraged us to explore the role of this bioactive compound on other wound healing players, closely related to epithelial cells and their migration. In an acute wound, to reach wound closure, sequential phases must occur with the involvement of different cell types. The proliferative phase and the remodeling phase are critical for a correct wound resolution (12). These two stages need to take place after a correct inflammation mitigation in the wound, which is produced after skin injury and defines the inflammatory phase (13). At this point, in the injured blood vessels of the wound, endothelial cells respond by expressing adhesion molecules on the endothelium surface in order to facilitate the recruitment of immune cells to the wound site. In particular, they recruit immune cells that are known for their reparative properties, such as M2 macrophages and type T lymphocytes, which release anti-inflammatory cytokines to modulate the wound inflammation milieu (14). The adequate resolution of this phase allows the wound to progress into the subsequent proliferative and remodeling phases, including angiogenesis and tissue regeneration. During angiogenesis, endothelial cells proliferate, migrate, and form a tube for the correct supply of nutrients, oxygen, and growth factors to the newly formed wound bed (15, 16). Briefly, angiogenesis is critical and occurs with cell migration during the proliferative and remodeling phases, supporting skin reepithelization.

However, when the wound is subjected to continuous inflammation, the other stages come to a halt, resulting in a chronic, non-healing wound that may progress to an ulcer (17, 18). Indeed, there are many causes that trigger this condition, including trauma, burns, infections, or underlying chronic diseases such as diabetes (19). In fact, diabetes is one of the leading causes of impaired wound healing, and represents a complex issue due to its socioeconomic impact and the elevated number of patients (20, 21). For instance, one of its most severe complications is diabetic foot ulcer (DFU), in which the patient's ulcer shows poor reepithelization and vascularization, leading to the amputation of the limb (20).

Diabetic ulcers display an excessive inflammatory response and deficient angiogenesis due to endothelium malfunction, which causes delayed healing and uncontrolled scar tissue formation (22–24). Thus, the use of *in vitro* cell models that can mimic endothelium diabetic features seems very relevant to studying possible strategies or agents that help rescue endothelial cells from this condition, and eventually restore their regular function. This is the case of human umbilical cord vein endothelial cells (HUVECs) exposed to hyperglycemia during pregnancy in mothers affected by gestational diabetes (GD) (25). Interestingly enough, this unique endothelial cell model (GD-HUVECs) displays an altered phenotype that has been exhaustively studied and described (26). Although regular primary HUVECs are a well-known *in vitro* model to study the process and molecular mechanisms related to inflammation and neo-angiogenesis (27, 28), GD-HUVECs are permanently damaged by hyperglycemia, thus showing a senescent pro-inflammatory phenotype that leads to endothelial dysfunction (26). Therefore, GD-HUVECs are a suitable model to study and to try to rescue an endothelium that is affected by diabetic ulcers and causes either a delay or even a halt on wound healing. Indeed, previous studies have shown that OA attenuates adhesion molecule overexpression under inflammation stimuli in C-HUVECs (29, 30). Nevertheless, it might be very interesting to carry out these studies on GD-HUVECs, which are endothelial cells experiencing a pathologic condition.

In this article, we have investigated the effects of OA on C-HUVECs and GD-HUVECs. Our results show that OA attenuates inflammatory responses, improves migration, and favors tube formation in both types of cells. Furthermore, these aspects are especially relevant in GD-HUVECs.

Materials and methods

HUVEC isolation and culture

All procedures adhered to the ethical standards of the Institutional Committee on Human Experimentation (reference number 1879/09COET) and to the principles of the Declaration of Helsinki. The protocol used was approved by the Institutional Review Board and informed consent was signed by every participating subject. Primary endothelial cells were collected from umbilical cord veins (HUVECs) of newborns delivered between the 36th and the 40th gestational week at the Hospital of Chieti and Pescara (Italy) from randomly selected Caucasian mothers affected by GD or not (control, C) following previously published methods (31). Briefly, veins of the umbilical cords were immediately collected after delivery, cannulated and perfused with 1 mg/mL collagenase 1A at 37°C. Obtained HUVECs were isolated in a base medium composed of DMEM/M199 (1:1) supplemented with 1% L-glutamine, 1% penicillin/streptomycin, and 20% fetal bovine serum (FBS) (all from Biowest, Nuaillé, France). Then, the cell suspension was centrifuged at 1,200 rpm for 10 min, and the cell pellet was re-suspended in HUVEC base medium and plated on 1.5% gelatin-coated (Sigma-Aldrich, St Louis, MO, USA) tissue culture flasks. HUVECs were confirmed by the presence of specific markers such as von Willebrand factor, CD31 and CD34 positive, together with the induced expression of cell adhesion molecules

ICAM1, VCAM1, and E-selectin, and cytokines IL-6 and IL-8 under pro-inflammatory stimuli, as well as the formation of cord-like structures on Matrigel (25, 32). For all experiments, the cells were used *in vitro* between the 3rd and 5th passage, never exceeding the 5th passage. The HUVECs selected for the assays were grown on 1.5% gelatin-coated tissue culture plates in HUVEC complete medium: low-glucose (1 g/L) DMEM and M199 medium (ratio 1:1), supplemented with 10 µg/mL heparin (Sigma-Aldrich, St Louis, MO, USA), 50 µg/mL endothelial cell growth factor (ECGF), 20% FBS, 1% penicillin/streptomycin, and 1% L-glutamine. All experiments were performed, at least, in technical triplicate, using three different cellular strains (n = 3) of C- and GD-HUVECs.

Oleanolic acid preparation

OA (purity > 97%) (Merck, Darmstadt, Germany) was solubilized to a 25 mM final concentration in dimethyl sulfoxide (DMSO) (Sigma-Aldrich, St Louis, MO, USA). Assay concentrations are indicated for each experiment in figure legends. MTT assays were performed in C- and GD-HUVECs prior to functional assays, in order to optimize the OA/DMSO effect (see Supplementary Figure 1). In all the assays, DMSO concentration never exceeded 1% to avoid cytotoxic effects.

RNA extraction and quantitative PCR

C- and GD-HUVECs were seeded in 5-cm-diameter Petri dishes coated with 1.5% gelatin in HUVEC complete medium. When cells reached sub-confluence (60%), cells were pre-treated for 24 h with OA or DMSO (basal condition) in HUVEC complete medium with 10% FBS. After this, a 2-h serum-starvation period was established in HUVEC serum-starvation medium: low-glucose (1 g/L) DMEM with 0.1% FBS, supplemented with 10 µg/mL heparin, 50 µg/mL endothelial cell growth factor (ECGF), 0.3% bovine serum albumin (BSA, from Sigma-Aldrich, St Louis, MO, USA), 1% penicillin/streptomycin, and 1% L-glutamine. After serum starvation, cells were treated with TNF-α at 1 ng/mL, using this concentration for subsequent assays as well (28, 33, 34). Then, cells were incubated for 2, 6, and 24 h to induce the gene expression of adhesion molecules: vascular cell adhesion molecule 1, *VCAM1*, intercellular adhesion molecule 1, *ICAM1*, and, E-selectin, *SELE*. At the times indicated above, RNA was extracted using the RNeasy-mini system (Qiagen, Venlo, The Netherlands). Usually, 800 ng of RNA from independent samples was retro-transcribed using iScript reagents (Bio-Rad, Hercules, CA, USA). The obtained cDNA was used for quantitative PCR (qPCR) using the SYBR premix ex Taq kit (Takara Bio Europe/Clontech, Saint-Germain-en-Laye, France) according to the manufacturer's protocol. The primers used for the analyzed genes related to inflammation are indicated in Table 1. For gene expression analysis, qPCR cycles were normalized with glyceraldehyde 3-phosphate dehydrogenase (*GAPDH*) gene expression according to the $2^{-\Delta\Delta Ct}$ method (35). The experiment was carried out on four different strains for C-HUVECs and four different strains for GD-HUVECs, each in technical triplicate. Analyzed data represent mean ± SEM.

MTT assay

The effects of increasing concentrations of OA on C-HUVEC and GD-HUVEC viability were assessed with the 3-(4,5-dimethylthiazolyl-2)-2, 5-diphenyltetrazolium bromide (MTT, Sigma-Aldrich) method (36). C- and GD-HUVECs were seeded in 96-well microplates, 2×10^4 cells/cm^2 (approximately 6500 cells per well), coated with 1.5% gelatin in HUVEC complete medium. When cells reached sub-confluence (80%), a 24-h serum-starvation period was established in HUVEC serum-starvation medium (0.1% FBS). After this, cells were treated with vehicle control DMSO or OA, as indicated in Supplementary Figure 1, in 0.5% FBS media. After 24-h incubation, 20 µL of MTT 5 mg/mL in PBS was added to each well. Plates were incubated for 3 h at 37 °C and finally the absorbance at 540 nm was detected by a microplate reader (SpectraMAX 190, Molecular Devices, Sunnyvale, CA, USA).

Western blot

C- and GD-HUVECs were seeded in 5-cm-diameter Petri dishes coated with 1.5% gelatin in HUVEC complete medium. When cells reached sub-confluence (60%), cells were pre-treated for 24 h with OA or DMSO (basal) in HUVEC complete medium with 10% FBS. After this, a 2-h serum-starvation period (0.1% FBS) was established in HUVEC serum-starvation medium. Then, cells were treated with TNF-α (1 ng/mL) for 1, 3, 6, or 24 h to induce inflammation. At the indicated times, cells were collected, washed twice with cold PBS, and lysed with 20 mM Tris, pH 7.5, 150 mM NaCl, 1 mM EDTA, 1.2 mM $MgCl_2$, 0.5%, Nonidet p-40, 1 mM DTT, 25 mM NaF, and 25 mM β-glycerophosphate supplemented

TABLE 1 Different primers used to study the expression of several genes.

Gene name (GeneCards)/ Primer name	Primer sequence 5′-3′
GAPDH Fwd	AGCTCAGGCCTCAAGACCTT
GAPDH Rev	AAGAAGATGCGGCTGACTGT
ICAM1 Fwd	ACCATCTACAGCTTTCCG (Sigma KiCqStart)
ICAM1 Rev	TCACACTTCACTGTCACC (Sigma KiCqStart)
SELE Fwd	GAGAATTCACCTACAAGTCC (Sigma KiCqStart)
SELE Rev	AGGCTTGAACATTTTACCAC (Sigma KiCqStart)
VCAM1 (mix Fwd/Rev)	Proprietary sequence (Qiagen QuantiTect®) QT00018347

GADPH, glyceraldehyde-3-phosphate dehydrogenase; ICAM1, intercellular adhesion molecule 1; SELE, E-Selectin; VCAM1, vascular cell adhesion molecule 1.

with phosphatase inhibitor cocktails (I and II) and protease inhibitors (all from Sigma-Aldrich, St Louis, MO, USA). Total protein amount of all samples was measured and normalized by Bradford assay (37) (Sigma-Aldrich, St Louis, MO, USA). Samples were analyzed by SDS-PAGE followed by Western blot using the indicated antibodies (see the *Antibodies* section). Blots were revealed by using horseradish peroxidase substrate (ECL) (GE Healthcare, GE, Little Chalfont, United Kingdom) and images were taken with a ChemiDoc MP (Bio-Rad, Hercules, CA, USA). To quantify Western blot protein bands, pictures in 8-bit format were processed in ImageJ software. In every picture, a lane was established for each sample. In each lane, only the band with the specific size (kDa) of the protein of interest was quantified. For each total protein and its phosphorylated form, each band's intensity peak was plotted, and subsequently, the area under the plot was measured by using "Wand tool" of ImageJ to finally obtain pixel intensity value. In order to normalize data, obtained intensity values were referred to those of the unphosphorylated form of the protein (total) or a loading control protein (β-actin) if the unphosphorylated form was undetectable (non-available antibody for the unphosphorylated form).

Monocyte-HUVEC adhesion assay

C- and GD-HUVECs were seeded in six-well plates (200,000 cells/well) coated with 1.5% gelatin in HUVEC complete medium until they reached 60% confluence. At this time, cells were pre-treated for 24 h with 20 μM OA in HUVEC complete medium with 10% FBS. When confluent, a 2-h serum-starvation period was established washing and adding HUVEC serum starvation media. After this, cells were stimulated with TNF-α (1 ng/mL) for 16 h. The U937 monocyte cell line (European Collection of Authenticated Cell Cultures, ECACC) was used to evaluate the adhesion to C- and GD-HUVEC monolayers, as previously described (28, 33, 34). Briefly, the medium was removed from each HUVEC well, cells were gently washed with DMEM, and a suspension with 1 million monocytes was added to each well. Plates were incubated for 20 min, with gentle shaking at room temperature. Finally, to remove non-adhered monocytes, HUVECs were gently washed and fixed with 1% paraformaldehyde. To identify the number of adherent monocytes for each tested strain, 12 counts were performed for every experimental condition (by using at least three different randomly selected high-power fields, at 10× magnification) using Paula Nuc microscope (Leica Microsystems, Wetzlar, Germany). Images were acquired by using Paula software version 1.2.2. For this experiment, four different strains of both C-HUVECs and GD-HUVECs were used.

Matrigel tube formation assay

C- and GD-HUVECs were seeded on 12-well plates coated with growth factor-reduced basement membrane matrix gel, known as Matrigel (BD Biosciences, Franklin Lakes, NJ, USA) all in 10% FBS HUVEC complete medium. A number of 1.4×10^5 cells/well was the suitable amount for the assay. After plating, cells were incubated for 15 min at 37°C to induce cellular adhesion to Matrigel. Then, 20 μM OA and DMSO equivalent volume as control were ready to add to cells. After 6 h, representative images were taken using a Paula Nuc microscope (Leica Microsystems, Wetzlar, Germany). Images were processed and measured by ImageJ software. In this software, "Angiogenesis Analyzer" plugin (38) was used to analyze key neo-angiogenesis markers: number of isolated segments, total length of isolated branches, number of master segments, number of meshes, number of nodes, number of segments, number of master junctions, total length of branches, and total length. The data presented are the data gathered from four C-HUVEC strains and four GD-HUVEC strains.

Wound healing scratch assay

C- and GD-HUVECs were grown in 24-well plates coated with 1.5% gelatin until they reached 100% confluence in HUVEC complete medium. At this point, a serum-starvation period was performed in 1% FBS HUVEC serum starvation medium for 24 h. Cells were scratched using a sterile p-40 μL pipette tip and then the resulting wounds were gently washed with free-FBS DMEM low glucose to remove released cells. Treatments were performed in the plates by adding DMSO and 20 μM OA in 0.5% FBS media. Additionally, 20% FBS was added as a positive control. After 12 h, the assay was stopped by fixing the cells with 4% formaldehyde (Applichem GmbH, Darmstadt, Germany) in PBS (Biowest, Nuaillé, France) for 10 min. Finally, cells were washed twice with PBS. Pictures were taken at 10× magnification using an optical microscope equipped with a digital camera (Motic Optic AE31, Motic Spain, Barcelona, Spain). Areas in the wounds at 0 h and 12 h were measured by ImageJ software. The initial cell area (0 h) was subtracted from the final cell area (12 h) and plotted in a graph as migration percentage (39).

Focal adhesion quantification assay

C- and GD-HUVECs were grown on round-glass coverslips coated with 1.5% gelatin until they were sub-confluent (60%) in HUVEC complete medium. At this time, cells were washed with serum-deprived medium and then treated with 20 μM OA and DMSO equivalent volume (basal) in 0.1% FBS HUVEC starvation medium. After 24-h incubation, coverslips were fixed with 4% formaldehyde (Applichem GmbH, Darmstadt, Germany) in PBS (Biowest, Nuaillé, France) for 10 min and washed twice with PBS. Then, cells were permeabilized with 0.3% Triton X-100 (Sigma-Aldrich, St Louis, MO, USA) in PBS for 10 min. For immunostaining, a 30-min blocking was performed in PBS solution with 10% FBS, 5% skim milk (Beckton Dickinson, Franklin Lakes, NJ, USA), 0.3% bovine serum albumin (BSA, Sigma-Aldrich, St Louis, MO, USA) and 0.1% Triton X-100. Subsequently, cells were incubated for 1 h with anti-paxillin antibody, diluted in the above-mentioned blocking solution without skim milk. Proper fluorescent-labeled secondary

antibodies (see the *Antibodies* section) were co-incubated for 30 min with Alexa Fluor 594 conjugated phalloidin (Molecular Probes, Thermo Fisher Scientific, Waltham, MA, USA) and Hoechst 33258 (Fluka, Biochemika, Sigma-Aldrich, St Louis, MO, USA) to reveal actin cytoskeleton and nuclei, respectively. Once the immunostaining was completed, representative pictures were acquired with a confocal microscope at 40x magnification (LSM 510 META from ZEISS, Jena, Germany). The setting of images was performed using Zeiss Efficient Navigation (ZEN) interface software (ZEISS, Jena, Germany). The "Z stack" ZEN tool was used in order to observe deep cytoskeleton structures (paxillin), taking picture slices along the *Z* axis. Then, picture slices were merged by the "Maximum intensity projection" ZEN tool. FA quantification was carried out as previously described by using CLAHE and Log3D macros for ImageJ (40). Essentially, FAs were quantified from paxillin-stained acquired pictures. We used four different replicates for each condition. Specifically, cell filopodia were selected as regions of interest (ROIs) and the resulting areas (containing FAs) were considered for further analysis. A number of five filopodia were considered from each picture. Then, the number of FAs were calculated in each filopodia by using the previously mentioned macros. The obtained number was divided by the total filopodia area to determine FA density in the cells.

Antibodies

The following commercial primary antibodies were used: 1:1,000 anti-phospho-NF-κB (Cell Signaling Technology, Danvers, MA, USA); 1:1,000 anti-NF-kB and 1:1,000 anti-VCAM1 (Abcam, Cambridge, United Kingdom); 1:200 anti-paxillin (Santa Cruz Biotechnology, Heidelberg, Germany); and 1:4,000 anti-β-actin (Sigma-Aldrich, St Louis, MO, USA). Secondary antibodies were as follows: 1:1,000 anti-rabbit IgG Horseradish peroxidase linked F(ab')2 I fragment (from donkey) (GE Healthcare, GE, Little Chalfont, United Kingdom); 1:3,000 anti-mouse IgG1 (BD Pharmingen, Beckton Dickinson, Franklin Lakes, NJ, USA); and 1:400 Alexa Fluor 488 conjugated anti-mouse (from donkey) (Thermo Fisher Scientific, Rockford, IL, USA).

Statistical analysis

The gathered data were represented and analyzed using GraphPad Prism v7 software. Classical statistical parameters were calculated and statistical tests were performed with a 95% confidence interval. Consequently, in each test, *p*-values lower than 0.05 were considered to be statistically significant. At the figure legends, asterisks indicate statistically significant differences between assay conditions (*$p < 0.05$, **$p < 0.005$, ***$p < 0.001$, and ****$p < 0.0001$). Data were analyzed by a one-way ANOVA test, comparing the mean of each condition with the mean of every other condition. Subsequently, a Tukey's multiple comparisons test was performed. *p*-values lower than 0.05 indicate statistically significant differences between the means of conditions.

Results

Oleanolic acid attenuates adhesion molecule overexpression induced by TNF-α in C- and GD-HUVEC

Adhesion molecule expression on endothelial cell surface is needed for immune cell recruitment to endothelial surface and, finally, migration to the inflammation source at the wound (41). However, an uncontrolled recruitment triggers endothelium dysfunction (42). Adhesion molecule gene expression, which is upregulated in endothelial cells in response to the pro-inflammatory cytokine TNF-α, was tested on HUVECs. Both C- and GD-HUVECs were treated with 20 μM OA and then TNF-α stimulated for the indicated times. On the whole, no gene expression differences were detected after 24 h pre-treatment with OA (Supplementary Figure 1) (0 h). Generally speaking, adhesion molecule expression in untreated C- and GD-HUVECs showed a strong response by TNF-α at 2 and 6 h in all genes tested. However, beginning with the *VCAM1* gene (Figure 1A), a patent attenuation with OA was detected at 2 and 6 h in both C- and GD-HUVECs. Strikingly, this reduction was even more significant in GD-HUVECs at 6 h. Regarding *ICAM1* (Figure 1B), this OA-dependent decrease was less patent but remained significant, mostly at 6 h, in C- and GD-HUVECs. The expression of the third adhesion molecule tested *SELE* (Figure 1C) also showed a strong attenuation with OA, which was more patent in the GD phenotype. At 24 h, in both types of endothelial cells and both conditions, all adhesion molecules showed a drop in their expression; therefore, we could not see any statistically significant differences.

Subsequently, we studied VCAM1 total protein amount in C- and GD-HUVECs using the same experimental design (Figure 2). At basal conditions, total VCAM1 protein levels were detected in both cell lines after 3 h of TNF-α stimulation, showing its highest level at 6 h, whereas 24 h later, the levels plummeted. To begin with, GD-HUVECs showed higher protein levels than control ones. Interestingly, C- and GD-HUVEC lysates with OA pre-treatment showed significantly lower total VCAM1 protein levels than control, which suggested a strong OA attenuation on the TNF-α stimulation. Endothelial cell stimulation with TNF-α induces the expression of adhesion molecules through the participation of nuclear factor-κB (NF-κB) that is phosphorylated at Ser 536 and then translocates to the nucleus where it activates the expression of *VCAM1*, among others (43–45). However, when Ser 536 phosphorylated NF-κB was assayed in response to TNF-α stimulation, no significant differences were found between 20 μM OA treated and non-treated C- or GD-HUVECs. Only a slight decrease of phospho-NF-κB level was noticed in C-HUVECs after 24 h OA stimulation and only in the TNF-α sample.

All these data suggest that OA attenuates the expression of VCAM1 protein and of the *VCAM1, SELE*, and *ICAM1* genes in response to TNF-α in HUVECs regardless of its glucose-affected condition.

10.3389/fendo.2023.1308606

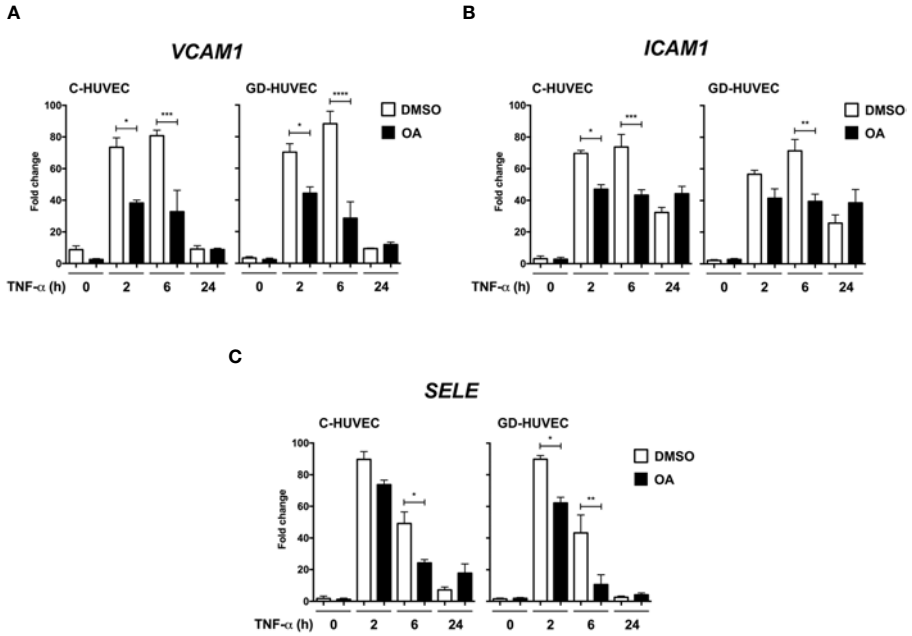

FIGURE 1
Oleanolic acid reduces the expression of adhesion molecule genes induced by TNF-α. Gene expression analysis of **(A)** *VCAM-1*, **(B)** *ICAM-1*, and **(C)** *SELE* in C- and GD-HUVECs pre-treated 24 h with 20 μM OA (black) or DMSO equivalent volume (white, DMSO). After pre-treatments, cells were stimulated with TNF-α at 2, 6, and 24 h. Histograms represent mRNA relative expression of each gene (normalized with GAPDH expression) for both C- and GD-HUVECs. Each condition represents the mean ± SEM using four different strains for C-HUVECs and four other different strains for GD-HUVECs. Asterisks indicate statistically significant differences between the selected conditions according to a one-way ANOVA statistical analysis (*$p < 0.05$, **$p < 0.005$, ***$p < 0.001$ and ****$p < 0.0001$).

Oleanolic acid reduces the number of monocytes adhered to GD-HUVECs

Given the attenuation effect of OA on adhesion molecule expression, a monocyte adhesion assay was conducted on C- and GD-HUVEC monolayers (Figure 3). HUVECs pre-treated or not with OA were subjected to 16 h TNF-α, to study whether the OA effect on adhesion molecules correlated with the number of monocytes adhered to their surface. When C- and GD-HUVECs were stimulated with TNF-α, there was a clear increase in the number of adhered monocytes, which was slightly higher on GD-HUVECs (Figure 3). Interestingly, OA pre-treatment decreased the number of monocytes in both C- and GD-HUVECs (Figure 3) before and after treatment with TNF-α.

Overall, this functional assay reveals less monocyte–endothelial interaction triggered by TNF-α in both C- and GD-HUVECs when the cells are previously treated with OA.

Oleanolic acid improves neo-angiogenesis in GD-HUVECs

Matrigel tube formation assay with HUVEC is a well-established and informative test to evaluate the angiogenesis function of endothelial cells *in vitro* (28, 38, 46). C- and GD-HUVECs were seeded in Matrigel and treated with OA for 6 h. Representative pictures indicated a greater network complexity in both HUVEC phenotypes under OA conditions (Figure 4A); however, the possible effects of OA on the GD-HUVEC versus the C-HUVEC were difficult to interpret. To gain more knowledge about angiogenesis features with OA, nine key parameters related to this meshed network were measured (Figure 4B). The number of isolated segments were higher in GD- compared to C-HUVEC, as it was reduced with OA. Similarly, total length of isolated branches was reduced with OA in GD-HUVEC. In addition, the number of master segments, which were affected in GD-HUVEC, was ameliorated with OA. Finally, both the number of master junctions and total length of branches were deficient in GD-HUVEC when compared to C-HUVEC. In all cases, the presence of OA produced and improvement of the parameters. Finally, the number of nodes, the number of segments and total length, all representing the complexity of the network, were all increased by OA in both C- and GD-HUVEC, but showed a more powerful effect on GD-HUVEC.

Altogether, GD-HUVEC exhibited poor performance for most of the measured tube-formation parameters. Generally, the quantification of all these parameters suggested that OA generally improved angiogenesis, with clear healing tendencies for the GD-HUVECs.

Oleanolic acid enhances C- and GD-HUVEC migration

Cell migration, a crucial process in wound healing to restore skin integrity, is enhanced by OA in epithelial cells (7, 8).

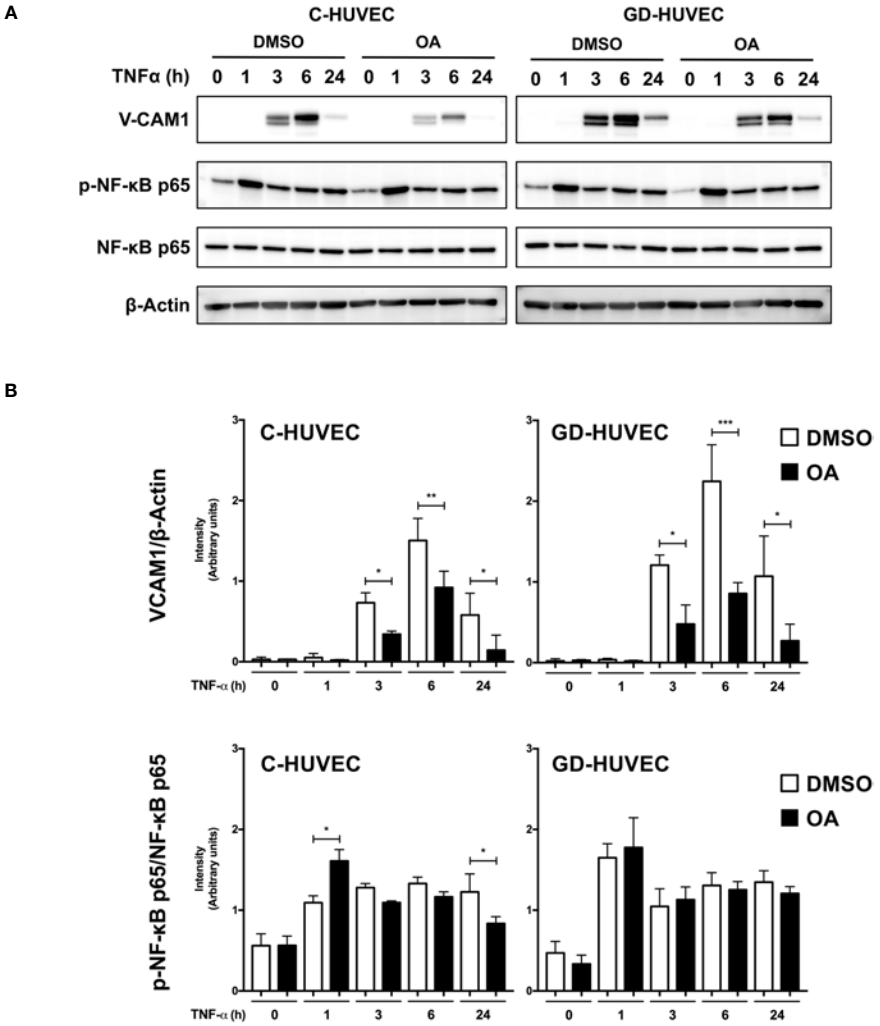

FIGURE 2
Oleanolic acid reduces total VCAM1 protein expression in C- and GD-HUVECs induced by TNF-α. **(A)** Total protein extracts from sub-confluent C- and GD-HUVECs pre-treated with 20 μM OA or DMSO equivalent volume, and then stimulated with TNF-α at 1, 3, 6, and 24 h. These extracts were assayed at these times targeting the following: VCAM1, phospho-NF-κB, and NF-κB. β-Actin was used as a loading control. A representative experiment is shown. **(B)** Column bar graphs represent intensity values of each protein assayed by Western blot, by collecting the data of four C-HUVEC and four GD-HUVEC strains. Intensity values were quantified and gathered by ImageJ software. Asterisks indicate statistically significant differences between the selected conditions according to a one-way ANOVA statistical analysis: (*$p < 0.05$, **$p < 0.005$, and ***$p < 0.001$).

Interestingly enough, migration also contributes to the organization and formation of new vessels (47). Therefore, we performed scratch assays on confluent C- and GD-HUVECs to see whether OA could also have this effect on endothelial cells. C- and GD-HUVECs were scratched and allowed to migrate for 12 h in the presence of OA (Figure 5A). Strikingly, OA activity promoted the migration of both C- and GD-HUVECs from the wound edges, since the wound gap area was surrounded with endothelial cells. To better comprehend the level of this promoting effect of OA, cell migration was quantified measuring the resulting areas of the wounds (Figure 5B). Thus, the obtained migration percentages in both C- and GD-HUVECs were clearly significant between basal condition and OA. Interestingly, 20% FBS was used as a positive control of cell migration, but the resulting migration with GD-HUVEC under this condition was significantly lower than with OA.

Given these results with wound healing scratch assays on HUVECs, OA showed cell migration promoting effects on endothelial cells that could probably enhance the wound healing process together with neo-angiogenesis.

Oleanolic acid increases focal adhesion number in C- and GD-HUVECs and their dynamization

It is known that OA-triggered molecular effects on cell migration include the role of cell architecture, by dynamizing actin cytoskeleton and FA remodeling (9, 48, 49). We performed immunocytochemistry assays in sub-confluent C- and GD-HUVECs targeting actin fibbers (F-actin) and paxillin to reveal

10.3389/fendo.2023.1308606

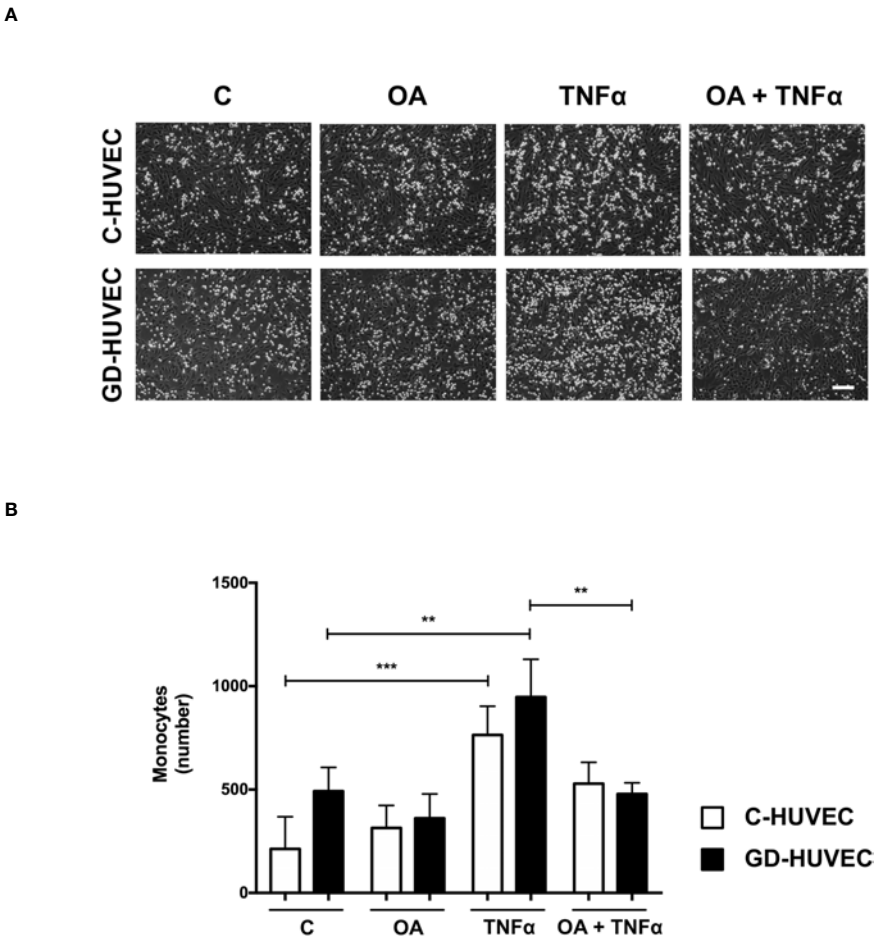

FIGURE 3
Oleanolic acid reduces the number of monocytes adhered to C- and GD-HUVECs. **(A)** For monocyte adhesion experiment, C- and GD-HUVEC monolayers were left untreated unless otherwise indicated (OA), where they were pre-treated with 20 μM OA for 24 h. Subsequently, TNF-α was added for 16 h to either untreated or OA pre-treated HUVECs (TNF-α and OA+TNF-α conditions). At this point, monocytes were added and the experiment was completed. Representative pictures of C- and GD-HUVECs are shown for each condition. **(B)** Graph represents the number of adhered U937 monocytes in each field of 12 fields. Each condition represents the mean ± SEM obtained from the data collection of four different strains for both C-HUVECs and GD-HUVECs. Asterisks indicate statistically significant differences between the selected conditions according to a one-way ANOVA statistical analysis (*$p < 0.05$, **$p < 0.001$). The scale bar indicates 100 μm.

FAs. With regard to cell morphology, untreated C- and GD-HUVECs exhibited a morphology related to a stressed condition due to the low amount of FBS (0.1%), with no apparent FA-like structures (Figure 6A). By contrast, C- and GD-HUVECs treated with OA displayed filopodia and lamellipodia garnished with FAs. Actin fibers were also modified by OA presence, because they were encompassing the newly formed filopodia and lamellipodia in response to OA. Interestingly and in line with this, the quantified FA density, revealed by paxillin staining, exhibited a significant increase in OA-treated C- and GD-HUVECs versus untreated ones (Figure 6B). This increase was even more significant in GD-HUVECs than in C-HUVECs.

Actin fiber and FA data revealed that HUVECs changed their cell architecture during OA-stimulated cell migration, thus suggesting a high dynamization of the migration-related machinery in both C- and GD-HUVECs.

Discussion

The results of this study provide intriguing insights into the effects of OA treatment on C- and GD-HUVECs in the context of inflammation and angiogenesis.

Plant-derived bioactive compounds present in various dietary sources have been widely studied for their significant effects to rescue endothelial cell function (50–52). Their antioxidant, anti-inflammatory, vasodilatory, angiogenic, and protective properties collectively contribute to the preservation of vascular health and the prevention of endothelial dysfunction-associated diseases (53–55). Indeed, a large number of these bioactive molecules or peptides modulate the signaling pathway of nuclear factor-kappa B (NF-κB), which is needed for adhesion molecules and pro-inflammatory cytokine expression (43, 56). For instance, studies have shown that carotenoids lycopene and β-carotene have anti-inflammatory

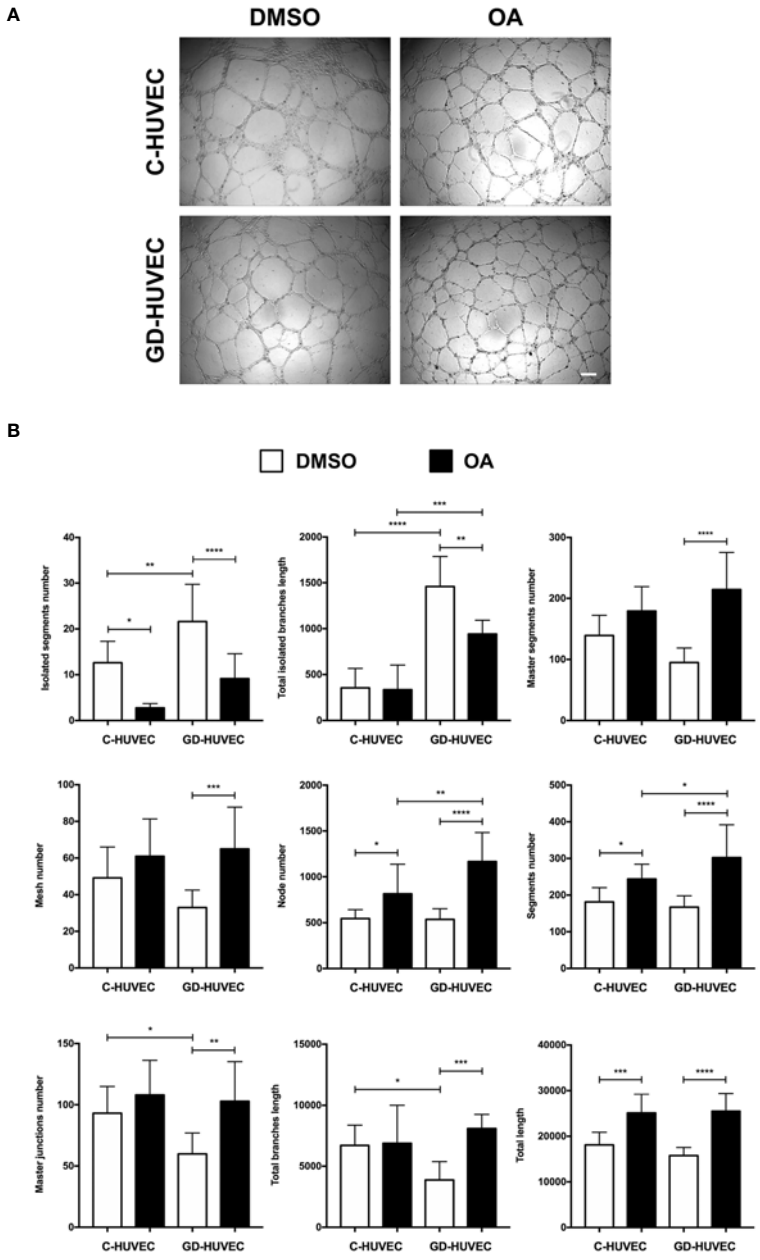

FIGURE 4
Effect of OA on tube-like structure formation capacity on Matrigel. Tube-like structure formation ability on Matrigel after 6-h treatment with 20 μM OA; a DMSO equivalent volume was added as control condition. **(A)** Representative pictures of C- and GD-HUVECs for both experimental conditions. Scale bar indicates 200 μm. **(B)** Graphs representing multiple angiogenic parameters analyzed: number of isolated segments, total length of isolated branches, number of master segments, number of meshes, number of nodes, number of segments, number of master junctions, total length of branches, and total length. Each bar in the plot represents the mean ± SEM using three different strains for C-HUVECs and also three for GD-HUVECs. Asterisks indicate statistically significant differences between the selected conditions according to a one-way ANOVA statistical analysis (*$p < 0.05$, **$p < 0.005$, ***$p < 0.001$, and ****$p < 0.0001$).

effects on both C- and GD-HUVECs (31, 33). Indeed, the addition of these carotenoids under TNF-α stimulation show less monocyte–endothelial cell interaction, enhanced by less ICAM1 and VCAM1 membrane exposure and total expression. All these effects depend on the attenuation that these carotenoids have on NF-κB phosphorylation and translocation to the cell nucleus (31, 33). In fact, the effects of pentacyclic triterpenes, OA, and its isomers ursolic acid (UA) and maslinic acid (MA) are similar to carotenoids and have been addressed *in vitro* by using regular HUVEC phenotype. Thus, these studies showed attenuation effects on adhesion molecule expression under inflammation conditions (29, 30, 57). However, there are no studies so far on the effects of OA on hyperglycemia-modified cells (GD-HUVECs), which have remarkably impaired functionality. Moreover, the concentration of serum used in those assays was not always clarified, a factor that is critical to properly study OA effects *in vitro*, since serum proteins

10.3389/fendo.2023.1308606

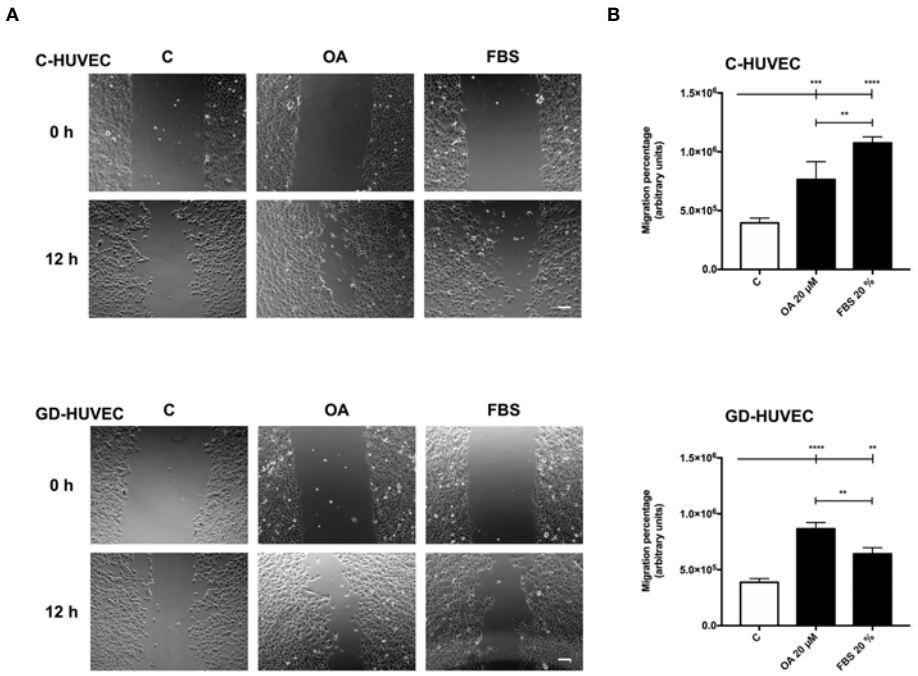

FIGURE 5
Oleanolic acid induces C- and GD-HUVEC migration in wound healing scratch assays. Confluent C- and GD-HUVECs were scratched with a pipette tip and allowed to migrate for 12 h. **(A)** Representative images of the wound healing assay with cell migration under basal conditions (control, C), compared to those with 20 µM OA after 24-h treatment. A condition with 20% FBS was added as positive-migration control. Scale bar indicates 200 µm. **(B)** Graphs represent C- and GD-HUVEC migration as the difference between areas at 0 h and 12 h in each condition, named as migration percentage. Asterisks indicate statistically significant differences between conditions according to a one-way ANOVA statistical analysis (**$p < 0.005$, ***$p < 0.001$, and ****$p < 0.0001$).

buffer OA activity and modify its optimal concentration of use (7, 8). Indeed, OA effects and bioavailability depend on the final OA concentration, the cell type used, and the serum concentration. High concentrations of OA produce cytotoxic and antiproliferative effects, while low concentrations do not produce any beneficial effect on cells (8, 58, 59). This is the reason why, in the present study, an MTT assay was conducted with C- and GD-HUVECs under the lowest possible serum concentration (0.5% FBS). In this way, a 20 µM OA concentration was established seeking a compromise between the optimal effects of OA and the abolition of the serum buffer effect, together with cell viability compatibility.

Furthermore, it should be noted that OA treatments, followed by TNF-α induction, should be performed at longer incubation times to unravel OA ameliorative effects on inflammation (30). Indeed, the highest expression of adhesion molecules *ICAM1*, *VCAM1*, and *SELE* in C- and GD-HUVECs was detected at 2 h and 6 h after TNF-α addition, thus showing a clear inflammatory profile. Strikingly, pre-treating the same endothelial cells with OA before TNF-α clearly attenuated adhesion molecule overexpression by the cytokine, especially on *VCAM1* and *SELE*. In addition to this, the preventive effect produced by OA was even more patent in GD-HUVECs, probably because of their senescent phenotype and endothelial dysfunction (26). Interestingly enough, in the case of *ICAM1*, at 24 h, gene expression levels were not fully abrogated by OA in C- and GD-HUVECs. This could be explained by other functions of this integrin, since controlled levels of ICAM1 on the cell surface are needed during wound healing to promote endothelial cell migration, thus leading to neo-angiogenesis (60). In particular, *VCAM1* showed the strongest attenuation by OA in C- and GD-HUVECs, and also showed decreased protein amount. However, we saw a window transient effect of TNF-α, since VCAM1 levels decreased at 24 h. Despite this, we still observed the mitigating effect of OA on VCAM1 protein levels. It should be highlighted that *in vitro* assays have this limitation, because, in a tissue with chronic inflammation, we would see sustained high levels of VCAM1 and other adhesion molecules due to the constant production of TNF-α and other pro-inflammatory cytokines (61). VCAM1 is endothelium-specific and this TNF-α inducible molecule is necessary for monocyte extravasation (44). NF-κB activation by its phosphorylation on the p65 subunit is required to promote adhesion molecule expression in the cell nucleus, such as *VCAM1*, among others (43). Although we observed lower VCAM1 protein levels with OA pre-treatment, we did not observe any differences on phospho-NF-κB p65. In contrast, in a similar set of experiments, the precondition of HUVECs with amniotic membrane was able to reduce the levels of phosphorylation of phospho-Ser-536 NF-κB p65 in response to TNF-α, which was coherent with an attenuation of the NF-κB p65 nuclear translocation and a reduction of the expression of *VCAM1* (28). Thus, our results have to be explained by the fact that the OA attenuation effect on VCAM1 could be due to different molecular mechanisms or also to the way it is synthesized. In fact, it has been

10.3389/fendo.2023.1308606

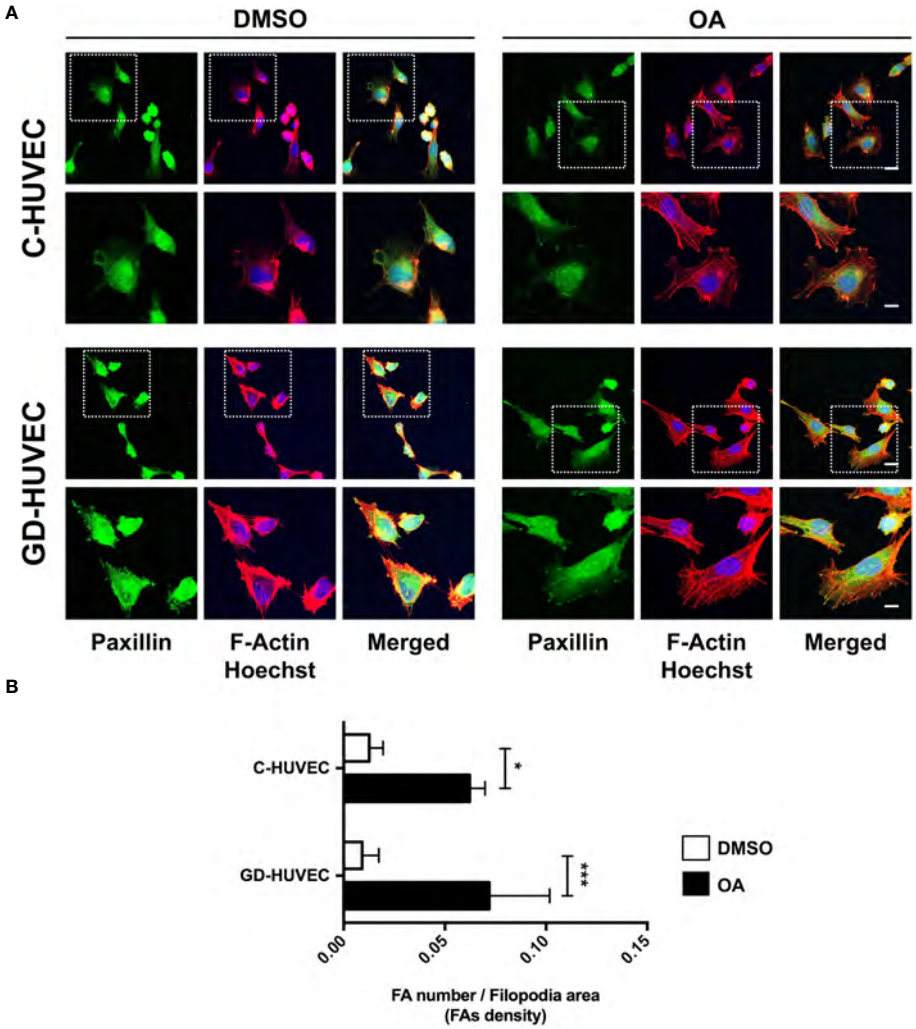

FIGURE 6
Oleanolic acid triggers focal adhesion remodeling in C- and GD-HUVECs revealed by paxillin. **(A)** Sub-confluent C- and GD-HUVECs were treated for 24 h with 20 μM OA and DMSO equivalent volume. Cells were immunostained with specific antibodies against paxillin. Co-staining with phalloidin and Hoechst-33258 was used to show actin cytoskeleton and nuclei, respectively. Paxillin: green. Actin fibers (F-Actin): red. Nuclei: blue. Images obtained with a confocal microscope at 63× magnification and their corresponding insets for a detailed view of paxillin structures. This experiment was repeated at least three times. 63× picture scale bar indicates 25 μm. Inset scale bar indicates 5 μm. **(B)** Column bar graphs show the quantification of the density of FAs (as FA number per filopodia area). Asterisks indicate statistically significant differences between conditions according to a one-way ANOVA statistical analysis (*$p < 0.05$ and ***$p < 0.001$).

shown that UA, an OA isomer, blocks VCAM1 traffic to the membrane (62). Another possibility could be that the amount of anchored-membrane VCAM1 is regulated by proteases, where specifically TNF-α converting enzyme (TACE/ADAM17) proteolyzes this molecule and releases it to the extracellular medium (44). Therefore, OA could be enhancing TACE/ADAM17 protease activity on VCAM1, thus decreasing its protein levels in endothelial cells. However, a complicated regulation must be involved, since the expression of *VCAM1* is effectively attenuated by the presence of OA. A more plausible, although uncertain, mechanism of regulation could be related to something different from NF-κB transcription factor or even its phosphorylation at Ser 536 residue. Further research is necessary to better clarify the mechanism behind *VCAM1* regulation in this context.

An excessive release of TNF-α in chronic inflammation conditions produces the overexpression of adhesion molecules on the endothelium surface. As a consequence, the uncontrolled adhesion and transmigration of immune cells occur, thus triggering endothelial cell apoptosis (42). E-selectin acts at the first steps of monocyte recruiting to produce their tethering and rolling (63). Then, integrins ICAM1 and VCAM1 secure the adhesion and allow monocyte extravasation to the injured wound (64). In a chronic wound, the high recruitment of monocytes leads to an uncontrolled population of M1 macrophages in the wound, which have hyperinflammatory, reduced phagocytic activity, and increase oxidative stress (14). By

contrast, a regular recruitment of monocyte population swings toward M2 macrophages, with anti-inflammatory, regenerative, and tissue remodeling properties, all in line with a healing wound (14). OA effects regarding monocyte adhesion are strongly coherent with the observed changes of adhesion molecule levels. In the context of either chronic or diabetic wounds, OA-reduced levels of VCAM1 on endothelial cells surely imply a better inflammation resolution.

Diabetes negatively affects angiogenesis (22, 24). Considering tube formation assays, GD-HUVEC exhibited a poorer tube formation; for instance, the number and length of isolated segments in basal condition was higher in GD-HUVEC. Strikingly, OA treatment clearly ameliorated this impairment in GD-HUVECs and, although more lightly, also in C-HUVECs. Coherently, positive features such as the number of master segments, the number of meshes, and the length of branches were significantly improved by OA only in GD-HUVECs. Indeed, this could be explained by the GD phenotype, which, in contrast to C-HUVEC, showed poorer performance for these parameters in basal conditions. This behaviour strongly suggests that OA restores GD-HUVEC to a more regular angiogenic phenotype, but does not intrinsically affect C-HUVEC's capability of achieving a full network. Overall, the network complexities achieved for both types of cells were higher with OA, as reflected by the observed incremented number of nodes, branches, master junctions, and the total length of the networks. These changes indicate that OA enhances all aspects of the complexity of the vascular network, which may have a positive impact on tissue regeneration in a complex healing wound milieu. Nonetheless, a good line of research could be testing the effects of OA on more complex systems, because tube formation assays on Matrigel do not compile/integrate endothelial cell interaction with other cell types, as happens during neo-angiogenesis in a real wound. Therefore, a 3D co-culture of endothelial cells with both primary fibroblasts and keratinocytes, which exhibit features more similar to natural skin, could be considered a good option to further assess the effects of OA on wound healing (65). Moreover, there are well-established *in vivo* angiogenesis assays that can unravel potential OA effects; for instance, one of the best is chorionallantoic membrane assays in chicken embryo, which are widely used in vascular biology (66). Regarding the potential molecular effects behind OA angiogenesis promotion, we would like to conduct future experiments in order to study the effects of OA on the stimulation of VEGFR-2, given its importance in angiogenesis (15, 67, 68), and due to the fact that OA has been directly involved in the activation of the similar function and structure receptor: EGFR (7, 8).

Cell migration is carried out by endothelial cells together with proliferation to enhance angiogenesis and vasculogenesis (69). According to the data of the scratch assays, OA was also capable of enhancing this process in both C- and GD-HUVECs to the same extent. However, FBS stimulation was unable to match the levels achieved by the OA stimulation for the GD phenotype. These data indicate that OA, but not FBS, rescues, in GD-HUVEC, an impaired migration mechanism resistant to the serum rescue. Thus, OA may trigger a particular molecular mechanism that is revealed only in the GD-HUVEC-impaired cells. Indeed, the quantification of FA density upon treatment with OA, detected by paxillin immunostaining, was stronger in GD-HUVECs than in C-HUVECs. Overall, the collected data of FAs strongly suggest that, generally, OA promotes a better endothelial cell movement to manage migration in both GD- and C-HUVECs. OA also contributes positively to angiogenesis by cell migration promotion, which is a favorable condition for tissue repair in a wound healing context (69).

Our findings suggest a clear OA ability to rescue the altered features of an endothelium affected by high blood sugar levels, which correlate with impaired metabolism and inflammation (25, 42, 70). It is well-known that, in order to ameliorate these processes, signaling pathways depending on the activation of G protein-coupled receptors (GPCRs) take place to protect cells from injury and malfunction. Concretely, the Takeda G protein-coupled receptor (TGR5), also known as Gpbbar1, is a transmembrane-type bile acid receptor that has been found to regulate a large number of specific molecular pathways (71, 72). Interestingly, TGR5 modulates inflammation by decreasing adhesion molecule expression in endothelial cells and blocking pro-inflammatory cytokines released by immune cells (71). Moreover, this receptor is also linked to tyrosine kinase receptor (RTK) transactivation by second messengers (73, 74). Strikingly, some evidence points out the interaction between OA, which has a similar chemical structure to bile acids, and TGR5, with OA behaving as a clear agonist of TGR5 (75). For these reasons, it is remarkable to suggest that probably all OA promotion and modulation effects related to monocyte adhesion, angiogenesis, and cell migration on C- and GD-HUVECs could be related to the interaction between TGR5 and OA. Thus, more research is needed to decipher this molecular mechanism, which may solve some of the conundrums revealed in our data. In addition, other mechanisms may be involved under OA effects regarding regulatory non-coding RNA expression, as microRNAs (miRs) have recently gained prominence due to their role in regulating several essential processes in endothelial cells (76, 77). For instance, it is shown that miR-4432 controls the expression of fibroblast growth factor binding protein 1 (FGFBP1), which is needed to preserve endothelial barrier function in the brain (78). On top of that, other studies reported that low expression levels of miR-145 and miR-885 cause thrombotic risk and mortality in COVID-19 patients; thus, the expression of these miRs in endothelial cells is critical to prevent a prothrombotic condition during the infection (79). Therefore, further studies focusing on OA's contribution to these miR expressions in endothelial cells seem very pertinent.

To sum up, this study sheds some light on the multifaceted effects of OA on inflammation, angiogenesis, and migration in C- and GD-HUVECs (Figure 7). The findings underline the potential of OA as a therapeutic agent for restoring vascular function and ameliorating inflammation excess in diabetic wounds. However,

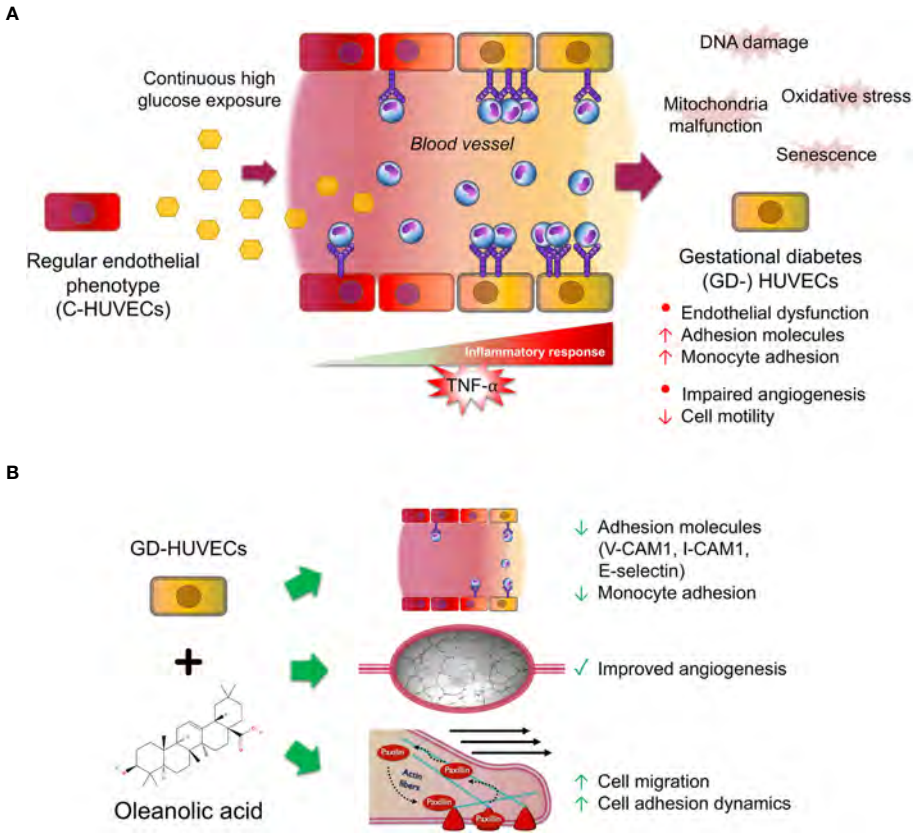

FIGURE 7
Oleanolic acid rescues multi-affected GD-HUVEC features caused by high blood glucose levels. **(A)** When regular endothelial cells (C-HUVECs) are exposed to a continuous high glucose exposure in blood vessels, several changes on their phenotype occur. These cells undergo the effects of high oxidative stress and damages on their DNA and mitochondria malfunction, thus triggering cellular senescence. As a result, these cells have an excessive and uncontrolled inflammation response when stimulated by pro-inflammatory cytokines such as TNF-α, triggering high adhesion molecule exposure on endothelium surface, subsequently displaying a high recruitment of circulating monocytes, and resulting in endothelial dysfunction. Moreover, these cells have an aberrant and limp tube formation (angiogenesis). **(B)** Strikingly, OA pre-treatment in GD-HUVECs before TNF-α addition attenuates key adhesion molecule overexpression of VCAM1, ICAM1, and E-selectin, resulting in less adhesion of the monocytes. Furthermore, OA displayed promotion effects on GD-HUVECs by restoring the impaired angiogenesis. Moreover, cell migration, a crucial process for angiogenesis, is also promoted by OA because it increases endothelial cell migration and adhesion dynamics by focal adhesion formation.

further research is needed to unravel the precise underlying molecular mechanisms driving these effects in order to evaluate the translational potential of OA clinical treatments for the management of complex wounds.

Data availability statement

The original contributions presented in the study are included in the article/Supplementary Material. Further inquiries can be directed to the corresponding authors.

Ethics statement

The studies involving humans were approved by Institutional Committee on Human Experimentation (reference number 1879/09COET). The studies were conducted in accordance with the local legislation and institutional requirements. The participants provided their written informed consent to participate in this study.

Author contributions

JS-F: Data curation, Formal Analysis, Investigation, Methodology, Writing – original draft, Writing – review & editing. IC: Data curation, Investigation, Methodology, Writing – review & editing. AP: Conceptualization, Data curation, Funding acquisition, Supervision, Validation, Writing – review & editing. JG: Funding acquisition, Project administration, Supervision, Writing – review & editing. CP: Conceptualization, Data curation, Investigation, Methodology, Supervision, Writing – review & editing. FN: Conceptualization, Funding acquisition, Investigation, Methodology, Project administration, Supervision, Validation, Writing – review & editing.

Funding

The author(s) declare financial support was received for the research, authorship, and/or publication of this article. The authors would like to acknowledge Hospital Clínico Universitario Virgen de la Arrixaca (HUVA, Murcia, Spain) and Hospitals of Chieti and Pescara (Italy), which supported and funded this research. JS-F was supported by a "Contrato Predoctoral para la Formación de Personal Investigador" from Universidad Católica de San Antonio de Murcia (UCAM) Projects "PI17/02164 and PI21/01339", funded by Instituto de Salud Carlos III (ISCIII) and co-funded by the European Union.

Acknowledgments

We want to thank people at Assunta Pandolfi's lab for technical support and helpful comments. Also, people at Francisco J. Nicolás' lab for helpful comments, reagents and support.

Conflict of interest

The authors declare that the research was conducted in the absence of any commercial or financial relationships that could be construed as a potential conflict of interest.

Publisher's note

All claims expressed in this article are solely those of the authors and do not necessarily represent those of their affiliated organizations, or those of the publisher, the editors and the reviewers. Any product that may be evaluated in this article, or claim that may be made by its manufacturer, is not guaranteed or endorsed by the publisher.

Supplementary material

The Supplementary Material for this article can be found online at: https://www.frontiersin.org/articles/10.3389/fendo.2023.1308606/full#supplementary-material

References

1. Vicente-Manzanares M, Horwitz AR. Cell migration: an overview. *Methods Mol Biol* (2011) 769:1–24. doi: 10.1007/978-1-61779-207-6_1

2. Trepat X, Chen Z, Jacobson K. Cell migration. *Compr Physiol* (2012) 2(4):2369–92. doi: 10.1002/cphy.c110012

3. Moura-Letts G, Villegas LF, Marcalo A, Vaisberg AJ, Hammond GB. *In vivo* wound-healing activity of oleanolic acid derived from the acid hydrolysis of Anredera diffusa. *J Nat Prod* (2006) 69(6):978–9. doi: 10.1021/np0601152

4. Pollier J, Goossens A. Oleanolic acid. *Phytochemistry* (2012) 77:10–5. doi: 10.1016/j.phytochem.2011.12.022

5. Ayeleso TB, Matumba MG, Mukwevho E. Oleanolic acid and its derivatives: biological activities and therapeutic potential in chronic diseases. *Molecules* (2017) 22 (11). doi: 10.3390/molecules22111915

6. Kuonen R, Weissenstein U, Urech K, Kunz M, Hostanska K, Estko M, et al. Effects of lipophilic extract of viscum album L. and oleanolic acid on migratory activity of NIH/3T3 fibroblasts and on haCat keratinocytes. *Evid Based Complement Alternat Med* (2013) 2013:718105. doi: 10.1155/2013/718105

7. Stelling-Ferez J, Gabaldon JA, Nicolas FJ. Oleanolic acid stimulation of cell migration involves a biphasic signaling mechanism. *Sci Rep* (2022) 12(1):15065. doi: 10.1038/s41598-022-17553-w

8. Bernabe-Garcia A, Armero-Barranco D, Liarte S, Ruzafa-Martinez M, Ramos-Morcillo AJ, Nicolas FJ. Oleanolic acid induces migration in Mv1Lu and MDA-MB-231 epithelial cells involving EGF receptor and MAP kinases activation. *PloS One* (2017) 12 (2):e0172574. doi: 10.1371/journal.pone.0172574

9. Turner CE. Paxillin and focal adhesion signalling. *Nat Cell Biol* (2000) 2(12): E231–6. doi: 10.1038/35046659

10. Schaller MD. Paxillin: a focal adhesion-associated adaptor protein. *Oncogene* (2001) 20(44):6459–72. doi: 10.1038/sj.onc.1204786

11. Schaks M, Giannone G, Rottner K. Actin dynamics in cell migration. *Essays Biochem* (2019) 63(5):483–95. doi: 10.1042/EBC20190015

12. Singer AJ, Clark RA. Cutaneous wound healing. *N Engl J Med* (1999) 341 (10):738–46. doi: 10.1056/NEJM199909023411006

13. Childs DR, Murthy AS. Overview of wound healing and management. *Surg Clin North Am* (2017) 97(1):189–207. doi: 10.1016/j.suc.2016.08.013

14. Aitcheson SM, Frentiu FD, Hurn SE, Edwards K, Murray RZ. Skin wound healing: normal macrophage function and macrophage dysfunction in diabetic wounds. *Molecules* (2021) 26(16):4917. doi: 10.3390/molecules26164917

15. Tonnesen MG, Feng X, Clark RA. Angiogenesis in wound healing. *J Investig Dermatol Symp Proc* (2000) 5(1):40–6. doi: 10.1046/j.1087-0024.2000.00014.x

16. Guerra A, Belinha J, Jorge RN. Modelling skin wound healing angiogenesis: A review. *J Theor Biol* (2018) 459:1–17. doi: 10.1016/j.jtbi.2018.09.020

17. Menke NB, Ward KR, Witten TM, Bonchev DG, Diegelmann RF. Impaired wound healing. *Clin Dermatol* (2007) 25(1):19–25. doi: 10.1016/j.clindermatol.2006.12.005

18. Qing C. The molecular biology in wound healing & non-healing wound. *Chin J Traumatol.* (2017) 20(4):189–93. doi: 10.1016/j.cjtee.2017.06.001

19. Schultz GS, Sibbald RG, Falanga V, Ayello EA, Dowsett C, Harding K, et al. Wound bed preparation: a systematic approach to wound management. *Wound Repair Regen.* (2003) 11 Suppl 1:S1–28. doi: 10.1046/j.1524-475X.11.s2.1.x

20. Greenhalgh DG. Wound healing and diabetes mellitus. *Clin Plast Surg* (2003) 30 (1):37–45. doi: 10.1016/S0094-1298(02)00066-4

21. Ferreira MC, Tuma P Jr., Carvalho VF, Kamamoto F. Complex wounds. *Clinics (Sao Paulo).* (2006) 61(6):571–8. doi: 10.1590/S1807-59322006000600014

22. Burgess JL, Wyant WA, Abdo Abujamra B, Kirsner RS, Jozic I. Diabetic wound-healing science. *Medicina (Kaunas).* (2021) 57(10):1072. doi: 10.3390/medicina57101072

23. Stachura A, Khanna I, Krysiak P, Paskal W, Wlodarski P. Wound healing impairment in type 2 diabetes model of leptin-deficient mice-A mechanistic systematic review. *Int J Mol Sci* (2022) 23(15):8621. doi: 10.3390/ijms23158621

24. Okonkwo UA, DiPietro LA. Diabetes and wound angiogenesis. *Int J Mol Sci* (2017) 18(7):1419. doi: 10.3390/ijms18071419

25. Di Fulvio P, Pandolfi A, Formoso G, Di Silvestre S, Di Tomo P, Giardinelli A, et al. Features of endothelial dysfunction in umbilical cord vessels of women with gestational diabetes. *Nutr Metab Cardiovasc Dis* (2014) 24(12):1337–45. doi: 10.1016/j.numecd.2014.06.005

26. Di Tomo P, Alessio N, Falone S, Pietrangelo L, Lanuti P, Cordone V, et al. Endothelial cells from umbilical cord of women affected by gestational diabetes: A suitable in *vitro* model to study mechanisms of early vascular senescence in diabetes. *FASEB J* (2021) 35(6):e21662. doi: 10.1096/fj.202002072RR

27. Medina-Leyte DJ, Domínguez-Pérez M, Mercado I, Villarreal-Molina MT, Jacobo-Albavera L. Use of human umbilical vein endothelial cells (HUVEC) as a model to study cardiovascular disease: A review. *Appl Sci* (2020) 10(3):938. doi: 10.3390/app10030938

28. Pipino C, Bernabe-Garcia A, Cappellacci I, Stelling-Ferez J, Di Tomo P, Santalucia M, et al. Effect of the human amniotic membrane on the umbilical vein endothelial cells of gestational diabetic mothers: new insight on inflammation and angiogenesis. *Front Bioeng Biotechnol* (2022) 10:854845. doi: 10.3389/fbioe.2022.854845

29. Lee W, Yang EJ, Ku SK, Song KS, Bae JS. Anti-inflammatory effects of oleanolic acid on LPS-induced inflammation in *vitro* and in vivo. *Inflammation* (2013) 36(1):94–102. doi: 10.1007/s10753-012-9523-9

30. Takada K, Nakane T, Masuda K, Ishii H. Ursolic acid and oleanolic acid, members of pentacyclic triterpenoid acids, suppress TNF-alpha-induced E-selectin

expression by cultured umbilical vein endothelial cells. *Phytomedicine* (2010) 17 (14):1114–9. doi: 10.1016/j.phymed.2010.04.006

31. Ucci M, Di Tomo P, Tritschler F, Cordone VGP, Lanuti P, Bologna G, et al. Anti-inflammatory role of carotenoids in endothelial cells derived from umbilical cord of women affected by gestational diabetes mellitus. *Oxid Med Cell Longev* (2019) 2019:8184656. doi: 10.1155/2019/8184656

32. Unger RE, Krump-Konvalinkova V, Peters K, Kirkpatrick CJ. *In vitro* expression of the endothelial phenotype: comparative study of primary isolated cells and cell lines, including the novel cell line HPMEC-ST1.6R. *Microvasc Res* (2002) 64(3):384–97. doi: 10.1006/mvre.2002.2434

33. Di Tomo P, Canali R, Ciavardelli D, Di Silvestre S, De Marco A, Giardinelli A, et al. beta-Carotene and lycopene affect endothelial response to TNF-alpha reducing nitro-oxidative stress and interaction with monocytes. *Mol Nutr Food Res* (2012) 56 (2):217–27. doi: 10.1002/mnfr.201100500

34. Di Tomo P, Di Silvestre S, Cordone VGP, Giardinelli A, Faricelli B, Pipino C, et al. Centella Asiatica and Lipoic Acid, or a combination thereof, inhibit monocyte adhesion to endothelial cells from umbilical cords of gestational diabetic women. *Nutrition Metab Cardiovasc Dis* (2015) 25(7):659–66. doi: 10.1016/j.numecd.2015.04.002

35. Livak KJ, Schmittgen TD. Analysis of relative gene expression data using real-time quantitative PCR and the 2(-Delta Delta C(T)) Method. *Methods* (2001) 25 (4):402–8. doi: 10.1006/meth.2001.1262

36. Kumar P, Nagarajan A, Uchil PD. Analysis of cell viability by the MTT assay. *Cold Spring Harb Protoc* (2018) 2018(6). doi: 10.1101/pdb.prot095505

37. Ernst O, Zor T. Linearization of the bradford protein assay. *J Vis Exp* (2010) 38). doi: 10.3791/1918-v

38. Carpentier G, Berndt S, Ferratge S, Rasband W, Cuendet M, Uzan G, et al. Angiogenesis Analyzer for ImageJ — A comparative morphometric analysis of "Endothelial Tube Formation Assay" and "Fibrin Bead Assay". *Sci Rep* (2020) 10 (1):11568. doi: 10.1038/s41598-020-67289-8

39. Liarte S, Bernabe-Garcia A, Armero-Barranco D, Nicolas FJ. Microscopy based methods for the assessment of epithelial cell migration during *in vitro* wound healing. *J Vis Exp* (2018) 131). doi: 10.3791/56799

40. Horzum U, Ozdil B, Pesen-Okvur D. Step-by-step quantitative analysis of focal adhesions. *MethodsX* (2014) 1:56–9. doi: 10.1016/j.mex.2014.06.004

41. Reglero-Real N, Colom B, Bodkin JV, Nourshargh S. Endothelial cell junctional adhesion molecules: role and regulation of expression in inflammation. *Arterioscler Thromb Vasc Biol* (2016) 36(10):2048–57. doi: 10.1161/ATVBAHA.116.307610

42. Theofilis P, Sagris M, Oikonomou E, Antonopoulos AS, Siasos G, Tsioufis C, et al. Inflammatory mechanisms contributing to endothelial dysfunction. *Biomedicines* (2021) 9(7):781. doi: 10.3390/biomedicines9070781

43. Lawrence T. The nuclear factor NF-kappaB pathway in inflammation. *Cold Spring Harb Perspect Biol* (2009) 1(6):a001651. doi: 10.1101/cshperspect.a001651

44. Troncoso MF, Ortiz-Quintero J, Garrido-Moreno V, Sanhueza-Olivares F, Guerrero-Moncayo A, Chiong M, et al. VCAM-1 as a predictor biomarker in cardiovascular disease. *Biochim Biophys Acta Mol Basis Dis* (2021) 1867(9):166170. doi: 10.1016/j.bbadis.2021.166170

45. Sakurai H, Suzuki S, Kawasaki N, Nakano H, Okazaki T, Chino A, et al. Tumor Necrosis Factor-α-induced IKK Phosphorylation of NF-κB p65 on Serine 536 Is Mediated through the TRAF2, TRAF5, and TAK1 Signaling Pathway*. *J Biol Chem* (2003) 278(38):36916–23. doi: 10.1074/jbc.M301598200

46. Flores AI, Pipino C, Jerman UD, Liarte S, Gindraux F, Kreft ME, et al. Perinatal derivatives: How to best characterize their multimodal functions in vitro. *Part C: Inflammation angiogenesis Wound healing. Front Bioeng Biotechnol* (2022) 10:965006. doi: 10.3389/fbioe.2022.965006

47. Lamalice L, Le Boeuf F, Huot J. Endothelial cell migration during angiogenesis. *Circ Res* (2007) 100(6):782–94. doi: 10.1161/01.RES.0000259593.07661.1e

48. Mitra SK, Hanson DA, Schlaepfer DD. Focal adhesion kinase: in command and control of cell motility. *Nat Rev Mol Cell Biol* (2005) 6(1):56–68. doi: 10.1038/nrm1549

49. Hu YL, Lu S, Szeto KW, Sun J, Wang Y, Lasheras JC, et al. FAK and paxillin dynamics at focal adhesions in the protrusions of migrating cells. *Sci Rep* (2014) 4:6024. doi: 10.1038/srep06024

50. Duffy SJ, Keaney JF Jr., Holbrook M, Gokce N, Swerdloff PL, Frei B, et al. Short- and long-term black tea consumption reverses endothelial dysfunction in patients with coronary artery disease. *Circulation* (2001) 104(2):151–6. doi: 10.1161/01.CIR.104.2.151

51. Jia Z, Babu PV, Si H, Nallasamy P, Zhu H, Zhen W, et al. Genistein inhibits TNF-alpha-induced endothelial inflammation through the protein kinase pathway A and improves vascular inflammation in C57BL/6 mice. *Int J Cardiol* (2013) 168(3):2637–45. doi: 10.1016/j.ijcard.2013.03.035

52. Ried K, Frank OR, Stocks NP. Aged garlic extract reduces blood pressure in hypertensives: a dose-response trial. *Eur J Clin Nutr* (2013) 67(1):64–70. doi: 10.1038/ejcn.2012.178

53. Kanitkar M, Gokhale K, Galande S, Bhonde RR. Novel role of curcumin in the prevention of cytokine-induced islet death in *vitro* and diabetogenesis in vivo. *Br J Pharmacol* (2008) 155(5):702–13. doi: 10.1038/bjp.2008.311

54. Bagul PK, Middela H, Matapally S, Padiya R, Bastia T, MadhuSudana K, et al. Attenuation of insulin resistance, metabolic syndrome and hepatic oxidative stress by resveratrol in fructose-fed rats. *Pharmacol Res* (2012) 66(3):260–8. doi: 10.1016/j.phrs.2012.05.003

55. Montezano AC, Dulak-Lis M, Tsiropoulou S, Harvey A, Briones AM, Touyz RM. Oxidative stress and human hypertension: vascular mechanisms, biomarkers, and novel therapies. *Can J Cardiol* (2015) 31(5):631–41. doi: 10.1016/j.cjca.2015.02.008

56. Martinez-Sanchez SM, Perez-Sanchez H, Antonio Gabaldon J, Abellan-Aleman J, Montoro-Garcia S. Multifunctional peptides from spanish dry-cured pork ham: endothelial responses and molecular modeling studies. *Int J Mol Sci* (2019) 20(17):4204. doi: 10.3390/ijms20174204

57. Hsuan CF, Hsu HF, Tseng WK, Lee TL, Wei YF, Hsu KL, et al. Glossogyne tenuifolia Extract Inhibits TNF-alpha-Induced Expression of Adhesion Molecules in Human Umbilical Vein Endothelial Cells *via* Blocking the NF-kB Signaling Pathway. *Molecules* (2015) 20(9):16908–23. doi: 10.3390/molecules200916908

58. He Y, Liu X, Huang M, Wei Z, Zhang M, He M, et al. Oleanolic acid inhibits the migration and invasion of hepatocellular carcinoma cells by promoting microRNA-122 expression. *Pharmazie* (2021) 76(9):422–7. doi: 10.1691/ph.2021.1366

59. Liu J, Ban H, Liu Y, Ni J. The expression and significance of AKR1B10 in laryngeal squamous cell carcinoma. *Sci Rep* (2021) 11(1):18228. doi: 10.1038/s41598-021-97648-y

60. Bui TM, Wiesolek HL, Sumagin R. ICAM-1: A master regulator of cellular responses in inflammation, injury resolution, and tumorigenesis. *J Leukoc Biol* (2020) 108(3):787–99. doi: 10.1002/JLB.2MR0220-549R

61. Hong YK, Chang YH, Lin YC, Chen B, Guevara BEK, Hsu CK. Inflammation in wound healing and pathological scarring. *Adv Wound Care (New Rochelle).* (2023) 12 (5):288–300. doi: 10.1089/wound.2021.0161

62. Mitsuda S, Yokomichi T, Yokoigawa J, Kataoka T. Ursolic acid, a natural pentacyclic triterpenoid, inhibits intracellular trafficking of proteins and induces accumulation of intercellular adhesion molecule-1 linked to high-mannose-type glycans in the endoplasmic reticulum. *FEBS Open Bio.* (2014) 4:229–39. doi: 10.1016/j.fob.2014.02.009

63. Silva M, Videira PA, Sackstein R. E-selectin ligands in the human mononuclear phagocyte system: implications for infection, inflammation, and immunotherapy. *Front Immunol* (2017) 8:1878. doi: 10.3389/fimmu.2017.01878

64. Medrano-Bosch M, Simon-Codina B, Jimenez W, Edelman ER, Melgar-Lesmes P. Monocyte-endothelial cell interactions in vascular and tissue remodeling. *Front Immunol* (2023) 14:1196033. doi: 10.3389/fimmu.2023.1196033

65. Ribatti D, Nico B, Crivellato E. Morphological and molecular aspects of physiological vascular morphogenesis. *Angiogenesis* (2009) 12(2):101–11. doi: 10.1007/s10456-008-9125-1

66. Nowak-Sliwinska P, Alitalo K, Allen E, Anisimov A, Aplin AC, Auerbach R, et al. Consensus guidelines for the use and interpretation of angiogenesis assays. *Angiogenesis* (2018) 21(3):425–532. doi: 10.1007/s10456-018-9613-x

67. Hoeben A, Landuyt B, Highley MS, Wildiers H, Van Oosterom AT, De Bruijn EA. Vascular endothelial growth factor and angiogenesis. *Pharmacol Rev* (2004) 56 (4):549–80. doi: 10.1124/pr.56.4.3

68. Apte RS, Chen DS, Ferrara N. VEGF in signaling and disease: beyond discovery and development. *Cell* (2019) 176(6):1248–64. doi: 10.1016/j.cell.2019.01.021

69. Reinke JM, Sorg H. Wound repair and regeneration. *Eur Surg Res* (2012) 49 (1):35–43. doi: 10.1159/000339613

70. Muller MM, Griesmacher A. Markers of endothelial dysfunction. *Clin Chem Lab Med* (2000) 38(2):77–85. doi: 10.1515/CCLM.2000.013

71. Pols T, Eggink H, Soeters M. TGR5 ligands as potential therapeutics in inflammatory diseases. *Int J Interferon Cytokine Mediator Res* (2014) 2014(6):27–38. doi: 10.2147/IJICMR.S40102

72. Guo C, Chen WD, Wang YD. TGR5, not only a metabolic regulator. *Front Physiol* (2016) 7:646. doi: 10.3389/fphys.2016.00646

73. Yasuda H, Hirata S, Inoue K, Mashima H, Ohnishi H, Yoshiba M. Involvement of membrane-type bile acid receptor M-BAR/TGR5 in bile acid-induced activation of epidermal growth factor receptor and mitogen-activated protein kinases in gastric carcinoma cells. *Biochem Biophys Res Commun* (2007) 354(1):154–9. doi: 10.1016/j.bbrc.2006.12.168

74. Marinissen MJ, Gutkind JS. G-protein-coupled receptors and signaling networks: emerging paradigms. *Trends Pharmacol Sci* (2001) 22(7):368–76. doi: 10.1016/S0165-6147(00)01678-3

75. Sato H, Genet C, Strehle A, Thomas C, Lobstein A, Wagner A, et al. Anti-hyperglycemic activity of a TGR5 agonist isolated from Olea europaea. *Biochem Biophys Res Commun* (2007) 362(4):793–8. doi: 10.1016/j.bbrc.2007.06.130

76. Kir D, Schnettler E, Modi S, Ramakrishnan S. Regulation of angiogenesis by microRNAs in cardiovascular diseases. *Angiogenesis* (2018) 21(4):699–710. doi: 10.1007/s10456-018-9632-7

77. Felicetta A, Condorelli G. RNA binding protein and microRNA control of endothelial cell function. *Cardiovasc Res* (2019) 115(12):1690–1. doi: 10.1093/cvr/cvz144

78. Avvisato R, Mone P, Jankauskas SS, Varzideh F, Kansakar U, Gambardella J, et al. miR-4432 targets FGFBP1 in human endothelial cells. *Biol (Basel)* (2023) 12 (3):459. doi: 10.3390/biology12030459

79. Gambardella J, Kansakar U, Sardu C, Messina V, Jankauskas SS, Marfella R, et al. Exosomal miR-145 and miR-885 Regulate Thrombosis in COVID-19. *J Pharmacol Exp Ther* (2023) 384(1):109–15. doi: 10.1124/jpet.122.001209

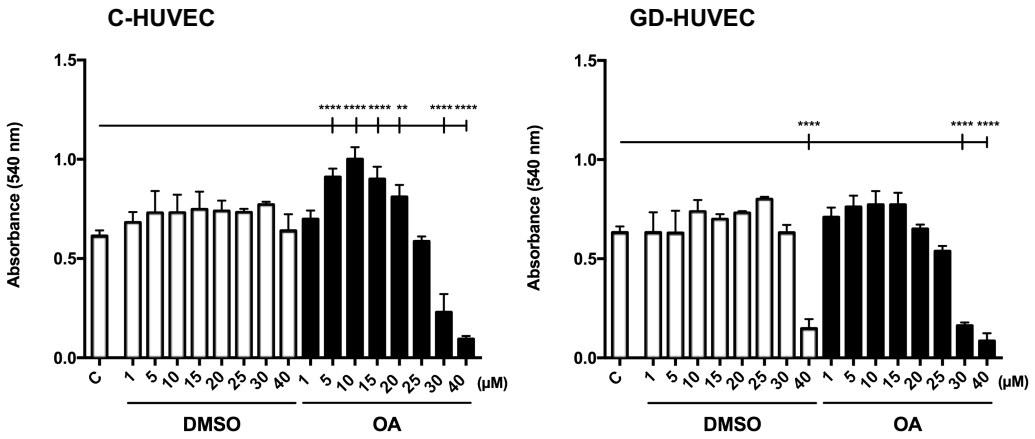

Supplemental Figure 1. Oleanolic acid MTT assay on C- and GD-HUVECs. Plots represent the registered absorbance values at 540 nm wave length of sub confluent C- and GD-HUVECs. DMSO and OA concentrations are indicated in X axis. A basal (control, C) condition was performed with any treatments added, in order to compare its cell viability with the rest of conditions. Asterisks indicate statistically significant differences between conditions according to a One-way ANOVA statistical analysis (**p<0.005 and ****p<0.0001).

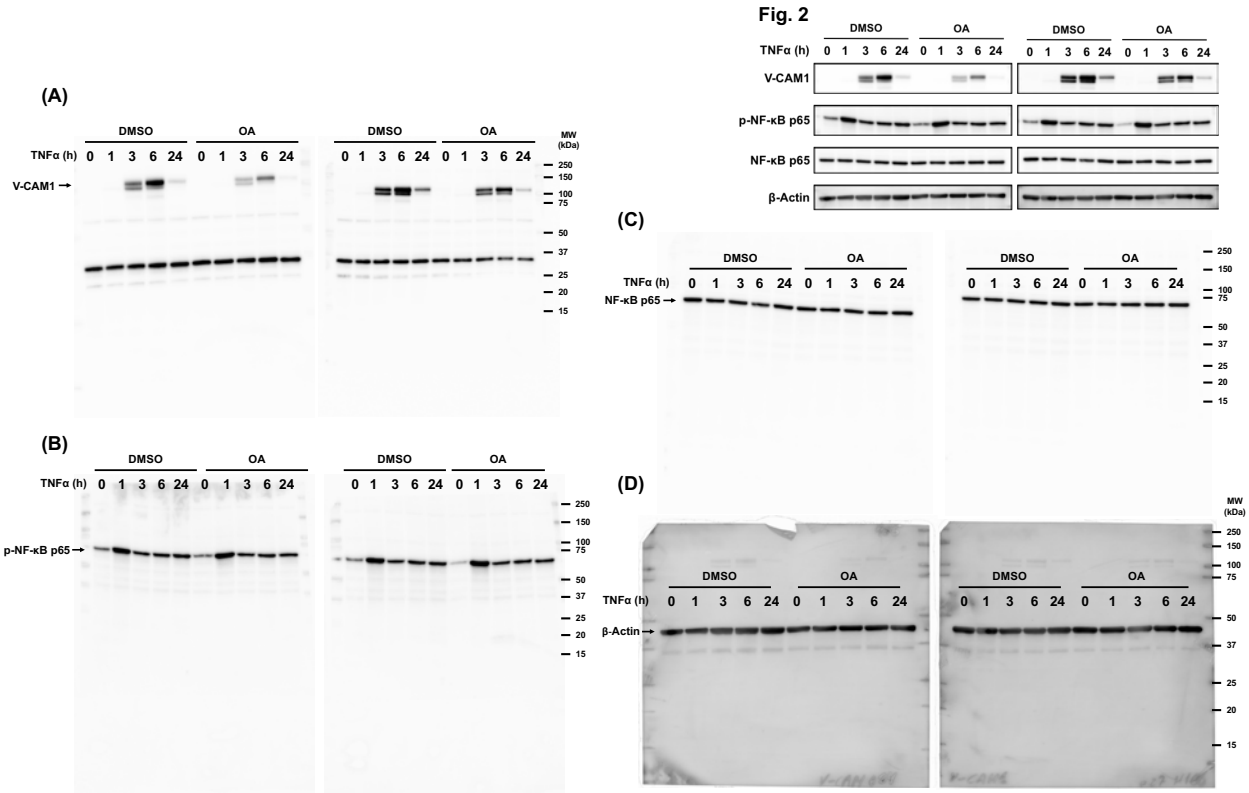

Supplemental Figure 2. Full-length blots corresponding to crops showed in Fig 2. **(A)** V-CAM1. **(B)** Ser 536 Phosphorylated NF-κB. **(C)** NF-κB **(D)** Beta-actin loading.

4.3. ARTICLE 3: OLEANOLIC ACID COMPLEXATION WITH CYCLODEXTRINS IMPROVES ITS CELL BIO-AVAILABILITY AND BIOLOGICAL ACTIVITIES FOR CELL MIGRATION

Stelling-Férez J, López-Miranda S, Gabaldón JA, Nicolás FJ. (2023) **Oleanolic Acid Complexation with Cyclodextrins Improves Its Cell Bio-Availability and Biological Activities for Cell Migration**. *International Journal of Molecular Sciences*, 3;24(19):14860. PMID: 37834307. doi: 10.3390/ijms241914860.

International Journal of
Molecular Sciences

MDPI

Article

Oleanolic Acid Complexation with Cyclodextrins Improves Its Cell Bio-Availability and Biological Activities for Cell Migration

Javier Stelling-Férez [1,2], Santiago López-Miranda [1], José Antonio Gabaldón [1] and Francisco José Nicolás [2,*]

[1] Department of Nutrition and Food Technology, Health Sciences PhD Program, Universidad Católica de San Antonio Murcia (UCAM), Campus de los Jerónimos n°135, Guadalupe, 30107 Murcia, Spain; javier.stelling.ferez@gmail.com (J.S.-F.); slmiranda@ucam.edu (S.L.-M.); jagabaldon@ucam.edu (J.A.G.)
[2] Regeneration, Molecular Oncology and TGF-β, Instituto Murciano de Investigación Biosanitaria (IMIB)-Arrixaca, Hospital Clínico Universitario Virgen de la Arrixaca, El Palmar, 30120 Murcia, Spain
* Correspondence: franciscoj.nicolas2@carm.es

Abstract: Wound healing is a complex process to restore skin. Plant-derived bioactive compounds might be a source of substances for the treatment of wounds stalled in a non-resolving stage of wound healing. Oleanolic acid (OA), a pentacyclic triterpene, has shown favorable wound healing properties both in vitro and in vivo. Unfortunately, OA cannot be solubilized in aqueous media, and it needs to be helped by the use of dimethyl sulfoxide (DMSO). In this paper, we have shown that cyclodextrins (CDs) are a good alternative to DMSO as agents to deliver OA to cells, providing better features than DMSO. Cyclodextrins are natural macromolecules that show a unique tridimensional structure that can encapsulate a wide variety of hydrophobic compounds. We have studied the cyclodextrin-encapsulated form of OA with OA/DMSO, comparing their stability, biological properties for cell migration, and cell viability. In addition, detailed parameters related to cell migration and cytoskeletal reorganization have been measured and compared. Our results show that OA-encapsulateds compound exhibit several advantages when compared to non-encapsulated OA in terms of chemical stability, migration enhancement, and preservation of cell viability.

Keywords: hydroxypropyl cyclodextrins (HP-CDs); oleanolic acid (OA); cell migration; MAP kinases; epidermal growth factor receptor (EGR); c-Jun; wound healing

Citation: Stelling-Férez, J.; López-Miranda, S.; Gabaldón, J.A.; Nicolás, F.J. Oleanolic Acid Complexation with Cyclodextrins Improves Its Cell Bio-Availability and Biological Activities for Cell Migration. *Int. J. Mol. Sci.* **2023**, *24*, 14860. https://doi.org/10.3390/ijms241914860

Academic Editors: Elia Ranzato and Simona Martinotti

Received: 7 September 2023
Revised: 26 September 2023
Accepted: 29 September 2023
Published: 3 October 2023

1. Introduction

The skin acts as a physical barrier against pathogens, ultraviolet radiation, or temperature [1], and its integrity is restored through the coordinated action of different signaling molecules and cell types in a process called wound healing [2–4]. Complications in wound healing may cause an uncomplete wound closure that may lead to an ulcer [5,6], a lesion that severely complicates a patient's life quality [7–11], and it is a great burden for health care systems for its high costs and time-consuming treatments [12–14].

Plant-derived bioactive compounds arise as a good alternative for the treatment of complex wounds because of their potential to improve cell migration [15–17]. Among them, oleanolic acid (OA) is a pentacyclic triterpene that has shown promising wound healing properties in vitro and in vivo [18,19]. Indeed, it has been shown that OA enhances cell migration, a crucial process for wound healing. Concretely, the test of OA in various in vitro scratch assays with cell migration models such as Mink lung epithelial (Mv1Lu) and Human Mammary Gland (MDA-MB-231) cell lines has demonstrated its important pro-migratory effect, which is comprised by a complex kinase regulatory system that turns on in response to OA [20,21]. Thus, OA induces the phosphorylation of epidermal growth factor receptor (EGFR), triggering the activation of both extracellular signal-regulated kinase (ERK1/2)

and c-Jun N-terminal kinase (JNK1/2) [20–23]. As a consequence, OA stimulation leads to the activation of a master regulator for cell migration, c-Jun, a transcription factor [24–27]. Specifically, in response to OA, c-Jun is mainly phosphorylated and overexpressed at the scratch edge of in vitro scratch assays both in Mv1Lu and in MDA-MB-231 cells [21]. Together with inhibitor experiments, this indicates that c-Jun participates in OA-enhanced cell migration. Additionally, these pathways are intimately related to other proteins in charge of cytoskeleton remodeling: focal adhesion kinase (FAK) and paxillin [28,29], which interact to execute an assembling-disassembling loop of actin cytoskeleton and focal adhesions (FAs), structures that allow migration of epithelial cells [30–33]. Thus, we have shown that OA promotes paxillin remodeling, increasing the number of FAs and decreasing FA size, a result reinforced by the fact that OA also promotes FAK-paxillin interaction [21]. These results indicate a high cytoskeleton dynamization induced by OA, needed for cell migration [34]. Because of these, in vitro scratch assays with Mv1Lu and MDA-MB-231 can be used as good biosensors for the improvement of OA application in migration as a foreseeable use in human skin wound healing [20,21,23,35,36].

The main constraint for OA application is its lipophilic nature. Usually, OA can be solubilized in aqueous solutions by using dimethyl sulfoxide (DMSO). Unfortunately, DMSO has mild cytotoxic effects, which compromise cell viability [37,38]. In addition to this, meticulous care is needed to manage OA/DMSO solutions in cell assays due to the fact that OA often precipitates and crystalizes, loosing bioavailability [20,21]. To help with all these issues, OA can be complexed with cyclodextrins, which allows it to be carried into aqueous solutions [39]. Cyclodextrins are natural macromolecules that show a unique tridimensional structure; they have a hydrophilic surface that confers high water solubility and a hydrophobic cavity that encapsulates a wide variety of hydrophobic compounds [39–42]. Many authors have shown the potency of cyclodextrins to deliver drugs since they reinforce their biological activities [39,43–47]. There are three types of native cyclodextrins, α, β, and γ, that differ in the number of D-glucose units that formed them, 6, 7, or 8, respectively, which progressively increase the size of the hydrophobic cavity [48]. Additionally, chemical groups can be added to native cyclodextrins for several purposes, such as increasing their water solubility [37,49–51]. Interestingly, using native cyclodextrins (α-, β-, and γ-CDs) and the same ones with hydroxypropyl groups (HP-α-, HP-β-, and HP-γ-CDs), a recent study determined which cyclodextrin had the highest performance to encapsulate OA [52]. Complexation constant (K_c) and encapsulation efficiency (EE) have been used to evaluate OA complexation, which revealed the highest K_c for β- and γ-CDs, followed by their homologues HP-β- and HP-γ-CDs [52]. Seeking a compromise between adequate complex stability and sufficiently high solubility of oleanolic acid, the modified cyclodextrins HP-β- and HP-γ-CDs emerged as the most suitable candidates for complex formation. However, the biological activity of the OA/HP-β-CD and OA/HP-γ-CD complexes has not been tested in vitro yet. In this paper, we have shown that OA can be maintained stable in a conjugated and dehydratable form to be applied to biological hydrophilic systems. Using cell and biochemistry models, we have assessed the effect of the complex on migration and cell viability, finding a better performance than the DMSO solubilized form. Therefore, a future application of these complexes to wound healing is more feasible.

2. Materials and Methods

2.1. Preparation of Oleanolic Acid in DMSO

Oleanolic acid (OA, purity > 97%) (Merck, Darmstadt, Germany) was dissolved in dimethyl sulfoxide (DMSO) (Merck, Darmstadt, Germany) to a 25 mM concentration. Final assay concentrations are indicated for each experiment in the figure legends. The DMSO concentration in all assays never exceeded 1% to avoid cytotoxic effects. In any case, a DMSO control condition was performed in each experiment.

2.2. Oleanolic/Cyclodextrin Complexes Preparation: Solid Complexes by Freeze Drying

The modified hydroxypropyl beta and gamma (HP-β- and HP-γ-) cyclodextrins (CDs) were used to encapsulate OA (Winplus International Limited, Ningbo, China). OA and CDs were added to 250 mL of aqueous solutions with a molar ratio of 0.2/50 (OA/CD) for both HP-β- and HP-γ-CDs. These molar proportions were selected according to phase solubility diagrams previously published by López-Miranda et al. (2018) [52]. Phase diagrams allow for the determination of the optimal molar ratio between cyclodextrin and the guest molecule to maximize their dissolution. Furthermore, the stoichiometry of the complexes formed is 1:1, indicating that when the complex is formed, one molecule of cyclodextrin complexes with a single molecule of oleanolic acid [52]. Solutions were constantly stirred for 24 h at 20 °C in the dark for complex formation in aqueous solutions. After that, OA/CD solid complexes were obtained by dehydrating a 250 mL volume of dissolved complexes by freeze drying. Solutions of OA/CD complexes (OA/HP-β-CD and OA/HP-γ-CD) were dehydrated in a Christ Alpha 1–2 LD Plus (Martin Christ, Osterode am Harz, Germany) freeze dryer at −48 °C for three days. This step was critical to obtaining an optimal formulation for its application to in vitro cell culture (see Figure S1). The recovered freeze-dried solid complexes were stored in plastic containers protected from light for posterior analysis and characterization.

The dehydration yield (DY) was calculated using the following equation:

$$\mathrm{DY}(\%) = \frac{\text{solid complexes obtained}(\mathrm{g})}{\text{total solids in solution}(\mathrm{g})} \cdot 100$$

The encapsulation efficiency (EE) was calculated using the equation:

$$\mathrm{EE}(\%) = \frac{\text{total compound encapsulated in solid complex}(\mathrm{mg})}{\text{initial total compound in solution}(\mathrm{mg})} \cdot 100$$

The drug load (DL) was calculated using the equation:

$$\mathrm{DL}\left(\mathrm{mg}\, g^{-1}\right) = \frac{\text{total compound encapsulated in solid complex}(\mathrm{mg})}{\text{total solid complexes}(\mathrm{g})}$$

Final assay OA/CD complex concentrations are indicated at each experiment in figure legends, which indicate their molar ratio in terms of μM for OA and mM for both HP-β-CD and HP-γ-CD (μM/mM).

2.3. Oleanolic Acid Determination by HPLC

OA that was complexed in cyclodextrins was quantified by High-performance liquid chromatography (HPLC) analysis, using an HPLC Agilent Technologies model 1200 (Santa Clara, CA, USA). Firstly, a calibration line was set with 1 mg/mL free OA (OA, purity > 97%) (Merck, Darmstadt, Germany) to refine the quantification. Then, complexed OA was analyzed by HPLC equipped with a DAD detector set at a 210 nm wavelength, injecting 20 μL of complexed OA. Separations were performed on a plugged (5 μm) HPLC Catridge 250-4 LiChospher 100 RP-18 (Sigma-Aldrich, St. Louis, MO, USA). The column temperature was set to 30 °C, and the flow rate was 1 mL/min. The mobile phase used was 20% water and 80% acetonitrile for a total running time of 30 min. During this time, an OA-specific absorbance peak at 210 nm appeared for close to 10 min. Finally, the data were processed, and OA concentrations were expressed in OA mg per CD g; this is the drug load (DL), as defined above.

2.4. Cell Culture

Mink Lung Epithelial (Mv1Lu) [36,53,54] cells were grown in Eagle's Minimum Essential Medium (EMEM) (Biowest, Nuaillé, France) supplemented with 10% Fetal Bovine Serum (FBS, Gibco, Thermo Fisher Scientific, Rockford, IL, USA), 1% Penicillin/Streptomycin, and

1% L-Glutamine (both from Biowest, Nuaillé, France). Mv1Lu cells were cultured in an incubator at 37 °C in a 5% CO_2-humified atmosphere. Human mammary gland cells (MDA-MB-231) [23,35] were grown in Dulbecco's Modified Eagle Medium (DMEM) supplemented as mentioned above for EMEM. MDA-MB-231 cells were incubated in an incubator at 37 °C with a 7.5% CO_2 humified atmosphere.

2.5. Cell Proliferation Assay

Cell proliferation over 10 days was evaluated by cell counting. Essentially, cells were seeded in 5 cm diameter plates at a density of 10^5 cells/plate in a complete medium supplemented with 10% FBS. Mv1Lu or MDA-MB-231 cells were treated in duplicate with DMSO, OA/DMSO, HP-β-CD, and OA/HP-β-CD; final concentrations are indicated in figure legends. At even days until day 10, cells from all conditions were detached using trypsin/EDTA, and the viable cell count was calculated using a TC10 automated cell counter (BioRad, Hercules, CA, USA) and a trypan blue dye (Sigma-Aldrich, St. Louis, MO, USA) exclusion assay. Data were gathered and plotted in Graph Pad Prism 7 software as a growth curve.

2.6. Cell-Front Migration Assay, Subcellular Localization Assay

Mv1Lu cells were grown until they reached confluence on round glass coverslips in 10% FBS-EMEM medium. At this time, cells were washed, and a 24 h serum-starvation period was set by replacing the medium with FBS-free EMEM. After this, the epithelium was scratched using a razor blade, which produced an artificial wound (it will be called "scratch" throughout the paper) with enough space to allow cells to migrate. The newly scratched wound was set as time 0 h of the experiment, and then 5 μM OA/DMSO or 12.5/3.125 μM/mM OA/HP-β-CD were added to the medium. As parallel conditions, DMSO or HP-β-CD (3.125 mM) equivalent volumes were added as vehicle controls. After the selected times of incubation, glass coverslips were fixed with 4% formaldehyde (Applichem GmbH, Darmstadt, Germany) in PBS (Biowest, Nuaillé, France) for 10 min and washed twice with PBS. After this, cells were permeabilized with 0.3% Triton X-100 (Sigma-Aldrich, St. Louis, MO, USA) in PBS for 10 min. For immunostaining, blocking was performed for 30 min at room temperature in a PBS solution with 10% FBS, 5% skim milk (Beckton Dickinson, Franklin Lakes, NJ, USA), 0.3% bovine serum albumin (BSA, Sigma-Aldrich, St. Louis, MO, USA), and 0.1% Triton X-100. Then, cells were incubated for 1 h at room temperature with anti-paxillin or anti-phospho-c-Jun antibodies, diluted in blocking solution without skim milk. Proper fluorescently labeled secondary antibodies (see Section 2.9) were co-incubated for 30 min with Alexa Fluor 594 conjugated phalloidin (Molecular Probes, Thermo Fisher Scientific, Waltham, MA, USA) and Hoechst 33258 (Fluka, Biochemika, Sigma-Aldrich, St. Louis, MO, USA) to reveal actin cytoskeleton and nuclei, respectively. Once samples were inmunostained, image acquisition was performed with a confocal microscope (LSM 510 META from ZEISS, Jena, Germany). The setting of images was performed using Zeiss Efficient Navigation (ZEN) interface software (ZEISS, Jena, Germany). When a wider view of the migration front was required, concretely in phospho-c-Jun staining (indicated in Figures), 4 × 3 linked fields were acquired by the "Tile scan" ZEN tool. Subsequently, tile scan fluorescent signals were converted to a linear mode and covered with a full data range using the Rainbow look up table (Rainbow LUT) in Image J software. In order to quantify phospho-c-Jun levels in immunofluorescence pictures, images were analyzed and quantified by Image J software. For this purpose, pictures in 8-bit, three-channel format (Red, Green, Blue, and RGB) were divided into three separate color channels (three pictures). By using the blue channel picture (Hoechst staining), regions of interest (ROIs) were established to define each nucleus, creating as many ROIs as nuclei in the image. Then, by overlapping these masks onto the corresponding green channel picture (p-c-Jun staining), we calculated the green intensity value of each nucleus (ROI). Because of the large area covered in each picture (tile scan), they were divided into three equal sectors (S1, S2, and S3), with S1 being the outermost edge on the scratch (Figure S4a). Within

each sector, the quantified signal of each nucleus was used as a replicate to obtain p-c-Jun intensity data in each of the conditions performed. For a better understanding, the relation between the number of p-c-Jun positive nuclei and the total nuclei number was calculated. For this purpose, a basal p-c-Jun intensity mean was calculated considering the control condition of the assays, set as a threshold. In this sense, nuclei with p-c-Jun intensity over the threshold were set as positive nuclei. On the other hand, the "Z stack" ZEN feature was used when deep cytoskeleton structure observance was required, taking a proper number of pictures along the Z axis. Focal adhesion (FA) quantifications were performed as described in Horzum et al., 2014 by using CLAHE and Log3D macros for ImageJ [55]. Briefly, focal adhesions (FAs) were quantified from paxillin-stained acquired pictures. We used three different images for each condition. Specifically, cell filopodia were selected as regions of interest (ROIs), and the resulting areas (containing FAs) were considered for further analysis. A number of five filopodia were considered for each picture. Then, the number of FAs was calculated in each filopodia by using the previously mentioned macros. The obtained number was divided by the total filopodia area to determine FA density. In parallel, the size of each FA was measured using the macros mentioned above. Finally, the FA average size was calculated for each treatment.

2.7. In Vitro Scratch Assay

Mv1Lu or MDA-MB-231 were seeded in 24-well plates until they reached 100% confluence, using the appropriate medium for each line with all supplements. At that time, the medium was changed to a FBS-free medium for 24 h. At the initial time (time 0 h), a cross-shaped scratch was made on the cell monolayer using a sterile p-200 µL pipette tip. After replacing FBS-free culture medium to wash out released cells, OA, OA/HP-β-CD, or OA/HP-γ-CD (indicated concentration at each figure legend) were added. An equivalent volume of DMSO, HP-β-CD, and HP-γ-CD was added. In parallel, a positive control was set by adding 10 ng/mL epidermal growth factor (EGF, Sigma-Aldrich, St. Louis, MO, USA). Additionally, pharmacological inhibitors against key proteins on migration regulation were added to OA conditions: 2.5 µM PD153035 (Epidermal Growth Factor inhibitor, EGFRi), 50 µM PD098059 (Mitogen-activated protein kinase kinase inhibitor, MEKi), and 15 µM SP600125 (c-Jun N-terminal kinase inhibitor, JNKi) [56–58]. After a 24-hour incubation period, cells were fixed with 4% formaldehyde (Applichem GmbH, Darmstadt, Germany) in PBS (Biowest, Nuaillé, France) for 10 min. Finally, well plates were washed twice with PBS. Pictures were taken at 10× magnification using an optical microscope equipped with a digital camera (Motic Optic AE31, Motic Spain, Barcelona, Spain). To quantify cell migration, the areas of the gaps in the scratches were measured by ImageJ software. The initial cell-free surface (time 0 h) was subtracted from the endpoint cell-free surface (time 24 h) and plotted in a graph [59].

2.8. Western Blot

Mv1Lu or MDA-MB-231 cells were seeded and allowed to reach 60% confluence in 10 cm diameter plates. At this time, culture medium containing 10% FBS was replaced by an FBS-free medium, incubating the cells for a 24-hour period. Serum-deprived cells were treated with either OA, OA/HP-β-CD, DMSO, HP-β-CD, or 10 ng/mL EGF. After time incubations, cells were harvested, washed twice with ice-cold PBS, and lysed with 20 mM TRIS pH 7.5, 150 mM NaCl, 1 mM EDTA, 1.2 mM MgCl2, 0.5% Nonidet p-40, 1 mM DTT, 25 mM NaF, and 25 mM β-glycerophosphate supplemented with phosphatase inhibitors (I and II) and protease inhibitors (all from Sigma-Aldrich, St. Louis, MO, USA). The total protein amount of all extracts was measured and normalized by the Bradford assay [60] (Sigma-Aldrich, St. Louis, MO, USA). The extracts were analyzed by SDS-PAGE followed by western blot (WB) using the indicated antibodies. Blots were revealed by using Horseradish peroxidase substrate (ECL) (GE Healthcare, GE, Little Chalfont, UK), and images were taken with a Chemidoc XRS1 (Bio-Rad, Hercules, CA, USA). For protein quantification, western blot pictures in 8-bit format were processed in ImageJ software.

Subsequently, in all western blot pictures, a lane was established for each of the samples. In each lane, the band was selected according to the specific size (kDa) of the protein of interest. For each total protein and their phosphorylated version, each band's intensity peak was plotted, and next, the area under the plot was measured by using the "Wand (tracing) tool" of ImageJ to obtain the intensity value. In order to normalize, obtained intensity values were referred to as obtained intensity values of either the unphosphorylated form of the protein (total) or a loading control protein such as β-actin, only if the unphosphorylated form was undetectable (non-available antibody for detecting the unphosphorylated form).

2.9. Antibodies

The following commercial primary antibodies were used: anti-phospho-ERK1/2, anti ERK1/2, anti-JNK1/2, anti-phospho-JNK1/2 and anti-phospho-c-Jun (all from Cell Signaling Technology, Danvers, MA, USA); anti-phospho-EGFR (Thermo Fisher Scientific, Rockford, IL, USA); anti-EGFR, anti-paxillin and anti-c-Jun (Santa Cruz Biotechnology, Heidelberg, Germany); and anti-β-actin (Sigma-Aldrich, St. Louis, MO, USA). Secondary antibodies were anti-rabbit IgG Horseradish peroxidase-linked F(ab')2 I fragment (from donkey) (GE Healthcare, GE, Little Chalfont, United Kingdom), anti-mouse IgG_1 (BD Pharmingen, Beckton Dickinson, Franklin Lakes, NJ, USA), and Alexa Fluor 488 conjugated anti-mouse (from donkey) (Thermo Fisher Scientific, Rockford, IL, USA).

2.10. Statistical Analysis

All the collected data were analyzed using Graph Pad Prism 7 software. In every analysis, classic statistical parameters were calculated and statistical tests were performed with a 95% confidence interval, consequently, *p*-values lower than 0.05 were considered to be statistically significant. In the figure legends, the asterisks denote statistically significant differences between conditions (* $p < 0.05$, ** $p < 0.005$, *** $p < 0.001$, and **** $p < 0.0001$). Data on intensity values, collected from western blots, were analyzed by a one-way ANOVA test, comparing the mean of each condition with the mean of every other condition. Then, a Tukey's multiple comparisons test was performed. The same parameters and tests were applied for migration percentage values of scratch assays.

Data of intensity values obtained from p-c-Jun nuclei quantifications in immunofluorescence pictures were analyzed by using two statistical tests: a two-way ANOVA test and a one-way ANOVA test. Concretely, a two-way ANOVA following Tukey's multiple comparison test was performed to compare the p-c-Jun intensity mean between sectors from different conditions (e.g., S1 DMSO versus S1 OA). On the other hand, a One-way ANOVA, following Tukey's multiple comparison test, was performed to compare the p-c-Jun intensity mean between sectors from the same condition (e. g., S1 DMSO versus S2 DMSO).

3. Results

3.1. HP-β- and HP-γ- Cyclodextrins SHOW High Rates Complexation Parameters with OA

Different parameters of the dehydrated by freeze drying solid complexes of OA with HP-β- and HP-γ-CD were measured (Table 1).

Table 1. Hydroxypropyl beta and gamma cyclodextrins (HP-β- and HP-γ-CDs) show high rates od complexation parameters with oleanolic acid (OA). Dehydration yield (DY), encapsulation efficiency (EE), and drug load (DL) of solid complexes obtained by freeze drying for OA encapsulated with HP-β- or HP-γ-CDs. Values represent means of triplicate determination; the data presented in the table represent the mean ± standard error of the mean.

	DY (%)	EE (5%)	DL (mg/g)
HP-β-CD	89.4 ± 6.7	80.0 ± 7.6	1.06 ± 0.07
HP-γ-CD	91.6 ± 0.7	91.9 ± 9.2	1.17 ± 0.18

The dehydration yield (DY) values were around 90% for both CDs. These values indicate a high level of complex recovery and were similar to those previously obtained in complex dehydration using the freeze drying technique [43].

Encapsulation Efficiency (EE) represents the percentage of OA that has been recovered after the dehydration process, indicating whether significant compound losses occur during the dehydration process. On average, EE was 80.0% for HP-β-CD, and 91.9% for HP-γ-CD. The amount of OA finally encapsulated per gram of complex (DL mg/g) was 1.06 and 1.17 for HP-β- and HP-γ-CD complexes, respectively (Table 1).

These results show that properly encapsulated solid complexes of oleanolic acid with HP-β- and HP-γ-CDs can be obtained, allowing for subsequent dosing and handling in an aqueous medium.

3.2. Freeze-Dried OA/HP-β-CD and OA/HP-γ-CD Complexes Stimulate Migration in Mv1Lu Cells

To measure OA/HP-β-CD and OA/HP-γ-CD complexes migration activity, we used mink lung epithelial cells, Mv1Lu, a very well-known epithelial model for the study of cell motility and cytoskeleton structures. They are also known for stopping proliferation when the cells reach confluence [36,54,61]. In previous papers, we have shown that OA 5 μM in DMSO stimulates Mv1Lu motility [20]. However, OA/DMSO levels beyond this concentration cause cell viability loss and cytotoxic effects [20,21,62]. It should be noted that the OA complexes used in the following in vitro assays were dehydrated by freeze drying to obtain a lyophilized powder compatible with in vitro cell culture. In fact, non-dried OA complexes did not exert any activity on cell migration (Figure S1a,b). However, freeze-dried OA/HP-β-CD and OA/HP-γ-CD complexes clearly stimulated Mv1Lu migration from the scratch edges (Figure 1a).

Consequently, migration percentages with OA/HP-β-CD and OA/HP-γ-CD complexes were statistically significant compared to basal conditions (C) (Figure 1b) and also to vehicle controls (empty HP-β-CD and HP-γ-CD) (Figure 1a,b). In particular, these complexes showed the highest migration activity at 12.5/3.12 μM/mM and 125/31.25 μM/mM for OA/HP-β-CD and OA/HP-γ-CD, respectively (Figure S2). Furthermore, no statistical differences were found between OA/DMSO and OA/CDs on Mv1Lu migration. However, a slight tendency was observed for OA complexes suggesting a higher migration activity than OA/DMSO, concretely for OA/HP-γ-CD complexes at 125/31.25 μM/mM concentration (Figure S2). Interestingly, when looking at a wider view at the scratch assay, we noticed a clear larger recruitment of Mv1Lu migrating cells in the OA/CDs condition than in the OA/DMSO condition, suggesting a more extensive and improved migratory effect of complexed OA with cyclodextrins (Figure S3).

All these data suggest a powerful effect of OA complexed with HP-β- and HP-γ-CDs on Mv1Lu cell migration. However, among the two cyclodextrins studied, it was deduced that HP-β-CD allows a better release of OA from the complex because a lower OA concentration (12.5 μM vs. 62.5 μM) is required for a similar cellular migration when HP-β-CD is used for complexation instead of HP-γ-CD. So then, the following experiments were performed exclusively with the OA HP-β-CD complexed form.

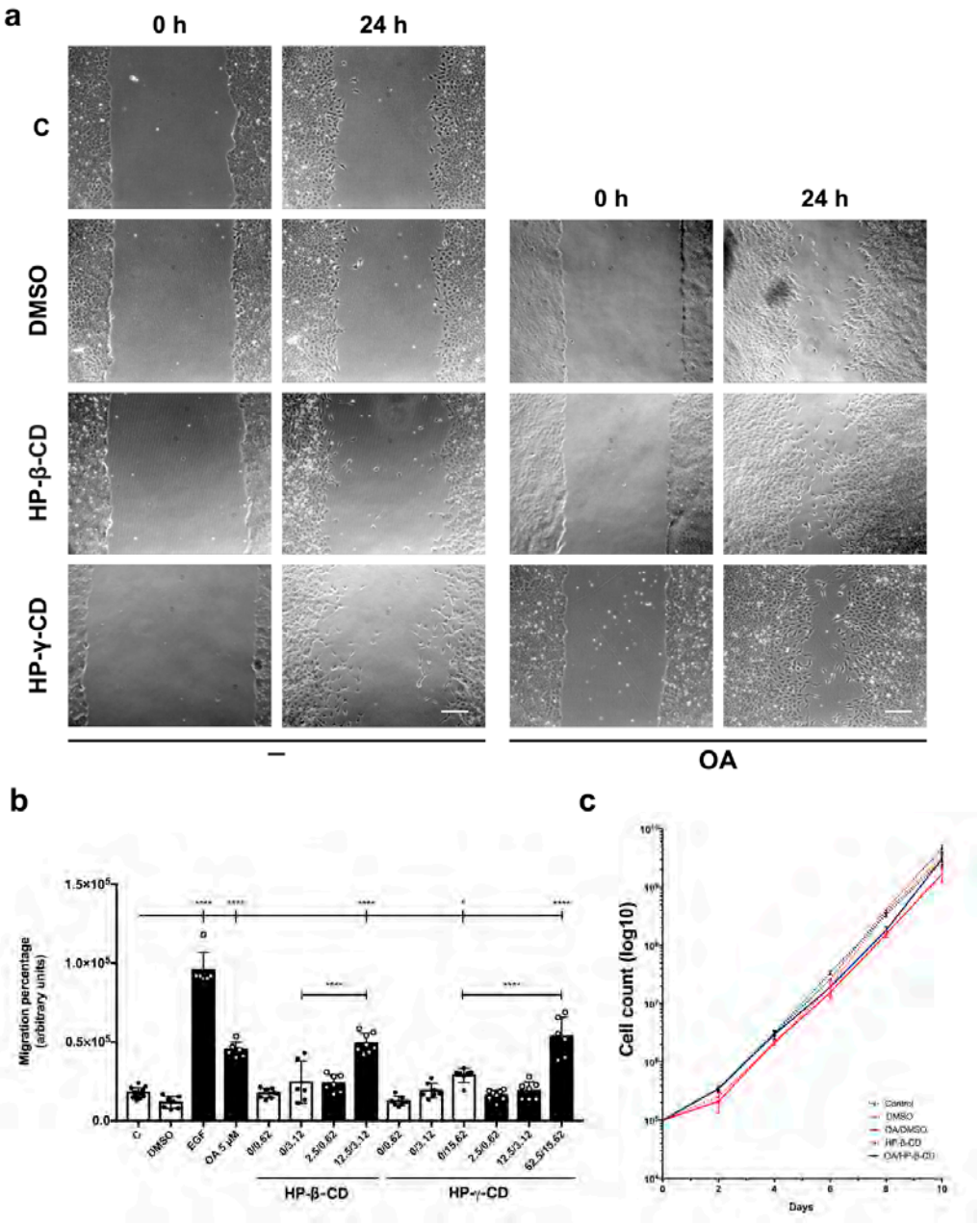

Figure 1. Freeze-dried OA/HP-β-CD and OA/HP-γ-CD complexes stimulate migration in Mv1Lu cells, minimizing OA/DMSO cytotoxic effects. Confluent My1Lu cells were scratched with a pipette tip and allowed to migrate for 24 h. (**a**) Representative images of the in vitro scratch assay with cell migration under basal conditions (C) compared to those with 5 µM OA/DMSO, 12.5/3.12 µM/mM OA/HP-β-CD, and 62.5/15.62 µM/mM OA/HP-γ-CD after 24 h treatment. Equivalent concentrations of DMSO, HP-β-CD, and HP-γ-CD were used as vehicle controls. The scale bar indicates 200 µm. (**b**) Plot represents cell migration as the difference between areas at time 0 h and time 24 h in each condition, named as migration percentage. Control conditions: white bars, black dots. Stimuli: black bars, white dots. The X axis indicates treatment conditions; for those with HP-β-CD and HP-γ-CD, the concentrations are represented as the molar ratio OA µM/CD mM. Epidermal growth factor (EGF) was added at 10 ng/mL as a positive migration control. Asterisks indicate statistically significant differences between conditions according to a one-way ANOVA statistical analysis (* $p < 0.05$ and **** $p < 0.0001$). (**c**) The long-term effects of 5 µM OA/DMSO and 12.5/3.12 µM/mM OA/HP-β-CD (with vehicle controls) on Mv1Lu proliferation were assessed by counting total cells at the indicated times. The logarithm of the mean number of cells against time is plotted.

3.3. Complexed OA at Freeze-Dried OA/HP-β-CDs Is Stable at Room Temperature

Conservation of OA in DMSO has always been a difficulty when the use of oleanolic in further applications has been envisaged. Once oleanolic acid is dissolved in DMSO, it needs to be preserved in liquid nitrogen. This is because factors such as exposure to light, oxygen, and temperature can influence its stability and reactivity. Generally speaking, molecule complexation with cyclodextrins adds an extra level of stability to such molecules [63,64]. Thus, after producing the OA HP-β-CD complexes, we tested OA stability in the complex that had been stored at different temperatures for different durations (Table 2).

Table 2. OA at freeze-dried OA/HP-β-CD complexes is stable at room temperature. The table shows OA analysis by HPLC to determine the OA amount in OA/HP-β-CD complexes, kept at different temperatures. Samples from these complexes were taken at 1, 2, 4, and 8 weeks after encapsulation. The table shows the OA areas corresponding to the absorbance peaks detected at 210 nm in the HPLC system. On the other side, the table indicates the amount of sample taken from the solid freeze-dried OA/HP-β-CD complexes. OA quantification was expressed as OA mg per HP-β-CD g, defined as drug load (DL). The data presented in the last row (Global) represents the mean ± standard error of the means of the different times (0 to 8 weeks).

Weeks after Encapsulation (w)	Storage Temperature (°C)	OA Peak Area at A_{210nm}	Solid Complex Weight (mg)	DL (mg/g)
0 w	20	489.0	21.3	1.11
	20	468.0	20.1	1.13
1 w	20	415.2	19.0	1.06
	4	517.6	21.0	1.19
	−80	527.5	22.0	1.16
2 w	20	489.8	21.4	1.11
	4	467.4	21.7	1.04
	−80	426.3	20.2	1.02
4 w	20	505.0	21.9	1.12
	4	501.0	22.2	1.09
	−80	514.0	21.9	1.14
8 w	20	459.6	20.2	1.10
	4	431.2	19.6	1.07
	−80	447.0	20.3	1.07
Global	20	471.25 ± 29.10	20.65 ± 0.98	1.11 ± 0.02
	4	479.30 ± 3.14	21.13 ± 0.98	1.10 ± 0.06
	−80	478.70 ± 42.95	21.10 ± 0.85	1.10 ± 0.06

Essentially, evaluation by HPLC of complexes showed that, after 8 weeks of conservation at different temperatures (−80 °C, 4 °C, or 20 °C), cyclodextrin-loaded OA values were very close to the initial ones, even in the less favorable case of conservation at room temperature (20 °C) (Table 2). All these data suggest that after HP-β-CD complexation, OA becomes a very stable molecule.

3.4. Freeze-Dried OA/HP-β-CD Complexes Do Not Compromise Cell Viability

According to previous reports, OA/DMSO has a mild antiproliferative effect on epithelial cells [20,65,66], so we decided to check this outcome when OA was complexed with cyclodextrins. We performed a cell proliferation assay by culturing Mv1Lu in supplemented medium with 5 µM OA/DMSO and 12.5/3.12 µM/mM OA/HP-β-CD for 10 days and counting total cells each 2 days. Generally speaking, although a slight decrease in

proliferation was noticed with OA/HP-β-CD by 6 and 8 days, at longer times, cyclodextrin vehiculation produced higher cell counts than the OA/DMSO condition (Figure 1c), being less counterproductive for cell proliferation when compared to OA/DMSO.

All these data suggest a less antiproliferative effect of OA complexed with HP-β- and HP-γ-CDs on Mv1Lu cell migration that exhibits an improvement in cell migration and better cell viability than the ones observed for OA/DMSO.

3.5. Specific Inhibitors against Migration-Related Proteins Decreased OA Migration Triggered by OA/HP-β-CD Complexes

Previously, it has been shown that OA/DMSO produces migration on Mv1Lu cells by activating the EGFR receptor and mitogen-activated protein kinases (MAP kinases) (mitogen-activated protein kinase kinase, MEK, and c-Jun N-terminal kinase, JNK) [18,20,21]. The role of these proteins has been shown by using pharmacological inhibitors in in vitro scratch assays, together with expression protein level and phosphorylation studies by western blot [20]. First of all, the use of an EGF receptor inhibitor (EGFRi, PD153035) has been reported to be a strong inhibitor of epithelial cell migration [20,56,67]. Indeed, the high migratory percentage with OA/HP-β-CD complexes observed in the scratch was also significantly abrogated by EGFRi (Figure 2a,b).

In contrast, the use of specific inhibitors against MEK and JNK partially blocked OA/HP-β-CD as well as OA/DMSO migratory activity. Thus, in any case, OA/HP-β-CD complexes migration activity was significantly compromised, in a very similar fashion observed with OA/DMSO with the different inhibitors. All these data suggest that OA/HP-β-CD complexes seemed to use triggered OA-enhanced biochemical pathways as OA/DMSO.

3.6. OA/HP-β-CD Complexes Induce c-Jun Phosphorylation Transcription Factor at Cells at Scratch Edge in Mv1Lu

The stimulation of OA produces an activation of c-Jun that is observed at the nuclear level. Moreover, migrating cells show an activation of transcription factor c-Jun at the nuclei in response to OA stimulation [21]. We monitored p-c-Jun subcellular localization along the scratch edge. Strikingly, cells at scratch edge overexpressed p-c-Jun at cell nuclei in response to OA/HP-β-CD complexes, similarly to the OA/DMSO condition (Figure 3).

Interestingly enough, OA/HP-β-CD was causing a wider recruitment of migrating cells in the scratched area compared to OA/DMSO. Although the quantification of c-Jun phosphorylation showed that OA/DMSO treatment produced a strong stimulation of p-c-Jun at the edge, OA/HP-β-CD treatment produced a higher intensity of p-c-Jun at nuclei, together with a greater number of cells revealing p-c-Jun (Figure S4b); the calculated ratio of positive p-c-Jun nuclei versus the total number of nuclei in the picture also showed a higher ratio of the OA/HP-β-CD compared to the OA/DMSO (Figure S4c). Additionally, we noticed that nuclear p-c-Jun intensity was higher at the scratch edge cells and decreased as the cells were far from the scratch edge, exhibiting a p-c-Jun intensity gradient, positively correlating with cells with a high migratory status.

3.7. OA/HP-β-CD Complexes Promote Changes in Actin Fibers and Paxillin Distribution in Mv1Lu Cells

We have recently observed that OA effects on cell migration include cytoskeleton and focal adhesion (FA) remodeling [21]. To assess the consequences of complexed OA with HP-β-CDs, we carried out immunocytochemistry assays in in vitro scratched Mv1Lu cells targeting actin fibbers (F-Actin) and paxillin. Just after scratching (time 0 h), cells displayed paxillin as compact FA (Figure 4), and they exhibited low FA density and size.

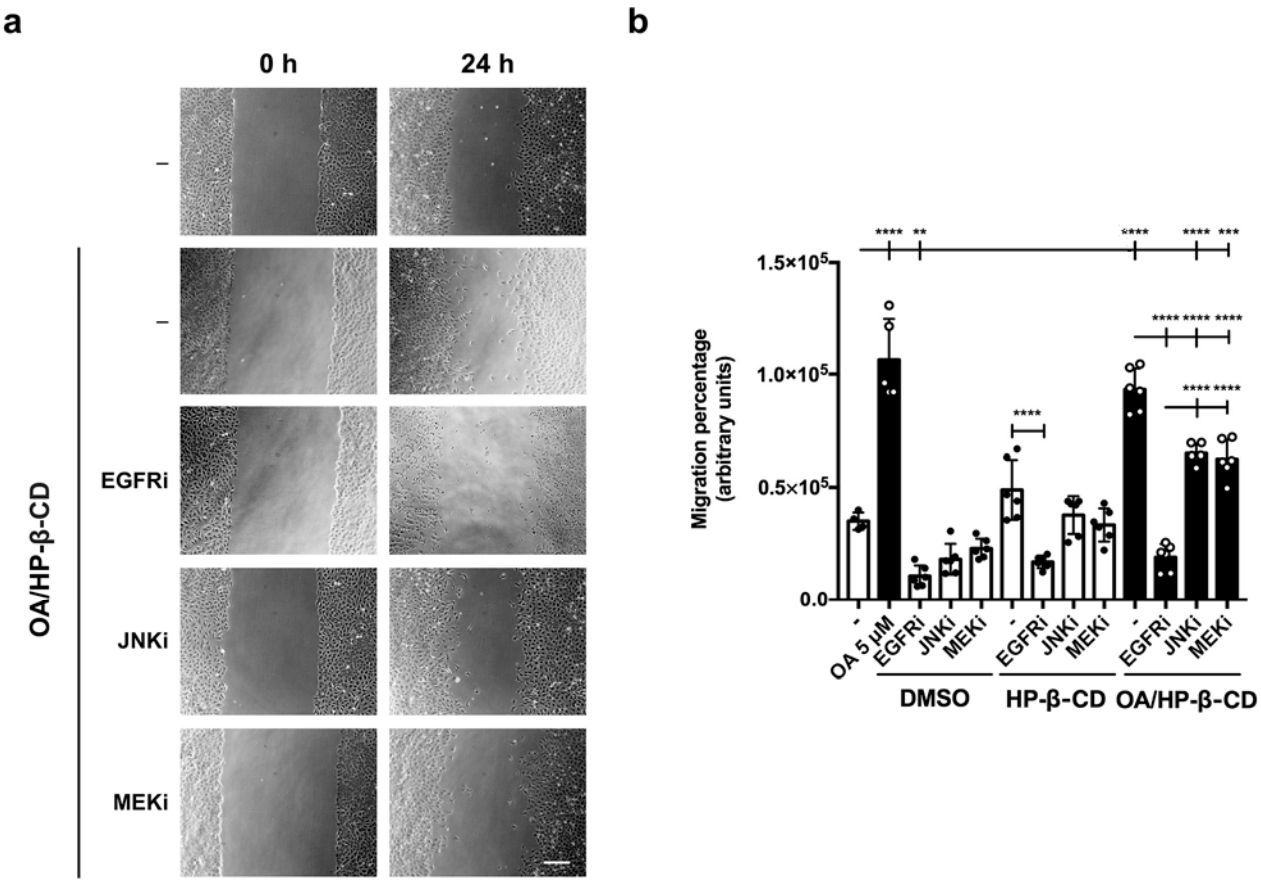

Figure 2. Pharmacological inhibitors against migration-related proteins decrease OA/HP-β-CD-induced cell migration in scratched Mv1Lu cells. Confluent Mv1Lu cells were scratched with a pipette tip and allowed to migrate for 24 h. Before adding treatments, EGFR, JNK, and MEK inhibitors were added to the medium (EGFRi, epidermal growth factor receptor inhibitor; JNKi, c-Jun N-terminal kinase inhibitor; MEKi, mitogen-activated protein kinase inhibitor). (**a**) The figure shows representative images of the in vitro scratch assay with cell migration under basal conditions (-) compared to those with 12.5/3.12 µM/mM OA/HP-β-CD alone (-) or with the above-mentioned inhibitors after 24 h treatment. The scale bar indicates 200 µm. (**b**) Plot represents cell migration as the difference between areas at time 0 h and time 24 h in each condition, named as migration percentage. Control conditions: white bars, black dots. Stimuli: black bars, white dots. Equivalent inhibitor concentrations were added too in vehicle control conditions DMSO and HP-β-CD. Asterisks indicate statistically significant differences between conditions according to a one-way ANOVA statistical analysis (** $p < 0.005$, *** $p < 0.001$, and **** $p < 0.0001$).

In contrast, the use of specific inhibitors against MEK and JNK partially blocked OA/HP-β-CD as well as OA/DMSO migratory activity. Thus, in any case, OA/HP-β-CD complexes migration activity was significantly compromised, in a very similar fashion observed with OA/DMSO with the different inhibitors. All these data suggest that OA/HP-β-CD complexes seemed to use triggered OA-enhanced biochemical pathways as both OA/DMSO and OA/HP-β-CD. Furthermore, after 12 h, FAs size was significantly smaller than basal control in OA/DMSO and OA/HP-β-CD conditions. Remarkably, we noticed that in the OA/HP-β-CD condition after 6 and 12 h exhibited a higher cell spreading along the scratch edge than with OA/DMSO when we took a look with more magnification (Figure S5). Interestingly, neither FAs size nor FAs density showed statistically significant differences between OA/DMSO and OA/HP-β-CD conditions. Regarding actin fibers, noticeable changes were observed in all conditions after 6 and 12 h; however, they were very evident after 12 h with OA/DMSO and OA/HP-β-CD, a time when cells displayed a lower actin intensity due to the actin disassembling during cell movement (Figure S5) [68].

Strikingly, after 6 h with OA/HP-β-CD treatment, we observed a high FAs density that was very noticeable at the pictures shown, being also coherent with the effects seen with OA/DMSO, however, with a slightly higher tendency than with OA/DMSO. Moreover, in terms of FAs size at 6 h, no statistical differences were observed between basal control and

The stimulation of OA produces an activation of c-Jun that is observed at the nuclear level. Moreover, migrating cells show an activation of transcription factor c-Jun at the nuclei in response to OA stimulation [21]. We monitored p-c-Jun subcellular localization along the scratch edge. Strikingly, cells at scratch edge overexpressed p-c-Jun at cell nuclei in response to OA/HP-β-CD complexes, similarly to the OA/DMSO condition (Figure 3).

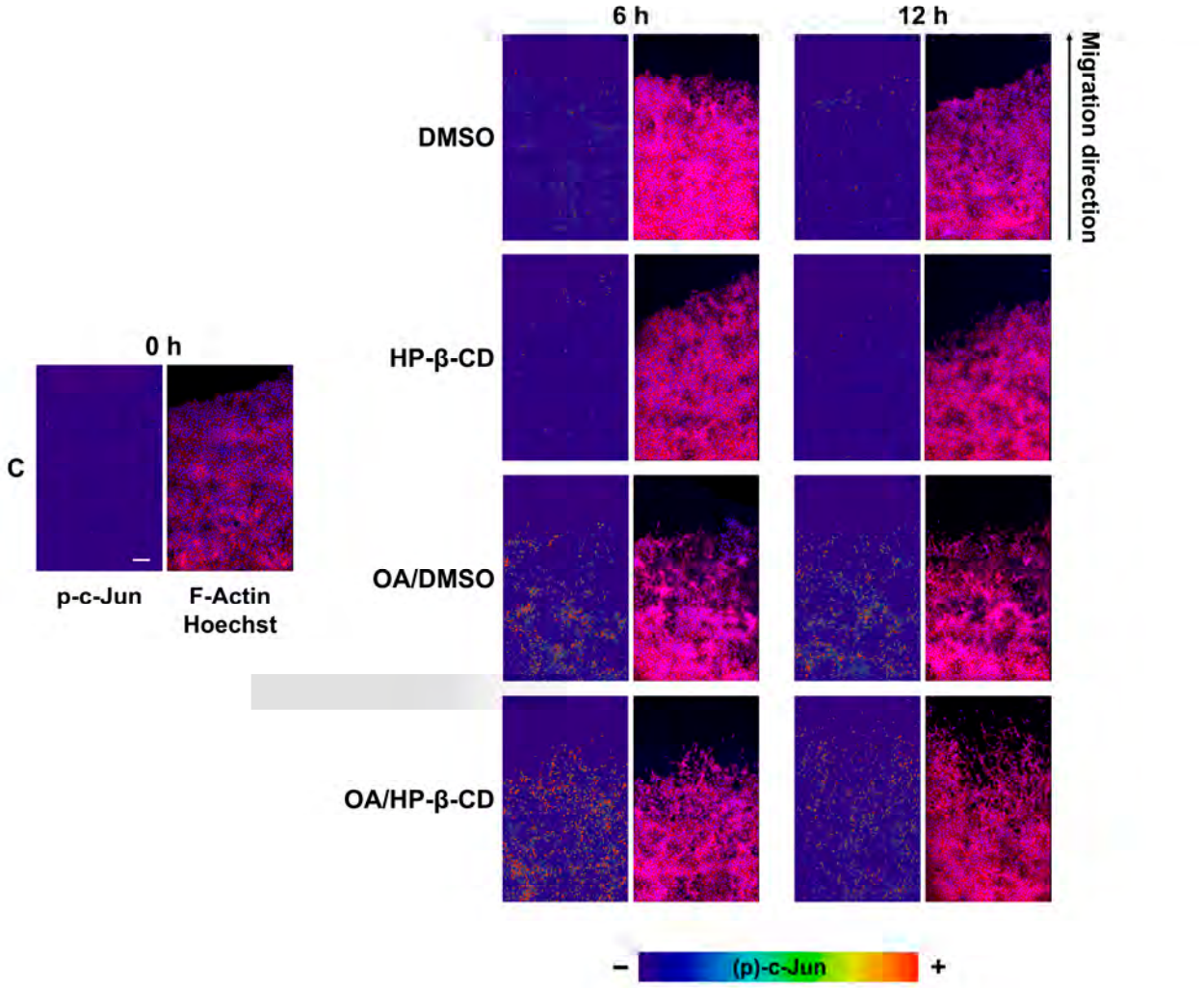

Figure 3. OA/HP-β-CD complexes promote c-Jun phosphorylation at the edge of scratched Mv1Lu cells. Confluent Mv1Lu cells were scratched and allowed to migrate for the indicated times (6 and 12 h). Cells were treated with 5 μM OA/DMSO or 12.5/3.12 μM/mM OA/HP-β-CD. Equivalent concentrations of DMSO and HP-β-CD were used as vehicle controls. Cells were immunostained with specific antibodies against c-Jun active phosphorylated form (p-c-Jun). Co-staining with phalloidin and Hoechst-33258 was used to show the actin cytoskeleton and nuclei, respectively. Images of p-c-Jun fluorescence were converted into pseudo-color with ImageJ software to show the intensity of p-c-Jun staining. Actin fibers (F-actin): red. Nuclei: blue. Images were obtained with a confocal microscope. This experiment was repeated at least three times. Representative images are shown. Scale bar indicates 100 μm.

Figure 3. OA/HP-β-CD complexes promote c-Jun phosphorylation at the edge of scratched Mv1Lu cells. Confluent Mv1Lu cells were scratched and allowed to migrate for the indicated times (6 and 12 h). Cells were treated with 5 μM OA/DMSO or 12.5/3.12 μM/mM OA/HP-β-CD. Equivalent concentrations of DMSO and HP-β-CD were used as vehicle controls. Cells were immunostained with specific antibodies against c-Jun active phosphorylated form (p-c-Jun). Co-staining with phalloidin and Hoechst-33258 was used to show the actin cytoskeleton and nuclei, respectively. Images of p-c-Jun fluorescence were converted into pseudo-color with ImageJ software to show the intensity of p-c-Jun staining. Actin fibers (F-actin): red. Nuclei: blue. Images were obtained with a confocal microscope. This experiment was repeated at least three times. Representative images are shown. Scale bar indicates 100 μm.

Interestingly enough, OA/HP-β-CD was causing a wider recruitment of migrating cells in the scratched area compared to OA/DMSO. Although the quantification of c-Jun

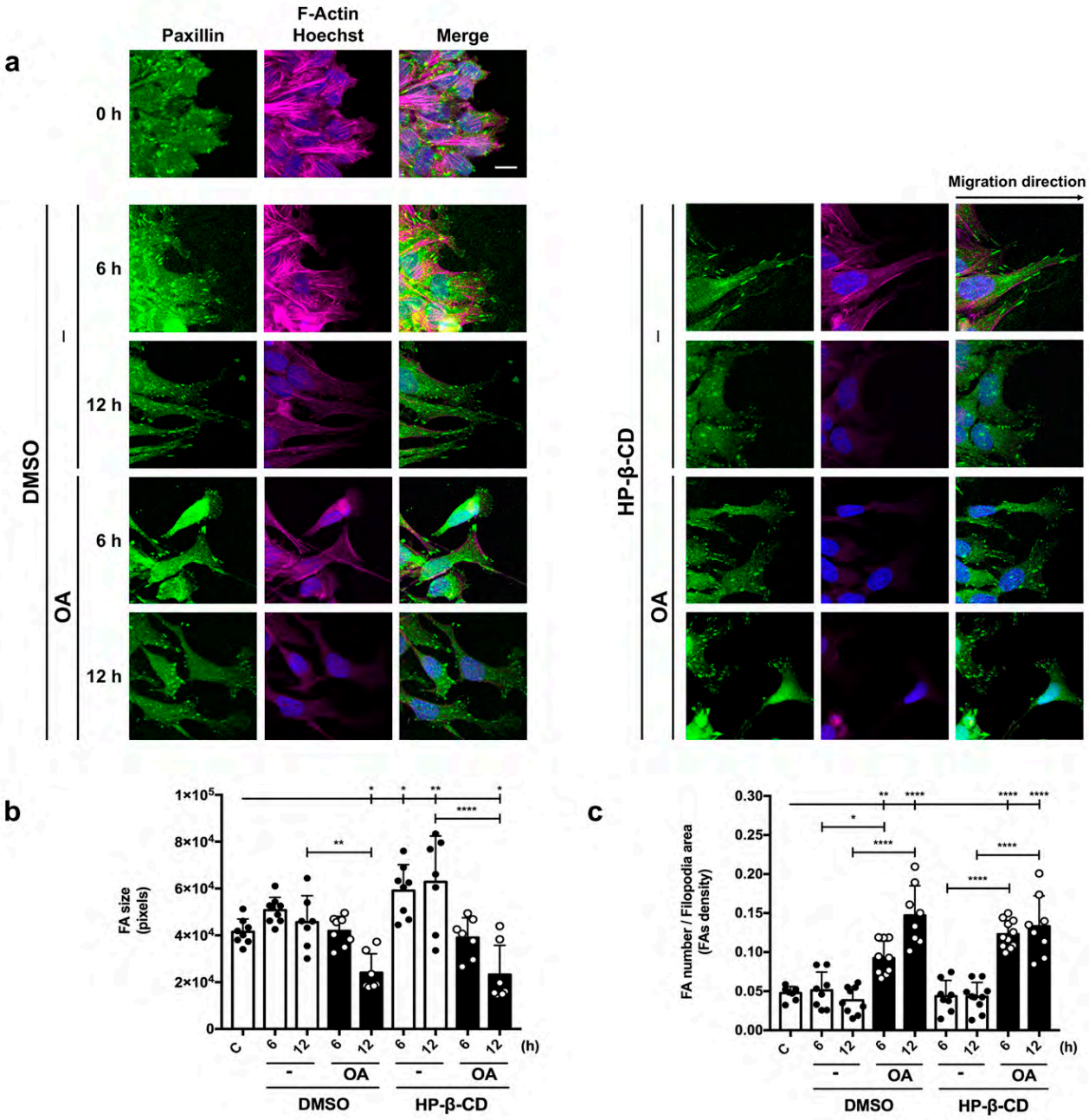

Figure 4. OA/HP-β-CD complexes promote changes in focal adhesions (FAs) revealed by Paxillin. (**a**) Confluent Mv1Lu cells were scratched and allowed to migrate for 6 and 12 h. Cells were treated with 5 µM OA/DMSO or 12.5/3.12 µM/mM OA/HP-β-CD. Equivalent concentrations of DMSO and HP-β-CD were used as vehicle controls. Cells were immunostained with specific antibodies against paxillin. Co-staining with phalloidin and Hoechst 33258 was used to show the actin cytoskeleton and nuclei, respectively. Paxillin: green. Actin fibers (F-Actin): red. Nuclei: blue. Images were obtained with a confocal microscope. Insets corresponding to 1/9 of the 63× original images (Figure S6) are shown for a detailed view of paxillin structures. This experiment was repeated at least three times. The scale bar indicates 6 µm. (**b**) FA size (average size) at the filopodia area. (**c**) Quantification of the density of FA (as FA number per filopodia area), Control conditions: white bars, black dots. Stimuli: black bars, white dots. A one-way ANOVA statistical analysis was performed (* $p < 0.05$, ** $p < 0.005$ and **** $p < 0.0001$).

Strikingly, after 6 h with OA/HP-β-CD treatment, we observed a high FAs density that was very noticeable at the pictures shown, being also coherent with the effects seen with OA/DMSO, however, with a slightly higher tendency than with OA/DMSO.

All these observations suggest that similarly to OA/DMSO, OA/HP-β-CD complexes produce high dynamization of the cytoskeleton and FA, compatible with a neat increment in migration rate.

3.8. OA/HP-β-CD Complexes Stimulate Migration in MDA-MB-231 Cells while Minimizing OA/DMSO Cytotoxic Effects

It has been seen that OA/DMSO stimulates MDA-MB-231 [23,35,69] migration in in vitro scratch assays at an optimal concentration of 10 μM [20,21]. We tested several concentrations of OA/HP-β-CD complexes, where MDA-MB-231 cells showed significant cell migration compared to basal (C) and vehicle control HP-β-CD conditions (Figure 5a,b).

Similar migration percentage values were observed between OA/DMSO and all OA/HP-β-CD concentrations tested, with no statistically significant differences reached. Nevertheless, there was a higher migration activity tendency within 17/4.25 μM/mM and 21/5.25 μM/mM OA/HP-β-CD concentration complexes. Furthermore, it was easy to notice that, in the case of OA/HP-β-CD, more cells could be found reaching the scratched gap area than in the OA/DMSO condition (Figure 5a).

OA/DMSO exhibits a mild antiproliferative effect on MDA-MB-231 cells [20]. OA/HP-β-CD treatment showed a nearly identical cell count to basal (control) and vehicle controls treatments in contrast to OA/DMSO, which was slightly affected since a lower number of cells was observed, a trend that was held for 10 days. Interestingly, these data suggest that MDA-MB-231 cell proliferation performed better, and near control samples, for OA/HP-β-CD complexes than for free OA/DMSO samples (Figure 5c).

All together, these experiments suggest that complexed OA with HP-β-CDs enhanced MDA-MB-231 cell migration while improving cell viability when compared to OA/DMSO.

3.9. Signaling Pathways Regulated by EGFR and c-Jun Activation, Necessary for Cell Migration, Are Induced by OA/HP-β-CD Complexes in MDA-MB-231 Cells

MDA-MB-231 cells are a suitable epithelial model for epidermal growth factor receptor (EGFR) expression regulation studies [21,23,70]. EGFR inhibitor (EGFRi), PD153035, is capable of reducing migration in MDA-MB-231 cells in OA/DMSO [20,21] and also in OA/HP-β-CD stimulated cells (see Figure 2).

With the objective of deeply deciphering the molecular mechanisms behind the OA/HP-β-CD complexes effect on cell migration, we decided to set up a whole study of key regulatory proteins involved in cell migration by using sub confluent cells [19,21,71]. Cells were stimulated with 10 μM OA/DMSO and 21/5.25 μM/mM OA/HP-β-CD, and the activation of different proteins was evaluated. Mainly, the phosphorylation consequences of all proteins studied were milder when cells were stimulated with OA/HP-β-CD in comparison to their DMSO-solubilized counterparts. To begin with, a p-EGFR stimulation was detected 2 h after treatment with OA/HP-β-CD, later increasing at 3 and 4 h; however, when compared to OA/DMSO, the stimulation was softer (Figure 6a,b).

When looking at a downstream EGFR kinase, p-ERK1/2, it was increased by OA/HP-β-CD treatment after 2 h following the same trend as EGFR phosphorylation (Figure 6a,b). Interestingly, OA/HP-β-CD showed significantly lower intensity values at time 2 h, and they were kept higher for longer periods of time. Regarding p-JNK1/2, both OA/HP-β-CD and OA/DMSO-induced stimulation stimulated this kinase at time 1 h; however, later in time, the dynamics were dissimilar. Interestingly, when blotting total c-Jun and active phosphorylated (p)-c-Jun forms, we observed changes on both antigens in response to OA/HP-β-CD, an effect that is evident also in the case of OA/DMSO [21]. In particular, in the case of p-c-Jun, the treatment with OA/HP-β-CD showed a mild increase at time 2 h that was sustained up to 6 h. In contrast, OA/DMSO produced a stronger stimulation of p-c-Jun at time 1 h; it was sustained in time up to 6 h and exhibited higher values than cyclodextrin-complexed OA. In any case, no increases in p-JNK1/2 and p-c-Jun regulatory proteins were observed with DMSO and HP-β-CD vehicle controls. Finally, total c-Jun levels were clearly increased by OA/HP-β-CD with a 2 h delay (3, 4, and 6 h) when compared to OA/DMSO, which stimulated c-Jun overexpression at the early time

All these observations suggest that similarly to OA/DMSO, OA/HP-β-CD complexes produce high dynamization of the cytoskeleton and FA, compatible with a neat increment in migration rate.

3.8. OA/HP-β-CD Complexes Stimulate Migration in MDA-MB-231 Cells while Minimizing OA/DMSO Cytotoxic Effects

It has been seen that OA/DMSO stimulates MDA-MB-231 [23,35,70] migration in in vitro scratch assays at an optimal concentration of 10 μM [20,21]. We tested several concentrations of OA/HP-β-CD complexes, where MDA-MB-231 cells showed significant cell migration compared to basal (C) and vehicle control HP-β-CD conditions (Figure 5a,b).

of 1 h. The overexpression and activation of the above-mentioned proteins in response to OA/HP-β-CD imply their participation in the cell migration phenomenon promoted by cyclodextrin-complexed OA.

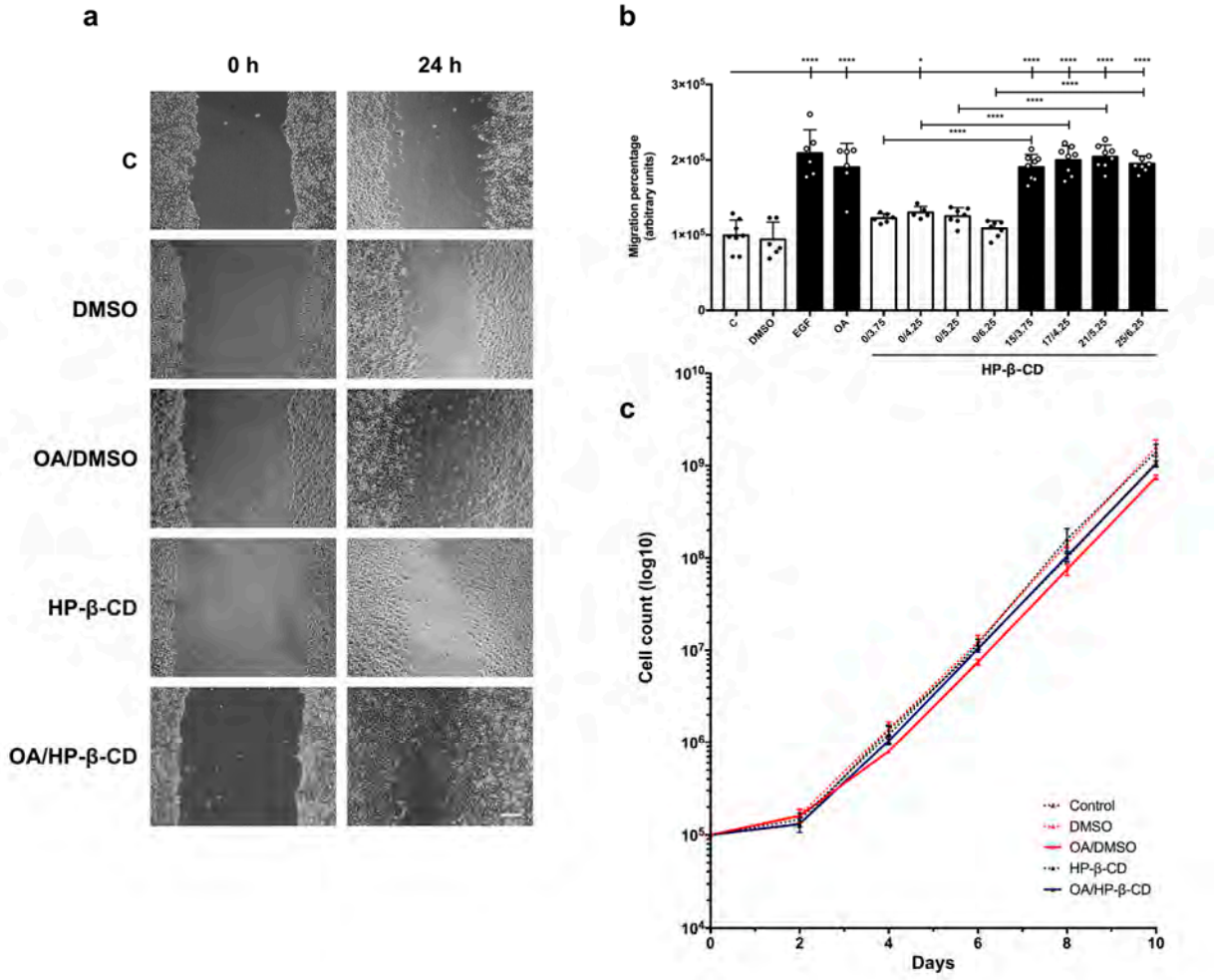

Figure 5. OA complexes with modified cyclodextrins HP-β-CD promote cell migration in MDA-MB-231 cells. Confluent MDA-MB-231 cells were scratched with a pipette tip and allowed to migrate for 24 h. (**a**) Representative images of the in vitro scratch assay with cell migration under basal conditions (C) compared to those with 5 μM OA/DMSO, 21/5.25 μM/mM OA/HP-β-CD, and equivalent concentrations of DMSO or HP-β-CD after 24 h treatment. The scale bar indicates 200 μm. (**b**) Plot represents cell migration as the difference between areas at time 0 h and time 24 h in each condition, named as migration percentage. Control conditions: white bars, black dots. Stimuli: black bars, white dots. The X axis indicates treatment conditions; for those with HP-β-CD concentrations are represented as the molar ratio OA μM/CD mM. Epidermal growth factor (EGF) was added at 10 ng/mL as a positive migration control. Asterisks indicate statistically significant differences between conditions according to a one-way ANOVA statistical analysis (* $p < 0.05$ and **** $p < 0.0001$). (**c**) The long term effects of 5 μM OA/DMSO and 21/5.25 μM/mM OA/HP-β-CD (with vehicle controls) on MDA-MB-231 proliferation were assessed by counting total cells at the indicated times. The logarithm of the mean number of cells against time is plotted.

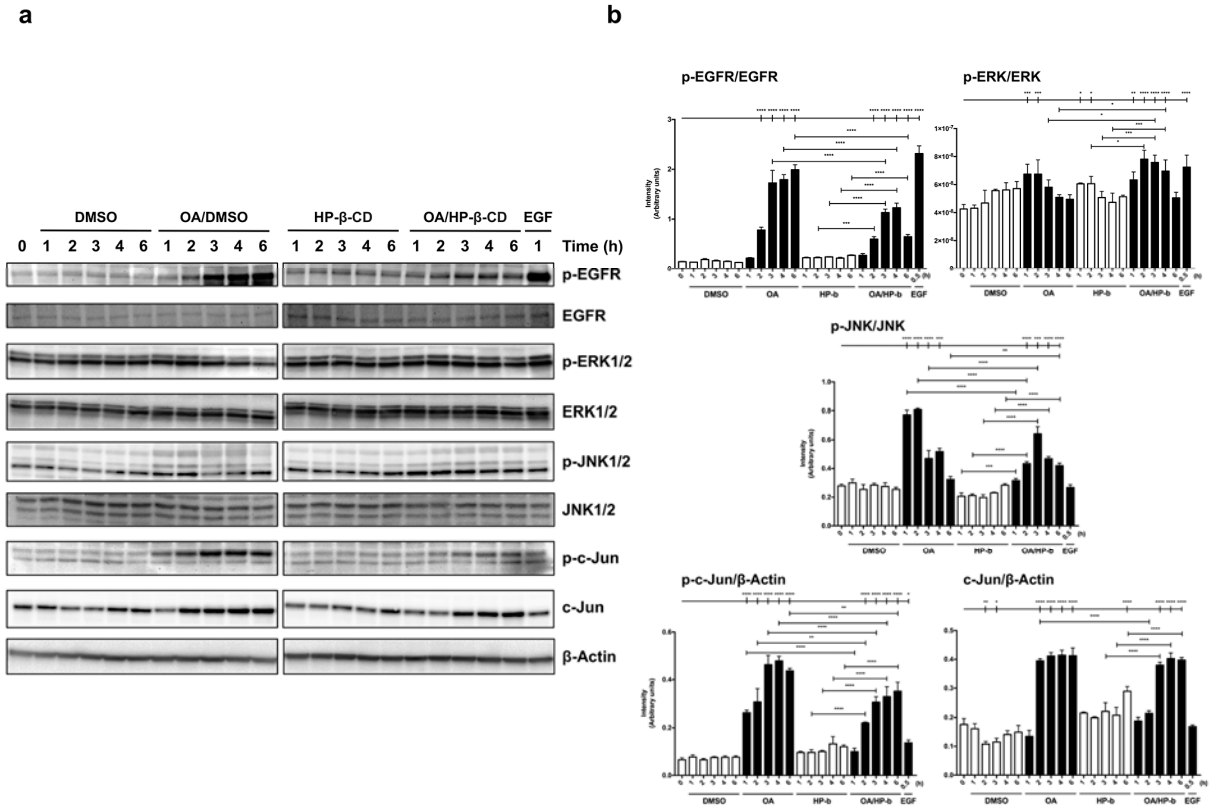

Figure 6. Signaling pathways regulated by EGFR and c-Jun activation, necessary for cell migration, are induced by OA/HP-β-CD complexes in MDA-MB-231 cells. (**a**) Total protein extracts from serum-starved sub-confluent MDA-MB-231 cells treated with 10 µM OA/DMSO, 2/5.25 µM/mM OA/HP-β-CD, or 10 ng/mL EGF. These extracts were assayed at the indicated times (hours) targeting: phospho-EGFR (Tyr 1068), phospho-ERK1/2 (Thr 202/Tyr 204), phospho-JNK1/2 (Thr 183/Tyr 185) and phospho-c-Jun (Ser 63). Total protein expression was assayed for the above-mentioned active protein forms: EGFR, ERK1/2, JNK1/2, and c-Jun. β-Actin was used as a loading control. DMSO and HP-β-CD equivalent concentrations were added as vehicle controls. A representative experiment was shown. (EGFR, epidermal growth factor receptor; ERK1/2, extracellular signal-regulated kinases 1 and 2; JNK1/2, c-Jun N-terminal kinases 1 and 2). (**b**) Column bar graphs represent the intensity values of each protein assayed by western blot by collecting the data from three independent experiments. Intensity values were quantified and gathered by ImageJ software. Asterisks indicate statistically significant differences between the selected conditions according to a one-way ANOVA statistical analysis. (* $p < 0.05$, ** $p < 0.005$, *** $p < 0.001$, and **** $p < 0.0001$).

Figure 6. Signaling pathways regulated by EGFR and c-Jun activation, necessary for cell migration, are induced by OA/HP-β-CD complexes in MDA-MB-231 cells. (**a**) Total protein extracts from serum-starved sub-confluent MDA-MB-231 cells treated with 10 µM OA/DMSO, 2/5.25 µM/mM OA/HP-β-CD, or 10 ng/mL EGF. These extracts were assayed at the indicated times (hours) targeting: phospho-EGFR (Tyr 1068), phospho-ERK1/2 (Thr 202/Tyr 204), phospho-JNK1/2 (Thr 183/Tyr 185) and phospho-c-Jun (Ser 63). Total protein expression was assayed for the above-mentioned active protein forms: EGFR, ERK1/2, JNK1/2, and c-Jun. β-Actin was used as a loading control. DMSO and HP-β-CD equivalent concentrations were added as vehicle controls. A representative experiment was shown. (EGFR, epidermal growth factor receptor; ERK1/2, extracellular signal-regulated kinases 1 and 2; JNK1/2, c-Jun N-terminal kinases 1 and 2). (**b**) Column bar graphs represent the intensity values of each protein assayed by western blot by collecting the data from three independent experiments. Intensity values were quantified and gathered by ImageJ software. Asterisks indicate statistically significant differences between the selected conditions according to a one-way ANOVA statistical analysis. (* $p < 0.05$, ** $p < 0.005$, *** $p < 0.001$, and **** $p < 0.0001$).

When looking at a downstream EGFR kinase, p-ERK1/2, it was increased by OA/DMSO stimulation of Mv1Lu shows similar molecular mechanisms as the MDA-MB-231 cell line [21]. Thus, we studied changes at the level of protein profiling in response to OA/HP-β-CD and compared them to OA/DMSO (Figure S7). Once again, OA/HP-β-CD complexes were capable of stimulating EGFR with similar phosphorylation patterns between OA/DMSO and OA/HP-β-CD and only differing in intensity values (Figure S7a,b). Strikingly, when looking at p-ERK1/2, OA/HP-β-CD stimulated p-ERK1/2 in a manner that differed from OA/DMSO, since p-ERK1/2 levels were significantly increased at earlier times (1 and 2 h) while OA/HP-β-CD produced a later response at times 4 and 6 h (Figure S7a,b). OA/DMSO and OA/HP-β-CD showed the same phosphorylation dynamic for p-JNK1/2, noticing in both cases an early response (time 1 h) with the highest levels of p-JNK1/2. Finally, c-Jun activation and overexpression were enhanced by OA/HP-β-CD values than cyclodextrin-complexed OA. In any case, no increases in p-JNK1/2, and p-c-Jun regulatory proteins were observed with DMSO and HP-β-CD vehicle controls. Finally, total c-Jun levels were clearly increased by OA/HP-β-CD with a 2 h delay (3, 4, and 6 h) when compared to OA/DMSO, which stimulated c-Jun overexpression at the early

OA/HP-β-CD treatment after 2 h following the same trend as EGFR phosphorylation (Figure 6a,b). Interestingly, OA/HP-β-CD showed significantly lower intensity values at time 2 h, and they were kept higher for longer periods of time. Regarding p-JNK1/2, both OA/HP-β-CD and OA/DMSO-induced stimulation stimulated this kinase at time 1 h, however, later in time, the dynamics were dissimilar. Interestingly, when blotting total c-Jun and active phosphorylated (p)-c-Jun forms, we observed changes on both antigens in response to OA/HP-β-CD, an effect that is evident also in the case of OA/DMSO [21]. In particular, in the case of p-c-Jun, the treatment with OA/HP-β-CD showed a mild increase at time 2 h that was sustained up to 6 h. In contrast, OA/DMSO produced a stronger stimulation of p-c-Jun at time 1 h; it was sustained in time up to 6 h and exhibited higher complexes. Regarding p-c-Jun, OA/HP-β-CD showed a clear increase on this active form such as OA/DMSO, but, remarkably, this increase was sustained until later times. In addition to this, c-Jun total levels were slightly increased by OA/HP-β-CD at time 1 h and

then at time 4 and 6 h, remaining as a trend compared to basal conditions, as this induction on total c-Jun was not as higher as with OA/DMSO.

Altogether, these results on protein expression and activation by phosphorylation on MDA-MB-231 and Mv1Lu cells point to the fact that complexed OA with modified cyclodextrins, as seen with OA/DMSO, clearly triggered different protein kinase targets to induce biochemical pathways, which are necessary to lead to cell migration.

4. Discussion

Oleanolic acid-triggered molecular mechanisms are compatible with improved cell migration, making them a potential wound healing agent [20,21]. Nevertheless, its hydrophobic nature stunts its application in hydrophilic contexts [52]. In this paper, we have shown how OA complexation in HP-β- and HP-γ- modified cyclodextrins can improve OA application and OA activity on in vitro cell culture models Mv1Lu and MDA-MB-231 [20,21].

The lipophilic nature of OA implies the need for improved delivery with new carriers, which could allow its conservation, protection, and application. For OA delivery, many studies have shown its vehiculation by a variety of macromolecules in several applications. For instance, nanoparticles made from polymers such as polyethylene glycol, cellulose, or silicone have been used to encapsulate OA [72–76]. Despite this, these nanoparticles require a long chemical synthesis and further 3D structure analyses, which are expensive and time-consuming. That is why cyclodextrins might be considered a better option to improve OA delivery and application. Remarkably, a dehydration step, performed by freeze drying, improves the effect on OA from cyclodextrins since they protect and preserve OA in long-term storage by keeping OA loaded for weeks at 4 °C and even at 20 °C. Conversely, OA/DMSO required specific storage conditions in liquid nitrogen (−190 °C) to maintain it long-term [20,21]. What is more, the OA/CDs powder formulation can be easily diluted in cell culture media or other desired aqueous solutions, avoiding microbial contamination and preserving the osmolarity of cell culture media.

HP-β- and HP-γ-CDs were chosen for OA complexation and subsequent in vitro assays for their improved water solubility compared to native cyclodextrins [48,77]. Both HP-β- and HP-γ-CD have shown that they can properly encapsulate OA, and dried solid complexes of OA can be obtained. However, it has been noticed that there is different behavior between them. The higher encapsulation constant (K_c) of the HP-γ-CD (K_c = 645 M^{-1}) complexes compared to the HP-β-CD complexes (K_c = 201 M^{-1}) [52] is associated with higher complex stability. This could contribute to a reduced loss of OA during the encapsulation and dehydration processes of the complex, resulting in higher encapsulation efficiency (EE) and a higher final retention of the active compound. As a consequence, this leads to a higher drug loading (DL mg/g) in the ultimately obtained solid complexes of OA/HP-γ-CD. This may represent an advantage at first, but it is necessary to determine whether the stability of the complex, dependent on its K_c value, allows a proper release of the host compound into the medium so that it can exert its biological activity.

The stability of the obtained complexes, defined by the K_c values of the complexes and dependent on the type of CD, can modulate the activity of the host molecule of the complex. In this regard, the results of cell migration show that, for the same concentration of 12.5 µM of OA, the level of cell migration has been higher for HP-β- than for HP-γ-CD complexes. The complex OA/HP-β-CD has a lower complexation constant (K_c) [52], indicating that OA is released more easily from the hydrophobic cavity of the CD, as it is a less stable complex compared to the one formed with HP-γ-CD. For this reason, HP-β-CD appears to be the most suitable CD for the complexation of OA, as it demonstrates a better compromise between adequate compound release capability and the high aqueous solubility of OA.

Furthermore, the results obtained demonstrate that the complexation of OA in CD partially limits its ability to stimulate cell migration, as it is necessary to increase the concentration of OA to 12.5 µM and 62.5 µM to achieve the same level of cell migration obtained with 5 µM of OA dissolved in DMSO. This limitation in the biological activity of

different encapsulated active compounds, previously described by other authors [43,78–80], is expected since encapsulation traps the active molecule and its release is conditioned by the stability of the complexes. On the other hand, it is known that, when solubilized with DMSO, OA acts at a very tight range of concentrations to see its cell migration activity on Mv1Lu and MDA-MB-231 epithelial cell lines [20,21]. Concentrations out of this range have cytotoxic effects and cell viability loss. Indeed, OA biological effects are cell-type specific, as OA is used as an antiproliferative in some tumor cell lines [62,81,82]. With our gathered data on scratch and proliferation assays, we observed that cyclodextrin complexation changed the OA dose-effect. First, OA/HP-β-CD complex concentrations that show cell migration activity peaks were mainly two times higher than the ones with OA/DMSO for both cell lines Mv1Lu and MDA-MB-231. Additionally, proliferation assays in these two cell lines showed a slightly higher cell count than OA/DMSO conditions, suggesting a protective effect of the cyclodextrin. These data could be explained by the non-direct and slow OA delivery to cells because of the OA lodging into the cyclodextrins, which produces a sustained OA release [83]. This improved delivery suggests better OA bioavailability for epithelial cells, which in fact could mitigate cell viability loss and improve cell migration from the scratch edges.

We noticed that complexed OA showed reinforced cell migration activity on Mv1Lu. On in vitro scratch assays, we observed that scratch treated with OA/HP-β-CD complexes displayed higher recruitment of migrating cells than OA/DMSO, as a migration morphology was very patent in several lines from the scratch edge. Even though this recruitment was less patent, it could also be seen in MDA-MB-231 scratch assays. Interestingly, this phenomenon correlated positively with immunocytochemistry assays in Mv1Lu, in which we study p-c-Jun activation and its subcellular location, which are crucial to express cell migration genes [84,85]. We saw a different pattern of activation when comparing OA/DMSO and OA/HP-β-CD scratched cells. Strikingly, scratched cells treated with OA/HP-β-CD showed a wider belt of cells with nuclear overexpressed and activated c-Jun. Indeed, the ratio of positive nuclei and total nuclei was higher in the OA/HP-β-CD condition than in the OA/DMSO condition, showing a decrease as the cells became far from the scratch edge. These results point out that OA complexation with cyclodextrins endows the oleanolic with improved properties on cell migration.

In terms of paxillin remodeling, OA/DMSO and OA/HP-β-CD conditions displayed quite similar patterns, especially when looking at focal adhesion size. We could not identify differences between the two treatments, so more studies must be carried out to decipher these mechanisms, such as paxillin/FAK colocalization assays by confocal microscopy [21]. However, regarding F-Actin distribution at cells at scratch edges, we could observe filopodia and ruffle formation during OA-triggered migration. Indeed, Mv1Lu scratch-edge cells treated with OA/HP-β-CD showed qualitatively a greater number of filopodia and ruffles since the cells were more spread along the scratched area. This, together with the fact that in OA/HP-β-CD condition F-Actin filaments were less patent than in OA/DMSO condition, suggests a highest degree of mobilization of structures in response to oleanolic when it was complexed. This could be related to the activation of c-Jun, the master regulator of cell migration [26,84,85], which lasted longer when the cells were stimulated with OA/HP-β-CD.

Some of the molecular events happening in cells when they are stimulated with OA suggest a general activation of several kinases related to cell movement. In order to deepen the molecular mechanisms underlaying the effects of OA/HP-β-CD complexes on cell migration, the same key regulatory proteins were examined [23,84–89]. Generally speaking, the responses obtained with OA/HP-β-CD were similar to those obtained with OA/DMSO. Surprisingly, the activation (phosphorylation) of many of the different proteins studied was milder with complexed OA compared to its DMSO-solubilized counterpart. However, in the case of MDA-MB-231, the activation pattern showed a delayed response in the OA/HP-β-CD condition than in the OA/DMSO condition. Furthermore, the levels of

the proteins assayed were lower in the OA/HP-β-CD condition than in the OA/DMSO condition, probably due to the different dynamics that cyclodextrins brought.

What is more, this study found that cell migration promoted by OA/HP-β-CD complexes in Mv1Lu cells exhibited similar molecular mechanisms to MDA-MB-231 cells, as it was previously described for OA/DMSO [21]. Interestingly, as seen with OA/DMSO, the cell migration that OA/HP-β-CD complexes produced was compromised when specific inhibitors against EGFR, MEK, and JNK were added to the media in scratch assays. Moreover, similar phosphorylation patterns were observed between OA/DMSO and OA/HP-β-CD for p-EGFR and p-JNK proteins. By contrast, OA/HP-β-CD complexes stimulated p-ERK1/2 at later times compared to OA/DMSO. Regarding c-Jun and p-c-Jun blots, the expression of both forms was increased and sustained at later times in the OA/HP-β-CD condition. These results suggest a sustained effect of complexed OA on this transcription factor, which also correlates positively with immunocytochemistry assays, where a greater number of cells with high p-c-Jun were observed at scratch edges. Altogether, these observations in western blots led us to think that these regulator proteins show a delayed response with OA complexes, probably due to the cyclodextrin slow-release dynamic. This response could be beneficial because, over time, OA complexes provided more migrating cells than OA/DMSO covering the scratched area.

Altogether, the evidence shown by the in vitro scratch assays favors the higher efficacy of cyclodextrins delivering OA to cells, based on the wide spread of activation caused. However, to make a perfect correlation, a western blot should be performed on the area that is activated by OA/HP-β-CD and compared to the rest of the epithelia, but, at present, we have not found a way of analyzing the samples in such a way. This may reflect the fact that using confluent cultures to depict what is happening at the scratch edge has some limitations that, with the current technology, cannot been overcome.

In summary, the study on key regulatory proteins indicates that complexed OA with modified cyclodextrins triggers the same biochemical pathways as OA/DMSO, which is necessary for cell migration of both MDA-MB-231 and Mv1Lu cells. In this study, we highlighted the potential of these epithelial cell models for investigating EGFR and key regulatory kinases expression in cell migration under OA/HP-β-CD complexes effects.

All in all, here we showed how cyclodextrin complexation allows OA application improvement, making it suitable to develop a product that could be used topically on skin for wound healing. Given the enhanced OA solubilization and improved activity on epithelial cells, we are prone to performing in vivo assays in the future. In this sense, many assays can be carried out on in vivo models to study complex OA effects on wound healing [90,91].

In this paper, we have deciphered how OA complexation with modified cyclodextrins could improve OA application and activity in vitro. Our results showed that OA/CDs, mainly OA/HP-β-CD complexes, showed significant activity on cell migration and toxicity protection in Mv1Lu and MDA-MB-231 cells. In addition to this, OA/HP-β-CD complexes induce a whole signaling system compatible with cell migration, such as OA/DMSO. Even though both agents triggered the same mechanisms, OA/HP-β-CD complexes showed greater migrating cell recruitment powered by greater c-Jun activation and displaying a sustained OA effect on cell migration provided by cyclodextrins slow release to the media. Validating that OA maintains its biological activity when it is complexed in the form of a solid complex with HP-β-CD is a key aspect of drug application because solid-state complexes improve the handling and stability of compounds, enabling better dose standardization [43]. This represents a clear technical advantage for the pharmaceutical industry. Furthermore, the complexation of OA with CD enables achieving effective OA concentrations in an aqueous medium, eliminating the need for organic solvents such as DMSO. Finally, given the implications that this paper shows, the research on OA complexed with cyclodextrins for developing an effective treatment for difficult wounds seems very promising.

5. Conclusions

Oleanolic acid conjugated to cyclodextrins (OA/CDs) exhibits enhanced properties compared to OA solubilized with DMSO. Specifically, OA/HP-β-CD not only enhances cell migration but also improves cell viability. It also plays a role in cytoskeleton reorganization and in mobilizing focal adhesions. Much like OA/DMSO, OA/HP-β-CD activates specific migration pathways. Moreover, complexing OA with cyclodextrins significantly enhances the molecule's stability and enables its solubility in aqueous solutions. This crucial enhancement extends its practical applications. Consequently, we now have a hydrophilic conjugate that is more bioavailable, stable, and readily applicable to wound care.

Supplementary Materials: The following supporting information can be downloaded at: https://www.mdpi.com/article/10.3390/ijms241914860/s1.

Author Contributions: J.S.-F. conceived, prepared, and performed the experiments, complexed OA with cyclodextrins, gathered the data, analyzed the data, discussed the data, drew the figures, and wrote the manuscript; S.L.-M. conceived and prepared OA complexes, discussed the experiments, and wrote the manuscript; J.A.G. supervised the experiments and supervised the writing of the manuscript; and F.J.N. conceived the experiments, discussed the data, gathered funding, supervised the writing of the manuscript, and wrote the final version of the manuscript. All authors have read and agreed to the published version of the manuscript.

Funding: Instituto de Salud Carlos III, Fondo de Investigaciones Sanitarias. Plan Estatal I+D+I and Instituto de Salud Carlos III-Subdirección General de Evaluación y Fomento de la Investigación (Grant nos.: PI17/02164 and PI21/01339) http://www.isciii.es/ (accessed on 29 September 2023). Fondos FEDER (EDRF) "Una manera de hacer Europa" A way of making Europe.

Institutional Review Board Statement: Not applicable.

Informed Consent Statement: Not applicable.

Data Availability Statement: All data supporting this paper had been included. In order to clarify western blot data, we displayed cropped blots of each figure in the paper as (Figures S8 and S9). These figures contain original blots of each protein assayed with molecular weight markers for a better identification.

Acknowledgments: We thank Gareth J. Inman for Mv1Lu cells and Ander Izeta for MDA-MB-231 cells. J.S.-F. was supported with a "Contrato Predoctoral para la Formación de Personal Investigador" from Universidad Católica San Antonio de Murcia (UCAM). We are indebted to the Hospital Clínico Universitario Virgen de la Arrixaca for strongly supporting and providing funding to conduct this research.

Conflicts of Interest: The authors declare no conflict of interest.

References

1. Nguyen, A.V.; Soulika, A.M. The Dynamics of the Skin's Immune System. *Int. J. Mol. Sci.* **2019**, *20*, 1811. [CrossRef] [PubMed]
2. Ridiandries, A.; Tan, J.T.M.; Bursill, C.A. The Role of Chemokines in Wound Healing. *Int. J. Mol. Sci.* **2018**, *19*, 3217. [CrossRef]
3. Wang, P.H.; Huang, B.S.; Horng, H.C.; Yeh, C.C.; Chen, Y.J. Wound healing. *J. Chin. Med. Assoc.* **2018**, *81*, 94–101. [CrossRef]
4. Eming, S.A.; Martin, P.; Tomic-Canic, M. Wound repair and regeneration: Mechanisms, signaling, and translation. *Sci. Transl. Med.* **2014**, *6*, 265sr6. [CrossRef]
5. Eming, S.A.; Krieg, T.; Davidson, J.M. Inflammation in wound repair: Molecular and cellular mechanisms. *J. Investig. Dermatol.* **2007**, *127*, 514–525. [CrossRef] [PubMed]
6. Janis, J.E.; Harrison, B. Wound Healing: Part I. *Basic. Science. Plast. Reconstr. Surg.* **2016**, *138* (Suppl. 3), 9S–17S. [CrossRef] [PubMed]
7. Okonkwo, U.A.; DiPietro, L.A. Diabetes and Wound Angiogenesis. *Int. J. Mol. Sci.* **2017**, *18*, 1419. [CrossRef]
8. Blair, M.J.; Jones, J.D.; Woessner, A.E.; Quinn, K.P. Skin Structure-Function Relationships and the Wound Healing Response to Intrinsic Aging. *Adv. Wound Care* **2020**, *9*, 127–143. [CrossRef]
9. Bonifant, H.; Holloway, S. A review of the effects of ageing on skin integrity and wound healing. *Br. J. Community Nurs.* **2019**, *24* (Suppl. 3), S28–S33. [CrossRef]
10. Burgess, J.L.; Wyant, W.A.; Abdo Abujamra, B.; Kirsner, R.S.; Jozic, I. Diabetic Wound-Healing Science. *Medicina* **2021**, *57*, 1072. [CrossRef]

11. Patel, S.; Srivastava, S.; Singh, M.R.; Singh, D. Mechanistic insight into diabetic wounds: Pathogenesis, molecular targets and treatment strategies to pace wound healing. *Biomed. Pharmacother.* **2019**, *112*, 108615. [CrossRef] [PubMed]
12. Kasuya, A.; Tokura, Y. Attempts to accelerate wound healing. *J. Dermatol. Sci.* **2014**, *76*, 169–172. [CrossRef] [PubMed]
13. Neuhaus, K.; Meuli, M.; Koenigs, I.; Schiestl, C. Management of "difficult" wounds. *Eur. J. Pediatr. Surg.* **2013**, *23*, 365–374.
14. Ball, V.; Younggren, B.N. Emergency management of difficult wounds: Part I. *Emerg. Med. Clin. North. Am.* **2007**, *25*, 101–121. [CrossRef]
15. Zhao, P.; Sui, B.D.; Liu, N.; Lv, Y.J.; Zheng, C.X.; Lu, Y.B.; Huang, W.T.; Zhou, C.H.; Chen, J.; Pang, D.L.; et al. Anti-aging pharmacology in cutaneous wound healing: Effects of metformin, resveratrol, and rapamycin by local application. *Aging Cell* **2017**, *16*, 1083–1093. [CrossRef]
16. Shin, S.A.; Joo, B.J.; Lee, J.S.; Ryu, G.; Han, M.; Kim, W.Y.; Park, H.H.; Lee, J.H.; Lee, C.S. Phytochemicals as Anti-Inflammatory Agents in Animal Models of Prevalent Inflammatory Diseases. *Molecules* **2020**, *25*, 5932. [CrossRef]
17. Ghiulai, R.; Rosca, O.J.; Antal, D.S.; Mioc, M.; Mioc, A.; Racoviceanu, R.; Macaşoi, I.; Olariu, T.; Dehelean, C.; Creţu, O.M.; et al. Tetracyclic and Pentacyclic Triterpenes with High Therapeutic Efficiency in Wound Healing Approaches. *Molecules* **2020**, *25*, 5557. [CrossRef]
18. Ayeleso, T.B.; Matumba, M.G.; Mukwevho, E. Oleanolic Acid and Its Derivatives: Biological Activities and Therapeutic Potential in Chronic Diseases. *Molecules* **2017**, *22*, 1915. [CrossRef]
19. Moura-Letts, G.; Villegas, L.F.; Marcalo, A.; Vaisberg, A.J.; Hammond, G.B. In vivo wound-healing activity of oleanolic acid derived from the acid hydrolysis of Anredera diffusa. *J. Nat. Prod.* **2006**, *69*, 978–979. [CrossRef] [PubMed]
20. Bernabe-Garcia, A.; Armero-Barranco, D.; Liarte, S.; Ruzafa-Martinez, M.; Ramos-Morcillo, A.J.; Nicolas, F.J. Oleanolic acid induces migration in Mv1Lu and MDA-MB-231 epithelial cells involving EGF receptor and MAP kinases activation. *PLoS ONE* **2017**, *12*, e0172574. [CrossRef]
21. Stelling-Ferez, J.; Gabaldon, J.A.; Nicolas, F.J. Oleanolic acid stimulation of cell migration involves a biphasic signaling mechanism. *Sci. Rep.* **2022**, *12*, 15065. [CrossRef] [PubMed]
22. Leserer, M.; Gschwind, A.; Ullrich, A. Epidermal growth factor receptor signal transactivation. *IUBMB Life* **2000**, *49*, 405–409. [PubMed]
23. Islam, T.; Resat, H. Quantitative investigation of MDA-MB-231 breast cancer cell motility: Dependence on epidermal growth factor concentration and its gradient. *Mol. Biosyst.* **2017**, *13*, 2069–2082. [CrossRef] [PubMed]
24. Herdegen, T.; Skene, P.; Bahr, M. The c-Jun transcription factor-bipotential mediator of neuronal death, survival and regeneration. *Trends Neurosci.* **1997**, *20*, 227–231. [CrossRef]
25. Meng, Q.; Xia, Y. c-Jun, at the crossroad of the signaling network. *Protein Cell* **2011**, *2*, 889–898. [CrossRef] [PubMed]
26. Yue, C.; Guo, Z.; Luo, Y.; Yuan, J.; Wan, X.; Mo, Z. c-Jun Overexpression Accelerates Wound Healing in Diabetic Rats by Human Umbilical Cord-Derived Mesenchymal Stem Cells. *Stem Cells Int.* **2020**, *2020*, 7430968. [CrossRef]
27. Neub, A.; Houdek, P.; Ohnemus, U.; Moll, I.; Brandner, J.M. Biphasic regulation of AP-1 subunits during human epidermal wound healing. *J. Invest. Dermatol.* **2007**, *127*, 2453–2462. [CrossRef]
28. Brown, M.C.; Turner, C.E. Paxillin: Adapting to change. *Physiol. Rev.* **2004**, *84*, 1315–1339. [CrossRef]
29. Schlaepfer, D.D.; Hauck, C.R.; Sieg, D.J. Signaling through focal adhesion kinase. *Prog. Biophys. Mol. Biol.* **1999**, *71*, 435–478. [CrossRef]
30. Mitra, S.K.; Hanson, D.A.; Schlaepfer, D.D. Focal adhesion kinase: In command and control of cell motility. *Nat. Rev. Mol. Cell Biol.* **2005**, *6*, 56–68. [CrossRef]
31. Deramaudt, T.B.; Dujardin, D.; Hamadi, A.; Noulet, F.; Kolli, K.; De Mey, J.; Takeda, K.; Rondé, P.; Bellance, C.; Khan, J.A.; et al. FAK phosphorylation at Tyr-925 regulates cross-talk between focal adhesion turnover and cell protrusion. *Mol. Biol. Cell* **2011**, *22*, 964–975. [CrossRef] [PubMed]
32. Turner, C.E. Paxillin and focal adhesion signalling. *Nat. Cell Biol.* **2000**, *2*, E231–E236. [CrossRef] [PubMed]
33. Zaidel-Bar, R.; Milo, R.; Kam, Z.; Geiger, B. A paxillin tyrosine phosphorylation switch regulates the assembly and form of cell-matrix adhesions. *J. Cell Sci.* **2007**, *120 Pt 1*, 137–148. [CrossRef]
34. Deramaudt, T.B.; Dujardin, D.; Noulet, F.; Martin, S.; Vauchelles, R.; Takeda, K.; Rondé, P. Altering FAK-paxillin interactions reduces adhesion, migration and invasion processes. *PLoS ONE* **2014**, *9*, e92059. [CrossRef]
35. Pontillo, C.A.; Garcia, M.A.; Pena, D.; Cocca, C.; Chiappini, F.; Alvarez, L.; Kleiman de Pisarev, D.; Randi, A.S. Activation of c-Src/HER1/STAT5b and HER1/ERK1/2 signaling pathways and cell migration by hexachlorobenzene in MDA-MB-231 human breast cancer cell line. *Toxicol. Sci.* **2011**, *120*, 284–296. [CrossRef]
36. Rahimi, N.; Hung, W.; Tremblay, E.; Saulnier, R.; Elliott, B. c-Src kinase activity is required for hepatocyte growth factor-induced motility and anchorage-independent growth of mammary carcinoma cells. *J. Biol. Chem.* **1998**, *273*, 33714–33721. [CrossRef]
37. Smith, E.R.; Hadidian, Z.; Mason, M.M. The single-and repeated-dose toxicity of dimethyl sulfoxide. *Ann. N. Y. Acad. Sci.* **1967**, *141*, 96–109. [CrossRef]
38. Galvao, J.; Davis, B.; Tilley, M.; Normando, E.; Duchen, M.R.; Cordeiro, M.F. Unexpected low-dose toxicity of the universal solvent DMSO. *FASEB J.* **2014**, *28*, 1317–1330. [CrossRef] [PubMed]
39. Pinho, E.; Grootveld, M.; Soares, G.; Henriques, M. Cyclodextrins as encapsulation agents for plant bioactive compounds. *Carbohydr. Polym.* **2014**, *101*, 121–135. [CrossRef]
40. Del Valle, E.M.M. Cyclodextrins and their uses: A review. *Process Biochem.* **2004**, *39*, 1033–1046. [CrossRef]

41. Kurkov, S.V.; Loftsson, T. Cyclodextrins. *Int. J. Pharm.* **2013**, *453*, 167–180. [CrossRef]
42. Poulson, B.G.; Alsulami, Q.A.; Sharfalddin, A.; El Agammy, E.F.; Mouffouk, F.; Emwas, A.-H.; Jaremko, L.; Jaremko, M. Cyclodextrins: Structural, Chemical, and Physical Properties, and Applications. *Polysaccharides* **2021**, *3*, 1–31. [CrossRef]
43. Lopez-Miranda, S.; Berdejo, D.; Pagan, E.; Garcia-Gonzalo, D.; Pagan, R. Modified cyclodextrin type and dehydration methods exert a significant effect on the antimicrobial activity of encapsulated carvacrol and thymol. *J. Sci. Food Agric.* **2021**, *101*, 3827–3835. [CrossRef]
44. Pitha, J.; Gerloczy, A.; Olivi, A. Parenteral hydroxypropyl cyclodextrins: Intravenous and intracerebral administration of lipophiles. *J. Pharm. Sci.* **1994**, *83*, 833–837. [CrossRef]
45. Soica, C.; Oprean, C.; Borcan, F.; Danciu, C.; Trandafirescu, C.; Coricovac, D.; Crăiniceanu, Z.; Dehelean, C.A.; Munteanu, M. The synergistic biologic activity of oleanolic and ursolic acids in complex with hydroxypropyl-gamma-cyclodextrin. *Molecules* **2014**, *19*, 4924–4940. [CrossRef] [PubMed]
46. Capelezzo, A.P.; Mohr, L.C.; Dalcanton, F.; Mello JMMd Fiori, M.A. β-Cyclodextrins as Encapsulating Agents of Essential Oils. In *Cyclodextrin—A Versatile Ingredient 2018*; IntechOpen: London, UK, 2018.
47. Saokham, P.; Muankaew, C.; Jansook, P.; Loftsson, T. Solubility of Cyclodextrins and Drug/Cyclodextrin Complexes. *Molecules* **2018**, *23*, 1161. [CrossRef] [PubMed]
48. Duchene, D.; Bochot, A. Thirty years with cyclodextrins. *Int. J. Pharm.* **2016**, *514*, 58–72. [CrossRef]
49. Lucas-Abellán, C.; Fortea, M.I.; Gabaldón, J.A.; Núñez-Delicado, E. Complexation of resveratrol by native and modified cyclodextrins: Determination of complexation constant by enzymatic, solubility and fluorimetric assays. *Food Chem.* **2008**, *111*, 262–267. [CrossRef]
50. Mercader-Ros, M.T.; Lucas-Abellán, C.; Fortea, M.I.; Gabaldón, J.A.; Núñez-Delicado, E. Effect of HP-β-cyclodextrins complexation on the antioxidant activity of flavonols. *Food Chem.* **2010**, *118*, 769–773. [CrossRef]
51. Rajewski, R.A.; Stella, V.J. Pharmaceutical applications of cyclodextrins. 2. In vivo drug delivery. *J. Pharm. Sci.* **1996**, *85*, 1142–1169. [CrossRef]
52. Lopez-Miranda, S.; Guardiola, L.; Hernandez-Sanchez, P.; Nunez-Delicado, E. Complexation between oleanolic and maslinic acids with native and modified cyclodextrins. *Food Chem.* **2018**, *240*, 139–146. [CrossRef]
53. Zou, Y.; Lim, S.; Lee, K.; Deng, X.; Friedman, E. Serine/threonine kinase Mirk/Dyrk1B is an inhibitor of epithelial cell migration and is negatively regulated by the Met adaptor Ran-binding protein M. *J. Biol. Chem.* **2003**, *278*, 49573–49581. [CrossRef] [PubMed]
54. Demetriou, M.; Nabi, I.R.; Coppolino, M.; Dedhar, S.; Dennis, J.W. Reduced contact-inhibition and substratum adhesion in epithelial cells expressing GlcNAc-transferase V. *J. Cell Biol.* **1995**, *130*, 383–392. [CrossRef] [PubMed]
55. Horzum, U.; Ozdil, B.; Pesen-Okvur, D. Step-by-step quantitative analysis of focal adhesions. *MethodsX* **2014**, *1*, 56–59. [CrossRef] [PubMed]
56. Bos, M.; Mendelsohn, J.; Kim, Y.M.; Albanell, J.; Fry, D.W.; Baselga, J. PD153035, a tyrosine kinase inhibitor, prevents epidermal growth factor receptor activation and inhibits growth of cancer cells in a receptor number-dependent manner. *Clin. Cancer Res.* **1997**, *3*, 2099–2106.
57. Bennett, B.L.; Sasaki, D.T.; Murray, B.W.; O'Leary, E.C.; Sakata, S.T.; Xu, W.; Leisten, J.C.; Motiwala, A.; Pierce, S.; Satoh, Y.; et al. SP600125, an anthrapyrazolone inhibitor of Jun N-terminal kinase. *Proc. Natl. Acad. Sci. USA* **2001**, *98*, 13681–13686. [CrossRef] [PubMed]
58. Shang, J.; Lu, S.; Jiang, Y.; Zhang, J. Allosteric modulators of MEK1: Drug design and discovery. *Chem. Biol. Drug Des.* **2016**, *88*, 485–497. [CrossRef]
59. Liarte, S.; Bernabe-Garcia, A.; Armero-Barranco, D.; Nicolas, F.J. Microscopy Based Methods for the Assessment of Epithelial Cell Migration During In Vitro Wound Healing. *J. Vis. Exp.* **2018**, *131*, e56799.
60. Ernst, O.; Zor, T. Linearization of the bradford protein assay. *J. Vis. Exp.* **2010**, *38*, e1918.
61. Wu, F.; Buckley, S.; Bui, K.C.; Yee, A.; Wu, H.Y.; Liu, J.; Warburton, D. Cell cycle arrest in G0/G1 phase by contact inhibition and TGF-beta 1 in mink Mv1Lu lung epithelial cells. *Am. J. Physiol.* **1996**, *270*, L879–L888. [CrossRef]
62. He, Y.; Liu, X.; Huang, M.; Wei, Z.; Zhang, M.; He, M.; Zheng, Z.; Dong, H.; Liu, D. Oleanolic acid inhibits the migration and invasion of hepatocellular carcinoma cells by promoting microRNA-122 expression. *Pharmazie* **2021**, *76*, 422–427. [PubMed]
63. Astray, G.; Gonzalez-Barreiro, C.; Mejuto, J.C.; Rial-Otero, R.; Simal-Gándara, J. A review on the use of cyclodextrins in foods. *Food Hydrocoll.* **2009**, *23*, 1631–1640. [CrossRef]
64. Morin-Crini, N.; Fourmentin, S.; Fenyvesi, É.; Lichtfouse, E.; Torri, G.; Fourmentin, M.; Crini, G. 130 years of cyclodextrin discovery for health, food, agriculture, and the industry: A review. *Environ. Chem. Lett.* **2021**, *19*, 2581–2617. [CrossRef]
65. Wojciak-Kosior, M.; Paduch, R.; Matysik-Wozniak, A.; Niedziela, P.; Donica, H. The effect of ursolic and oleanolic acids on human skin fibroblast cells. *Folia Histochem. Cytobiol.* **2011**, *49*, 664–669. [CrossRef] [PubMed]
66. Kuonen, R.; Weissenstein, U.; Urech, K.; Kunz, M.; Hostanska, K.; Estko, M.; Heusser, P.; Baumgartner, S. Effects of Lipophilic Extract of Viscum album L. and Oleanolic Acid on Migratory Activity of NIH/3T3 Fibroblasts and on HaCat Keratinocytes. *Evid. Based Complement. Alternat. Med.* **2013**, *2013*, 718105. [CrossRef] [PubMed]
67. Cole, G.W., Jr.; Alleva, A.M.; Reddy, R.M.; Maxhimer, J.B.; Zuo, J.; Schrump, D.S.; Nguyen, D.M. The selective epidermal growth factor receptor tyrosine kinase inhibitor PD153035 suppresses expression of prometastasis phenotypes in malignant pleural mesothelioma cells in vitro. *J. Thorac. Cardiovasc. Surg.* **2005**, *129*, 1010–1017. [CrossRef]
68. Schaks, M.; Giannone, G.; Rottner, K. Actin dynamics in cell migration. *Essays Biochem.* **2019**, *63*, 483–495.

69. McInroy, L.; Maatta, A. Down-regulation of vimentin expression inhibits carcinoma cell migration and adhesion. *Biochem. Biophys. Res. Commun.* **2007**, *360*, 109–114. [CrossRef] [PubMed]
70. Herbst, R.S. Review of epidermal growth factor receptor biology. *Int. J. Radiat. Oncol. Biol. Phys.* **2004**, *59* (Suppl. 2), 21–26. [CrossRef]
71. Xia, Y.; Makris, C.; Su, B.; Li, E.; Yang, J.; Nemerow, G.R.; Karin, M. MEK kinase 1 is critically required for c-Jun N-terminal kinase activation by proinflammatory stimuli and growth factor-induced cell migration. *Proc. Natl. Acad. Sci. USA* **2000**, *97*, 5243–5248. [CrossRef]
72. Man, D.K.; Casettari, L.; Cespi, M.; Bonacucina, G.; Palmieri, G.F.; Sze, S.C.; Leung, G.P.H.; Lam, J.K.W.; Kwok, P.C.L. Oleanolic Acid Loaded PEGylated PLA and PLGA Nanoparticles with Enhanced Cytotoxic Activity against Cancer Cells. *Mol. Pharm.* **2015**, *12*, 2112–2125. [CrossRef]
73. Wang, Y.; Zhu, P.; Li, G.; Zhu, S.; Liu, K.; Liu, Y.; He, J.; Lei, J. Amphiphilic carboxylated cellulose-g-poly(l-lactide) copolymer nanoparticles for oleanolic acid delivery. *Carbohydr. Polym.* **2019**, *214*, 100–109. [CrossRef] [PubMed]
74. Kumbham, S.; Paul, M.; Itoo, A.; Ghosh, B.; Biswas, S. Oleanolic acid-conjugated human serum albumin nanoparticles encapsulating doxorubicin as synergistic combination chemotherapy in oropharyngeal carcinoma and melanoma. *Int. J. Pharm.* **2022**, *614*, 121479. [CrossRef]
75. Zhang, S.; Peng, B.; Chen, Z.; Yu, J.; Deng, G.; Bao, Y.; Ma, C.; Du, F.; Sheu, W.C.; Kimberly, W.T.; et al. Brain-targeting, acid-responsive antioxidant nanoparticles for stroke treatment and drug delivery. *Bioact. Mater.* **2022**, *16*, 57–65. [CrossRef]
76. Leilei, L.; Wenke, Q.; Yuyuan, L.; Sihang, L.; Xue, S.; Weiqiang, C.; Lianbao, Y.; Ying, W.; Yan, L.; Ming, L. Oleanolic acid-loaded nanoparticles attenuate activation of hepatic stellate cells via suppressing TGF-beta1 and oxidative stress in PM2.5-exposed hepatocytes. *Toxicol. Appl. Pharmacol.* **2022**, *437*, 115891. [CrossRef] [PubMed]
77. George, S.; Vasudevan, D. Studies on the Preparation, Characterization, and Solubility of 2-HP-beta-Cyclodextrin-Meclizine HCl Inclusion Complexes. *J. Young Pharm.* **2012**, *4*, 220–227. [CrossRef] [PubMed]
78. Del Toro-Sánchez, C.L.; Ayala-Zavala, J.F.; Machi, L.; Santacruz, H.; Villegas-Ochoa, M.A.; Alvarez-Parrilla, E.; González-Aguilar, G.A. Controlled release of antifungal volatiles of thyme essential oil from β-cyclodextrin capsules. *J. Incl. Phenom. Macrocycl. Chem.* **2010**, *67*, 431–441. [CrossRef]
79. Kfoury, M.; Auezova, L.; Ruellan, S.; Greige-Gerges, H.; Fourmentin, S. Complexation of estragole as pure compound and as main component of basil and tarragon essential oils with cyclodextrins. *Carbohydr. Polym.* **2015**, *118*, 156–164. [CrossRef]
80. Silva, F.; Caldera, F.; Trotta, F.; Nerín, C.; Domingues, F.C. Encapsulation of coriander essential oil in cyclodextrin nanosponges: A new strategy to promote its use in controlled-release active packaging. *Innov. Food Sci. Emerg. Technol.* **2019**, *56*, 102177. [CrossRef]
81. Edathara, P.M.; Chintalapally, S.; Makani, V.K.K.; Pant, C.; Yerramsetty, S.; Rao, M.D.; Bhadra, M.P. Inhibitory role of oleanolic acid and esculetin in HeLa cells involve multiple signaling pathways. *Gene* **2021**, *771*, 145370. [CrossRef]
82. Liu, J.; Ban, H.; Liu, Y.; Ni, J. The expression and significance of AKR1B10 in laryngeal squamous cell carcinoma. *Sci. Rep.* **2021**, *11*, 18228. [CrossRef]
83. Loftsson, T.; Jarho, P.; Másson, M.; Järvinen, T. Cyclodextrins in drug delivery. *Expert. Opin. Drug Deliv.* **2005**, *2*, 335–351. [CrossRef]
84. Li, G.; Gustafson-Brown, C.; Hanks, S.K.; Nason, K.; Arbeit, J.M.; Pogliano, K.; Wisdom, R.M.; Johnson, R.S. c-Jun is essential for organization of the epidermal leading edge. *Dev. Cell* **2003**, *4*, 865–877. [CrossRef] [PubMed]
85. Altan, Z.M.; Fenteany, G. c-Jun N-terminal kinase regulates lamellipodial protrusion and cell sheet migration during epithelial wound closure by a gene expression-independent mechanism. *Biochem. Biophys. Res. Commun.* **2004**, *322*, 56–67. [CrossRef]
86. Matsubayashi, Y.; Ebisuya, M.; Honjoh, S.; Nishida, E. ERK activation propagates in epithelial cell sheets and regulates their migration during wound healing. *Curr. Biol.* **2004**, *14*, 731–735. [CrossRef]
87. Yujiri, T.; Ware, M.; Widmann, C.; Oyer, R.; Russell, D.; Chan, E.; Zaitsu, Y.; Clarke, P.; Tyler, K.; Oka, Y.; et al. MEK kinase 1 gene disruption alters cell migration and c-Jun NH2-terminal kinase regulation but does not cause a measurable defect in NF-kappa B activation. *Proc. Natl. Acad. Sci. USA* **2000**, *97*, 7272–7277. [CrossRef] [PubMed]
88. Huang, C.; Rajfur, Z.; Borchers, C.; Schaller, M.D.; Jacobson, K. JNK phosphorylates paxillin and regulates cell migration. *Nature* **2003**, *424*, 219–223. [CrossRef]
89. Huang, Z.; Yan, D.P.; Ge, B.X. JNK regulates cell migration through promotion of tyrosine phosphorylation of paxillin. *Cell Signal* **2008**, *20*, 2002–2012. [CrossRef] [PubMed]
90. Davidson, J.M. Animal models for wound repair. *Arch. Dermatol. Res.* **1998**, *290*, S1–S11. [CrossRef]
91. Grambow, E.; Sorg, H.; Sorg, C.G.G.; Struder, D. Experimental Models to Study Skin Wound Healing with a Focus on Angiogenesis. *Med. Sci.* **2021**, *9*, 55. [CrossRef]

Figure S 1

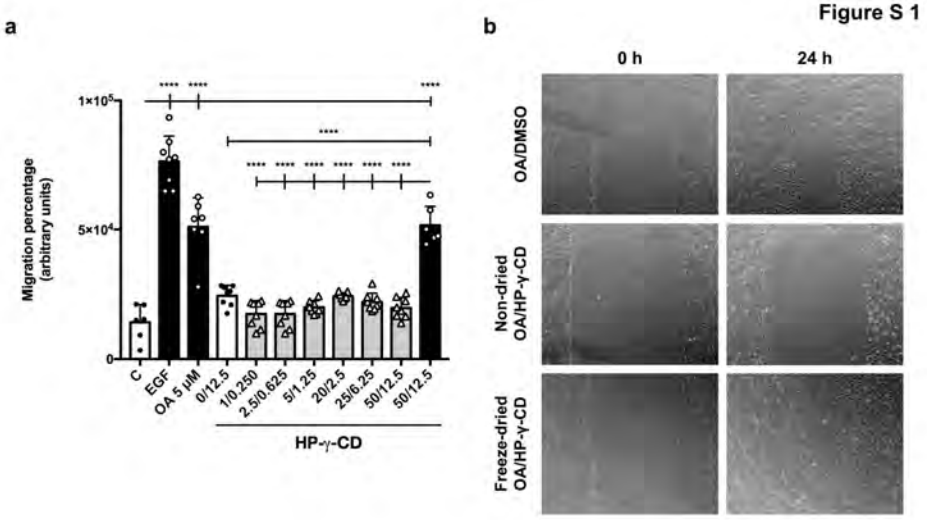

Figure S1. Non-dried OA/CDs complexes have poor effectivity on cell migration as opposed to freeze dried OA/CDs complexes in Mv1Lu cells. Confluent Mv1Lu cells were scratched with a pipette tip and allowed to migrate for 24 hours. (a) Plot represents cell migration as the difference between areas at time 0 hours and time 24 hours in each condition, named as migration percentage. X axis indicates treatment conditions, for those with HP-γ-CD, the concentrations are represented as molar ratio OA μM /CD mM. Non-dried OA/HP-γ-CD complexes concentrations used are represented in grey bars and white triangles. Freeze dried 50/12.5 μM/mM OA/HP-γ-CD complexes and 5 μM OA/DMSO were used as positive control (black bars). Empty HP-γ-CDs at 0/12.5 μM/mM were used as vehicle control. Epidermal growth factor (EGF) was added at 10 ng/ml as a positive migration control. Asterisks indicate statistically significant differences between conditions according to a One-way ANOVA statistical analysis (****p<0.0001). (b) Representative images of the wound healing assay with cell migration under 5 μM OA/DMSO compared to those non-dried OA/HP-γ-CD complexes after 24 h treatment. DMSO, and 0/12.5 μM/mM HP-γ-CD were used as vehicle controls.

Figure S 2

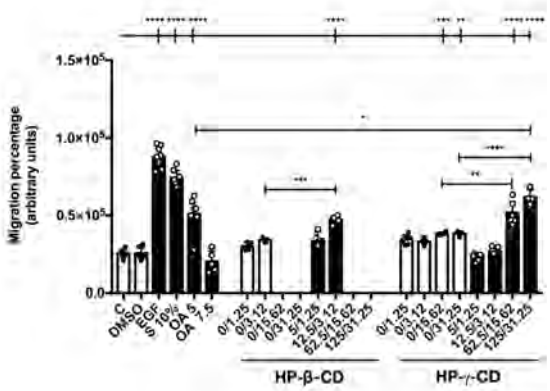

Figure S2. OA complexes with modified cyclodextrins HP-β-CD and HP-γ-CD promote cell migration in scratched Mv1Lu cells. Plot represents cell migration as the difference between areas at time 0 hours and time 24 hours in each condition, named as migration percentage. X axis indicates treatment conditions, for those with HP-β-CD and HP-γ-CD, the concentrations are represented as molar ratio OA μM/CD mM. Additional concentrations of OA/CDs are shown. Note that concentrations without any data point indicate cell viability loss as a consequence of the OA cytotoxic effect at high OA concentrations. 10 % FBS (S 10%) and 10 ng/ml EGF were also added to the experiment as positive migration controls. Asterisks indicate statistically significant differences between conditions according to a One-way ANOVA statistical analysis (*p<0.05, **p<0.005, ***p<0.001 and ****p<0.0001).

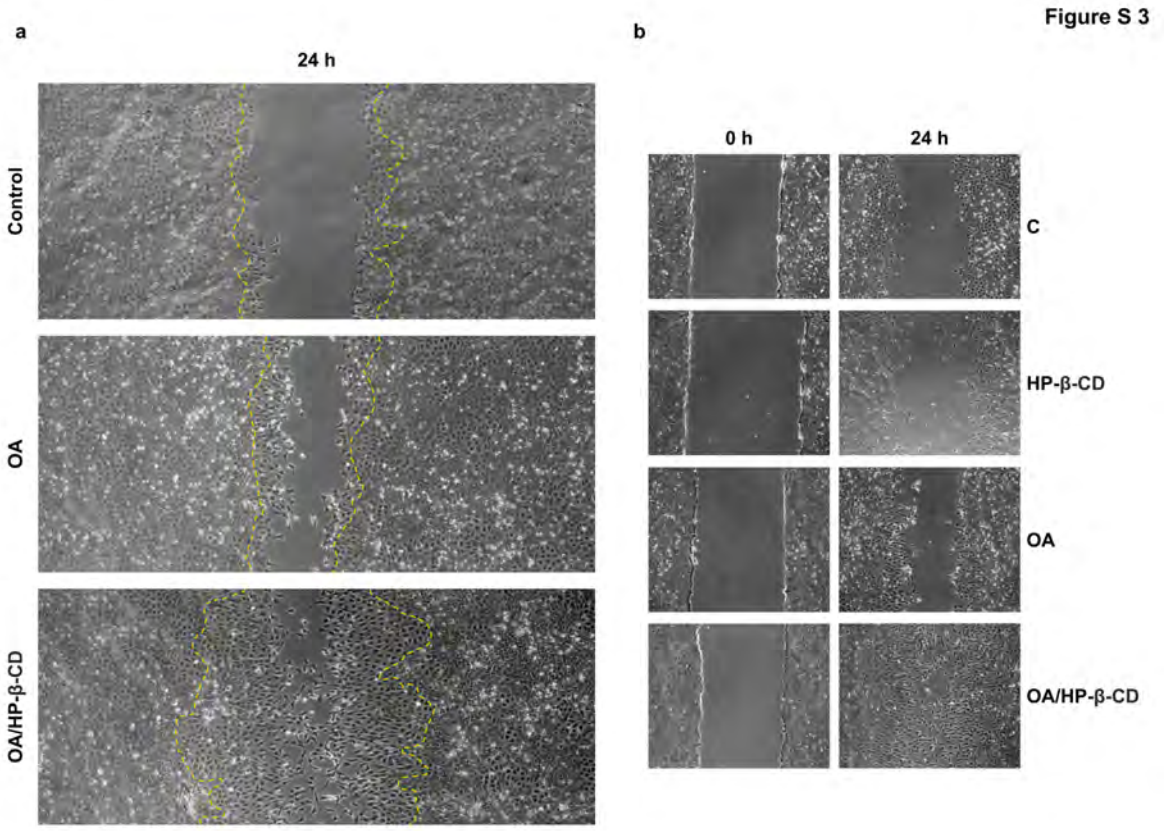

Figure S3. OA complexes recruit a higher number of Mv1Lu migratory-cells than OA/DMSO on in vitro scratch assays. (a) Composite pictures of the in vitro scratch assay showing the first lines of cells at the scratch edge and cells far away from the edge. Images show cell migration under basal conditions (Control) compared to those with 5 μM OA/DMSO and 12.5/3.12 μM/mM OA/HP-β-CD after 24 hours treatment. Note that with OA/HP-β-CD complexes a greater number of cell lines are recruited to migrate along the scratch. (b) Pictures corresponding to the same assay showing vehicle control conditions with equivalent concentrations. Scale bar 200 μM.

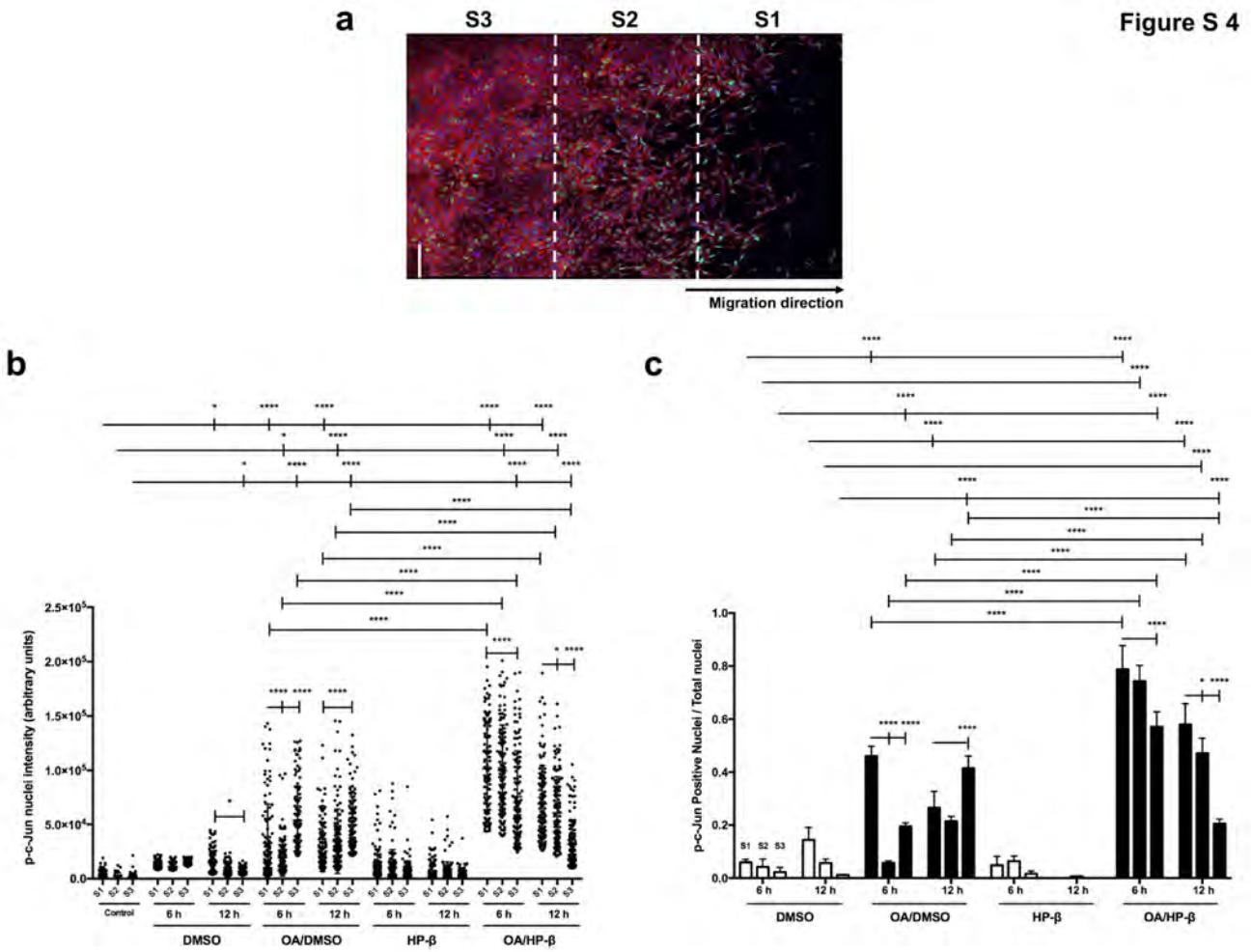

Figure S4. OA/HP β CD complexes promote higher c Jun transcription factor phosphorylation than OA/DMSO at the scratch edge. (a) The image represents how a Tile Scan image is divided in three equal sectors for better analyze active c Jun (p c Jun) expression. Scale bar indicates 100 μm. (b) Plot represents the p c Jun intensity in cell nuclei. Each point represents the intensity of p c Jun intensity in one nucleus. (c) Plot represents the relation between the number of positive p c Jun nuclei and total number nuclei existent in each sector. In order to exclude negative p c Jun nuclei, an intensity p c Jun threshold was set using the p c Jun intensity mean in basal (control) condition.

Figure S 5

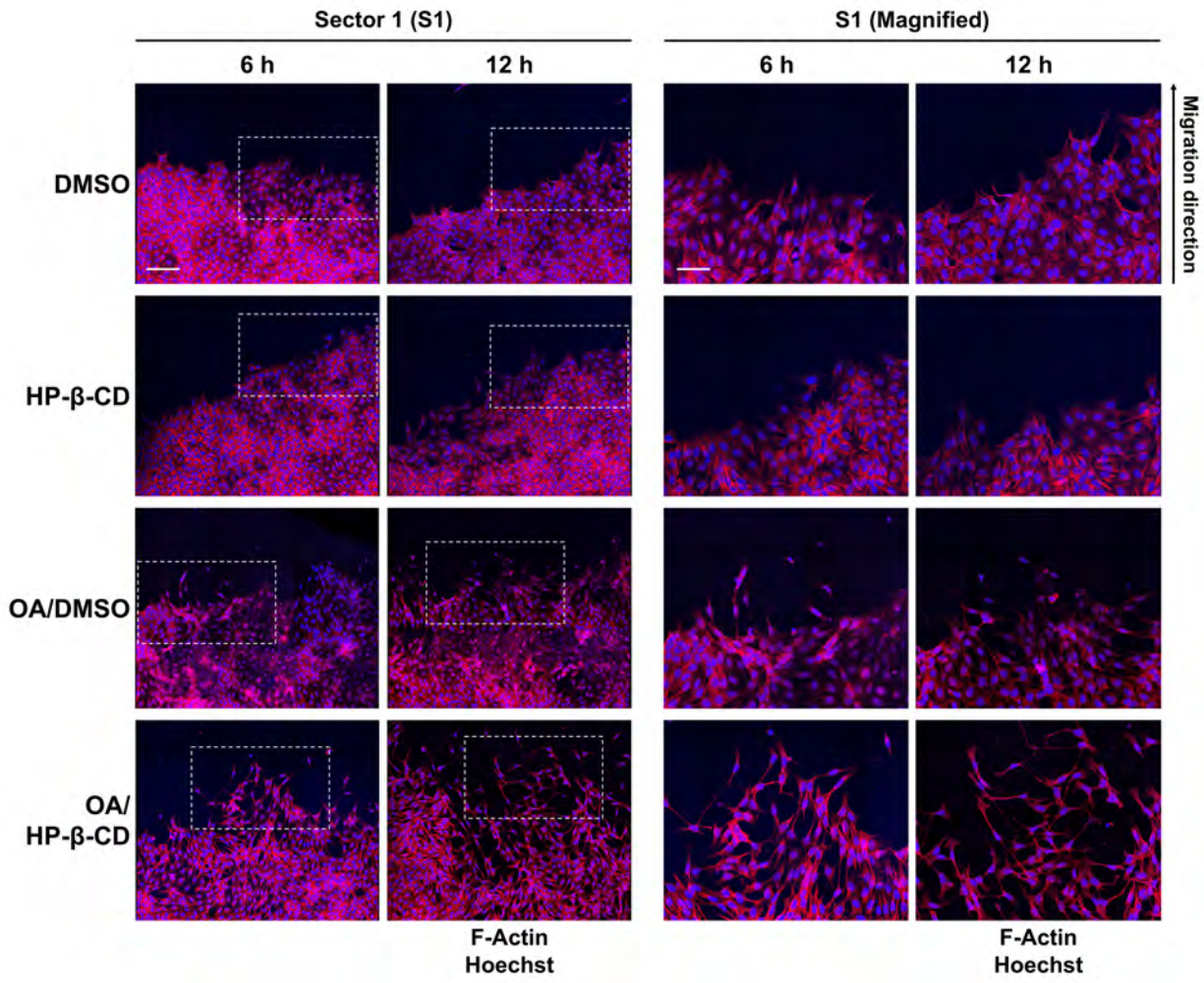

Figure S5. OA/HP β CD complexes change the distribution of actin cytoskeleton, revealed by Phalloidin staining. Confluent Mv1Lu cells were scratched and allowed to migrate for 6 and 12 hours. Cells were treated with 5 μM OA/DMSO or 12.5/3.12 μM/mM OA/HP β CD. Equivalent concentrations of DMSO and HP β CD were used as vehicle controls. Detailed images of the staining showed in Figure 4, corresponding to the cells at the scratch edge (sector 1, S1, area) and their 2 times magnified homologue. Actin fibers (F Actin): red. Nuclei: blue. Images obtained with a confocal microscope at 40X. Sector 1 scale bar indicates 50 μm. Magnified Sector 1 scale bar indicates 25 μm.

Figure S 6

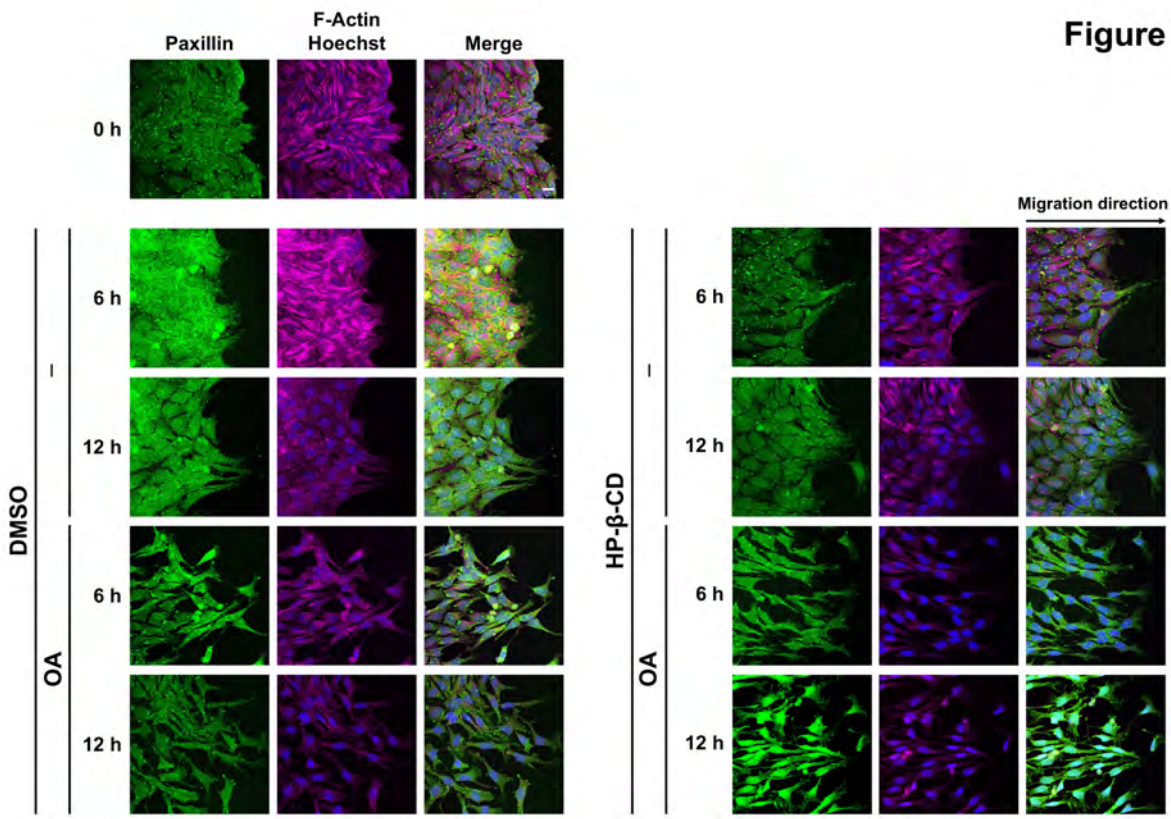

Figure S6. OA/HP β CD complexes promote changes in focal adhesions (FAs) revealed by Paxillin. Confluent Mv1Lu cells were scratched and allowed to migrate for 6 and 12 hours. Cells were treated with 5 μM OA/DMSO or 12.5/3.12 μM/mM OA/HP β CD. Equivalent concentrations of DMSO and HP β CD were used as vehicle controls. Cells were immunostained with specific antibodies against Paxillin. Co-staining with phalloidin and Hoechst 33258 was used to show actin cytoskeleton and nuclei, respectively. Paxillin: green. Actin fibers (F Actin): red. Nuclei: blue. Images obtained with a confocal microscope at 40X. This experiment was repeated at least three times. Scale bar indicates 25 μm.

Figure S 7

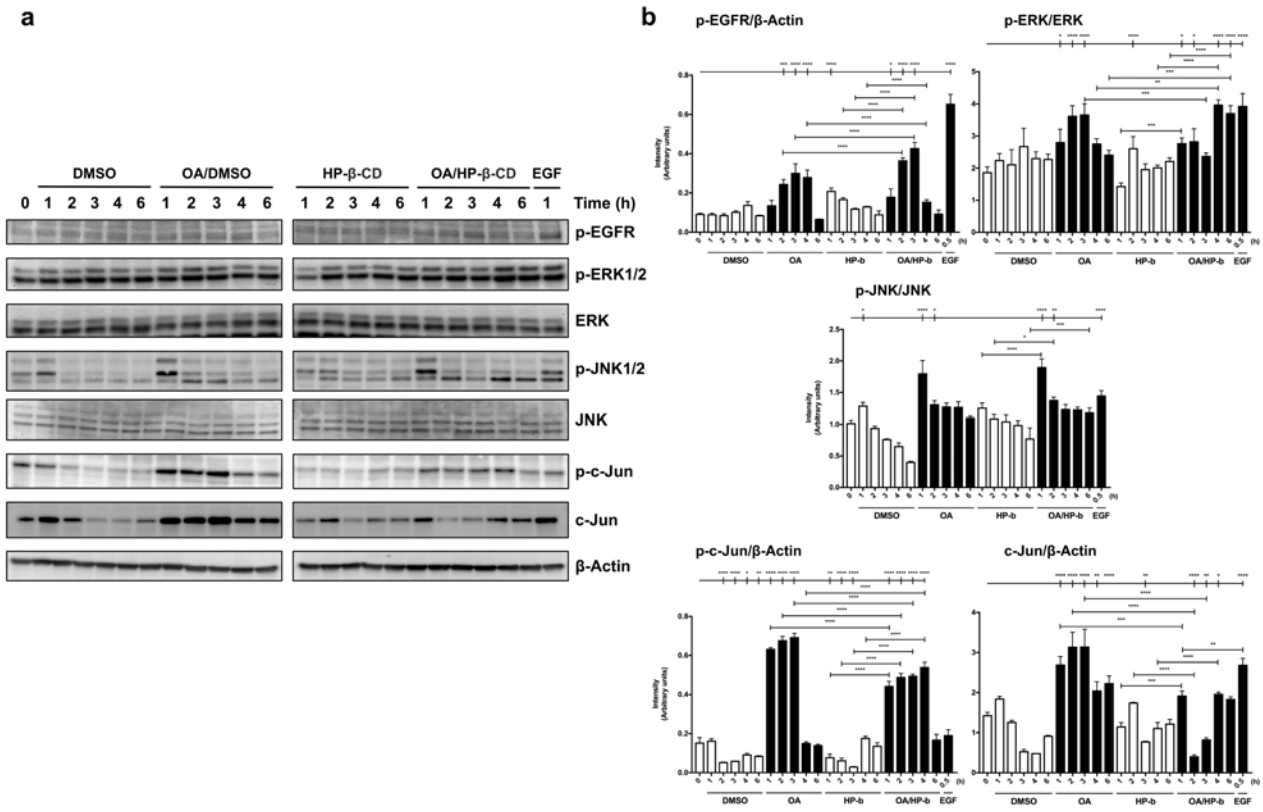

Figure S7. Cell migration necessary signaling pathways regulated by EGFR and c-Jun activation, are induced by OA/HP-β-CD complexes in Mv1Lu cells. (a) Total protein extracts from sub-confluent Mv1Lu cells in FBS-free media treated with 10 μM OA/DMSO or 12.5/3.12 μM/mM. DMSO and HP-β-CD equivalent concentrations were added as vehicle controls. Different proteins were assayed at the indicated times (hours): phospho-EGFR (Tur 1068), phospho-ERK1/2 (Thr 202/Tyr 204), phospho-JNK1/2 (Thr 183/Tyr 185) and phospho-c-Jun (Ser 63). Total protein expression was assayed for the above-mentioned active forms: ERK1/2, JNK1/2 and c-Jun. β-Actin was used as a loading control. A representative experiment was shown (EGFR, epidermal growth factor receptor; ERK1/2, extracellular signal-regulated kinases 1 and 2; c-Jun N-terminal kinases 1 and 2). (b) Column bar graphs represent intensity values of each protein assayed by Western blot, by collecting the data of three independent experiments. Intensity values were quantified and gathered by ImageJ software. Asterisks indicate statistically significant differences between the selected conditions according to a One-way ANOVA statistical analysis: (*$p<0.05$, **$p<0.005$, ***$p<0.001$ and ****$p<0.0001$).

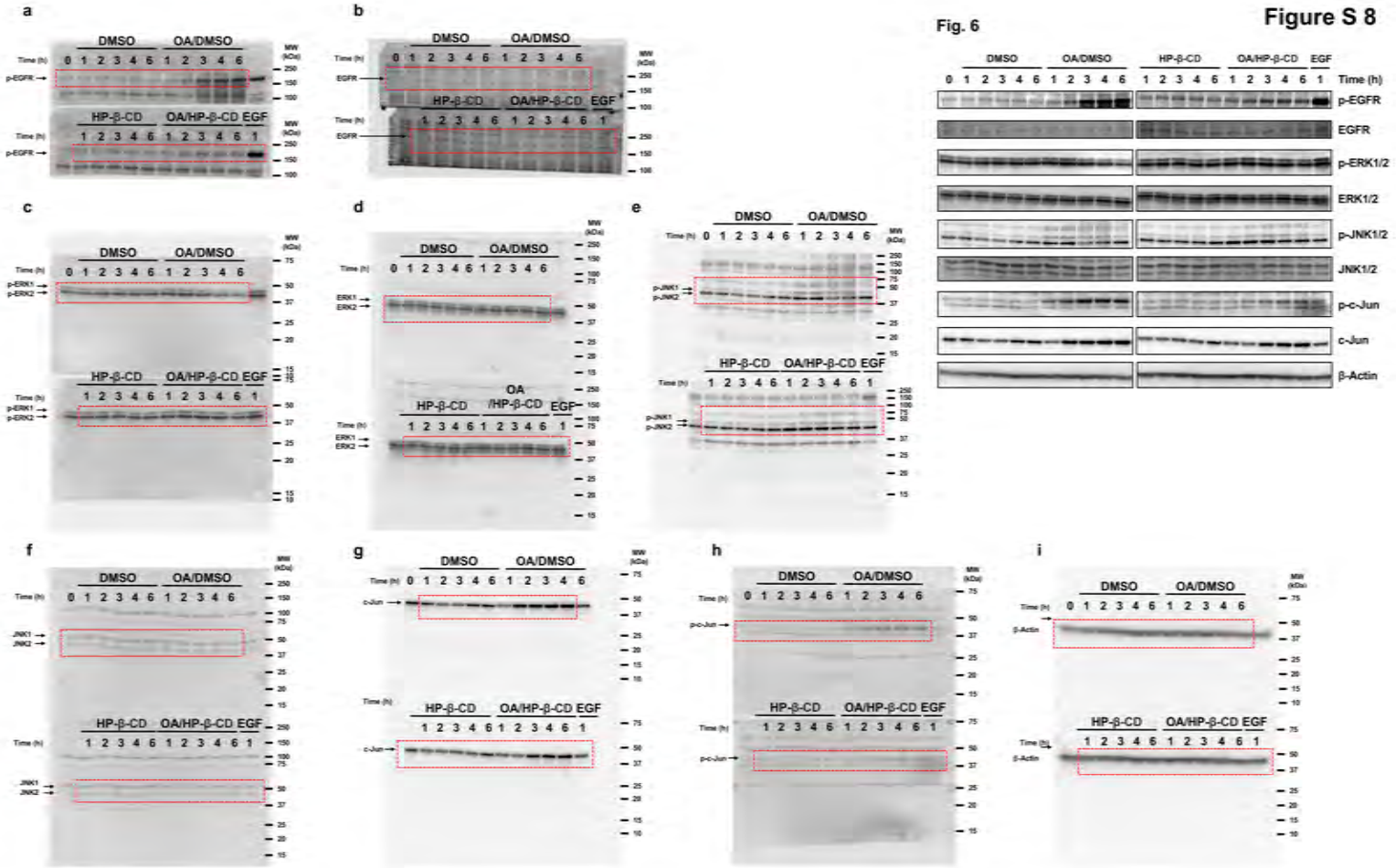

Supplemental Figure 8. Full-length blots corresponding to crops showed in Fig 6. (a) Tyr 1068 Phosphorylated-EGFR. (b) EGFR. (c) Thr 202/Tyr 204 Phosphorylated ERK (d) ERK1/2. (e) Thr 183/Tyr 185 Phosphorylated JNK. (f) JNK1/2. (g) c-Jun. (h) Ser 63 Phosphorylated c-Jun. (i) Beta-actin loading. Dashed red rectangle indicates the portion of the blot that was used in the figure.

Figure S 9

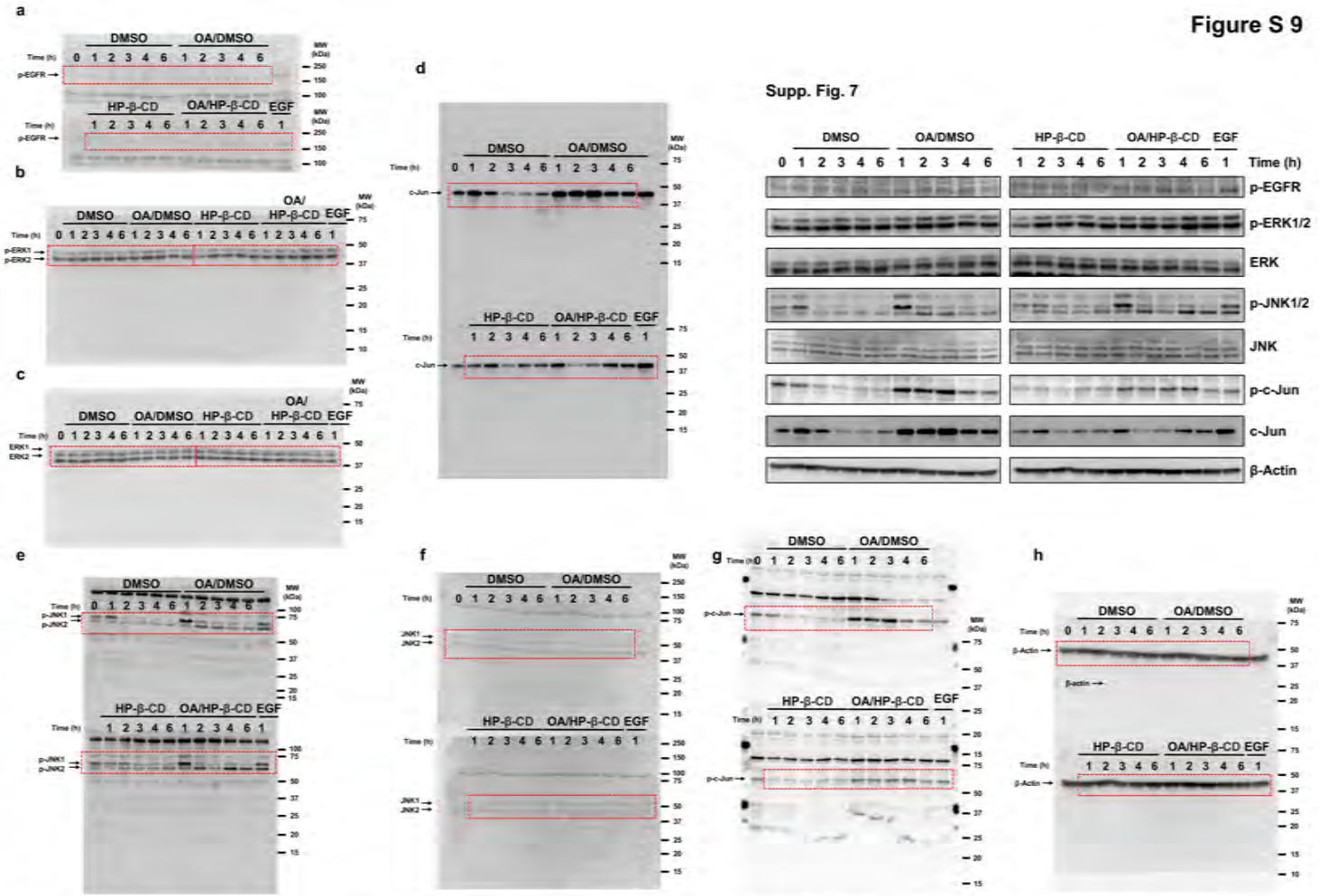

Supplemental Figure 9. Full-length blots corresponding to crops showed in Supplemental Fig 7. (a) Tyr 1068 Phosphorylated-EGFR. (b) Thr 202/Tyr 204 Phosphorylated ERK. (c) ERK1/2. (d) c-Jun. (e) Thr 183/Tyr 185 Phosphorylated JNK. (f) JNK1/2. (g) Ser 63 Phosphorylated c-Jun. (h) Beta-actin loading. Dashed red rectangle indicates the portion of the blot that was used in the figure.

V – DISCUSSION

V - DISCUSSION

The research on plant-derived bioactive compounds has revealed substances with promising therapeutical effects on human health. Oleanolic acid (OA) is a remarkable compound because of its multiple properties that can restore impaired physiologic processes, promote repairing processes, and attenuate several damages in vivo and in vitro. The present doctoral thesis focused on the cellular processes regulated during wound healing to accomplish skin regeneration: cell migration and motility, and the effect that OA might have on them. Indeed, we have disclosed some of the molecular effects of OA behind these processes by using epithelial cell in vitro models. Additionally, this thesis has unraveled new cellular processes promoted by OA in other wound-healing players, such as endothelial cells. Lastly, improved OA effects have been shown by using cyclodextrin complexation to ameliorate the use of OA in in vitro models. In this chapter, the results achieved in these areas of study and their implications in the field are discussed.

5.1. NEW INSIGHTS IN EPITHELIAL CELL MIGRATION PROMOTION BY OA

We have elucidated new molecular insights into OA's mode of action on epithelial cell models Mv1Lu and MDA-MB-231. This mode of action is encompassed in cell migration promotion by OA. In addition to this, a comprehensive study of OA effects on cell architecture and machinery was conducted to extend the knowledge of OA-triggered migration.

5.1.1. Migration-promoting effects of OA depend on its concentration and cell type tested

In recent years, the effects of OA on migration and invasion have been reported in various in vitro cellular models, regarding OA as an antitumoral agent. For instance, OA inhibits the migration of HeLa cells and HepG2 liver cancer cells when these cells are treated with high doses of OA: 25, 50, 100, and 200 μM (226, 228). Another study showed an inhibition of monocyte transmigration on

endothelial cells at 35 and 50 μM of OA (89). Other authors observed an OA suppression of migration and invasion, together with MAP kinase inhibition, in malignant glioma cells (309). Additionally, other authors point out that OA synthetic derivatives can inhibit cell migration via cytoskeleton remodeling alteration (310). Although this evidence could be paradoxical to explain OA promotion of cell migration, its negative or positive effects rely on the amount of concentrations used. It is worth noting that the concentrations of OA used in the aforementioned assays are relatively high, thus producing reduced cell viability and triggering apoptosis. Indeed, our previous research with epithelial cell lines revealed that OA positive effects are produced in a narrow spectrum of concentrations, specifically 5 μM for Mv1Lu cells and 10 μM for MDA-MB-231 cells (126, 311). On the contrary, in higher concentrations, OA exhibits inhibitory effects on cell migration (126, 225). Remarkably, these precise OA doses for Mv1Lu and MDA-MB-231 were optimized in serum-deprived growth conditions. Hence, fetal bovine serum (FBS) concentration in the cell medium used for each assay is a critical parameter that must be considered, since migration is also influenced by cell proliferation (312, 313). When serum is present in the cell culture, growth factors promote both migration and proliferation, making it difficult to ascertain OA's precise effects on migration, together with the fact that OA cell migration promotion is independent of cell proliferation (126). For example, in vitro scratch assays need to be done with null or the lowest FBS concentration possible to prevent serum protein or growth factors from masking OA effects (126). Nevertheless, it is imperative to acknowledge the potential existence of cell-type-specific differences that might underlie disparities in research outcomes.

5.1.2. C-Jun activation and regulation in response to OA stimulation in epithelial cells

C-Jun plays a pivotal role in promoting cell migration (151, 314) because it is the end point of the integration of signaling cascades triggered by growth factors, including EGF (149, 153). Remarkably, the research carried out with Mv1Lu and MDA-MB-231 cells showed that OA induces the activation of c-Jun by its phosphorylation on Ser 63 in both Mv1Lu and MDA-MB-231 cells. Interestingly, Western blot time courses showed increments in both phosphorylation and total

protein levels (p-c-Jun and c-Jun) of c-Jun under OA treatment. This could be explained by the fact that c-Jun upregulates its own transcription when it is phosphorylated by binding to its own gene promoter, thus establishing a positive feedback loop (145). On the other hand, this study has revealed the significance of c-Jun overexpression and phosphorylation at the leading edge of scratched epithelia by OA, improving the migration of epithelial cells (151, 314). Similarly, OA demonstrated a clear specificity for the activation of wound-edge migrating cells, a phenomenon that indicated a minimized stimulation of cell migration beyond the necessary scope. Coherently with this, leading-edge cells usually overexpress c-Jun to trigger cell-junction removal and protrusion formation in order to gain movement (193, 315, 316). Strikingly, this effect is different from the activation of c-Jun in response to EGF, which is extended to all cells of the epithelium (317, 318). Thus, this phenomenon unravels the specific OA-activity impact on epithelial cell migration driven by c-Jun master regulator.

5.1.3. Uncovering the molecular mechanisms behind OA-triggered cell migration

The pharmacologic inhibition on EGFR, MEK1, and JNK1/2 in scratch assays revealed a different contribution of these key proteins on OA-triggered cell migration in Mv1Lu and MDA-MB-231 cell lines (126). Therefore, a possible pathway induced by OA was elucidated by focusing on its beginning in EGFR with an unknown interaction with OA, subsequently triggering the activation of two EGFR-dependent pathways driven by ERK1/2 and JNK1/2, both finally leading to c-Jun activation in the cell nucleus (126). Intriguingly, our study revealed that, although EGFRi abrogated cell migration, it did not suppress the increase of both Ser 63-phosphorylated c-Jun and the overexpression of this protein by OA. This was in line with unaffected p-c-Jun levels and subcellular localization at wound-edge cells under EGFRi+OA condition in cell front migration assays. Certainly, detected phosphoprotein levels under OA treatment in Western blot time courses showed a different activation timing between EGFR and c-Jun, since c-Jun was stimulated by OA before EGFR, and therefore, independently of EGFR stimulation.

All these data did not support the previously conceived pathway, suggesting a non-linear, multiple-step mechanism induced by OA in Mv1Lu and MDA-MB-231 cells, where more regulatory elements must be playing a role. In Mv1Lu cells, where ERK1/2 is not constitutively active, ERK1/2 activation by OA exhibited delayed phosphorylation in line with EGFR activation, thus reinforcing the theory that OA might induce the activation of both JNK1/2/c-Jun and EGFR/ERK1/2 pathways, but these two are decoupled in time. Unfortunately, this result was not perceptible in MDA-MD-231 cells, since the excessive overexpression of EGFR in this cell line produces a high level of phosphorylated ERK and it was complicated to differentiate between the experimental conditions tested (319). Nevertheless, it was clear that early c-Jun phosphorylation was mediated by OA-activated JNK1/2, as indicated by Western blots and cell front migration assays, because JNKi produced the total inhibition of c-Jun phosphorylation and cell nuclei localization despite OA treatment. Nonetheless, a comprehensive exploration is necessary to elucidate the potential pathway upstream of JNK, which is responsible for inducing c-Jun activation. In any event, despite early response (JNK1/2/c-Jun) and late response (EGFR/ERK1/2), the assays pointed out that MAP kinases are implicated in both pathways, because the MEKi strikingly blocked the activation of EGFR, ERK1/2, JNK1/2, and c-Jun under OA stimulation. In this sense, it is possible that MEK1/2 (MAPKK) could be the node that links JNK1/2 with EGFR/ERK1/2 pathway during OA stimulation. This phenomenon was observed in both cell lines.

A mechanism compatible with this complexity could be the transactivation of EGFR, a way of activation that differs from the canonical external stimuli by growth factors (320). This mechanism has been studied for its pivotal function in signal transduction pathways (320, 321). It is plausible that OA stimulation on EGFR might occur through EGFR receptor transactivation. It has been shown that this particular mechanism starts at the cell surface by G protein-coupled receptors (GPCRs) (322, 323). GPCRs are proteins with seven transmembrane domains and, despite their lack of intrinsic kinase activity like RTs, they activate signal cascades by the binding of ligands of different nature in the extracellular domain: proteins, peptides, nucleotides, ions, amino acids, and lipids (321, 324, 325). When activated, these receptors interact with heterotrimeric G proteins (Gα, Gβ, and Gγ), which produce the exchange of GDP for GTP and consecutively activate numerous

effector proteins (321, 325, 326). Among them, a non-receptor tyrosine kinase is activated, proto-oncogene tyrosine kinase c-Src (230, 327, 328). This kinase phosphorylates EGFR to regulate cell motility (119, 327). Apart from this mechanism of EGFR activation, it is known that EGF and other growth factors signal in an autocrine fashion, so production, release, and binding to EGFR occur in the same cell, thus regulating its own proliferation and migration (123, 329). In this sense, there is evidence that GPCRs may act in this autocrine loop by the shedding of growth factors from the cell membrane, such as EGF (119, 320, 330). Indeed, EGFR activation and exposure are regulated by endocytosis, which is removed from cell membranes with GPCRs in endosomes (125, 331, 332). Strikingly, EGFR internalization is observed in MDA-MB-231 cells during OA stimulation (126). For instance, in the context of corneal cell injury, EGFR activation is mediated by a shedding mechanism associated with GPCR receptors (333). Intriguingly, the use of PD098059, inhibiting ERK1/2 phosphorylation, led to the blocking of EGFR activation, suggesting that besides serving as an effector downstream of EGFR, ERK1/2 can also mediate EGFR transactivation (333). Additionally, it has been reported that GPCRs activate different MEK isoforms, which subsequently activate ERK and JNK kinases, thus supporting the idea that MEK might be the node interconnecting JNK1/2/c-Jun and EGFR/ERK1/2 pathways (321). Altogether, the existence of this GPCR mechanism goes in line with the results and dynamics of EGFR and MAP kinase stimulation by OA observed in this study. Indeed, this could explain the crosstalk between the early response of MEK/JNK/c-Jun and the later response of EGFR/MEK/ERK, which might be linking both GPCR and EGFR receptors (Figure V-1). First, GPCR could be triggering JNK and c-Jun early activations, and later, EGFR could be phosphorylated because of GPCR activation. However, at this level of observance, we could not ascertain whether EGFR is activated via c-Src kinase or via EGF shedding. Nonetheless, this second mechanism might be more plausible given the timing of EGFR and ERK displayed in Mv1Lu and MDA-MB-231 cells in response to OA. Interestingly, an anchored-membrane enzyme that cleaves proteins, A disintegrin and metalloproteinase 17 (ADAM 17), also called tumor necrosis factor-converting enzyme (TACE), has been identified as a key player for EGFR activation, which has many functions involved in inflammation regulation, tissue regeneration, and cell differentiation (334, 335). Indeed, one of the substrates of ADAM17/TACE is EGF

pro-ligand, which remains inactive and attached to the membrane until ADAM17 cleaves it to produce the shedding and binding to EGFR (330). ADAM17 role needs to be deciphered to confirm its involvement in OA stimulation. This will most probably exclude the fact that EGFR stimulation by OA is caused by its direct receptor interaction, and confirm that it is indeed caused by its interaction with GPRCs. This mode of action would be supported by the identification of OA as a weak agonist for a specific GPCR, concretely Takeda G protein-coupled receptor 5 (TGR5) (14, 336). TGR5 is involved in regulating metabolism and has bile acids as ligands, with a similar structure to OA (14, 337, 338). Overall, there is no doubt that both JNK/c-Jun and EGFR/ERK axes are necessary, and that the latter contributes positively to c-Jun overexpression and phosphorylation during OA-triggered migration.

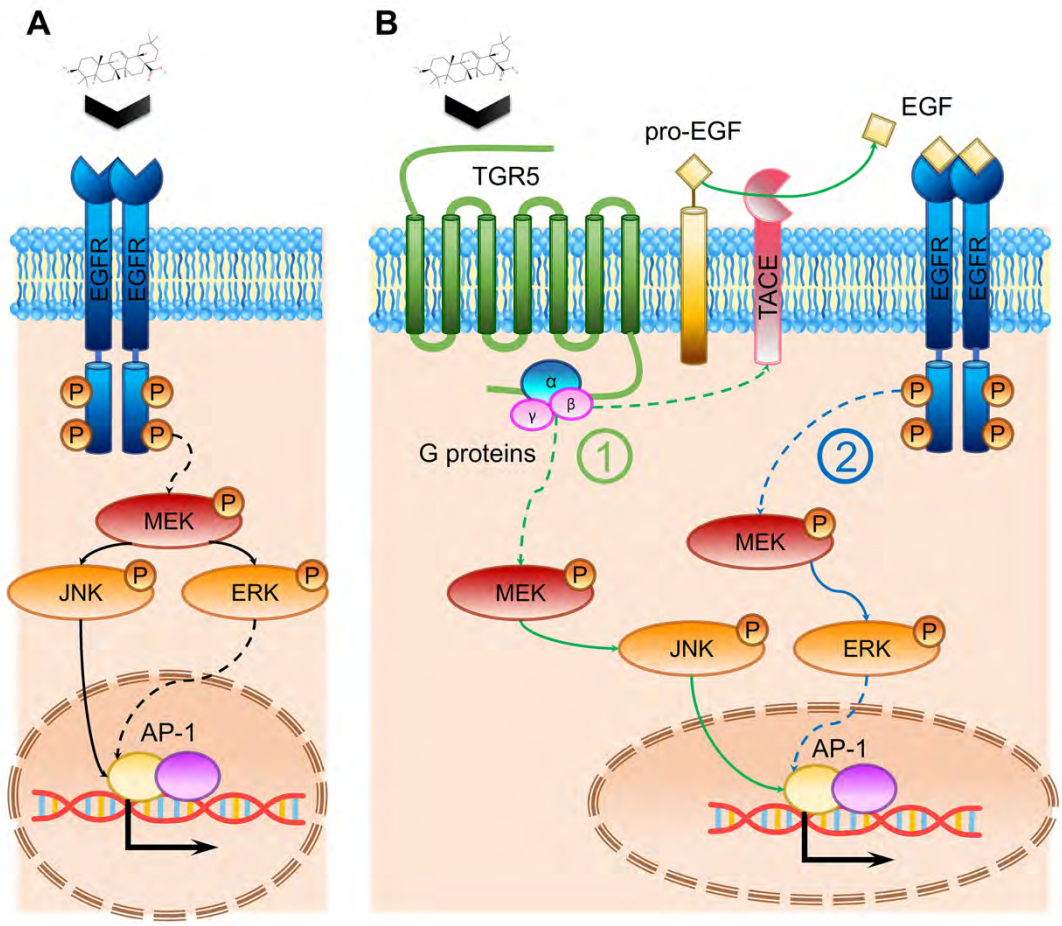

Figure V-1. Oleanolic acid induces a biphasic mechanism. A. *Previously, the activation of EFGR and MAP kinases by OA was thought to be due to OA's interaction with EGFR, leading to MAP kinases activation and AP-1 transcription factor (c-Jun) activation.* ***B.*** *However, this research strongly questions the previous mechanism of action. Mechanism of action that is now known to be more complex with two stages in time. Instead, OA, as an agonist of TGR5, interacts with this GPCR to induce G protein activation. Subsequently, MEK is activated, and JNK and AP-1 are immediately phosphorylated and activated in the nucleus. G proteins may activate proteases anchored in the cell membrane TACE/ADAM17, which produce growth factor shedding, including EGF. Later, by EGF release, EGFR activation and phosphorylation cause a second phase of induction, which ultimately triggers the complete MAP kinase module activation with ERK involved, which contributes to AP-1 activation in the nucleus. Several proposed steps still need to be thoroughly confirmed by research. Dashed arrows indicate multiple steps in the figure.*

5.1.4. Cell architecture morphology and regulation in response to OA

The thorough study of EGFR, ERK, JNK, and c-Jun regulation upon OA treatment, together with the molecular implications discussed, suggest distinctive morphological changes in Mv1Lu and MDA-MB-231 cells at the wound edge, observed in *in vitro* scratch and cell front migration assays. Wound-edge cells showed protrusions, lamellipodia, and ruffles, all promoted by OA (315, 316). Moreover, OA induced modifications of the density and the arrangement of actin fibers (F-actin) in the wound edge, which are suggestive of a high polymerization-depolymerization turnover of actin, compatible with an active migratory effect. This is necessary for the dynamization of the F-actin network that makes the lamellipodia movement possible (161, 167, 339). Altogether, these effects suggest an active migratory state of the cells (158, 160, 167, 339). Additionally, paxillin integrates multiple signaling pathways, as it is the adaptor protein critical for focal adhesion (FA) formation from focal complex (FC) maturation during cell migration (167, 183, 184, 189). Indeed, paxillin displayed a distinct reorganization in the cells at the wound edge under OA treatment. Because of paxillin localization in FAs, the staining showed an increased number and a decreased size of FAs in OA condition (340, 341). Coherently with this, phospho-paxillin Ser 178 residue is phosphorylated by JNK, an event that enhances FA dynamics and cell motility (191, 342). In fact, this residue was phosphorylated by OA in a time-dependent fashion. However, the presence of JNKi did not affect the density and size of FAs in response to OA, thus suggesting the existence of further more regulatory inputs on FAs, which are independent of JNK activation. Importantly, FAs are produced as a result of the activation of integrins and RTKs, such as EGFR (180, 183, 343). This event brought together FAK with adaptor proteins and kinases (183, 342, 344). Indeed, Tyr 925 phosphorylation of FAK can occur as a consequence of cell integrin assembly or stimulation by growth factors (179, 345). This event was observed with OA, since the triterpenoid induced FAK-tyrosine 925 phosphorylation in a very similar dynamics to EGFR, which is characterized by a response later than c-Jun, together with EGFRi suppression. Remarkably, both EGFR and FAK are closely located to drive their functions in the cell (346). Moreover, OA stimulation of this phosphorylation was inhibited by MEKi, suggesting the direct involvement of EGFR/MEK/ERK in FAK activation. Interestingly, it has been shown that ERK

targets FAK to trigger migration in corneal epithelial cells (342). These observations correlated positively with the study conducted on FAs, since the presence of EGFRi or MEKi upon OA stimulation reduced FA density and increased FA size. Hence, this pathway is one of the other inputs necessary for FA formation and a successful OA-driven migration. It has been reported that enhanced localization of active FAK to focal adhesions increases its turnover at the protrusion front (185, 347). Remarkably, active FAK (phospho-Tyr 925) co-localized with paxillin in response to OA in cell front migration assays, indicating an active remodeling of FAs in Mv1Lu and MDA-MB-231 cells. This event, in line with FAs conformation, was completely abrogated when EGFRi and MEKi were added before OA stimulation. All these results underscored an OA-responsive pathway by involving EGFR/MEK/ERK/FAK to trigger FAs and cytoskeleton dynamization, as previously described (342). In contrast, JNKi did not produce the inhibitory effect on FAK to FA localization; however, it substantiated the notion of the existence of early JNK/c-Jun response and might be contributing in other FA sites (348). This was underpinned by the observation that JNKi partially inhibits, but does not abrogate, OA-triggered cell migration (126).

Overall, the molecular effects of OA on these key cell-migration regulators have revealed an intricate signaling mechanism that acts in response to OA in order to enhance cell migration. These results have uncovered that OA influences the signaling of the cell, with a fine complex biphasic mechanism to reach a better cell migration (Figure V-1). Considering the robust influence of OA on cell migration, further elucidation of these mechanisms implies great significance and relevance. These findings may offer a compelling mode of action for OA and prompt extrapolation to its isomers or synthetic derivatives, thus warranting further research.

5.2. NEW OLEANOLIC ACID FEATURES ON ENDOTHELIAL CELL FUNCTION

The potential of plant-derived compounds for preserving endothelial cell function is well known (30, 349-351). They have shown multiple positive effects in protecting vascular health and preventing diseases associated with endothelial cell dysfunction (6, 7, 352, 353). Among them, terpenoids are a noteworthy group of active molecules that, like OA, have anti-inflammatory effects (354). OA's beneficial effects on epithelial cells prompted us to test OA on other cellular models and to study its role in endothelial function and its possible relation with wound healing. Hence, the conducted investigation offered new insights into the effects of OA on the endothelium by studying its effects on human umbilical cord vein endothelial cells (HUVECs) model, which were obtained from control (C) and gestational diabetes (GD) contexts, particularly focusing on inflammation and angiogenesis. First of all, the present study conducted MTT assays and OA dose-effect optimizations to test its activity in primary HUVECs. Given the limitations of OA dose effects, these assays were performed seeking a compromise between cell viability, the read out of OA positive effects and the lowest serum concentration possible (0.1%, 0.5%) in order to avoid OA masking. Finally, we set up a working concentration for OA of 20 μM.

5.2.1. Inflammation attenuation in HUVECs

Studies with terpenoid molecules, the same family as that of OA, concretely carotenoids lycopene and β-carotene, have shown anti-inflammatory effects on both C- and GD-HUVECs (355). These molecules, under inflammatory stimulus by TNF-α, reduce monocyte-endothelial cell interaction, attenuate the expression of adhesion molecules (I-CAM1 and V-CAM1), and decrease NF-κB phosphorylation and translocation to the cell nucleus (354, 355). Indeed, OA and its isomers, ursolic acid (UA) and maslinic acid (MA), have shown similar effects using regular HUVEC phenotypes, showing attenuation effects on adhesion molecule expression (77, 356, 357). However, prior studies on OA have not specifically addressed hyperglycemia-modified cells (GD-HUVECs), which have notably impaired functionality (358, 359). Furthermore, previous investigations have consistently failed to clarify the concentration of serum used in cell growth assays, a critical factor for studying OA effects in vitro. Another parameter that should be

considered for this kind of studies is the timing of drug treatment and TNF-α inflammation induction, since these times might be critical to deciphering OA-positive effects. Therefore, in our research, the TNF-α incubation period was extended to 24 hours.

The stimulation with TNF-α produced an acute overexpression of adhesion molecules in C- and GD-HUVECs. Interestingly, the pre-treatment with 20 μM of OA produced a clear attenuation of adhesion molecules overexpression by TNF-α, particularly V-CAM1 and *SELE*. This preventive effect of OA was more pronounced in the GD phenotype, probably due to its cell senescence and endothelial dysfunction (360). On the other hand, I-CAM1 gene expression levels at 24 hours were not fully abrogated by OA pre-treatment in both cell phenotypes. This feature could be explained by other functions of I-CAM1 since this integrin's constitutive expression levels are crucial for promoting endothelial cell migration and neo-angiogenesis during wound healing (202, 361). Regarding V-CAM1, it is an endothelium-specific molecule and it is inducible by TNF-α release, crucial for monocyte extravasation (203). Nevertheless, under OA pre-treatment, V-CAM1 exhibited the strongest attenuation in both C- and GD-HUVECs, a result that positively correlated with V-CAM1 protein levels, which were also decreased by OA, showing a significant decrease of total protein levels even at 24 hours. However, it is essential to acknowledge the limitations of in vitro assays, because a chronic inflammation milieu has persistent V-CAM1 levels due to tissue injury and constant release of TNF-α (362). Paradoxically, no significant differences were observed at the phospho-serine 536 residue of p65 subunit of NF-κB. In contrast, other bioactive compounds have shown NF-κB attenuation by inhibiting either its phosphorylation or its translocation to the cell nucleus (354, 363). Thus, the effects of OA on V-CAM1 might involve distinct molecular mechanisms. For example, OA isomer, UA, has been shown to block V-CAM1 trafficking in vesicles from the endoplasmic reticulum to the cell membrane (364). On the other hand, as might occur in epithelial cells to trigger MAP kinases activation and cell migration, OA could potentially enhance the proteolysis of V-CAM1. It is worth noting that the activity of ADAM17/TACE processes not only growth factors but also V-CAM1, thus inhibiting its function by releasing the integrin into the extracellular medium (203, 365). Given the molecular effects of OA seen in epithelial cells and its potential role in EGF shedding by ADAM17, this mechanism is plausible but needs to be

confirmed with future research. Regardless of the mechanism involved, OA effectively attenuated both V-CAM1 gene expression and total protein levels.

During the chronic inflammation that occurs in a non-healing wound, excessive TNF-α release increases the presence of adhesion molecules at the endothelium, increasing both the adhesion and the transmigration of immune cells, thus leading to endothelial cell apoptosis and dysfunction (366). During monocyte immune cell recruitment, while selectins (E-selectin) capture and roll monocytes on the endothelium, integrins I-CAM1 and V-CAM1 firm monocyte adhesion to endothelial cells and mediate transmigration (361). In chronic non-healing wounds, the excessive recruitment of monocytes results in an uncontrolled population of M1 macrophages, characterized by hyperinflammation, reduced phagocytic activity, and increased oxidative stress (367). Conversely, regular monocyte recruitment leads to M2 macrophages, contributing to an anti-inflammatory, regenerative, and tissue-remodeling environment (367). The effects of OA on monocyte adhesion, especially on GD-HUVECs, were coherent with altered adhesion molecule levels, particularly with the reduced levels in V-CAM1, implying a potential resolution of inflammation in vitro with a remarkable relevance for treating both chronic and diabetic wounds in the future.

5.2.2. Angiogenesis promotion, rescue of impaired angiogenesis features in GD-HUVECs, and cell migration and motility promotion by OA

Diabetes produces a pernicious effect on the vascular system and the angiogenesis process, causing poor tissue vascularization (300, 301). The tube formation assay on Matrigel showed that GD-HUVECs had impaired tube formation, characterized by an elevated number of aberrant isolated segments under basal conditions, as opposed to C-HUVECs. Strikingly, the treatment with OA rescued this impairment in GD-HUVECs and, to a lesser extent, in C-HUVECs, by reducing the number and length of isolated segments. Furthermore, positive angiogenic features, such as number of master segments, meshes, and branch length, were notably improved by OA, particularly in GD-HUVECs. This improvement in GD-HUVECs could be attributed to their inherently poorer angiogenic performance for these parameters under basal conditions. Overall, these data indicated that OA restores GD-HUVEC phenotype to a more regular

angiogenic phenotype, without significantly affecting C-HUVECs, which intrinsically have the capability of forming more complex networks. Nevertheless, both types of HUVEC cell phenotypes displayed better complexity of vascular network under OA conditions, as evidenced by an increased number of nodes, branches, master junctions, and total network length. Therefore, this OA ability could potentially have a positive impact in the context of tissue regeneration in whether acute, chronic, or diabetic wounds.

It should be noted that to comprehend OA effects in a wound context, it might be desirable to study its impact on more complex systems, as will be discussed below. Moreover, it would be interesting to study the molecular effects behind OA angiogenesis, focusing on the stimulation and the signaling pathway of Vascular Endothelial Growth Factor Receptor 2 (V-EGFR2). This is even more significant if we consider its crucial role in angiogenesis, especially because of its similarity to the epidermal growth factor receptor (EGFR) structure and function, which has been activated by OA in previous assays (126, 194, 220, 368).

During angiogenesis, cell migration is a crucial process for endothelial cells (110). The outcome of scratch assays revealed that OA significantly increases migration in both C- and GD-HUVECs. Notably, the stimulation with fetal bovine serum (FBS) failed to attain the levels achieved by OA stimulation in the case of the GD phenotype. This effect suggests that OA, in contrast to FBS, specifically rescues an impaired migration mechanism of GD-HUVECs that cannot be rescued by serum stimulation. Therefore, OA might activate a distinct molecular mechanism that appears particularly helpful to the impaired cells. The quantification of focal adhesions (FAs), assessed through paxillin immunostaining, indicates a more robust enhancement in FA density in GD-HUVECs compared to C-HUVECs under OA treatment. Then, collectively, the FA data strongly imply that OA generally fosters superior endothelial cell movement, facilitating migration in both C- and GD- HUVECs. All in all, OA activity enhances angiogenesis by triggering cell migration, presenting multifaceted properties that are beneficial in a wound-healing context, and are revealed especially in the GD-HUVEC phenotype (110).

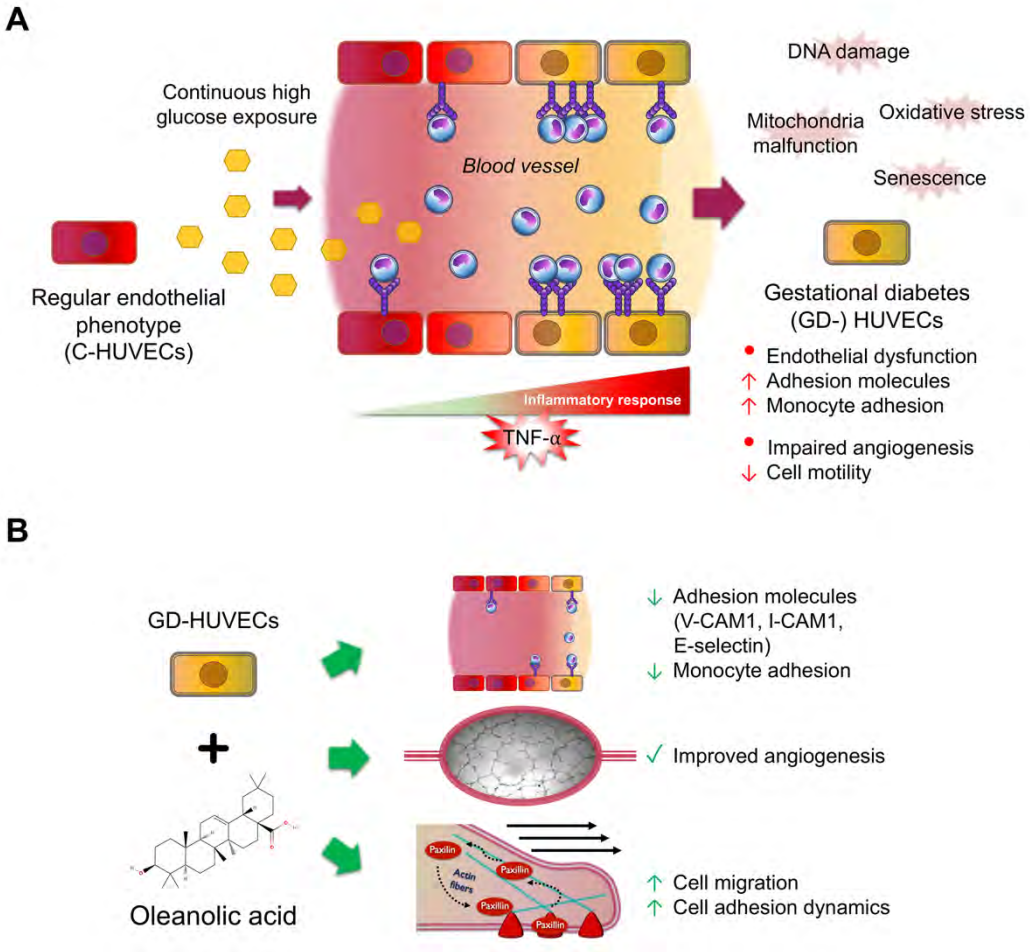

Figure V-2. Oleanolic acid rescues critical features of GD-HUVEC. A. *When regular endothelial cells are exposed to high glucose levels in the bloodstream, their function is harmed. Consequently, high oxidative stress, DNA damage, and mitochondrial damage cause cellular senescence. As a result, these cells exhibit an altered phenotype (GD-HUVEC) with an excessive inflammation response upon stimulation by TNF-α, resulting in an abnormal exposure of adhesion molecules on the endothelium. This, in turn, leads to heightened recruitment of circulating monocytes and ultimately results in endothelial dysfunction. Additionally, these cells display impaired tube formation and poor angiogenesis features.* ***B.*** *Strikingly, OA pre-treatment in the GD-HUVEC model before TNF-α addition was found to attenuate the overexpression of adhesion molecules V-CAM1, I-CAM1, and E-selectin, leading to reduced monocyte recruitment. Simultaneously, OA had a positive impact on GD-HUVEC angiogenesis and migration, by restoring affected tube formation features and increasing cell motility.*

5.2.3. The role of GPCRs in OA multifaceted effects on HUVECs

The different OA effects on endothelial cells indicate a complex signaling mechanism induced by OA, which might be very similar to the one observed in epithelial cells. Remarkably, this OA capacity indicated that this mechanism ameliorated the malfunction of the endothelium when subjected to high blood sugar levels, which is the cause of an impaired metabolism and inflammation (359, 360, 366, 369). In this sense, GPCRs are known to safeguard cells from inflammation, radical oxygen species (ROS), and damage, thus preventing endothelial dysfunction (323, 325). As seen in epithelial cells, behind this protective function lies transmembrane bile acid receptor TGR5, a receptor that is becoming more and more relevant due to its regulatory role, not only in metabolism but also in key processes for the cell, such as proliferation, muscle relaxation, and migration (338, 370). Intriguingly, TGR5 has been shown to modulate the inflammation milieu by controlling adhesion molecule expression and pro-inflammatory cytokine release of endothelial cells, monocytes, and macrophages (371). In addition, it should be emphasized that this receptor produces RTKs transactivation of V-EGFR2, among others, as does its counterpart in epithelial cells EGFR (321, 372, 373). Because of the resemblance of OA to bile acids and the evidence of its interaction with TGR5, it is very plausible that the unraveled OA-positive effects on HUVECs are driven by OA/TGR5 interaction (14, 336). Furthermore, this mechanism may elucidate the multiple effects of OA on monocyte adhesion, adhesion molecules, angiogenesis, and cell migration in both C- and GD-HUVECs. Therefore, further studies in the near future seem very pertinent to unveil this possible molecular mechanism.

To summarize, this performance underscores the therapeutic potential of OA for restoring vascular function and ameliorating excessive inflammation, which are impairing features that contribute to the non-healing of chronic and diabetic wounds (Figure V-2). Thus, thorough research on OA should be conducted due to its potential positive impact on the health care system.

5.3. OLEANOLIC ACID IMPROVEMENT BY COMPLEXATION WITH MODIFIED CYCLODEXTRINS

The molecular mechanisms unraveled by OA align with enhanced epithelial cell migration. Moreover, OA's positive effects could be seen in other cell types relevant for wound healing in endothelial cells. These findings position OA as a remarkable agent for treating wounds. Unfortunately, OA's hydrophobic chemical nature limits its applicability to hydrophilic environments, thus forcing the use of amphipathic molecules such as DMSO, which has cytotoxic effects (307). In this study, novel OA application on epithelial cells was tested through OA complexation with hydroxypropyl-β- and hydroxypropyl-γ-cyclodextrins (HP-β- and HP-γ-CDs), by making OA/HP-β-CD and OA/HP-γ-CD complexes. The use of these complexes showcased improvements in OA efficacy in both in vitro epithelial cell models: Mv1Lu and MDA-MB-231.

5.3.1. Technical OA improvement by cyclodextrin properties

OA's poor water-solubility needs novel microcarriers to ensure its protection and optimal application. Strikingly, the process of OA complexation with modified CDs respected OA stability, since its complexation was usually done at room temperature (25 °C) and neutral pH (pH = 7.5) (270). Significantly, the innovation of adding a dehydration step for OA/CD complexes in this study was critical to improving both OA/CD complexes' in vitro applicability and biocompatibility (374). The biocompatibility was achieved because a dehydrated powder allowed us to dissolve the complexes in osmolarity solutions compatible with cell culture, thus respecting cell viability. Besides, it allowed for the dissolution of complexes in sterile solutions, thus reducing the risk of contamination by bacteria or fungi. It should be noted that the high solubility of OA complexes enabled their dissolution at a desired concentration, which was usually high, in order to apply small volumes for the assays carried out on cell culture. In this case, the method of choice was freeze drying, which significantly enhanced OA efficacy (see below), as with many other drugs for pharmaceutical applications (255, 374, 375). Of course, other dehydration methods are available, but they do not accomplish 100% dehydration of the product or they compromise the drug stability (308, 376, 377). Furthermore, the freeze-drying method for OA complexes is appropriate to have a homogenous

dispersion of the complexes and, since it is applied under a vacuum, it is recommended due to OA's sensitivity to oxygen (308). Alternatively, the spray drying method could also be considered in the future for OA/CD complexes production, since it dehydrates faster than freeze drying – half an hour versus three days – beside the fact that it is a more energy-efficient process and the device used is cheaper than the one used for freeze drying (308, 378-380). In addition to the intrinsic properties of the powder formulation, freeze drying also improved the handling of OA for in vitro assays. Remarkably, another advantage was the prolonged preservation of OA, as indicated in the studies of different temperatures, where CDs effectively safeguarded and maintained OA stability for extended periods, even at harsh storage temperatures of 4 °C and 20 °C. In contrast, the traditional OA/DMSO formulation used required specific long-term storage conditions in liquid nitrogen (-190 °C). Finally, improved preservation of OA with CDs could allow an easy long-distance transport of the complexes as it does not necessarily require low temperatures.

5.3.2. Cyclodextrin complexation modifies OA in vitro dose-responses

Freeze-dried OA complexes, namely OA/HP-β-CD and OA/HP-γ-CDs, were tested in vitro in Mv1Lu and MDA-MB-231 cell lines because they were good biosensors for OA activity, as showed in previous and the present study (126). The addition of the hydroxypropyl groups provides cyclodextrins with a superior water solubility compared to native cyclodextrins. Therefore, HP-β- and HP-γ-CDs were chosen to complex OA (243, 381). Indeed, both HP-β- and HP-γ-CDs have demonstrated their effectiveness in encapsulating OA (270). Surprisingly, distinctions in behavior between the two cyclodextrins have been unraveled in in vitro assays. A higher complexation constant (K_c) for HP-γ-CDs (K_c = 645 M−1) in comparison to HP-β-CDs (K_c = 201 M−1) is indicative of greater complex stability (270). This feature results in a diminished loss of OA during the encapsulation and dehydration processes, thus contributing to higher encapsulation efficiency (EE). While these results present an advantage, it is imperative to ascertain whether the stability of the complex, as dictated by its K_c value, facilitates an appropriate release and activity of the host compound into the cell medium. The stability of the resulting OA complexes, as established by the K_c values and contingent on the

cyclodextrin type, holds the capacity to modulate the activity of OA within the complex. In this context, the outcomes of in vitro scratch assays revealed that, at an identical concentration of 12.5 μM of complexed OA, the extent of cell migration was higher for OA/HP-β-CD complexes than for OA/HP-γ-CD complexes. The effect of OA/HP-β-CD complexes, with lower K_c than OA/HP-γ-CD complexes, suggests an easier release of OA from the hydrophobic cavity of the cyclodextrin, which is indicative of a less stable complex compared to its counterpart formed with HP-γ-CDs. Consequently, HP-β-CD emerges as the more suitable cyclodextrin for OA complexation in terms of OA potency in scratch assays, showing a superior balance between effective compound release and the heightened aqueous solubility of OA.

First of all, Mv1Lu and MDA-MB-231 scratch assays with OA complexes revealed that cyclodextrins partially curtail OA activity on cell migration, as observed with the use of 12.5 μM of OA/HP-β-CD and 62.5 μM of OA/HP-γ-CD to attain a comparable level of cell migration as the one achieved with 5 μM of OA/DMSO. This constraint on the biological activity of various encapsulated active compounds, as reported by prior studies, was expected since encapsulation confines the active molecule and limits its release at the cost of the complex stability (255, 287, 288, 382). Conversely, OA/DMSO formulation demonstrates a narrow range of concentrations for eliciting cell migration activity on Mv1Lu and MDA-MB-231 epithelial cell lines, beyond which cytotoxic effects and cell viability loss occur (126). The data obtained from scratch assays, together with the proliferation assays, have shown that cyclodextrin complexation modified the dose-response of OA in vitro. Specifically, concentrations of the OA/HP-β-CD complexes displayed peaks in cell migration activity two times higher than those with OA/DMSO for both Mv1Lu and MDA-MB-231 cell lines. In addition to this, proliferation assays in these cell lines indicate a slightly elevated cell count compared to conditions with OA/DMSO, suggesting a potential protective effect given by cyclodextrins. This phenomenon could be attributed to the gradual delivery of OA to cells, which ensures OA positive effects without compromising cell viability (245).

5.3.3. Improved cell migration features with OA/CD stimulation

Mv1Lu *in vitro* scratch assays revealed an enhanced cell migration activity by OA/CD complexes. Interestingly, heightened recruitment of migrating cells was observed when treating the scratched epithelium with OA/HP-β-CD complexes compared to OA/DMSO, by showing a distinct morphology in multiple rows from the scratch edge. Although this recruitment was less conspicuous, a similar trend was observed in scratch assays with MDA-MB-231 cells. Notably, this phenomenon exhibited a positive correlation with immunocytochemistry assays conducted on Mv1Lu cells, focusing on F-actin morphology and the activation and subcellular localization of phosphorylated c-Jun (p-c-Jun). Remarkably, cells treated with OA/HP-β-CD complexes exhibited a broader recruitment zone of cells than OA/DMSO, characterized by nuclear overexpression and activation of c-Jun. Indeed, the ratio of positive nuclei to total nuclei was notably higher in the OA/HP-β-CD condition than in its DMSO counterpart, and it gradually decreased as cells were farther from the scratch edge. These results underscore that the complexation of OA with cyclodextrins enhances its properties in activating cell migration.

Regarding the study of cytoskeleton structures, focal adhesion remodeling, revealed by paxillin staining, exhibited similar patterns in both OA/DMSO and OA/HP-β-CD formulations. Hence, as no discernible differences were identified between these conditions, further studies are necessary to delve into these mechanisms, including paxillin/FAK interaction studies, as done previously with OA/DMSO. Despite this, the observance of F-actin distribution in Mv1Lu cells at the edges of scratches, showed the formation of filopodia and ruffles with OA/HP-β-CD complexes, with a qualitatively greater presence of these movement structures than OA/DMSO and less pronounced visibility of F-actin, thus reinforcing the great recruitment and high dynamization seen at the scratch assays. These phenomena could be associated with the prolonged activation by OA/HP-β-CD complexes of c-Jun, recognized as the master regulator of cell migration (151, 153, 193).

As discussed above, OA triggers a complex molecular mechanism that drives cell migration. To delve into the OA/HP-β-CD effects on this mechanism of action, the same key regulatory proteins that were stimulated by OA/DMSO were studied.

Overall, the responses elicited by OA/HP-β-CD complexes were akin to those seen with OA/DMSO, showing analogous phosphorylation patterns, mainly on EGFR and JNK proteins. Intriguingly, several proteins' activation (phosphorylation) was comparatively milder with OA complexes than with its DMSO-solubilized counterpart. However, for MDA-MB-231, the activation pattern displayed a delayed response in the OA/HP-β-CD condition compared to OA/DMSO. This could be attributed to the distinct dynamics of cyclodextrins, which might provide a sustained OA release. It should be noted that this study also revealed that cell migration induced by OA/HP-β-CD complexes in Mv1Lu cells shared similar molecular mechanisms with MDA-MB-231 cells, as previously observed for OA/DMSO. In this line, the migration prompted by OA/HP-β-CD complexes was compromised when specific inhibitors EGFRi, MEKi, and JNKi were added to scratch assays. Concerning c-Jun and p-c-Jun blots, both forms exhibited increased and sustained expression at later times in the OA/HP-β-CD condition. These findings imply a sustained effect of complexed OA on this transcription factor, correlating positively with immunocytochemistry assays. Altogether, EGFR, ERK1/2, JNK1/2, and c-Jun activation dynamics exhibit a delayed response by OA/HP-β-CD complexes in Mv1Lu and MDA-MB-231 cells, provided by the slow-release dynamics of cyclodextrins. This particular response appears to be advantageous over time, since OA complexes in turn yielded more recruited migrating cells that covered the scratched area in the wound, without compromising cell viability.

In light of these results, the developed formulations of complexed OA with cyclodextrins allow for a suitable topical use for skin wound healing. Therefore, future in vivo assays should be considered (Figure V-3). Numerous in vivo models can be employed to explore the complex effects of OA on wound healing (383, 384). The enhanced delivery provided by cyclodextrins, followed by the dehydration process, showed improved OA in vitro bioavailability for epithelial cells, improving cell viability and enhancing cell migration. This formulation did not only improve cell migration features, but also demonstrated that OA biological activity was preserved as a solid complex with CDs, which holds a crucial significance for drug application, improving sustainability, conservation, dose standardization, DMSO cytotoxic solvent elimination, and handling (Figure V-3).

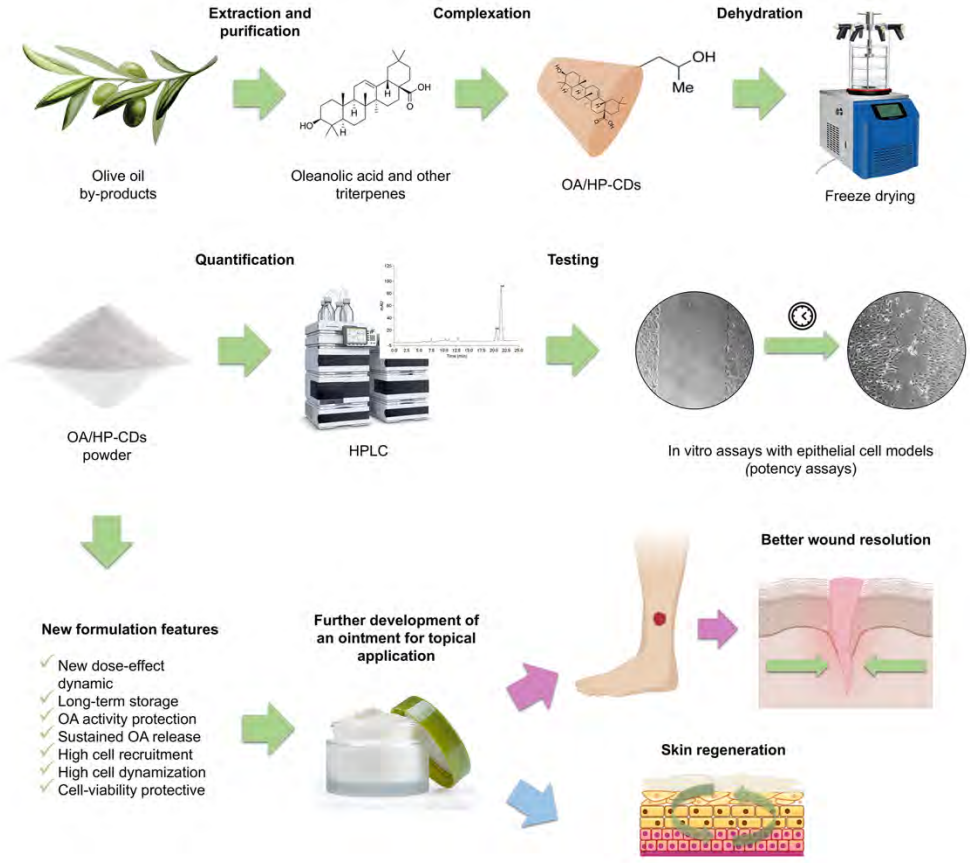

Figure V-3. A new formulation has been developed to enhance the applicability and bioavailability of OA. *Oleanolic acid and other bioactive triterpenes are obtained from olive oil by-products. These compounds can be complexed with hydroxypropyl cyclodextrins (HP-CDs), a CD type with extra water-solubility. Proper in vitro application of OA/HP-CDs complexes requires their dehydration using non-harmful freeze-drying devices. The concentration of OA in the powder is measured by HPLC before its testing on in vitro cultures through potency assays, including scratch assays. The effects of this new formulation seen in epithelial cells will lead to further research on advanced formulations that incorporate dried OA/HP-CDs into creams, gels, or ointments which can be topically applied for pharmacological or cosmetic use on wounds or skin.*

VI – CONCLUSIONS

VI -CONCLUSIONS

1. OA induces the overexpression and activation of transcription factor c-Jun in the cell nuclei during migration, with a precise organization across rows of wound edge cells.
2. OA changes actin conformation, paxillin distribution and FAK activity; thus triggering actin turnover, increasing focal adhesions, paxillin and FAK activation and colocalization; resulting in high cell motility.
3. OA produces an earlier activation of c-Jun, a mechanism that is independent from EGFR.
4. OA's biphasic signaling mechanism for cell migration is divided into an early first phase of MEK/JNK/c-Jun and a later second phase of EGFR/MEK/ERK/c-Jun; thus, both are required for c-Jun activation and paxillin/FAK crosstalk.
5. OA attenuates adhesion molecule overexpression and synthesis by TNF-α inflammatory stimulus in C- and GD-HUVEC endothelial cell models, therefore resulting in a reduced number of adhered monocytes.
6. OA rescues and improves neo-angiogenic features of GD-HUVEC.
7. OA enhances C- and GD-HUVEC cell migration, an event that contributes to neo-angiogenesis, and this positive effect is enhanced by the increase in focal adhesion number.
8. HP-β- and HP-γ- cyclodextrins are very productive for complexation of OA.
9. OA stability and preservation in the complexes is improved by freeze drying.
10. Freeze-dried OA/HP-β-CD and OA/HP-γ-CD complexes modify the OA dose-response dynamics in vitro, respecting cell viability, requiring higher working concentrations than OA/DMSO and resolving mild OA/DMSO cytotoxic effects.

11. Freeze-dried OA/HP-β-CD and OA/HP-γ-CD complexes exhibit substantial efficacy in promoting cell migration, showing a higher recruitment of migrating cells.
12. Freeze-dried OA/HP-β-CD complexes are compatible with high cell motility, as they induce actin and focal adhesion dynamization at wound edge cells.
13. Freeze-dried OA/HP-β-CD complexes induce the whole signaling system to trigger cell migration, as observed with OA/DMSO.

VII – LIMITATIONS AND FUTURE RESEARCH LINES

VII - LIMITATIONS AND FUTURE RESEARCH LINES

Overall, the data collected in this study and its implications for the field will enable new lines of research to be pursued in the future, as outlined below:

a. Understand the global effects of OA on GPCR pathways and regulatory proteins involved
b. Decipher potential OA effects on antioxidant pathways that regulate oxidative stress in endothelial cells
c. Test OA activity on primary keratinocytes and fibroblasts
d. Test OA activity on in vivo animal models

a. Understand the effects of OA on GPCR pathways and the regulatory proteins involved

Given the data collected in this study, it would be very profitable to study whether OA's effects on epithelial cell migration are driven by GPCR receptors (14, 336, 371). Additionally, the same approach could be done in C- and GD-HUVECs, because the observed positive effects of OA on these endothelial cells may be driven by GPCRs function (371). Additionally, it would be interesting to check MEK1/2 total protein and phosphorylation levels under these conditions as it might be interconnecting GPCRs and EGFR pathways to trigger c-Jun activation by OA. Related to this, GPCRs and EGFR receptors, since they are interconnected by growth factors shedding and cytosolic kinases, might be close together in the cell membrane, as many other cell surface receptors, in lipid rafts (385-387). Therefore, it is worth observing whether GPCRs and EGFR are located in the same lipid raft, thus establishing a better-integrated signal in the cell.

It is noteworthy that the Western blot assays carried out in this study and future ones should be performed specifically on the area that is activated by either OA or OA/CDs, compared to the rest of the epithelia. However, at present, we have performed Western blot assays in sub-confluent cells and we have not found a technology to analyze the lysates obtained specifically from the leading edge. Nevertheless, this issue was addressed with cell front migration assays and immunostaining.

Last but not least, OA has shown the capability to induce the phosphorylation of several proteins related to cell motility, especially the phosphorylation of regulatory kinases on their tyrosine residues. In this sense, further research is needed to elucidate the specific contribution of phosphorylated motility proteins paxillin, FAK, or vinculin in OA-induced migration. To better comprehend this OA effect, the study of the phospho-proteome of Mv1Lu and MDA-MB-231 cells could be performed.

b. Decipher potential OA effects on antioxidant pathways that regulate oxidative stress in endothelial cells

OA antioxidant activity has been shown in several studies (39, 73, 74, 76). This molecule can induce the expression of genes related to ROS defense and is also a scavenger of many of the ROS. C- and GD-HUVECs have been demonstrated to be a proper in vitro model to study endothelial cell function (359, 360). Furthermore, a correct endothelial function relies on oxidative stress management (353, 360). Therefore, several key proteins can be analyzed by treating HUVECs with OA, as oxidative stress enzymes regulate ROS levels in the endothelium by synthesizing nitric oxide (NO) with endothelial nitric oxide synthase (eNOS) and inducible nitric oxide synthase (iNOS) (355, 388-390).

c. Test OA activity on primary keratinocytes and fibroblasts

OA's in vitro capabilities should be expanded to include other cell models that have been widely used for wound healing studies. This study did not explore the effects of OA on fibroblasts, even though they are crucial for wound healing due to the production of ECM and skin integrity (94, 103). Hence, the study of primary fibroblasts under OA treatment could be considered as an interesting choice, by performing invasion assays, ECM synthesis study, and qPCR of key genes involved in ECM degradation and remodeling. Although the use of Mv1Lu and MDA-MB-231 cell models are good epithelial models and biosensors for OA activity, more research is necessary to test OA in a cell model that is closer to the skin keratinocytes phenotype, for instance, primary keratinocytes or human skin equivalents (391, 392). Indeed, they are preferable to other models, such as HaCaT cells, which show aberrant responses to growth factors and aneuploidy (391).

d. Test OA activity on in vivo animal models

One of the limitations of the present study is the level of the observed biological effects of OA, which has been shown on an in vitro study. For this reason, further assays should be conducted on in vivo models. There are several wound-healing animal models to establish a new research line testing the OA/CD formulation on wounds, depending on the type of wound present in the model, acute or chronic. For instance, murine models are known for different protocols to surgically wound their dorsal area or the tail (393, 394). Remarkably, a pathologic model to study diabetic wounds could be leptin-deficient mice, animals that develop type 2 diabetes and have delayed wound closure and deficient healing (395). Despite these, murine models for wound healing have thinner skin than other models (384). Interestingly, pig models are an advantage since they have a skin that is anatomically and physiologically more similar to humans, and they have a greater dorsal area for wounding (394).

Regarding angiogenesis, specific in vivo angiogenesis assays with OA could be carried out. One of the most common is angiogenesis in the chorio allantoic membrane of chicken embryos, which could provide new insights into OA angiogenesis-promoting effects since it is a well-established model in vascular biology (384, 396). Overall, these studies would allow for the translational use of OA for the treatment of complex wounds in the health care system.

VIII – BIBLIOGRAPHIC REFERENCES

VIII - BIBLIOGRAPHIC REFERENCES

1. Oracz J, Nebesny E, Zyzelewicz D, Budryn G, Luzak B. Bioavailability and metabolism of selected cocoa bioactive compounds: A comprehensive review. Crit Rev Food Sci Nutr. 2020;60(12):1947-85.
2. Zou H, Li Y, Liu X, Wu Z, Li J, Ma Z. Roles of plant-derived bioactive compounds and related microRNAs in cancer therapy. Phytother Res. 2021;35(3):1176-86.
3. Al-Warhi T, Elmaidomy AH, Maher SA, Abu-Baih DH, Selim S, Albqmi M, et al. The Wound-Healing Potential of Olea europaea L. Cv. Arbequina Leaves Extract: An Integrated In Vitro, In Silico, and In Vivo Investigation. Metabolites. 2022;12(9).
4. Esmeeta A, Adhikary S, Dharshnaa V, Swarnamughi P, Ummul Maqsummiya Z, Banerjee A, et al. Plant-derived bioactive compounds in colon cancer treatment: An updated review. Biomed Pharmacother. 2022;153:113384.
5. Kaur S, Panesar PS, Chopra HK. Citrus processing by-products: an overlooked repository of bioactive compounds. Crit Rev Food Sci Nutr. 2023;63(1):67-86.
6. Zhu F, Du B, Xu B. Anti-inflammatory effects of phytochemicals from fruits, vegetables, and food legumes: A review. Crit Rev Food Sci Nutr. 2018;58(8):1260-70.
7. Shin SA, Joo BJ, Lee JS, Ryu G, Han M, Kim WY, et al. Phytochemicals as Anti-Inflammatory Agents in Animal Models of Prevalent Inflammatory Diseases. Molecules. 2020;25(24).
8. Anand AV, Balamuralikrishnan B, Kaviya M, Bharathi K, Parithathvi A, Arun M, et al. Medicinal Plants, Phytochemicals, and Herbs to Combat Viral Pathogens Including SARS-CoV-2. Molecules. 2021;26(6).
9. Shen J, Shan J, Zhong L, Liang B, Zhang D, Li M, et al. Dietary Phytochemicals that Can Extend Longevity by Regulation of Metabolism. Plant Foods Hum Nutr. 2022;77(1):12-9.

10. Kussmann M, Abe Cunha DH, Berciano S. Bioactive compounds for human and planetary health. Frontiers in Nutrition. 2023;10.

11. Liu J. Pharmacology of oleanolic acid and ursolic acid. J Ethnopharmacol. 1995;49(2):57-68.

12. Ayeleso TB, Matumba MG, Mukwevho E. Oleanolic Acid and Its Derivatives: Biological Activities and Therapeutic Potential in Chronic Diseases. Molecules. 2017;22(11).

13. Singer AJ, Clark RA. Cutaneous wound healing. N Engl J Med. 1999;341(10):738-46.

14. Castellano JM, Ramos-Romero S, Perona JS. Oleanolic Acid: Extraction, Characterization and Biological Activity. Nutrients. 2022;14(3):623.

15. Phillips DR, Rasbery JM, Bartel B, Matsuda SPT. Biosynthetic diversity in plant triterpene cyclization. Current Opinion in Plant Biology. 2006;9(3):305-14.

16. Pollier J, Goossens A. Oleanolic acid. Phytochemistry. 2012;77:10-5.

17. Fukushima EO, Seki H, Ohyama K, Ono E, Umemoto N, Mizutani M, et al. CYP716A Subfamily Members are Multifunctional Oxidases in Triterpenoid Biosynthesis. Plant and Cell Physiology. 2011;52(12):2050-61.

18. Kushiro T, Shibuya M, Ebizuka Y. Beta-amyrin synthase--cloning of oxidosqualene cyclase that catalyzes the formation of the most popular triterpene among higher plants. Eur J Biochem. 1998;256(1):238-44.

19. Lin C, Wen X, Sun H. Oleanolic acid derivatives for pharmaceutical use: a patent review. Expert Opin Ther Pat. 2016;26(6):643-55.

20. Gudoityte E, Arandarcikaite O, Mazeikiene I, Bendokas V, Liobikas J. Ursolic and Oleanolic Acids: Plant Metabolites with Neuroprotective Potential. Int J Mol Sci. 2021;22(9).

21. Juang YP, Lin YY, Chan SH, Chang CK, Shie JJ, Hsieh YSY, et al. Synthesis, distribution analysis and mechanism studies of N-acyl glucosamine-bearing oleanolic saponins. Bioorg Chem. 2020;99:103835.

22. Szakiel A, Kasprzyk Z. Distribution of oleanolic acid glycosides in vacuoles and cell walls isolated from protoplasts and cells of Calendula officinalis leaves. Steroids. 1989;53(3-5):501-11.

23. Fai YM, Tao C.C. A review of presence of oleanolic acid in natural products. Natura Proda Medica. 2009;2:77-290.

24. Szakiel A, Paczkowski C, Pensec F, Bertsch C. Fruit cuticular waxes as a source of biologically active triterpenoids. Phytochem Rev. 2012;11(2-3):263-84.

25. Ludeña-Huaman MA, Ramos-Inquiltupa DA. Determination of the content of ursolic and oleanolic acid in the cuticular wax of fruits of different species of Rosaceae. Revista Colombiana de Química. 2019;48(2):15-20.

26. Jager S, Trojan H, Kopp T, Laszczyk MN, Scheffler A. Pentacyclic triterpene distribution in various plants - rich sources for a new group of multi-potent plant extracts. Molecules. 2009;14(6):2016-31.

27. Kowalski R. Studies of selected plant raw materials as alternative sources of triterpenes of oleanolic and ursolic acid types. J Agric Food Chem. 2007;55(3):656-62.

28. Bernardini E, Visioli F. High quality, good health: The case for olive oil. European Journal of Lipid Science and Technology. 2016;119(1).

29. Ministerio de Agricultura PyA. Aceite de oliva y aceituna de mesa: Gobierno de España, Ministerio de Agricultura, Pesca y Alimentación (MAPA)

; 2020 [Available from: https://www.mapa.gob.es/es/agricultura/temas/producciones-agricolas/aceite-oliva-y-aceituna-mesa/aceite.aspx.

30. Gorzynik-Debicka M, Przychodzen P, Cappello F, Kuban-Jankowska A, Marino Gammazza A, Knap N, et al. Potential Health Benefits of Olive Oil and Plant Polyphenols. Int J Mol Sci. 2018;19(3).

31. De Santis S, Cariello M, Piccinin E, Sabba C, Moschetta A. Extra Virgin Olive Oil: Lesson from Nutrigenomics. Nutrients. 2019;11(9).

32. Mora ‐ Ruiz ME, Reboredo ‐ Rodríguez P, Salvador MD, González ‐ Barreiro C, Cancho ‐ Grande B, Simal ‐ Gándara J, et al. Assessment of polar phenolic compounds of virgin olive oil by NIR and mid ‐ IR

spectroscopy and their impact on quality. European Journal of Lipid Science and Technology. 2016;119(1).

33. Claro-Cala CM, Quintela JC, Perez-Montero M, Minano J, de Sotomayor MA, Herrera MD, et al. Pomace Olive Oil Concentrated in Triterpenic Acids Restores Vascular Function, Glucose Tolerance and Obesity Progression in Mice. Nutrients. 2020;12(2).

34. Xie P, Cecchi L, Bellumori M, Balli D, Giovannelli L, Huang L, et al. Phenolic Compounds and Triterpenes in Different Olive Tissues and Olive Oil By-Products, and Cytotoxicity on Human Colorectal Cancer Cells: The Case of Frantoio, Moraiolo and Leccino Cultivars (Olea europaea L.). Foods. 2021;10(11).

35. Xia EQ, Yu YY, Xu XR, Deng GF, Guo YJ, Li HB. Ultrasound-assisted extraction of oleanolic acid and ursolic acid from Ligustrum lucidum Ait. Ultrason Sonochem. 2012;19(4):772-6.

36. Xia EQ, Wang BW, Xu XR, Zhu L, Song Y, Li HB. Microwave-assisted extraction of oleanolic acid and ursolic acid from Ligustrum lucidum Ait. Int J Mol Sci. 2011;12(8):5319-29.

37. Fu Q, Zhang L, Cheng N, Jia M, Zhang Y. Extraction optimization of oleanolic and ursolic acids from pomegranate (Punica granatum L.) flowers. Food and Bioproducts Processing. 2014;92(3):321-7.

38. Lim SW, Hong SP, Jeong SW, Kim B, Bak H, Ryoo HC, et al. Simultaneous effect of ursolic acid and oleanolic acid on epidermal permeability barrier function and epidermal keratinocyte differentiation via peroxisome proliferator-activated receptor-alpha. J Dermatol. 2007;34(9):625-34.

39. Somova LO, Nadar A, Rammanan P, Shode FO. Cardiovascular, antihyperlipidemic and antioxidant effects of oleanolic and ursolic acids in experimental hypertension. Phytomedicine. 2003;10(2-3):115-21.

40. Kim KA, Lee JS, Park HJ, Kim JW, Kim CJ, Shim IS, et al. Inhibition of cytochrome P450 activities by oleanolic acid and ursolic acid in human liver microsomes. Life Sci. 2004;74(22):2769-79.

41. Khwaza V, Oyedeji OO, Aderibigbe BA. Ursolic Acid-Based Derivatives as Potential Anti-Cancer Agents: An Update. Int J Mol Sci. 2020;21(16).

42. He Y, Wang Y, Yang K, Jiao J, Zhan H, Yang Y, et al. Maslinic Acid: A New Compound for the Treatment of Multiple Organ Diseases. Molecules [Internet]. 2022; 27(24).

43. Patočka J. Biologically active pentacyclic triterpenes and their current medicine signification. Journal of Applied Biomedicine. 2003;1(1):7-12.

44. Ramirez-Espinosa JJ, Garcia-Jimenez S, Rios MY, Medina-Franco JL, Lopez-Vallejo F, Webster SP, et al. Antihyperglycemic and sub-chronic antidiabetic actions of morolic and moronic acids, in vitro and in silico inhibition of 11beta-HSD 1. Phytomedicine. 2013;20(7):571-6.

45. Lehbili M, Alabdul Magid A, Kabouche A, Voutquenne-Nazabadioko L, Abedini A, Morjani H, et al. Oleanane-type triterpene saponins from Calendula stellata. Phytochemistry. 2017;144:33-42.

46. Petronelli A, Pannitteri G, Testa U. Triterpenoids as new promising anticancer drugs. Anticancer Drugs. 2009;20(10):880-92.

47. Ziberna L, Samec D, Mocan A, Nabavi SF, Bishayee A, Farooqi AA, et al. Oleanolic Acid Alters Multiple Cell Signaling Pathways: Implication in Cancer Prevention and Therapy. Int J Mol Sci. 2017;18(3).

48. Mu DW, Guo HQ, Zhou GB, Li JY, Su B. Oleanolic acid suppresses the proliferation of human bladder cancer by Akt/mTOR/S6K and ERK1/2 signaling. Int J Clin Exp Pathol. 2015;8(11):13864-70.

49. Gao D, Tang S, Tong Q. Oleanolic acid liposomes with polyethylene glycol modification: promising antitumor drug delivery. Int J Nanomedicine. 2012;7:3517-26.

50. Wang X, Bai H, Zhang X, Liu J, Cao P, Liao N, et al. Inhibitory effect of oleanolic acid on hepatocellular carcinoma via ERK-p53-mediated cell cycle arrest and mitochondrial-dependent apoptosis. Carcinogenesis. 2013;34(6):1323-30.

51. Zeisel MB, Pfeffer S, Baumert TF. miR-122 acts as a tumor suppressor in hepatocarcinogenesis in vivo. J Hepatol. 2013;58(4):821-3.

52. He Y, Liu X, Huang M, Wei Z, Zhang M, He M, et al. Oleanolic acid inhibits the migration and invasion of hepatocellular carcinoma cells by promoting microRNA-122 expression. Pharmazie. 2021;76(9):422-7.

53. Xiaofei J, Mingqing S, Miao S, Yizhen Y, Shuang Z, Qinhua X, et al. Oleanolic acid inhibits cervical cancer Hela cell proliferation through modulation of the ACSL4 ferroptosis signaling pathway. Biochem Biophys Res Commun. 2021;545:81-8.

54. Shanmugam MK, Dai X, Kumar AP, Tan BK, Sethi G, Bishayee A. Oleanolic acid and its synthetic derivatives for the prevention and therapy of cancer: preclinical and clinical evidence. Cancer Lett. 2014;346(2):206-16.

55. Baer-Dubowska W, Narozna M, Krajka-Kuzniak V. Anti-Cancer Potential of Synthetic Oleanolic Acid Derivatives and Their Conjugates with NSAIDs. Molecules. 2021;26(16).

56. Castellano JM, Guinda A, Delgado T, Rada M, Cayuela JA. Biochemical basis of the antidiabetic activity of oleanolic acid and related pentacyclic triterpenes. Diabetes. 2013;62(6):1791-9.

57. Carvalho E, Jansson PA, Nagaev I, Wenthzel AM, Smith U. Insulin resistance with low cellular IRS-1 expression is also associated with low GLUT4 expression and impaired insulin-stimulated glucose transport. FASEB J. 2001;15(6):1101-3.

58. Li M, Han Z, Bei W, Rong X, Guo J, Hu X. Oleanolic Acid Attenuates Insulin Resistance via NF-kappaB to Regulate the IRS1-GLUT4 Pathway in HepG2 Cells. Evid Based Complement Alternat Med. 2015;2015:643102.

59. Loza-Rodriguez H, Estrada-Soto S, Alarcon-Aguilar FJ, Huang F, Aquino-Jarquin G, Fortis-Barrera A, et al. Oleanolic acid induces a dual agonist action on PPARgamma/alpha and GLUT4 translocation: A pentacyclic triterpene for dyslipidemia and type 2 diabetes. Eur J Pharmacol. 2020;883:173252.

60. Li Y, Wang J, Gu T, Yamahara J, Li Y. Oleanolic acid supplement attenuates liquid fructose-induced adipose tissue insulin resistance through the insulin receptor substrate-1/phosphatidylinositol 3-kinase/Akt signaling pathway in rats. Toxicol Appl Pharmacol. 2014;277(2):155-63.

61. Fornasier M, Pireddu R, Del Giudice A, Sinico C, Nylander T, Schillen K, et al. Tuning lipid structure by bile salts: Hexosomes for topical administration of catechin. Colloids Surf B Biointerfaces. 2021;199:111564.

62. Liu J, Liu J, Meng C, Huang C, Liu F, Xia C. Oleanolic acid alleviates ANIT-induced cholestatic liver injury by activating Fxr and Nrf2 pathways to ameliorate disordered bile acids homeostasis. Phytomedicine. 2022;102:154173.

63. Xin C, Liu S, Qu H, Wang Z. The novel nanocomplexes containing deoxycholic acid-grafted chitosan and oleanolic acid displays the hepatoprotective effect against CCl(4)-induced liver injury in vivo. Int J Biol Macromol. 2021;185:338-49.

64. He F, Ru X, Wen T. NRF2, a Transcription Factor for Stress Response and Beyond. Int J Mol Sci. 2020;21(13).

65. Gabas-Rivera C, Martinez-Beamonte R, Rios JL, Navarro MA, Surra JC, Arnal C, et al. Dietary oleanolic acid mediates circadian clock gene expression in liver independently of diet and animal model but requires apolipoprotein A1. J Nutr Biochem. 2013;24(12):2100-9.

66. Luo HQ, Shen J, Chen CP, Ma X, Lin C, Ouyang Q, et al. Lipid-lowering effects of oleanolic acid in hyperlipidemic patients. Chin J Nat Med. 2018;16(5):339-46.

67. Rodriguez JA, Astudillo L, Schmeda-Hirschmann G. Oleanolic acid promotes healing of acetic acid-induced chronic gastric lesions in rats. Pharmacol Res. 2003;48(3):291-4.

68. Medina-O'Donnell M, Rivas F, Reyes-Zurita FJ, Cano-Munoz M, Martinez A, Lupianez JA, et al. Oleanolic Acid Derivatives as Potential Inhibitors of HIV-1 Protease. J Nat Prod. 2019;82(10):2886-96.

69. Kong L, Li S, Liao Q, Zhang Y, Sun R, Zhu X, et al. Oleanolic acid and ursolic acid: novel hepatitis C virus antivirals that inhibit NS5B activity. Antiviral Res. 2013;98(1):44-53.

70. Khwaza V, Oyedeji OO, Aderibigbe BA. Antiviral Activities of Oleanolic Acid and Its Analogues. Molecules. 2018;23(9).

71. Jesus JA, Lago JH, Laurenti MD, Yamamoto ES, Passero LF. Antimicrobial activity of oleanolic and ursolic acids: an update. Evid Based Complement Alternat Med. 2015;2015:620472.

72. Blanco-Cabra N, Vega-Granados K, Moya-Anderico L, Vukomanovic M, Parra A, Alvarez de Cienfuegos L, et al. Novel Oleanolic and Maslinic Acid Derivatives as a Promising Treatment against Bacterial Biofilm in Nosocomial Infections: An in Vitro and in Vivo Study. ACS Infect Dis. 2019;5(9):1581-9.

73. Wang X, Ye XL, Liu R, Chen HL, Bai H, Liang X, et al. Antioxidant activities of oleanolic acid in vitro: possible role of Nrf2 and MAP kinases. Chem Biol Interact. 2010;184(3):328-37.

74. Castellano JM, Garcia-Rodriguez S, Espinosa JM, Millan-Linares MC, Rada M, Perona JS. Oleanolic Acid Exerts a Neuroprotective Effect Against Microglial Cell Activation by Modulating Cytokine Release and Antioxidant Defense Systems. Biomolecules. 2019;9(11).

75. Msibi ZNP, Mabandla MV. Oleanolic Acid Mitigates 6-Hydroxydopamine Neurotoxicity by Attenuating Intracellular ROS in PC12 Cells and Striatal Microglial Activation in Rat Brains. Front Physiol. 2019;10:1059.

76. Rong ZT, Gong XJ, Sun HB, Li YM, Ji H. Protective effects of oleanolic acid on cerebral ischemic damage in vivo and H(2)O(2)-induced injury in vitro. Pharm Biol. 2011;49(1):78-85.

77. Lee W, Yang EJ, Ku SK, Song KS, Bae JS. Anti-inflammatory effects of oleanolic acid on LPS-induced inflammation in vitro and in vivo. Inflammation. 2013;36(1):94-102.

78. Martin R, Cordova C, San Roman JA, Gutierrez B, Cachofeiro V, Nieto ML. Oleanolic acid modulates the immune-inflammatory response in mice with experimental autoimmune myocarditis and protects from cardiac injury. Therapeutic implications for the human disease. J Mol Cell Cardiol. 2014;72:250-62.

79. Barrientos S, Stojadinovic O, Golinko MS, Brem H, Tomic-Canic M. Growth factors and cytokines in wound healing. Wound Repair Regen. 2008;16(5):585-601.

80. Behm B, Babilas P, Landthaler M, Schreml S. Cytokines, chemokines and growth factors in wound healing. J Eur Acad Dermatol Venereol. 2012;26(7):812-20.

81. Menke NB, Ward KR, Witten TM, Bonchev DG, Diegelmann RF. Impaired wound healing. Clin Dermatol. 2007;25(1):19-25.

82. Chambers ES, Vukmanovic-Stejic M. Skin barrier immunity and ageing. Immunology. 2020;160(2):116-25.

83. Dabrowska AK, Spano F, Derler S, Adlhart C, Spencer ND, Rossi RM. The relationship between skin function, barrier properties, and body-dependent factors. Skin Res Technol. 2018;24(2):165-74.

84. Rawlings AV, Harding CR. Moisturization and skin barrier function. Dermatol Ther. 2004;17 Suppl 1:43-8.

85. Gravitz L. Skin. Nature. 2018;563(7732):S83.

86. Abdo JM, Sopko NA, Milner SM. The applied anatomy of human skin: A model for regeneration. Wound Medicine. 2020;28.

87. Proksch E, Brandner JM, Jensen JM. The skin: an indispensable barrier. Exp Dermatol. 2008;17(12):1063-72.

88. McGovern JA, Heinemann JR, Burke LJ, Dawson R, Parker TJ, Upton Z, et al. Stratum basale keratinocyte expression of the cell-surface glycoprotein CDCP1 during epidermogenesis and its role in keratinocyte migration. Br J Dermatol. 2013;168(3):496-503.

89. Yang EJ, Lee W, Ku SK, Song KS, Bae JS. Anti-inflammatory activities of oleanolic acid on HMGB1 activated HUVECs. Food Chem Toxicol. 2012;50(5):1288-94.

90. Fuchs E, Raghavan S. Getting under the skin of epidermal morphogenesis. Nat Rev Genet. 2002;3(3):199-209.

91. Eckhart L, Lippens S, Tschachler E, Declercq W. Cell death by cornification. Biochim Biophys Acta. 2013;1833(12):3471-80.

92. Thulabandu V, Chen D, Atit RP. Dermal fibroblast in cutaneous development and healing. Wiley Interdiscip Rev Dev Biol. 2018;7(2).

93. Bressler RS, Bressler CH. Functional Anatomy of the Skin. Clinics in Podiatric Medicine and Surgery. 1989;6(2):229-46.

94. Bainbridge P. Wound healing and the role of fibroblasts. J Wound Care. 2013;22(8):407-8, 10-12.

95. Varani J, Dame MK, Rittie L, Fligiel SE, Kang S, Fisher GJ, et al. Decreased collagen production in chronologically aged skin: roles of age-dependent alteration in fibroblast function and defective mechanical stimulation. Am J Pathol. 2006;168(6):1861-8.

96. Yousef H, Alhajj M, Sharma S. Anatomy, Skin (Integument), Epidermis. StatPearls. Treasure Island (FL) ineligible companies. Disclosure: Mandy Alhajj declares no relevant financial relationships with ineligible companies. Disclosure: Sandeep Sharma declares no relevant financial relationships with ineligible companies.2023.

97. Arner P. Human fat cell lipolysis: biochemistry, regulation and clinical role. Best Pract Res Clin Endocrinol Metab. 2005;19(4):471-82.

98. Broughton G, 2nd, Janis JE, Attinger CE. Wound healing: an overview. Plast Reconstr Surg. 2006;117(7 Suppl):1e-S-32e-S.

99. Takeo M, Lee W, Ito M. Wound healing and skin regeneration. Cold Spring Harb Perspect Med. 2015;5(1):a023267.

100. Janis JE, Harrison B. Wound Healing: Part I. Basic Science. Plast Reconstr Surg. 2016;138(3 Suppl):9S-17S.

101. Sorg H, Tilkorn DJ, Hager S, Hauser J, Mirastschijski U. Skin Wound Healing: An Update on the Current Knowledge and Concepts. Eur Surg Res. 2017;58(1-2):81-94.

102. Rodrigues M, Kosaric N, Bonham CA, Gurtner GC. Wound Healing: A Cellular Perspective. Physiol Rev. 2019;99(1):665-706.

103. Wang PH, Huang BS, Horng HC, Yeh CC, Chen YJ. Wound healing. J Chin Med Assoc. 2018;81(2):94-101.

104. Ridiandries A, Tan JTM, Bursill CA. The Role of Chemokines in Wound Healing. Int J Mol Sci. 2018;19(10).

105. Byrd AL, Belkaid Y, Segre JA. The human skin microbiome. Nat Rev Microbiol. 2018;16(3):143-55.

106. Gurtner GC, Werner S, Barrandon Y, Longaker MT. Wound repair and regeneration. Nature. 2008;453(7193):314-21.

107. Werner S, Grose R. Regulation of wound healing by growth factors and cytokines. Physiol Rev. 2003;83(3):835-70.

108. Galiano RD, Tepper OM, Pelo CR, Bhatt KA, Callaghan M, Bastidas N, et al. Topical vascular endothelial growth factor accelerates diabetic wound healing through increased angiogenesis and by mobilizing and recruiting bone marrow-derived cells. Am J Pathol. 2004;164(6):1935-47.

109. Raja, Sivamani K, Garcia MS, Isseroff RR. Wound re-epithelialization: modulating keratinocyte migration in wound healing. Front Biosci. 2007;12:2849-68.

110. Reinke JM, Sorg H. Wound repair and regeneration. Eur Surg Res. 2012;49(1):35-43.

111. Schreier T, Degen E, Baschong W. Fibroblast migration and proliferation during in vitro wound healing. A quantitative comparison between various growth factors and a low molecular weight blood dialysate used in the clinic to normalize impaired wound healing. Res Exp Med (Berl). 1993;193(4):195-205.

112. Lamalice L, Le Boeuf F, Huot J. Endothelial cell migration during angiogenesis. Circ Res. 2007;100(6):782-94.

113. Kalluri R, Weinberg RA. The basics of epithelial-mesenchymal transition. J Clin Invest. 2009;119(6):1420-8.

114. Huber MA, Kraut N, Beug H. Molecular requirements for epithelial-mesenchymal transition during tumor progression. Curr Opin Cell Biol. 2005;17(5):548-58.

115. Du Z, Lovly CM. Mechanisms of receptor tyrosine kinase activation in cancer. Mol Cancer. 2018;17(1):58.

116. Esteban-Villarrubia J, Soto-Castillo JJ, Pozas J, San Roman-Gil M, Orejana-Martin I, Torres-Jimenez J, et al. Tyrosine Kinase Receptors in Oncology. Int J Mol Sci. 2020;21(22).

117. Herbst RS. Review of epidermal growth factor receptor biology. Int J Radiat Oncol Biol Phys. 2004;59(2 Suppl):21-6.

118. Fichter CD, Gudernatsch V, Przypadlo CM, Follo M, Schmidt G, Werner M, et al. ErbB targeting inhibitors repress cell migration of esophageal

squamous cell carcinoma and adenocarcinoma cells by distinct signaling pathways. J Mol Med (Berl). 2014;92(11):1209-23.

119. Edwin F, Wiepz GJ, Singh R, Peet CR, Chaturvedi D, Bertics PJ, et al. A historical perspective of the EGF receptor and related systems. Methods Mol Biol. 2006;327:1-24.

120. Hutson JM, Niall M, Evans D, Fowler R. Effect of salivary glands on wound contraction in mice. Nature. 1979;279(5716):793-5.

121. Boonstra J, Rijken P, Humbel B, Cremers F, Verkleij A, van Bergen en Henegouwen P. The epidermal growth factor. Cell Biol Int. 1995;19(5):413-30.

122. Purba ER, Saita EI, Maruyama IN. Activation of the EGF Receptor by Ligand Binding and Oncogenic Mutations: The "Rotation Model". Cells. 2017;6(2).

123. Wee P, Wang Z. Epidermal Growth Factor Receptor Cell Proliferation Signaling Pathways. Cancers (Basel). 2017;9(5).

124. Verma NK, Tran T, Kelleher D. Editorial: Adaptor Protein Regulation in Immune Signalling. Front Immunol. 2020;11:441.

125. Boucher I, Kehasse A, Marcincin M, Rich C, Rahimi N, Trinkaus-Randall V. Distinct activation of epidermal growth factor receptor by UTP contributes to epithelial cell wound repair. Am J Pathol. 2011;178(3):1092-105.

126. Bernabe-Garcia A, Armero-Barranco D, Liarte S, Ruzafa-Martinez M, Ramos-Morcillo AJ, Nicolas FJ. Oleanolic acid induces migration in Mv1Lu and MDA-MB-231 epithelial cells involving EGF receptor and MAP kinases activation. PLoS One. 2017;12(2):e0172574.

127. Boriack-Sjodin PA, Margarit SM, Bar-Sagi D, Kuriyan J. The structural basis of the activation of Ras by Sos. Nature. 1998;394(6691):337-43.

128. Lin CW, Nocka LM, Stinger BL, DeGrandchamp JB, Lew LJN, Alvarez S, et al. A two-component protein condensate of the EGFR cytoplasmic tail and Grb2 regulates Ras activation by SOS at the membrane. Proc Natl Acad Sci U S A. 2022;119(19):e2122531119.

129. Dhillon AS, Kolch W. Untying the regulation of the Raf-1 kinase. Arch Biochem Biophys. 2002;404(1):3-9.

130. Dhanasekaran N, Premkumar Reddy E. Signaling by dual specificity kinases. Oncogene. 1998;17(11 Reviews):1447-55.

131. Shang J, Lu S, Jiang Y, Zhang J. Allosteric modulators of MEK1: drug design and discovery. Chem Biol Drug Des. 2016;88(4):485-97.

132. Schnidar H, Eberl M, Klingler S, Mangelberger D, Kasper M, Hauser-Kronberger C, et al. Epidermal growth factor receptor signaling synergizes with Hedgehog/GLI in oncogenic transformation via activation of the MEK/ERK/JUN pathway. Cancer Res. 2009;69(4):1284-92.

133. Matsubayashi Y, Ebisuya M, Honjoh S, Nishida E. ERK activation propagates in epithelial cell sheets and regulates their migration during wound healing. Curr Biol. 2004;14(8):731-5.

134. Wortzel I, Seger R. The ERK Cascade: Distinct Functions within Various Subcellular Organelles. Genes Cancer. 2011;2(3):195-209.

135. Klemke RL, Cai S, Giannini AL, Gallagher PJ, de Lanerolle P, Cheresh DA. Regulation of cell motility by mitogen-activated protein kinase. J Cell Biol. 1997;137(2):481-92.

136. Dhillon AS, Hagan S, Rath O, Kolch W. MAP kinase signalling pathways in cancer. Oncogene. 2007;26(22):3279-90.

137. Morrison DK. MAP kinase pathways. Cold Spring Harb Perspect Biol. 2012;4(11).

138. Johnson GL, Nakamura K. The c-jun kinase/stress-activated pathway: regulation, function and role in human disease. Biochim Biophys Acta. 2007;1773(8):1341-8.

139. Xia Y, Makris C, Su B, Li E, Yang J, Nemerow GR, et al. MEK kinase 1 is critically required for c-Jun N-terminal kinase activation by proinflammatory stimuli and growth factor-induced cell migration. Proc Natl Acad Sci U S A. 2000;97(10):5243-8.

140. Yujiri T, Ware M, Widmann C, Oyer R, Russell D, Chan E, et al. MEK kinase 1 gene disruption alters cell migration and c-Jun NH2-terminal

kinase regulation but does not cause a measurable defect in NF-kappa B activation. Proc Natl Acad Sci U S A. 2000;97(13):7272-7.

141. White SR, Tse R, Marroquin BA. Stress-activated protein kinases mediate cell migration in human airway epithelial cells. Am J Respir Cell Mol Biol. 2005;32(4):301-10.

142. Bernabe-Garcia A, Liarte S, Moraleda JM, Castellanos G, Nicolas FJ. Amniotic membrane promotes focal adhesion remodeling to stimulate cell migration. Sci Rep. 2017;7(1):15262.

143. Wilhelm D, van Dam H, Herr I, Baumann B, Herrlich P, Angel P. Both ATF-2 and c-Jun are Phosphorylated by Stress-Activated Protein Kinases in Response to UV Irradiation. Immunobiology. 1995;193(2-4):143-8.

144. Morton S, Davis RJ, McLaren A, Cohen P. A reinvestigation of the multisite phosphorylation of the transcription factor c-Jun. EMBO J. 2003;22(15):3876-86.

145. Meng Q, Xia Y. c-Jun, at the crossroad of the signaling network. Protein Cell. 2011;2(11):889-98.

146. Herber B, Truss M, Beato M, Muller R. Inducible regulatory elements in the human cyclin D1 promoter. Oncogene. 1994;9(4):1295-304.

147. Herdegen T, Skene P, Bahr M. The c-Jun transcription factor--bipotential mediator of neuronal death, survival and regeneration. Trends Neurosci. 1997;20(5):227-31.

148. Shaulian E. AP-1--The Jun proteins: Oncogenes or tumor suppressors in disguise? Cell Signal. 2010;22(6):894-9.

149. Angel P, Szabowski A, Schorpp-Kistner M. Function and regulation of AP-1 subunits in skin physiology and pathology. Oncogene. 2001;20(19):2413-23.

150. Neub A, Houdek P, Ohnemus U, Moll I, Brandner JM. Biphasic regulation of AP-1 subunits during human epidermal wound healing. J Invest Dermatol. 2007;127(10):2453-62.

151. Yue C, Guo Z, Luo Y, Yuan J, Wan X, Mo Z. c-Jun Overexpression Accelerates Wound Healing in Diabetic Rats by Human Umbilical Cord-Derived Mesenchymal Stem Cells. Stem Cells Int. 2020;2020:7430968.

152. Kushnir T, Mezuman S, Bar-Cohen S, Lange R, Paroush Z, Helman A. Novel interplay between JNK and Egfr signaling in Drosophila dorsal closure. PLoS Genet. 2017;13(6):e1006860.

153. Li G, Gustafson-Brown C, Hanks SK, Nason K, Arbeit JM, Pogliano K, et al. c-Jun is essential for organization of the epidermal leading edge. Dev Cell. 2003;4(6):865-77.

154. Xue G, Hemmings BA. PKB/Akt-dependent regulation of cell motility. J Natl Cancer Inst. 2013;105(6):393-404.

155. Li Q, Li Z, Luo T, Shi H. Targeting the PI3K/AKT/mTOR and RAF/MEK/ERK pathways for cancer therapy. Mol Biomed. 2022;3(1):47.

156. Yang Y, Mlodzik M. Wnt-Frizzled/planar cell polarity signaling: cellular orientation by facing the wind (Wnt). Annu Rev Cell Dev Biol. 2015;31:623-46.

157. Webb DJ, Zhang H, Horwitz AF. Cell migration: an overview. Methods Mol Biol. 2005;294:3-11.

158. Lauffenburger DA, Horwitz AF. Cell migration: a physically integrated molecular process. Cell. 1996;84(3):359-69.

159. Manes S, Mira E, Gomez-Mouton C, Lacalle RA, Martinez C. Cells on the move: a dialogue between polarization and motility. IUBMB Life. 2000;49(2):89-96.

160. Ridley AJ, Schwartz MA, Burridge K, Firtel RA, Ginsberg MH, Borisy G, et al. Cell migration: integrating signals from front to back. Science. 2003;302(5651):1704-9.

161. Rottner K, Faix J, Bogdan S, Linder S, Kerkhoff E. Actin assembly mechanisms at a glance. J Cell Sci. 2017;130(20):3427-35.

162. Schaks M, Giannone G, Rottner K. Actin dynamics in cell migration. Essays Biochem. 2019;63(5):483-95.

163. Svitkina TM, Bulanova EA, Chaga OY, Vignjevic DM, Kojima S, Vasiliev JM, et al. Mechanism of filopodia initiation by reorganization of a dendritic network. J Cell Biol. 2003;160(3):409-21.

164. Dominguez R, Holmes KC. Actin structure and function. Annu Rev Biophys. 2011;40:169-86.

165. Pollard TD. Actin and Actin-Binding Proteins. Cold Spring Harb Perspect Biol. 2016;8(8).

166. Svitkina T. The Actin Cytoskeleton and Actin-Based Motility. Cold Spring Harb Perspect Biol. 2018;10(1).

167. Gardel ML, Schneider IC, Aratyn-Schaus Y, Waterman CM. Mechanical integration of actin and adhesion dynamics in cell migration. Annu Rev Cell Dev Biol. 2010;26:315-33.

168. Tang DD, Gerlach BD. The roles and regulation of the actin cytoskeleton, intermediate filaments and microtubules in smooth muscle cell migration. Respir Res. 2017;18(1):54.

169. Breuss JM, Gallo J, DeLisser HM, Klimanskaya IV, Folkesson HG, Pittet JF, et al. Expression of the beta 6 integrin subunit in development, neoplasia and tissue repair suggests a role in epithelial remodeling. J Cell Sci. 1995;108 (Pt 6):2241-51.

170. Zaidel-Bar R, Ballestrem C, Kam Z, Geiger B. Early molecular events in the assembly of matrix adhesions at the leading edge of migrating cells. J Cell Sci. 2003;116(Pt 22):4605-13.

171. Blystone SD. Integrating an integrin: a direct route to actin. Biochim Biophys Acta. 2004;1692(2-3):47-54.

172. Brunton VG, MacPherson IR, Frame MC. Cell adhesion receptors, tyrosine kinases and actin modulators: a complex three-way circuitry. Biochim Biophys Acta. 2004;1692(2-3):121-44.

173. Huttenlocher A, Horwitz AR. Integrins in cell migration. Cold Spring Harb Perspect Biol. 2011;3(9):a005074.

174. Wozniak MA, Modzelewska K, Kwong L, Keely PJ. Focal adhesion regulation of cell behavior. Biochim Biophys Acta. 2004;1692(2-3):103-19.

175. Geiger B, Spatz JP, Bershadsky AD. Environmental sensing through focal adhesions. Nat Rev Mol Cell Biol. 2009;10(1):21-33.

176. Heasman SJ, Ridley AJ. Mammalian Rho GTPases: new insights into their functions from in vivo studies. Nat Rev Mol Cell Biol. 2008;9(9):690-701.

177. Stupack DG, Cho SY, Klemke RL. Molecular signaling mechanisms of cell migration and invasion. Immunol Res. 2000;21(2-3):83-8.

178. Raman M, Chen W, Cobb MH. Differential regulation and properties of MAPKs. Oncogene. 2007;26(22):3100-12.

179. Sieg DJ, Hauck CR, Ilic D, Klingbeil CK, Schaefer E, Damsky CH, et al. FAK integrates growth-factor and integrin signals to promote cell migration. Nat Cell Biol. 2000;2(5):249-56.

180. Mitra SK, Hanson DA, Schlaepfer DD. Focal adhesion kinase: in command and control of cell motility. Nat Rev Mol Cell Biol. 2005;6(1):56-68.

181. Schlaepfer DD, Hauck CR, Sieg DJ. Signaling through focal adhesion kinase. Prog Biophys Mol Biol. 1999;71(3-4):435-78.

182. Sieg DJ, Hauck CR, Schlaepfer DD. Required role of focal adhesion kinase (FAK) for integrin-stimulated cell migration. J Cell Sci. 1999;112 (Pt 16):2677-91.

183. Turner CE. Paxillin and focal adhesion signalling. Nat Cell Biol. 2000;2(12):E231-6.

184. Schaller MD. Paxillin: a focal adhesion-associated adaptor protein. Oncogene. 2001;20(44):6459-72.

185. Hu YL, Lu S, Szeto KW, Sun J, Wang Y, Lasheras JC, et al. FAK and paxillin dynamics at focal adhesions in the protrusions of migrating cells. Sci Rep. 2014;4:6024.

186. Brown MC, Turner CE. Paxillin: adapting to change. Physiol Rev. 2004;84(4):1315-39.

187. Deramaudt TB, Dujardin D, Noulet F, Martin S, Vauchelles R, Takeda K, et al. Altering FAK-paxillin interactions reduces adhesion, migration and invasion processes. PLoS One. 2014;9(3):e92059.

188. Shen Y, Schaller MD. Focal adhesion targeting: the critical determinant of FAK regulation and substrate phosphorylation. Mol Biol Cell. 1999;10(8):2507-18.

189. Sero JE, Thodeti CK, Mammoto A, Bakal C, Thomas S, Ingber DE. Paxillin mediates sensing of physical cues and regulates directional cell motility by controlling lamellipodia positioning. PLoS One. 2011;6(12):e28303.

190. Ma X, Hammes SR. Paxillin actions in the nucleus. Steroids. 2018;133:87-92.

191. Huang C, Rajfur Z, Borchers C, Schaller MD, Jacobson K. JNK phosphorylates paxillin and regulates cell migration. Nature. 2003;424(6945):219-23.

192. Huang Z, Yan DP, Ge BX. JNK regulates cell migration through promotion of tyrosine phosphorylation of paxillin. Cell Signal. 2008;20(11):2002-12.

193. Altan ZM, Fenteany G. c-Jun N-terminal kinase regulates lamellipodial protrusion and cell sheet migration during epithelial wound closure by a gene expression-independent mechanism. Biochem Biophys Res Commun. 2004;322(1):56-67.

194. Tonnesen MG, Feng X, Clark RA. Angiogenesis in wound healing. J Investig Dermatol Symp Proc. 2000;5(1):40-6.

195. Eming SA, Krieg T, Davidson JM. Inflammation in wound repair: molecular and cellular mechanisms. J Invest Dermatol. 2007;127(3):514-25.

196. van Buul JD, Kanters E, Hordijk PL. Endothelial signaling by Ig-like cell adhesion molecules. Arterioscler Thromb Vasc Biol. 2007;27(9):1870-6.

197. Mestas J, Ley K. Monocyte-endothelial cell interactions in the development of atherosclerosis. Trends Cardiovasc Med. 2008;18(6):228-32.

198. Idriss HT, Naismith JH. TNF alpha and the TNF receptor superfamily: structure-function relationship(s). Microsc Res Tech. 2000;50(3):184-95.

199. Hayden MS, Ghosh S. Shared principles in NF-kappaB signaling. Cell. 2008;132(3):344-62.

200. Liu T, Zhang L, Joo D, Sun SC. NF-kappaB signaling in inflammation. Signal Transduct Target Ther. 2017;2:17023-.

201. Silva M, Videira PA, Sackstein R. E-Selectin Ligands in the Human Mononuclear Phagocyte System: Implications for Infection, Inflammation, and Immunotherapy. Front Immunol. 2017;8:1878.

202. Bui TM, Wiesolek HL, Sumagin R. ICAM-1: A master regulator of cellular responses in inflammation, injury resolution, and tumorigenesis. J Leukoc Biol. 2020;108(3):787-99.

203. Troncoso MF, Ortiz-Quintero J, Garrido-Moreno V, Sanhueza-Olivares F, Guerrero-Moncayo A, Chiong M, et al. VCAM-1 as a predictor biomarker

in cardiovascular disease. Biochim Biophys Acta Mol Basis Dis. 2021;1867(9):166170.

204. Medrano-Bosch M, Simon-Codina B, Jimenez W, Edelman ER, Melgar-Lesmes P. Monocyte-endothelial cell interactions in vascular and tissue remodeling. Front Immunol. 2023;14:1196033.

205. Jutila MA, Berg EL, Kishimoto TK, Picker LJ, Bargatze RF, Bishop DK, et al. Inflammation-induced endothelial cell adhesion to lymphocytes, neutrophils, and monocytes. Role of homing receptors and other adhesion molecules. Transplantation. 1989;48(5):727-31.

206. Gerszten RE, Lim YC, Ding HT, Snapp K, Kansas G, Dichek DA, et al. Adhesion of monocytes to vascular cell adhesion molecule-1-transduced human endothelial cells: implications for atherogenesis. Circ Res. 1998;82(8):871-8.

207. Imhof BA, Aurrand-Lions M. Adhesion mechanisms regulating the migration of monocytes. Nat Rev Immunol. 2004;4(6):432-44.

208. Jaipersad AS, Lip GYH, Silverman S, Shantsila E. The Role of Monocytes in Angiogenesis and Atherosclerosis. Journal of the American College of Cardiology. 2014;63(1):1-11.

209. Yunna C, Mengru H, Lei W, Weidong C. Macrophage M1/M2 polarization. Eur J Pharmacol. 2020;877:173090.

210. Arnold F, West DC. Angiogenesis in wound healing. Pharmacol Ther. 1991;52(3):407-22.

211. DiPietro LA. Angiogenesis and wound repair: when enough is enough. J Leukoc Biol. 2016;100(5):979-84.

212. Patan S. Vasculogenesis and angiogenesis. Cancer Treat Res. 2004;117:3-32.

213. Eilken HM, Adams RH. Dynamics of endothelial cell behavior in sprouting angiogenesis. Curr Opin Cell Biol. 2010;22(5):617-25.

214. Leibovich SJ, Polverini PJ, Shepard HM, Wiseman DM, Shively V, Nuseir N. Macrophage-induced angiogenesis is mediated by tumour necrosis factor-alpha. Nature. 1987;329(6140):630-2.

215. Murdoch C, Muthana M, Coffelt SB, Lewis CE. The role of myeloid cells in the promotion of tumour angiogenesis. Nat Rev Cancer. 2008;8(8):618-31.

216. Galli SJ, Borregaard N, Wynn TA. Phenotypic and functional plasticity of cells of innate immunity: macrophages, mast cells and neutrophils. Nat Immunol. 2011;12(11):1035-44.

217. Zachary I. VEGF signalling: integration and multi-tasking in endothelial cell biology. Biochem Soc Trans. 2003;31(Pt 6):1171-7.

218. Hicklin DJ, Ellis LM. Role of the vascular endothelial growth factor pathway in tumor growth and angiogenesis. J Clin Oncol. 2005;23(5):1011-27.

219. van der Meel R, Symons MH, Kudernatsch R, Kok RJ, Schiffelers RM, Storm G, et al. The VEGF/Rho GTPase signalling pathway: a promising target for anti-angiogenic/anti-invasion therapy. Drug Discov Today. 2011;16(5-6):219-28.

220. Hoeben A, Landuyt B, Highley MS, Wildiers H, Van Oosterom AT, De Bruijn EA. Vascular endothelial growth factor and angiogenesis. Pharmacol Rev. 2004;56(4):549-80.

221. Karaman S, Leppanen VM, Alitalo K. Vascular endothelial growth factor signaling in development and disease. Development. 2018;145(14).

222. Kiselyov A, Balakin KV, Tkachenko SE. VEGF/VEGFR signalling as a target for inhibiting angiogenesis. Expert Opin Investig Drugs. 2007;16(1):83-107.

223. Moura-Letts G, Villegas LF, Marcalo A, Vaisberg AJ, Hammond GB. In vivo wound-healing activity of oleanolic acid derived from the acid hydrolysis of Anredera diffusa. J Nat Prod. 2006;69(6):978-9.

224. Wojciak-Kosior M, Paduch R, Matysik-Wozniak A, Niedziela P, Donica H. The effect of ursolic and oleanolic acids on human skin fibroblast cells. Folia Histochem Cytobiol. 2011;49(4):664-9.

225. Kuonen R, Weissenstein U, Urech K, Kunz M, Hostanska K, Estko M, et al. Effects of Lipophilic Extract of Viscum album L. and Oleanolic Acid on

Migratory Activity of NIH/3T3 Fibroblasts and on HaCat Keratinocytes. Evid Based Complement Alternat Med. 2013;2013:718105.

226. Gao C, Li X, Yu S, Liang L. Inhibition of cancer cell growth by oleanolic acid in multidrug resistant liver carcinoma is mediated via suppression of cancer cell migration and invasion, mitochondrial apoptosis, G2/M cell cycle arrest and deactivation of JNK/p38 signalling pathway. J BUON. 2019;24(5):1964-9.

227. Liu J, Ban H, Liu Y, Ni J. The expression and significance of AKR1B10 in laryngeal squamous cell carcinoma. Sci Rep. 2021;11(1):18228.

228. Edathara PM, Chintalapally S, Makani VKK, Pant C, Yerramsetty S, M DR, et al. Inhibitory role of oleanolic acid and esculetin in HeLa cells involve multiple signaling pathways. Gene. 2021;771:145370.

229. Demetriou M, Nabi IR, Coppolino M, Dedhar S, Dennis JW. Reduced contact-inhibition and substratum adhesion in epithelial cells expressing GlcNAc-transferase V. J Cell Biol. 1995;130(2):383-92.

230. Rahimi N, Hung W, Tremblay E, Saulnier R, Elliott B. c-Src kinase activity is required for hepatocyte growth factor-induced motility and anchorage-independent growth of mammary carcinoma cells. J Biol Chem. 1998;273(50):33714-21.

231. Zou Y, Lim S, Lee K, Deng X, Friedman E. Serine/threonine kinase Mirk/Dyrk1B is an inhibitor of epithelial cell migration and is negatively regulated by the Met adaptor Ran-binding protein M. J Biol Chem. 2003;278(49):49573-81.

232. McInroy L, Maatta A. Down-regulation of vimentin expression inhibits carcinoma cell migration and adhesion. Biochem Biophys Res Commun. 2007;360(1):109-14.

233. Zhang N, Kong X, Yan S, Yuan C, Yang Q. Huaier aqueous extract inhibits proliferation of breast cancer cells by inducing apoptosis. Cancer Sci. 2010;101(11):2375-83.

234. Pontillo CA, Garcia MA, Pena D, Cocca C, Chiappini F, Alvarez L, et al. Activation of c-Src/HER1/STAT5b and HER1/ERK1/2 signaling pathways

and cell migration by hexachlorobenzene in MDA-MB-231 human breast cancer cell line. Toxicol Sci. 2011;120(2):284-96.

235. Burke P, Schooler K, Wiley HS. Regulation of epidermal growth factor receptor signaling by endocytosis and intracellular trafficking. Mol Biol Cell. 2001;12(6):1897-910.

236. Li R, Quan P, Liu DF, Wei FD, Zhang Q, Xu QW. The influence of cosolvent on the complexation of HP-beta-cyclodextrins with oleanolic acid and ursolic acid. AAPS PharmSciTech. 2009;10(4):1137-44.

237. Zhang K, Lv, Li, Feng, Li, Liu, et al. Preparation, characterization, and in vivo pharmacokinetics of nanostructured lipid carriers loaded with oleanolic acid and gentiopicrin. International Journal of Nanomedicine. 2013.

238. Man DK, Casettari L, Cespi M, Bonacucina G, Palmieri GF, Sze SC, et al. Oleanolic Acid Loaded PEGylated PLA and PLGA Nanoparticles with Enhanced Cytotoxic Activity against Cancer Cells. Mol Pharm. 2015;12(6):2112-25.

239. Wang Y, Zhu P, Li G, Zhu S, Liu K, Liu Y, et al. Amphiphilic carboxylated cellulose-g-poly(l-lactide) copolymer nanoparticles for oleanolic acid delivery. Carbohydr Polym. 2019;214:100-9.

240. Leilei L, Wenke Q, Yuyuan L, Sihang L, Xue S, Weiqiang C, et al. Oleanolic acid-loaded nanoparticles attenuate activation of hepatic stellate cells via suppressing TGF-beta1 and oxidative stress in PM2.5-exposed hepatocytes. Toxicol Appl Pharmacol. 2022;437:115891.

241. Kumbham S, Paul M, Itoo A, Ghosh B, Biswas S. Oleanolic acid-conjugated human serum albumin nanoparticles encapsulating doxorubicin as synergistic combination chemotherapy in oropharyngeal carcinoma and melanoma. Int J Pharm. 2022;614:121479.

242. Szejtli J. Introduction and General Overview of Cyclodextrin Chemistry. Chem Rev. 1998;98(5):1743-54.

243. Poulson BG, Alsulami QA, Sharfalddin A, El Agammy EF, Mouffouk F, Emwas A-H, et al. Cyclodextrins: Structural, Chemical, and Physical Properties, and Applications. Polysaccharides. 2021;3(1):1-31.

244. Wupper S, Luersen K, Rimbach G. Cyclodextrins, Natural Compounds, and Plant Bioactives-A Nutritional Perspective. Biomolecules. 2021;11(3).

245. Loftsson T, Jarho P, Masson M, Jarvinen T. Cyclodextrins in drug delivery. Expert Opin Drug Deliv. 2005;2(2):335-51.

246. Morin-Crini N, Fourmentin S, Fenyvesi É, Lichtfouse E, Torri G, Fourmentin M, et al. 130 years of cyclodextrin discovery for health, food, agriculture, and the industry: a review. Environmental Chemistry Letters. 2021;19(3):2581-617.

247. Hernandez-Sanchez P, Lopez-Miranda S, Guardiola L, Serrano-Martinez A, Gabaldon JA, Nunez-Delicado E. Optimization of a method for preparing solid complexes of essential clove oil with beta-cyclodextrins. J Sci Food Agric. 2017;97(2):420-6.

248. Del Valle EMM. Cyclodextrins and their uses: a review. Process Biochemistry. 2004;39(9):1033-46.

249. Loftsson T, Duchene D. Cyclodextrins and their pharmaceutical applications. Int J Pharm. 2007;329(1-2):1-11.

250. Astray G, Gonzalez-Barreiro C, Mejuto JC, Rial-Otero R, Simal-Gándara J. A review on the use of cyclodextrins in foods. Food Hydrocolloids. 2009;23(7):1631-40.

251. Lopez-Miranda S, Serrano-Martinez A, Hernandez-Sanchez P, Guardiola L, Perez-Sanchez H, Fortea I, et al. Use of cyclodextrins to recover catechin and epicatechin from red grape pomace. Food Chem. 2016;203:379-85.

252. Quilez M, Ferreres F, Lopez-Miranda S, Salazar E, Jordan MJ. Seed Oil from Mediterranean Aromatic and Medicinal Plants of the Lamiaceae Family as a Source of Bioactive Components with Nutritional. Antioxidants (Basel). 2020;9(6).

253. Pinho E, Grootveld M, Soares G, Henriques M. Cyclodextrins as encapsulation agents for plant bioactive compounds. Carbohydr Polym. 2014;101:121-35.

254. Capelezzo AP, Mohr LC, Dalcanton F, Mello JMMd, Fiori MA. β-Cyclodextrins as Encapsulating Agents of Essential Oils. Cyclodextrin - A Versatile Ingredient2018.

255. Lopez-Miranda S, Berdejo D, Pagan E, Garcia-Gonzalo D, Pagan R. Modified cyclodextrin type and dehydration methods exert a significant effect on the antimicrobial activity of encapsulated carvacrol and thymol. J Sci Food Agric. 2021;101(9):3827-35.

256. Biwer A, Antranikian G, Heinzle E. Enzymatic production of cyclodextrins. Appl Microbiol Biotechnol. 2002;59(6):609-17.

257. Li Z, Wang M, Wang F, Gu Z, Du G, Wu J, et al. gamma-Cyclodextrin: a review on enzymatic production and applications. Appl Microbiol Biotechnol. 2007;77(2):245-55.

258. Liu Y, Lin T, Cheng C, Wang Q, Lin S, Liu C, et al. Research Progress on Synthesis and Application of Cyclodextrin Polymers. Molecules. 2021;26(4).

259. Loftsson T, Brewster ME. Pharmaceutical applications of cyclodextrins. 1. Drug solubilization and stabilization. J Pharm Sci. 1996;85(10):1017-25.

260. Varan G, Varan C, Erdogar N, Hincal AA, Bilensoy E. Amphiphilic cyclodextrin nanoparticles. Int J Pharm. 2017;531(2):457-69.

261. Rajewski RA, Stella VJ. Pharmaceutical applications of cyclodextrins. 2. In vivo drug delivery. J Pharm Sci. 1996;85(11):1142-69.

262. Lucas-Abellán C, Fortea MI, Gabaldón JA, Núñez-Delicado E. Complexation of resveratrol by native and modified cyclodextrins: Determination of complexation constant by enzymatic, solubility and fluorimetric assays. Food Chemistry. 2008;111(1):262-7.

263. Mercader-Ros MT, Lucas-Abellán C, Fortea MI, Gabaldón JA, Núñez-Delicado E. Effect of HP-β-cyclodextrins complexation on the antioxidant activity of flavonols. Food Chemistry. 2010;118(3):769-73.

264. Araj SK, Szeleszczuk L. A Review on Cyclodextrins/Estrogens Inclusion Complexes. Int J Mol Sci. 2023;24(10).

265. Kim D-H, Lee S-E, Pyo Y-C, Tran P, Park J-S. Solubility enhancement and application of cyclodextrins in local drug delivery. Journal of Pharmaceutical Investigation. 2019;50(1):17-27.

266. Godínez LA, Schwartz L, Criss CM, Kaifer AE. Thermodynamic Studies on the Cyclodextrin Complexation of Aromatic and Aliphatic Guests in

Water and Water−Urea Mixtures. Experimental Evidence for the Interaction of Urea with Arene Surfaces. The Journal of Physical Chemistry B. 1997;101(17):3376-80.

267. da Silva Junior WF, Bezerra de Menezes DL, de Oliveira LC, Koester LS, Oliveira de Almeida PD, Lima ES, et al. Inclusion Complexes of beta and HPbeta-Cyclodextrin with alpha, beta Amyrin and In Vitro Anti-Inflammatory Activity. Biomolecules. 2019;9(6).

268. Mazurek AH, Szeleszczuk L. Current Status of Quantum Chemical Studies of Cyclodextrin Host-Guest Complexes. Molecules. 2022;27(12).

269. Popielec A, Loftsson T. Effects of cyclodextrins on the chemical stability of drugs. Int J Pharm. 2017;531(2):532-42.

270. Lopez-Miranda S, Guardiola L, Hernandez-Sanchez P, Nunez-Delicado E. Complexation between oleanolic and maslinic acids with native and modified cyclodextrins. Food Chem. 2018;240:139-46.

271. Samuelsen L, Holm R, Lathuile A, Schonbeck C. Correlation between the stability constant and pH for beta-cyclodextrin complexes. Int J Pharm. 2019;568:118523.

272. Tuz B, Noszal B, Hosztafi S, Mazak K. beta-cyclodextrin complex formation and protonation equilibria of morphine and other opioid compounds of therapeutic interest. Eur J Pharm Sci. 2022;171:106120.

273. Doile MM, Fortunato KA, Schmucker IC, Schucko SK, Silva MA, Rodrigues PO. Physicochemical properties and dissolution studies of dexamethasone acetate-beta-cyclodextrin inclusion complexes produced by different methods. AAPS PharmSciTech. 2008;9(1):314-21.

274. Sursyakova VV, Maksimov NG, Levdansky VA, Rubaylo AI. Combination of phase-solubility method and capillary zone electrophoresis to determine binding constants of cyclodextrins with practically water-insoluble compounds. J Pharm Biomed Anal. 2018;160:12-8.

275. Niu Y, Jia L, Li Y, Liu Y, Yin Q, Zhou L. Insights into Structural Features and Ternary Phase Diagrams of Prednisolone/β-Cyclodextrin Inclusion Complex. Crystal Growth & Design. 2023;23(9):6431-41.

276. Saokham P, Loftsson T. gamma-Cyclodextrin. Int J Pharm. 2017;516(1-2):278-92.

277. Saokham P, Muankaew C, Jansook P, Loftsson T. Solubility of Cyclodextrins and Drug/Cyclodextrin Complexes. Molecules. 2018;23(5).

278. Grecu M, Minea B, Foia LG, Bostanaru-Iliescu AC, Miron L, Nastasa V, et al. Short Review on the Biological Activity of Cyclodextrin-Drug Inclusion Complexes Applicable in Veterinary Therapy. Molecules. 2023;28(14).

279. Pitha J, Gerloczy A, Olivi A. Parenteral hydroxypropyl cyclodextrins: intravenous and intracerebral administration of lipophiles. J Pharm Sci. 1994;83(6):833-7.

280. Gould S, Scott RC. 2-Hydroxypropyl-beta-cyclodextrin (HP-beta-CD): a toxicology review. Food Chem Toxicol. 2005;43(10):1451-9.

281. Braga SS. Cyclodextrins: Emerging Medicines of the New Millennium. Biomolecules. 2019;9(12).

282. Kurkov SV, Loftsson T. Cyclodextrins. Int J Pharm. 2013;453(1):167-80.

283. Suvarna V, Bore B, Bhawar C, Mallya R. Complexation of phytochemicals with cyclodextrins and their derivatives- an update. Biomed Pharmacother. 2022;149:112862.

284. Huang Z, Xu R, Ge X, Cheng J. Complexation of capsaicin with hydroxypropyl-beta-cyclodextrin and its analytical application. Spectrochim Acta A Mol Biomol Spectrosc. 2019;223:117278.

285. Naguib YW, Saha S, Skeie JM, Acri T, Ebeid K, Abdel-Rahman S, et al. Solubilized ubiquinol for preserving corneal function. Biomaterials. 2021;275:120842.

286. Liu Y, Chen Y, Gao X, Fu J, Hu L. Application of cyclodextrin in food industry. Crit Rev Food Sci Nutr. 2022;62(10):2627-40.

287. Del Toro-Sánchez CL, Ayala-Zavala JF, Machi L, Santacruz H, Villegas-Ochoa MA, Alvarez-Parrilla E, et al. Controlled release of antifungal volatiles of thyme essential oil from β-cyclodextrin capsules. Journal of Inclusion Phenomena and Macrocyclic Chemistry. 2010;67(3):431-41.

288. Kfoury M, Auezova L, Ruellan S, Greige-Gerges H, Fourmentin S. Complexation of estragole as pure compound and as main component of

basil and tarragon essential oils with cyclodextrins. Carbohydrate Polymers. 2015;118:156-64.

289. Gidwani B, Vyas A. A Comprehensive Review on Cyclodextrin-Based Carriers for Delivery of Chemotherapeutic Cytotoxic Anticancer Drugs. Biomed Res Int. 2015;2015:198268.

290. Carneiro SB, Costa Duarte FI, Heimfarth L, Siqueira Quintans JS, Quintans-Junior LJ, Veiga Junior VFD, et al. Cyclodextrin(-)Drug Inclusion Complexes: In Vivo and In Vitro Approaches. Int J Mol Sci. 2019;20(3).

291. Gandhi SR, Quintans JSS, Gandhi GR, Araujo AAS, Quintans Junior LJ. The use of cyclodextrin inclusion complexes to improve anticancer drug profiles: a systematic review. Expert Opin Drug Deliv. 2020;17(8):1069-80.

292. Armstrong DW, Faulkner JR, Han SM. Use of hydroxypropyl- and hydroxyethyl-derivatized beta-cyclodextrins for the thin-layer chromatographic separation of enantiomers and diastereomers. J Chromatogr. 1988;452:323-30.

293. Jansook P, Ogawa N, Loftsson T. Cyclodextrins: structure, physicochemical properties and pharmaceutical applications. Int J Pharm. 2018;535(1-2):272-84.

294. Ferreira MC, Tuma P, Jr., Carvalho VF, Kamamoto F. Complex wounds. Clinics (Sao Paulo). 2006;61(6):571-8.

295. Martin P, Nunan R. Cellular and molecular mechanisms of repair in acute and chronic wound healing. Br J Dermatol. 2015;173(2):370-8.

296. Qing C. The molecular biology in wound healing & non-healing wound. Chin J Traumatol. 2017;20(4):189-93.

297. Fife CE, Carter MJ. Wound Care Outcomes and Associated Cost Among Patients Treated in US Outpatient Wound Centers: Data From the US Wound Registry. Wounds. 2012;24(1):10-7.

298. Leavitt T, Hu MS, Marshall CD, Barnes LA, Lorenz HP, Longaker MT. Scarless wound healing: finding the right cells and signals. Cell Tissue Res. 2016;365(3):483-93.

299. Diaz-Herrera MA, Martinez-Riera JR, Verdu-Soriano J, Capillas-Perez RM, Pont-Garcia C, Tenllado-Perez S, et al. Multicentre Study of Chronic Wounds Point Prevalence in Primary Health Care in the Southern Metropolitan Area of Barcelona. J Clin Med. 2021;10(4).

300. Okonkwo UA, DiPietro LA. Diabetes and Wound Angiogenesis. Int J Mol Sci. 2017;18(7).

301. Burgess JL, Wyant WA, Abdo Abujamra B, Kirsner RS, Jozic I. Diabetic Wound-Healing Science. Medicina (Kaunas). 2021;57(10).

302. Greenhalgh DG. Wound healing and diabetes mellitus. Clin Plast Surg. 2003;30(1):37-45.

303. Bonifant H, Holloway S. A review of the effects of ageing on skin integrity and wound healing. Br J Community Nurs. 2019;24(Sup3):S28-S33.

304. Grinnell F. Fibroblasts, myofibroblasts, and wound contraction. J Cell Biol. 1994;124(4):401-4.

305. Lampugnani MG. Cell migration into a wounded area in vitro. Methods Mol Biol. 1999;96:177-82.

306. Smith ER, Hadidian Z, Mason MM. The single--and repeated--dose toxicity of dimethyl sulfoxide. Ann N Y Acad Sci. 1967;141(1):96-109.

307. Galvao J, Davis B, Tilley M, Normando E, Duchen MR, Cordeiro MF. Unexpected low-dose toxicity of the universal solvent DMSO. FASEB J. 2014;28(3):1317-30.

308. Emami F, Vatanara A, Park E, Na D. Drying Technologies for the Stability and Bioavailability of Biopharmaceuticals. Pharmaceutics. 2018;10(3).

309. Guo G, Yao W, Zhang Q, Bo Y. Oleanolic acid suppresses migration and invasion of malignant glioma cells by inactivating MAPK/ERK signaling pathway. PLoS One. 2013;8(8):e72079.

310. To C, Roy A, Chan E, Prado MAM, Di Guglielmo GM. Synthetic triterpenoids inhibit GSK3beta activity and localization and affect focal adhesions and cell migration. Biochim Biophys Acta Mol Cell Res. 2017;1864(7):1274-84.

311. Stelling-Férez J, López-Miranda S, Gabaldón JA, Nicolás FJ. Oleanolic Acid Complexation with Cyclodextrins Improves Its Cell Bio-Availability

and Biological Activities for Cell Migration. International Journal of Molecular Sciences [Internet]. 2023; 24(19).

312. Vicente-Manzanares M, Horwitz AR. Cell migration: an overview. Methods Mol Biol. 2011;769:1-24.

313. Trepat X, Chen Z, Jacobson K. Cell migration. Compr Physiol. 2012;2(4):2369-92.

314. Nakano T, Uchiyama K, Ushiroda C, Kashiwagi S, Toyokawa Y, Mizushima K, et al. Promotion of wound healing by acetate in murine colonic epithelial cell via c-Jun N-terminal kinase activation. J Gastroenterol Hepatol. 2020;35(7):1171-9.

315. Mayor R, Carmona-Fontaine C. Keeping in touch with contact inhibition of locomotion. Trends Cell Biol. 2010;20(6):319-28.

316. Mayor R, Etienne-Manneville S. The front and rear of collective cell migration. Nat Rev Mol Cell Biol. 2016;17(2):97-109.

317. Alcaraz A, Mrowiec A, Insausti CL, Bernabe-Garcia A, Garcia-Vizcaino EM, Lopez-Martinez MC, et al. Amniotic Membrane Modifies the Genetic Program Induced by TGFss, Stimulating Keratinocyte Proliferation and Migration in Chronic Wounds. PLoS One. 2015;10(8):e0135324.

318. Ruiz-Canada C, Bernabe-Garcia A, Liarte S, Insausti CL, Angosto D, Moraleda JM, et al. Amniotic membrane stimulates cell migration by modulating transforming growth factor-beta signalling. J Tissue Eng Regen Med. 2018;12(3):808-20.

319. Li RH, Huang WH, Wu JD, Du CW, Zhang GJ. EGFR expression is associated with cytoplasmic staining of CXCR4 and predicts poor prognosis in triple-negative breast carcinomas. Oncol Lett. 2017;13(2):695-703.

320. Leserer M, Gschwind A, Ullrich A. Epidermal growth factor receptor signal transactivation. IUBMB Life. 2000;49(5):405-9.

321. Marinissen MJ, Gutkind JS. G-protein-coupled receptors and signaling networks: emerging paradigms. Trends Pharmacol Sci. 2001;22(7):368-76.

322. Grisanti LA, Guo S, Tilley DG. Cardiac GPCR-Mediated EGFR Transactivation: Impact and Therapeutic Implications. J Cardiovasc Pharmacol. 2017;70(1):3-9.

323. Palanisamy S, Xue C, Ishiyama S, Naga Prasad SV, Gabrielson K. GPCR-ErbB transactivation pathways and clinical implications. Cell Signal. 2021;86:110092.

324. Wang J, Hua T, Liu ZJ. Structural features of activated GPCR signaling complexes. Curr Opin Struct Biol. 2020;63:82-9.

325. Gusach A, Maslov I, Luginina A, Borshchevskiy V, Mishin A, Cherezov V. Beyond structure: emerging approaches to study GPCR dynamics. Curr Opin Struct Biol. 2020;63:18-25.

326. Hilger D, Masureel M, Kobilka BK. Structure and dynamics of GPCR signaling complexes. Nat Struct Mol Biol. 2018;25(1):4-12.

327. Roskoski R, Jr. Src protein-tyrosine kinase structure, mechanism, and small molecule inhibitors. Pharmacol Res. 2015;94:9-25.

328. Luo J, Zou H, Guo Y, Tong T, Ye L, Zhu C, et al. SRC kinase-mediated signaling pathways and targeted therapies in breast cancer. Breast Cancer Res. 2022;24(1):99.

329. Sporn MB, Roberts AB. Autocrine growth factors and cancer. Nature. 1985;313(6005):745-7.

330. Zunke F, Rose-John S. The shedding protease ADAM17: Physiology and pathophysiology. Biochim Biophys Acta Mol Cell Res. 2017;1864(11 Pt B):2059-70.

331. Trenker R, Jura N. Receptor tyrosine kinase activation: From the ligand perspective. Curr Opin Cell Biol. 2020;63:174-85.

332. Roepstorff K, Grandal MV, Henriksen L, Knudsen SL, Lerdrup M, Grovdal L, et al. Differential effects of EGFR ligands on endocytic sorting of the receptor. Traffic. 2009;10(8):1115-27.

333. Yin J, Yu FS. ERK1/2 mediate wounding- and G-protein-coupled receptor ligands-induced EGFR activation via regulating ADAM17 and HB-EGF shedding. Invest Ophthalmol Vis Sci. 2009;50(1):132-9.

334. Scheller J, Chalaris A, Garbers C, Rose-John S. ADAM17: a molecular switch to control inflammation and tissue regeneration. Trends Immunol. 2011;32(8):380-7.

335. Rose-John S. ADAM17, shedding, TACE as therapeutic targets. Pharmacol Res. 2013;71:19-22.

336. Sato H, Genet C, Strehle A, Thomas C, Lobstein A, Wagner A, et al. Anti-hyperglycemic activity of a TGR5 agonist isolated from Olea europaea. Biochem Biophys Res Commun. 2007;362(4):793-8.

337. Jensen DD, Godfrey CB, Niklas C, Canals M, Kocan M, Poole DP, et al. The bile acid receptor TGR5 does not interact with beta-arrestins or traffic to endosomes but transmits sustained signals from plasma membrane rafts. J Biol Chem. 2013;288(32):22942-60.

338. Guo C, Chen WD, Wang YD. TGR5, Not Only a Metabolic Regulator. Front Physiol. 2016;7:646.

339. Ponti A, Machacek M, Gupton SL, Waterman-Storer CM, Danuser G. Two distinct actin networks drive the protrusion of migrating cells. Science. 2004;305(5691):1782-6.

340. Horzum U, Ozdil B, Pesen-Okvur D. Step-by-step quantitative analysis of focal adhesions. MethodsX. 2014;1:56-9.

341. Legerstee K, Houtsmuller AB. A Layered View on Focal Adhesions. Biology (Basel). 2021;10(11).

342. Teranishi S, Kimura K, Nishida T. Role of formation of an ERK-FAK-paxillin complex in migration of human corneal epithelial cells during wound closure in vitro. Invest Ophthalmol Vis Sci. 2009;50(12):5646-52.

343. Guidetti GF, Torti M, Canobbio I. Focal Adhesion Kinases in Platelet Function and Thrombosis. Arterioscler Thromb Vasc Biol. 2019;39(5):857-68.

344. Subauste MC, Pertz O, Adamson ED, Turner CE, Junger S, Hahn KM. Vinculin modulation of paxillin-FAK interactions regulates ERK to control survival and motility. J Cell Biol. 2004;165(3):371-81.

345. Deramaudt TB, Dujardin D, Hamadi A, Noulet F, Kolli K, De Mey J, et al. FAK phosphorylation at Tyr-925 regulates cross-talk between focal adhesion turnover and cell protrusion. Mol Biol Cell. 2011;22(7):964-75.

346. Tomar A, Schlaepfer DD. A PAK-activated linker for EGFR and FAK. Dev Cell. 2010;18(2):170-2.

347. Bachmann M, Skripka A, Weissenbruch K, Wehrle-Haller B, Bastmeyer M. Phosphorylated paxillin and phosphorylated FAK constitute subregions within focal adhesions. J Cell Sci. 2022;135(7).

348. Kimura K, Teranishi S, Yamauchi J, Nishida T. Role of JNK-dependent serine phosphorylation of paxillin in migration of corneal epithelial cells during wound closure. Invest Ophthalmol Vis Sci. 2008;49(1):125-32.

349. Duffy SJ, Keaney JF, Jr., Holbrook M, Gokce N, Swerdloff PL, Frei B, et al. Short- and long-term black tea consumption reverses endothelial dysfunction in patients with coronary artery disease. Circulation. 2001;104(2):151-6.

350. Jia Z, Babu PV, Si H, Nallasamy P, Zhu H, Zhen W, et al. Genistein inhibits TNF-alpha-induced endothelial inflammation through the protein kinase pathway A and improves vascular inflammation in C57BL/6 mice. Int J Cardiol. 2013;168(3):2637-45.

351. Ried K, Frank OR, Stocks NP. Aged garlic extract reduces blood pressure in hypertensives: a dose-response trial. Eur J Clin Nutr. 2013;67(1):64-70.

352. Kanitkar M, Gokhale K, Galande S, Bhonde RR. Novel role of curcumin in the prevention of cytokine-induced islet death in vitro and diabetogenesis in vivo. Br J Pharmacol. 2008;155(5):702-13.

353. Montezano AC, Dulak-Lis M, Tsiropoulou S, Harvey A, Briones AM, Touyz RM. Oxidative stress and human hypertension: vascular mechanisms, biomarkers, and novel therapies. Can J Cardiol. 2015;31(5):631-41.

354. Ucci M, Di Tomo P, Tritschler F, Cordone VGP, Lanuti P, Bologna G, et al. Anti-inflammatory Role of Carotenoids in Endothelial Cells Derived from Umbilical Cord of Women Affected by Gestational Diabetes Mellitus. Oxid Med Cell Longev. 2019;2019:8184656.

355. Di Tomo P, Canali R, Ciavardelli D, Di Silvestre S, De Marco A, Giardinelli A, et al. beta-Carotene and lycopene affect endothelial response to TNF-alpha reducing nitro-oxidative stress and interaction with monocytes. Mol Nutr Food Res. 2012;56(2):217-27.

356. Takada K, Nakane T, Masuda K, Ishii H. Ursolic acid and oleanolic acid, members of pentacyclic triterpenoid acids, suppress TNF-alpha-induced E-selectin expression by cultured umbilical vein endothelial cells. Phytomedicine. 2010;17(14):1114-9.

357. Di Tomo P, Di Silvestre S, Cordone VGP, Giardinelli A, Faricelli B, Pipino C, et al. Centella Asiatica and Lipoic Acid, or a combination thereof, inhibit monocyte adhesion to endothelial cells from umbilical cords of gestational diabetic women. Nutrition, Metabolism and Cardiovascular Diseases. 2015;25(7):659-66.

358. Unger RE, Krump-Konvalinkova V, Peters K, Kirkpatrick CJ. In vitro expression of the endothelial phenotype: comparative study of primary isolated cells and cell lines, including the novel cell line HPMEC-ST1.6R. Microvasc Res. 2002;64(3):384-97.

359. Di Fulvio P, Pandolfi A, Formoso G, Di Silvestre S, Di Tomo P, Giardinelli A, et al. Features of endothelial dysfunction in umbilical cord vessels of women with gestational diabetes. Nutr Metab Cardiovasc Dis. 2014;24(12):1337-45.

360. Di Tomo P, Alessio N, Falone S, Pietrangelo L, Lanuti P, Cordone V, et al. Endothelial cells from umbilical cord of women affected by gestational diabetes: A suitable in vitro model to study mechanisms of early vascular senescence in diabetes. FASEB J. 2021;35(6):e21662.

361. Lawson C, Wolf S. ICAM-1 signaling in endothelial cells. Pharmacological Reports. 2009;61(1):22-32.

362. Hong YK, Chang YH, Lin YC, Chen B, Guevara BEK, Hsu CK. Inflammation in Wound Healing and Pathological Scarring. Adv Wound Care (New Rochelle). 2023;12(5):288-300.

363. Hsuan CF, Hsu HF, Tseng WK, Lee TL, Wei YF, Hsu KL, et al. Glossogyne tenuifolia Extract Inhibits TNF-alpha-Induced Expression of Adhesion

Molecules in Human Umbilical Vein Endothelial Cells via Blocking the NF-kB Signaling Pathway. Molecules. 2015;20(9):16908-23.

364. Mitsuda S, Yokomichi T, Yokoigawa J, Kataoka T. Ursolic acid, a natural pentacyclic triterpenoid, inhibits intracellular trafficking of proteins and induces accumulation of intercellular adhesion molecule-1 linked to high-mannose-type glycans in the endoplasmic reticulum. FEBS Open Bio. 2014;4:229-39.

365. Wang K, Xuan Z, Liu X, Zheng M, Yang C, Wang H. Immunomodulatory role of metalloproteinase ADAM17 in tumor development. Front Immunol. 2022;13:1059376.

366. Theofilis P, Sagris M, Oikonomou E, Antonopoulos AS, Siasos G, Tsioufis C, et al. Inflammatory Mechanisms Contributing to Endothelial Dysfunction. Biomedicines. 2021;9(7).

367. Aitcheson SM, Frentiu FD, Hurn SE, Edwards K, Murray RZ. Skin Wound Healing: Normal Macrophage Function and Macrophage Dysfunction in Diabetic Wounds. Molecules. 2021;26(16).

368. Apte RS, Chen DS, Ferrara N. VEGF in Signaling and Disease: Beyond Discovery and Development. Cell. 2019;176(6):1248-64.

369. Muller MM, Griesmacher A. Markers of endothelial dysfunction. Clin Chem Lab Med. 2000;38(2):77-85.

370. Chiang JYL. Bile Acid Metabolism and Signaling. Comprehensive Physiology2013. p. 1191-212.

371. Pols T, Eggink H, Soeters M. TGR5 ligands as potential therapeutics in inflammatory diseases. International Journal of Interferon, Cytokine and Mediator Research. 2014.

372. Yasuda H, Hirata S, Inoue K, Mashima H, Ohnishi H, Yoshiba M. Involvement of membrane-type bile acid receptor M-BAR/TGR5 in bile acid-induced activation of epidermal growth factor receptor and mitogen-activated protein kinases in gastric carcinoma cells. Biochem Biophys Res Commun. 2007;354(1):154-9.

373. Cattaneo F, Guerra G, Parisi M, De Marinis M, Tafuri D, Cinelli M, et al. Cell-surface receptors transactivation mediated by g protein-coupled receptors. Int J Mol Sci. 2014;15(11):19700-28.

374. Izutsu K-i. Applications of Freezing and Freeze-Drying in Pharmaceutical Formulations. Survival Strategies in Extreme Cold and Desiccation. Advances in Experimental Medicine and Biology2018. p. 371-83.

375. Siow CRS, Wan Sia Heng P, Chan LW. Application of freeze-drying in the development of oral drug delivery systems. Expert Opinion on Drug Delivery. 2016;13(11):1595-608.

376. Sebastiani A, Hirnet T, Jahn-Eimermacher A, Thal SC. Comparison of speed-vacuum method and heat-drying method to measure brain water content of small brain samples. Journal of Neuroscience Methods. 2017;276:73-8.

377. Kumar C, Karim MA. Microwave-convective drying of food materials: A critical review. Critical Reviews in Food Science and Nutrition. 2017;59(3):379-94.

378. Wanning S, Süverkrüp R, Lamprecht A. Pharmaceutical spray freeze drying. International Journal of Pharmaceutics. 2015;488(1-2):136-53.

379. Vishali DA, Monisha J, Sivakamasundari SK, Moses JA, Anandharamakrishnan C. Spray freeze drying: Emerging applications in drug delivery. Journal of Controlled Release. 2019;300:93-101.

380. Zimmermann CM, Baldassi D, Chan K, Adams NBP, Neumann A, Porras-Gonzalez DL, et al. Spray drying siRNA-lipid nanoparticles for dry powder pulmonary delivery. Journal of Controlled Release. 2022;351:137-50.

381. Duchene D, Bochot A. Thirty years with cyclodextrins. Int J Pharm. 2016;514(1):58-72.

382. Silva F, Caldera F, Trotta F, Nerín C, Domingues FC. Encapsulation of coriander essential oil in cyclodextrin nanosponges: A new strategy to promote its use in controlled-release active packaging. Innovative Food Science & Emerging Technologies. 2019;56:102177.

383. Davidson JM. Animal models for wound repair. Arch Dermatol Res. 1998;290 Suppl:S1-11.

384. Grambow E, Sorg H, Sorg CGG, Struder D. Experimental Models to Study Skin Wound Healing with a Focus on Angiogenesis. Med Sci (Basel). 2021;9(3).

385. Montenegro MF, Cabezas-Herrera J, Campoy FJ, Munoz-Delgado E, Vidal CJ. Lipid rafts of mouse liver contain nonextended and extended acetylcholinesterase variants along with M3 muscarinic receptors. FASEB J. 2017;31(2):544-55.

386. Lee J, Kim YJ, Choi LM, Lee K, Park HK, Choi SY. Muscarinic Receptors and BK Channels Are Affected by Lipid Raft Disruption of Salivary Gland Cells. Int J Mol Sci. 2021;22(9).

387. Roy A, Patra SK. Lipid Raft Facilitated Receptor Organization and Signaling: A Functional Rheostat in Embryonic Development, Stem Cell Biology and Cancer. Stem Cell Rev Rep. 2023;19(1):2-25.

388. Hickey MJ, Granger DN, Kubes P. Inducible nitric oxide synthase (iNOS) and regulation of leucocyte/endothelial cell interactions: studies in iNOS-deficient mice. Acta Physiol Scand. 2001;173(1):119-26.

389. Quaschning T, Voss F, Herzfeld S, Relle K, Kalk P, Godes M, et al. Lack of iNOS impairs endothelial function in endothelin-1 transgenic mice. Kidney Blood Press Res. 2008;31(2):127-34.

390. Zhang H, Zhang J, Ungvari Z, Zhang C. Resveratrol improves endothelial function: role of TNFalpha and vascular oxidative stress. Arterioscler Thromb Vasc Biol. 2009;29(8):1164-71.

391. Smits JPH, Niehues H, Rikken G, van Vlijmen-Willems I, van de Zande G, Zeeuwen P, et al. Immortalized N/TERT keratinocytes as an alternative cell source in 3D human epidermal models. Sci Rep. 2017;7(1):11838.

392. Rikken G, Niehues H, van den Bogaard EH. Organotypic 3D Skin Models: Human Epidermal Equivalent Cultures from Primary Keratinocytes and Immortalized Keratinocyte Cell Lines. Methods Mol Biol. 2020;2154:45-61.

393. Chen JS, Longaker MT, Gurtner GC. Murine models of human wound healing. Methods Mol Biol. 2013;1037:265-74.

394. Grada A, Mervis J, Falanga V. Research Techniques Made Simple: Animal Models of Wound Healing. J Invest Dermatol. 2018;138(10):2095-105 e1.

395. Stachura A, Khanna I, Krysiak P, Paskal W, Wlodarski P. Wound Healing Impairment in Type 2 Diabetes Model of Leptin-Deficient Mice-A Mechanistic Systematic Review. Int J Mol Sci. 2022;23(15).

396. Nowak-Sliwinska P, Alitalo K, Allen E, Anisimov A, Aplin AC, Auerbach R, et al. Consensus guidelines for the use and interpretation of angiogenesis assays. Angiogenesis. 2018;21(3):425-532.

IX - ANNEXES

IX - ANNEXES

Annex 1. Approval of the ethics committee for biomedical research with HUVEC cells.

COMITATO DI ETICA PER LA RICERCA BIOMEDICA
UNIVERSITA' DEGLI STUDI "G.D'ANNUNZIO"
AZIENDA SANITARIA LOCALE – CHIETI
E-mail: comitatodietica@unich.it

PROT.873 COET del 12.05.09

L'anno duemilanove, il giorno ventiquattro del mese di febbraio, alle ore 14,30, presso l'Aula 12 della Facoltà di Medicina dell'Università degli Studi "G. D'Annunzio" di Chieti, si è riunito il Comitato di Etica per la Ricerca Biomedica dell'Università /ASL di Chieti, formalmente istituito nel rispetto delle direttive europee della GCP DM 15.07.97 con deliberazione N° 7713/R del 21.07.94 e regolarmente accreditato dal Ministero della Salute.
Risultano presenti, assenti giustificati e assenti:

	Nominativo	Pres.	Giust.	Ass.
1	VACCA Michele	X		
2	NERI Matteo	X		
3	NATOLI Clara	X		
4	CIPOLLONE Francesco			X
5	CONSOLI Agostino			X
6	D'ALONZO Luigi			X
7	COTELLESE Roberto			X
8	DE BENEDETTO Fernando		X	
9	SALVATI Filippo	X		
10	ERRICHI Bruno Maria	X		
11	CARULLO Giuseppe	X		
12	MARINUCCI Riccardo	X		
13	CERULLI Aldo	X		
14	BALLONE Enzo	X		
15	SCHIOPPA Francesco	X		
16	SCLOCCO Tonino			X
17	STANISCIA Tommaso		X	
18	DI MASCIO Rocco	X		
20	PATRIGNANI Paola	X		
21	CICCARELLI Renata	X		
22	BRUNETTI Lugi	X		
23	MELENA Ennio	X		
24	D'AMICO Rossana	X		
25	PACE Valeria	X		
26	DE ROSA Pier Luigi	X		
27	ALBANESE Paolo		X	
28	LEPORE Anna Raffaella		X	
29	SAVINO Carlo	X		
30	SEBASTIANELLI Raffaele	X		
31	ZAPPACOSTA Luigi		X	
32	FARAONE Gabriele	X		
33	CASCAVILLA Michele	X		
34	RAZZOTTI Bernardo	X		
35	NARDONE Ginevra	X		
36	CIAMPOLI Rocco	X		
37	CIAVARELLI MACOZZI Sandro	X		
38	MASCELLANTI Marco			X

Il Presidente constatata la presenza del numero legale dichiara aperta la seduta.

OMISSIS

2. Valutazione protocolli:

2.4 Protocollo "Studio dei meccanismi cellulari delle complicanze vascolari dell'iperglicemia cronica" studio spontaneo della Prof.ssa Assunta Pandolfi c/o il Dipartimento di Scienze Biomediche dell'Università degli Studi "G. D'Annunzio" di Chieti e c/o l'U.O. di Ostetricia e Ginecologia del Policlinico SS. Annunziata di Chieti;

Il Comitato di Etica esaminata la documentazione di rito presentata all'unanimità, e dopo essersi pronunciato favorevolmente sulla competenza dello Sperimentatore e sull'idoneità della struttura, valutati i rischi e gli inconvenienti prevedibili, ritiene che il protocollo di studio soddisfi i criteri etici e scientifici che ne giustificano l'esecuzione. Il Comitato, pertanto, a norma di quanto previsto dall'art. 7 del Decreto Legislativo 24 giugno 2003, n. 211 esprime il seguente parere:

parere favorevole alla conduzione dello studio.

Il Comitato richiede che venga informato dell'inizio dello studio, della sua conclusione, della sua eventuale interruzione con le motivazioni di essa.

Al Comitato Etico vanno inviati anche i rapporti sull'avanzamento dello studio, nonché il rapporto finale. Eventuali eventi avversi devono essere tempestivamente comunicati nei termini e con le modalità previste dall'art. 16 del Decreto Legislativo 24 giugno 2003, n. 211.

Si precisa inoltre che tutta la documentazione relativa allo Studio (comprese le schede raccolta dati e in particolare i moduli di consenso informato) dovrà essere archiviata e conservata a cura degli Sperimentatori per un tempo non inferiore agli anni 15. Tale documentazione dovrà essere prontamente reperita ed esibita in caso di controlli da parte delle autorità competenti (Ministero della Salute, etc.).Nella corrispondenza si prega di citare sempre il protocollo e la data della seduta del Comitato Etico in cui è stata esaminata la documentazione.

OMISSIS

Null'altro essendovi da discutere o da deliberare la seduta è tolta alle ore 18,00.

Del che è verbale.

IL PRESIDENTE

Prof. Michele Vacca

UNIVERSITA' DEGLI STUDI "G. D'ANNUNZIO"- ASL/CHIETI

COMITATO DI ETICA PER LA RICERCA BIOMEDICA

UFFICIO PRESIDENZA **Allegato A) delibera n°** 1878/03c05 **del** 12.05.08

PRESIDENTE	*Prof. Michele Vacca*	*Preside Facoltà di Farmacia - Uni/ Chieti*	

COMPONENTI

QUALIFICA-DISCIPLINA	TITOLARE	STRUTTURA	TITOLARE	STRUTTURA
Clinico	*Matteo Neri, Clara Natoli, Francesco Cipollone, Agostino Consoli, Roberto Cotellese*	*Uni/Chieti*		
Clinico	*Fernando De Benedetto, Filippo Salvati, Bruno Maria Errichi, Riccardo Marinucci, Raffaele Sebastianelli*	*Asl/Chieti*		
Clinico	*Luigi D'Alonzo, Marco Mascellanti*	*Membro esterno*		
Biostatistico	*Enzo Ballone, Tonino Sclocco, Francesco Schioppa*	*Uni/Chieti*	*Rocco Di Mascio Tommaso Staniscia*	*Uni/Chieti*
Farmacologo	*Michele Vacca, Paola Patrignani*	*Uni/Chieti*	*Renata Ciccarelli Luigi Brunetti*	*Uni/Chieti*
Farmacista	*Ennio Melena, Rocco Ciampoli*	*Asl/Chieti*		
Direttore Sanitario	*Raffaella Lepore*	*Asl/Chieti*	*Carlo Savino*	*Asl/Chieti*
Esperto in materia giuridica	*Paolo Albanese*	*Asl/Chieti*	*Pier Luigi De Rosa*	*Membro esterno*
Medicina Generale Territoriale in rappresentanza Ordine Medici	*Valeria Pace, Gabriele Faraone*	*Ordine dei Medici*		
Bioetica	*Rossana D'Amico*	*Membro esterno*		
Bioetica	*Michele Cascavilla, Bernardo Razzotti*	*Uni/Chieti*		
Infermieristico	*Ginevra Nardone*	*Membro esterno*	*Luigi Zappacosta*	*Membro esterno*
Associazionismo tutela malati	*Giuseppe Carullo*	*Membro esterno*	*Aldo Cerulli*	*Asl/Chieti*
Psicologo	*Ciavarelli Macozzi Sandro*	*Membro esterno*		

UFFICIO SEGRETERIA

Funzionario Amm.vo	*Mauro Carabella*	*Asl/Chieti*		
Amm.vo lib/prof.	*Susanna Petaccia*	*Uni/Chieti*		

Annex 2. Registered intellectual property: "Process to complex oleanolic acid with cyclodextrins and products obtained thereof."

European patent. Application number: EP23382932.4. Date of application for European patent registration: 13/09/2023.

PROCESS TO COMPLEX OLEANOLIC ACID WITH CYCLODEXTRINS AND PRODUCTS OBTAINED THEREOF

Field of the Invention

The present invention relates to the field of biochemistry and cell biology, more particularly to a process to complex oleanolic acid with cyclodextrins and its use on normal and injured human skin.

Background

Oleanolic acid (OA) is a particularly noteworthy molecule, as it is easier to obtain from plants than its two isomers, ursolic and maslinic acid (UA, AM), being present at different concentrations in the seed and pericarp of some fruits. The properties of OA make it a molecule with high therapeutic potential. In fact, one of its least studied properties is its promoting effect on wound healing. For this reason, the study of the effect of OA on wound healing, together with its improvement for application in wounds, are the main objectives of the proposed invention.

However, the use of OA in free form presents a number of limitations mainly due to its hydrophobic nature. Such molecules are poorly soluble in water, making the development of aqueous preparations significantly more difficult, in anticipation of administration to wounds. In addition to this, OA addition to aqueous solutions requires organic solvents such as dimethyl sulfoxide (DMSO), which have cytotoxic effects. In relation to this, the low solubility compromises the amount of OA taken up by epithelial cells and the beneficial effects on cell migration are limited, given its low availability to the cells. On the other hand, the use of OA in free (OA/DMSO) form requires it to be used in very low concentrations to achieve its healing-promoting effect, rapidly depleting the OA supply.

Due to these limitations, there is a need for new vehicles to improve the preservation, protection, delivery and effect of OA in wound healing.

Cyclodextrins (CD) are polymers composed of glucose units linked by α-1,4-linkages which are produced from starch by an enzymatic process in plant cells. There are three forms of CDs: α-CD, β-CD, and γ-CD.

The scientific article Lopez-Miranda S, Guardiola L, Hernandez-Sanchez P, Nunez-Delicado E. Complexation between oleanolic and maslinic acids with native and modified

cyclodextrins. Food Chem. 2018;240:139-46 disclose encapsulations of oleanolic acid and maslinic acid with native cyclodextrins (α-CD, β-CD and γ-CD) and their equivalents modified with hydroxypropyl groups (HP-α-CD, HP-β-CD and HP-γ-CD).

However, this article does not disclose the complexation process of the present inventions and the advantages the final product has in comparison with the mentioned method. Particularly, this article does not disclose a dehydration step which make the final product more soluble and stable. The advantages of the process of the invention, and more concretely, the dehydration step, are the following:

- Better handling of the oleanolic acid

- Allows dissolving the complexes in solutions with osmolarity compatible with cell cultures, respecting their viability and biocompatibility.

- Allows the complexes to be dissolved in sterile solutions, thus allowing their use in cell cultures because it reduces the risk of contamination by bacteria or fungi.

- Better stability and preservation, as indicated in the study of different temperatures.

- It allows a better transport of the complexes as it does not necessarily require low temperatures.

Description of the invention

In the present specification the terms “drying” “dehydration” and the grammatical variations thereof are synonyms and can be used interchangeably.

In the present specification the term “OA/DMSO” refers to free OA in water that requires the presence of dimethyl sulfoxide (DMSO), an organic solvent, to increase the water solubility of OA.

In the present specification the terms “OA encapsulation” and “OA complexation” and the grammatical variations thereof are synonyms and can be used interchangeably.

The first object of the invention relates to a process to complex oleanolic acid that comprises:

a) putting in contact oleanolic acid and at least one cyclodextrin in an aqueous mixture

b) dehydrate the product obtained in the previous step to obtain a dry powder comprising oleanolic acid/cyclodextrin complexes.

The term “Dehydration” means to reduce the water content. The reduction of the water content can be total or partial compared to the initial water content of the product of step a). Dehydration can be a reduction of the water content of 1, 2, 3, 4, 5, 6, 7, 8, 9, 10, 11, 12, 13, 14, 15, 16, 17, 18, 19, 20, 21, 22, 23, 24, 25, 26, 27, 28, 29, 30, 31, 32, 33, 34, 35, 36, 37, 38, 39, 40, 41, 42, 43, 44, 45, 46, 47, 48, 49, 50, 51, 52, 53, 54, 55, 56, 57, 58, 59, 60, 61, 62, 63, 64,65, 66, 67, 68, 69, 70, 71, 72, 73, 74, 75, 76, 77, 78, 79, 80, 81, 82, 83, 84, 85, 86, 87, 88, 89, 90, 91, 92, 93, 94, 95, 96, 97, 98, 99, or 100% compared to the initial water content of step a)

The reduction of the water content is an essential step in the process of the invention. The technical effect of this feature is that as it allows to increase the concentration of the complexes when used in order to see a therapeutic effect.

In a particular embodiment oleanolic acid and the cyclodextrin are put in contact with aqueous solution simultaneously or immediately one after another.

In another particular embodiment the aqueous mixture may comprise any liquid miscible with water, for example an alcohol, in any proportion that do not alter the aqueous character of the solution. In a preferred embodiment the aqueous mixture is pure water

The complexes obtained in step a) are not useful for therapeutic uses as the OA concentration in the aqueous solution will not be high enough to achieve an effective amount in order to obtain a therapeutic effect.

By the term “effective amount” of the complexes as provided herein is meant a nontoxic but sufficient amount of the compound to provide the desired result. As will be pointed out below, the exact amount required will vary from subject to subject, depending on the species, age, and general condition of the subject, the severity of the disease that is being treated, the particular compound used, its mode of administration, and the like. Thus, it is not possible to specify an exact “effective amount.” However, an appropriate effective amount can be determined by one of ordinary skill in the art using only routine experimentation.

The product obtained can be rapidly dissolved in a polar liquid such as water, and be used on *in vitro* assays with cell lines.

In a particular embodiment, the cyclodextrin is selected from one or more of the groups consisting of: α-cyclodextrin, β-cyclodextrin, and γ-cyclodextrin, preferably β-cyclodextrin, and γ-cyclodextrin.

In another particular embodiment the cyclodextrin comprises at least one hydroxypropyl group. This chemical groups are added to the free hydroxyl (-OH) from the glucose units,

outside the cyclodextrin ring, on its surface. This modification confers extra water solubility.

In a preferred embodiment the cyclodextrin is hydroxypropyl-β-cyclodextrin or hydroxypropyl- γ-cyclodextrin.

In the present specification, the expression “oleanolic acid/cyclodextrin” can refer to both “oleanolic acid/cyclodextrin” and/or “oleanolic acid/hydroxypropyl-cyclodextrin”. Furthermore, cyclodextrin may also refer to hydroxypropyl-cyclodextrin.

In a particular embodiment the ratio oleanolic acid/cyclodextrin in step a) is between approximately 1:50 to 1:500, preferably approximately 1:100 to 1:400, more preferably approximately 1:150 to 1:300.

In a preferred embodiment the ratio oleanolic acid/cyclodextrin is between approximately 1:200 to 1:280, more preferably 1:220 to 1:260, even more preferably approximately 1:250.

Routine concentrations for example would be approximately 25 to 100 mM of a cyclodextrin and 12.5 to 50 mg OA in 125 to 500 ml deionized water, preferably approximately 50 mM of a cyclodextrin and 25 mg OA in 250 ml deionized water, this is a ratio of 0.2/50 µM/mM oleanolic acid/cyclodextrin (1:250)

Later in the examples of the inventions it will be seen that ratios are given in µM/mM oleanolic acid/cyclodextrin. Thus, in a particular embodiment of the invention the oleanolic acid/cyclodextrin in step a) is between 0.05 µM to 70 µM of OA per 0.03 mM to 18 mM cyclodextrin and keeping a ratio of approximately 1:100 to 1:400.

This ratio is important to achieve an effective OA encapsulation ensuring encapsulation dynamics during the process of the invention.

The main advantage of the method of the invention is that upon obtaining dried complexes, very concentrated solutions can be achieved by dissolving the complexes in the appropriate medium (e.g. 1 gram in just 1 ml), which makes it easy to work with when adding the final concentration required for the assay. This is impossible to do with liquid complexes.

The ratio of the formed complexes oleanolic acid/cyclodextrin in step a) is between approximately 3:1 to 1:3, preferably approximately 2:1 to 1:2, more preferably approximately 1.5:1 to 1:1.5.

In a preferred embodiment the ratio oleanolic acid/cyclodextrin of the formed complexes is between approximately 1.2:1 to 1:1.2

The oleanolic acid/cyclodextrin are putting in contact in step a) for a time comprised between approximately 5 h and 5 days, preferably, approximately 10 h and 3 days, more preferably approximately 15 h and 2 days.

The temperature in step a) is comprised approximately between 5ºC and 40ºC, preferably between approximately 10ºC and 30ºC.

In a preferred embodiment, the oleanolic acid/cyclodextrin are put in contact for a time comprised between approximately 15 h and 2 days and a temperature comprised between approximately 10ºC and 30ºC.

Step a) needs to be protected from light exposure.

The dehydration of step b) is performed by freeze-drying, spray drying, vacuum stove and/or rotary evaporator, preferably freeze-drying, spray drying as vacuum stove or rotary evaporator are less up-to-date.

The freeze drying comprises subjecting the product of step a) to a temperature of less than -30 ºC for an appropriate time, until the aqueous solution with the complexes is completely frozen, and them under a vacuum, subject said product to a temperature comprised between approximately -80ºC and -20ºC to obtain a dry powder.

In a particular embodiment, the freeze drying comprises subjecting the product of step a) to a temperature of less than approximately -70 ºC for an appropriate time, until the aqueous solution with the complexes is completely frozen, and them under a vacuum, subject said product to a temperature comprised between approximately -60ºC and -40ºC to obtain a dry powder, the required time until the water is completely removed can vary, it can be 1 day, 2 days, 3 days, 4 days or more.

In a particular embodiment, the the aqueous solutions with the complexes is subjected to a temperature of at least -10ºC, -20ºC, -30ºC, -40ºC, -50ºC, -60ºC, -70ºC, -80ºC, -90ºC, until said solution with the complexes is completely frozen.

In another particular embodiment, in the freeze dryer, a vacuum system and a temperature of -80 ºC and -20ºC, preferably -60ºC and -40ºC, even more preferably approximately -48°C, will be applied for three days until the water in which the complexes were dissolved is completely removed.

The spray drying comprises injecting the product of step a) into a circuit that sprays said product at a temperature between approximately 110ºC and 210ºC and then cool it to a temperature between approximately 40ºC and 90ºC to obtain a dry powder for a time between 10 min and 2 h.

In a particular embodiment, the temperature of the circuit is preferably 120ºC to 200ºC, more preferably 130ºC to 190ºC, and even more preferably 140ºC to 180ºC.

In another particular embodiment, the temperature to cool the solution with the complexes after the spray is between approximately 50ºC and 80ºC even more preferably 60ºC to 70ºC, for a time between 20 min and 1h.

The advantage of the spray drying technique compared to the freeze-drying technique is that dehydrates the complexes faster as there is no need to freeze them before. While freeze drying technique takes about 3 days to get the complexes dehydrated, spray drying only takes half an hour to obtain a completely dry powder. Generally speaking, spray drying is cheaper, faster and more energy efficient alternative to freeze drying, however, the spray drying stronger process using high temperatures could decrease OA activity.

The vacuum stove consists of reducing water boiling point (e.g. from 100 ºC to 60 ºC) by applying vacuum inside the stove. Thus, this technique eliminates most of the water content of the product. The disadvantage that this technique has is the high energy cost and time consuming, since it needs a long time period to remove 100 % of the water content. In the case of complexed OA, this procedure could also compromise OA activity due to the elevated temperature applied. This technique is close to the new ones: freeze drying and spray drying.

The rotary evaporator also applies heat and vacuum, together with a centrifugation that produces water evaporation. This procedure is used to concentrate products that are dissolved in a liquid, so it does not remove 100% of the water content. For this reason, is a procedure that may need to be complemented with freeze drying or spray drying.

Another object of the invention relates to a dry powder oleanolic acid/cyclodextrin complex obtained by the above-described process.

The dry powder oleanolic acid/cyclodextrin complex is a solid obtained after the dehydration step b) of the process of the invention.

Later in the examples of the invention it will be seen that this powder is stable over a long storage time.

In a particular embodiment, the cyclodextrin is selected from one or more of the groups consisting of: α-cyclodextrin, β-cyclodextrin, and γ-cyclodextrin, preferably β-cyclodextrin, and γ-cyclodextrin.

In another particular embodiment the cyclodextrin comprises at least one hydroxypropyl group. This chemical groups are added to the free hydroxyl (-OH) from the glucose units,

outside the cyclodextrin ring, on its surface. This modification confers extra water solubility.

In a preferred embodiment the cyclodextrin is hydroxypropyl-β-cyclodextrin or hydroxypropyl- γ-cyclodextrin.

In the present specification, the expression “oleanolic acid/cyclodextrin” can refer to both “oleanolic acid/cyclodextrin” and/or “oleanolic acid/hydroxypropyl-cyclodextrin”

Another object of the invention relates to a solution comprising the dry powder oleanolic acid/cyclodextrin complex which is diluted in an aqueous solution, which may be mixed any other liquids such as an alcohol or solid excipients dissolved on it.

The concentration of the dissolved dry powder oleanolic acid/cyclodextrin complex is higher than the maximum concentration that can be obtained in the step a) of the process of the invention.

The advantage of dissolving a dry powder oleanolic acid/cyclodextrin complex in an aqueous mixture (preferably water) is that high concentrations of said complex can be obtained,

In a particular embodiment, the concentration of the dissolved dry powder oleanolic acid/cyclodextrin complex in an aqueous mixture is at least 0.001 g/ml, or at least 0.01 g/ml 0.1 g/ml, or at least 0.5 g/ml, or at least 1g/ml, or at least 2 g/ml, or at least 3 g/ml, or at least 5 g/ml up to 10 g/ml. Preferably between 0.01 g/ml to 0.09 g/ml, more preferably 0.02 g/ml to 0.06 g/ml. So, the concentration of OA in the solution comprising the dry powder oleanolic acid/cyclodextrin complex and an aqueous mixture is approximately 25 mM. This is the therapeutically effective concentration of OA which is impossible to achieve unless the complexes are previously dehydrated.

Another object of the invention relates to the oleanolic acid/cyclodextrin complex, described above and/or obtained by the above-mentioned process for use in the treatment of skin disorders

In a particular embodiment, the skin disorders are one or more of the following: wound healing, scarring, eczema, psoriasis, acne, rosacea, ichthyosis, vitiligo, urticaria and seborrheic dermatitis. The complexes of the invention are also useful to prevent and/or trweat endothelial vascular disfunction, which is needed for skin regeneration.

The terms “treatment” and “treating” as used herein refer to the medical management of a subject with the intent to cure, ameliorate, stabilize, or prevent a disease, pathological condition, or disorder. This term includes active treatment, that is, treatment directed specifically toward the improvement of a disease, pathological condition, or disorder, and

also includes causal treatment, that is, treatment directed toward removal of the cause of the associated disease, pathological condition, or disorder. In addition, this term includes palliative treatment, that is, treatment designed for the relief of symptoms rather than the curing of the disease, pathological condition, or disorder; preventative treatment, that is, treatment directed to minimizing or partially or completely inhibiting the development of the associated disease, pathological condition, or disorder; and supportive treatment, that is, treatment employed to supplement another specific therapy directed toward the improvement of the associated disease, pathological condition, or disorder. It is understood that treatment, while intended to cure, ameliorate, stabilize, or prevent a disease, pathological condition, or disorder, need not actually result in the cure, amelioration, stabilization or prevention. The effects of treatment can be measured or assessed as described herein and as known in the art as is suitable for the disease, pathological condition, or disorder involved. Such measurements and assessments can be made in qualitative and/or quantitative terms. Thus, for example, characteristics or features of a disease, pathological condition, or disorder and/or symptoms of a disease, pathological condition, or disorder can be reduced to any effect or to any amount. In the context of a subject suffering from skin disorders, the terms “treatment” and “treating” refer to the medical management of a subject with the intent to cure, ameliorate, or stabilize skin disorders. In the context of a subject at risk of developing skin disorders, the terms “treatment” and “treating” refer to the medical management of a subject with the intent to prevent skin disorders.

Each of the terms “comprising,” “consisting essentially of,” and “consisting of” may be replaced with either of the other two terms. The term “a” or “an” can refer to one of or a plurality of the elements it modifies (e.g., “a reagent” can mean one or more reagents) unless it is contextually clear either one of the elements or more than one of the elements is described. The term “about” as used herein refers to a value within 10% of the underlying parameter (i.e., plus or minus 10%; e.g., a weight of “about 100 grams” can include a weight between 90 grams and 110 grams). Use of the term “about” at the beginning of a listing of values modifies each of the values (e.g., “about 1, 2 and 3” refers to "about 1, about 2 and about 3"). When a listing of values is described, the listing includes all intermediate values and all fractional values thereof (e.g., the listing of values "80%, 85% or 90%" includes the intermediate value 86% and the fractional value 86.4%). When a listing of values is followed by the term "or more," the term "or more" applies to each of the values listed (e.g., the listing of "80%, 90%, 95%, or more" or "80%, 90%, 95% or more" or "80%, 90%, or 95% or more" refers to "80% or more, 90% or more, or 95% or more"). When a listing of values is described, the listing includes all ranges

between any two of the values listed (e.g., the listing of "80%, 90% or 95%" includes ranges of "80% to 90%", "80% to 95%" and "90% to 95%"). Certain implementations of the technology are set forth in examples below

Brief description of the figures

Figure 1. Standard curve with OA by HPLC detection at 210 nm (OA specific absorbance).

Figure 2. Freeze dried OA/HP-β-CD and OA/HP-γ-CD complexes stimulate migration in Mv1Lu cells. Confluent Mv1Lu cells were scratched with a pipette tip and allowed to migrate for 24 hours. (a) Representative images of the wound healing assay with cell migration under basal conditions (C) compared to those with 5 µM OA/DMSO, 12.5/3.12 µM/mM OA/HP-β-CD and 62.5/15.62 µM/mM OA/HP-γ-CD; after 24h treatment. Equivalent concentrations of DMSO, HP-β-CD and HP-γ-CD were used as vehicle controls. Scale bar indicates 200 µm. (b) Plot represents cell migration as the difference between areas at time 0 hours and time 24 hours in each condition, named as migration percentage. X axis indicates treatment conditions, for those with HP-β-CD and HP-γ-CD, the concentrations are represented as molar ratio OA µM/CD mM. Epidermal growth factor (EGF) was added at 10 ng/ml as a positive migration control. Asterisks indicate statistically significant differences between conditions according to a One-way ANOVA statistical analysis (*p<0.05 and ****p<0.0001).

Figure 3. Freeze dried and spray-dried OA/HP-β-CD complexes stimulate migration in Mv1Lu cells. a) Representative images of the wound healing assay with cell migration under basal conditions (C) compared to those with 5 µM OA/DMSO, freeze dried (L) OA/HP-β-CD complexes and spray dried (S) OA/HP-β-CD, after 24h treatment. Equivalent concentrations of DMSO and HP-β-CD were used as vehicle controls. Scale bar indicates 200 µm. b) Plot represents cell migration as the difference between areas at time 0 hours and time 24 hours in each condition, named as migration percentage. X axis indicates treatment conditions, for those with HP-β-CD and HP-γ-CD, the concentrations are represented as molar ratio OA µM/CD mM. L (freeze dried); S (spray dried). Epidermal growth factor (EGF) was added at 10 ng/ml as a positive migration control. Asterisks indicate statistically significant differences between conditions according to a One-way ANOVA statistical analysis (*p<0.05, **p<0.005 and ****p<0.0001).

Figure 4. OA/HP-β-CD complexes promote c-Jun phosphorylation at the edge of wound scratched Mv1Lu cells. Confluent Mv1Lu cells were scratched and allowed to migrate for the indicated times (6 and 12 hours). Cells were treated with 5 µM OA/DMSO or 12.5/3.12 µM/mM OA/HP-β-CD. Equivalent concentrations of DMSO and HP-β-CD were used as vehicle controls. Cells were immunostained with specific antibodies against c-Jun active phosphorylated form (p-c-Jun). Co-staining with phalloidin and Hoechst-33258 was used to show actin cytoskeleton and nuclei, respectively. Images of p-c-Jun fluorescence were converted into pseudo-color with ImageJ software to show the intensity of p-c-Jun staining. Actin fibers (F-actin): red. Nuclei: blue. Images were obtained with a confocal microscope. This experiment was repeated at least three times. Representative images are shown. Scale bar indicates 100 µm.

Figure 5. OA/HP-β-CD complexes promote higher c-Jun transcription factor phosphorylation than OA/DMSO at wound edge. (a) The image represents how a Tile Scan image is divided in three equal sectors for better analyze active c-Jun (p-c-Jun) expression. Scale bar indicates 100 µm. (b) Plot represents the p-c-Jun intensity in cell nuclei. Each point represents the intensity of p-c-Jun intensity in one nucleus. (c) Plot represents the relation between the number of positive p-c-Jun nuclei and total number nuclei existent in each sector. In order to exclude negative p-c-Jun nuclei, an intensity p-c-Jun threshold was set using the p-c-Jun intensity mean in basal (control) condition.

Figure 6. OA/HP-β-CD complexes promote changes in focal adhesions (FAs) revealed by Paxillin. Confluent Mv1Lu cells were scratched and allowed to migrate for 6 and 12 hours. Cells were treated with 5 µM OA/DMSO or 12.5/3.12 µM/mM OA/HP-β-CD. Equivalent concentrations of DMSO and HP-β-CD were used as vehicle controls. Cells were immunostained with specific antibodies against paxillin Co-staining with phalloidin and Hoechst-33258 was used to show actin cytoskeleton and nuclei, respectively (Not shown). Quantification of the density of FA (as FA number per filopodia area). FA size (average size) at the filopodia area. A One-way ANOVA statistical analysis was performed (*p<0.05, **p<0.005 and ****p<0.0001)

Figure 7. OA complexes with modified cyclodextrins HP-β-CD promote cell migration in MDA-MB-231 cells. Confluent MDA-MB-231 cells were scratched with a pipette tip and allowed to migrate for 24 hours. (a) Representative images of the wound healing assay with cell migration under basal conditions (C) compared to those with 5 µM OA/DMSO, 21/5.25 µM/mM OA/HP-β-CD and equivalent concentrations of DMSO or HP-β-CD after 24h treatment. Scale bar indicates 200 µm. (b) Plot represents cell migration as the difference between areas at time 0 hours and time 24 hours in each condition, named as migration percentage. X axis indicates treatment conditions, for those with HP-β-CD the concentrations are represented as molar ratio OA µM/CD mM. Epidermal growth factor (EGF) was added at 10 ng/ml as a positive migration control.

Asterisks indicate statistically significant differences between conditions according to a One-way ANOVA statistical analysis (*p<0.05 and ****p<0.0001).

Figure 8. Signaling pathways regulated by EGFR and c-Jun activation, necessary for cell migration, are induced by OA/HP-β-CD complexes in MDA-MB-231 cells. (a) Total protein extracts from serum-starved sub-confluent MDA-MB-231 cells treated with 10 µM OA/DMSO, 21/5.25 µM/mM OA/HP-β-CD or 10 ng/ml EGF. These extracts were assayed at the indicated times (hours) targeting: phospho-EGFR (Tyr 1068), phospho-ERK1/2 (Thr 202/Tyr 204), phospho-JNK1/2 (Thr 183/Tyr 185) and phospho-c-Jun (Ser 63). Total protein expression was assayed for the above-mentioned active protein forms: EGFR, ERK1/2, JNK1/2 and c-Jun. β-Actin was used as a loading control. DMSO and HP-β-CD equivalent concentrations were added as vehicle controls. A representative experiment was shown. (EGFR, epidermal growth factor receptor; ERK1/2, extracellular signal-regulated kinases 1 and 2; c-Jun N-terminal kinases 1 and 2). (b) Column bar graphs represent intensity values of each protein assayed by Western blot, by collecting the data of three independent experiments. Intensity values were quantified and gathered by ImageJ software. Asterisks indicate statistically significant differences between the selected conditions according to a One-way ANOVA statistical analysis: (*p<0.05, **p<0.005, ***p<0.001 and ****p<0.0001).

Figure 9. **Liquid OA/CDs complexes do not have the same effectiveness on cell migration as dehydrated OA/CDs complexes in Mv1Lu cells.** Confluent Mv1Lu cells were scratched with a pipette tip and allowed to migrate for 24 hours. (a) Representative images of the wound healing assay with cell migration under 5 µM OA/DMSO compared to those liquid (no dehydrated) OA/HP-**γ**-CD complexes after 24h treatment. DMSO, and 0/12.5 µM/mM HP-**γ**-CD were used as vehicle controls. (b) Plot represents cell migration as the difference between areas at time 0 hours and time 24 hours in each condition, named as migration percentage. X axis indicates treatment conditions, for those with HP-γ-CD, the concentrations are represented as molar ratio OA µM/CD mM. Liquid OA/HP-γ-CD complexes concentrations used are represented in grey bars. Freeze dried 50/12.5 µM/mM OA/HP-γ-CD complexes were used as positive control. Epidermal growth factor (EGF) was added at 10 ng/ml as a positive migration control. Asterisks indicate statistically significant differences between conditions according to a One-way ANOVA statistical analysis (****p<0.0001).

Examples

Materials and Methods

EXAMPLE 1: COMPLEXATION OF OLEANOLIC ACID WITH CYCLODEXTRINS

Preparation of liquid oleanolic acid/cyclodextrin complexes.

The formation of liquid oleanolic acid/cyclodextrin complexes was performed as described in Lopez-Miranda 2018. Briefly, Excess amounts of OA was added to 10 ml of aqueous solutions of increasing concentrations from 0 to 13 mM for b-CDs and 0 to 50 mM for a-, g-, HP-a-, HP-b- and HP-g-CDs. The different phase solubility diagrams were prepared in glass test tubes and maintained in an ultrasonic bath (Ultrasons H.P. Selecta, Spain) for 60 min to reach equilibrium. The effect of temperature on the complexation process was studied by developing solubility experiments in distilled water at different temperatures (4 ºC, 25 ºC and 65 ºC). The effect of pH on the complexation process was studied by developing solubility diagrams in buffered solutions of CDs at pH 3.0 (sodium acetate buffer), 6.5 (sodium phosphate buffer) and pH 9 (sodium borate buffer). After 60 min of ultrasound treatment, solutions were centrifuged in a microcentrifuge (Eppendorf Centrifuge S415D, Germany) at 10000 xg for 10 min and filtered using 0.45 µm nylon membrane filters (Chromafil. Macherey-Nagel, Germany).

Given the need to standardize the conditions of pH and temperature for the encapsulation step and further assay oleanolic acid/cyclodextrins on cell cultures, a condition with 25 ºC and pH 7.0 was stablished since, as indicated below, they are the preferred parameters to obtain high encapsulation efficiency (EE) values.

On the other hand, given its better performance for oleanolic acid encapsulation and solubility, the modified hydroxypropyl beta and gamma (HP-β- and HP-γ-) cyclodextrin (CD) are chosen. They are purchased from Winplus International Limited (Ningbo, China). OA and cyclodextrins are added to 250 mL of aqueous solutions with a molar ratio of 0.2/50 (OA/CD) for both HP-β- and HP-γ-CDs. These molar proportions were selected according to phase solubility diagrams previously published by López-Miranda et al. (2018), since they formed type 1:1 complexes, one OA encapsulated molecule per one cyclodextrin molecule. Solutions are constantly stirred during 24 h at 20 ºC in the dark for complexes formation in said aqueous solutions.

Oleanolic acid/cyclodextrin (OA/CDs) complexes dehydration.

The aim of this step is to prepare an anhydrous presentation, i.e. a solid powder preparation with the formed OA/CDs complexes. This dehydration is necessary for testing the mentioned complexes in an *in vitro* model of epithelial cell cultures. The advantage of a dehydrated complex is that it allows its easy dissolution in the culture

media used to grow the cells, thus allowing the preparation of solutions at the desired concentration of OA/CDs. This culture media is an aqueous solution.

After Solutions were constantly stirred during 24 h at 20 ºC in the dark, OA/CD solid complexes are obtained by dehydrating 250 mL volume of dissolved complexes. The recovered dehydrated solid complexes are stored in plastic containers protected from light for posterior analysis and characterization. This samples, already with encapsulated OA, will be resuspended with ultrapure water and re-injected into a HPLC for OA detection and quantification. Previously, a standard curve is elaborated with pure OA to better quantify OA complexes solutions. HPLC allows the detection and quantification of a given compound by knowing its absorbance at a specific wavelength (λ). It consists of injecting a solution of the compound, in this case OA, to drive it through a mobile phase in the HPLC machine. The encapsulated OA solution is injected into the HPLC for detection and quantification of the OA. Due to the chemical structure of OA, it has a specific absorbance and can therefore be detected at a reference wavelength of 210 nm. Furthermore, using the absorbance peak at 210 nm recorded by the HPLC machine by the detection of OA, the amount of OA in solution can be calculated by determining the peak area.

OA/HP-β-CD and OA/HP-γ-CD complexes drying by freeze drying and spray drying methods

The formed OA/HP-β-CD complexes were subjected to drying by freeze drying or spray drying. First, for the freeze-drying method, the aqueous solutions with the complexes OA/HP-β-CDs and OA/HP-γ-CDs shall be subjected to -80°C to freeze them completely. Then, in the freeze dryer, a vacuum system and a temperature of -48°C will be applied for three days until the water in which the complexes were dissolved is completely removed. Secondly, the Spray Dry technique dehydrates the complexes in less time and without the need to freeze them beforehand. In this case, the solution with the complexes is injected into a circuit that sprays it at a temperature of 170ºC, eliminating the water from the solution and then cooling it to 68ºC. In just half an hour, the dried complexes are obtained in a dry powder form.

Evaluation of OA concentration in the complexes and measurement of their stability at different temperatures at different times

To determine the amount of encapsulated OA present in the powder preparations obtained by freeze drying or spray drying, several samples of the powder preparations

were reconstituted with ultrapure water, in order to be able to detect the OA by HPLC, as described above. Considering the amounts of OA before and after encapsulation (mg of OA in the initial solution), together with the new data of OA in the powdered preparations (mg of OA in solid complex and total g of complexes), the encapsulation efficiency (EE) and the OA load in the complexes (DL) are calculated according to the following formulae:

$$\text{EE}\ (\%) = \frac{\text{total compound encapsulated in solid complex (mg)}}{\text{total initial compound in solution (mg)}} \cdot 100$$

$$\text{DL}\ (\text{mg}\ g^{-1}) = \frac{\text{total compound encapsulated in solid complex (mg)}}{\text{total weight of solid complex (g)}}$$

In order to study the stability and conservation of the powdered complexes over time. Sais OA/CD complexes were stored at three different temperatures (20ºC, 4ºC and -80ºC) and were analyzed later to quantify the encapsulated OA by HPLC (days and weeks after complexation).

EXAMPLE 2: FUNCTIONAL TESTING OF THE COMPLEXES OF THE INVENTION

The complexes of the invention were tested in functional assays with epithelial cell models. In these assays, the promoter effect of OA on cell migration and the expression of proteins necessary for this phenomenon was evaluated.

Cell culture

Mink Lung Epithelial (Mv1Lu) cells are grown in Eagle's Minimum Essential Medium (EMEM) (Biowest, Nuaillé, France) supplemented with 10% Fetal Bovine Serum (FBS, Gibco, Thermo Fisher Scientific, Rockford, IL, USA), 1% Penicillin/Streptomycin and 1% L-Glutamine (both from Biowest, Nuaillé, France). Mv1Lu cells are cultured in an incubator at 37 ºC with a 5% CO_2 humified atmosphere. Human mammary gland cells (MDA-MB-231) are grown in Dulbecco's Modified Eagle Medium (DMEM) supplemented as mentioned above for EMEM. MDA-MB-231 cells are incubated in an incubator at 37 ºC with a 7.5% CO_2 humified atmosphere.

Wound-healing scratch assay on epithelial cell lines with OA/CDs complexes to measure their biological activity on cell migration

Mv1Lu or MDA-MB-231 are seeded in 24-well plates until they reach 100% confluence, using the appropriate medium for each line with all supplements. At that time, medium is changed to FBS-free medium for 24 hours. At the initial time (T0), a cross-shaped scratch is made on the cell monolayer using a sterile p-200 µl pipette tip. After replacing FBS-free culture medium to wash out released cells, OA, OA/HP-β-CD or OA/HP-γ-CD (the concentration used in each assay is indicated at each figure legend) are added. An equivalent volume of DMSO, HP-β-CD and HP-γ-CD is added. In parallel, a positive control is set by adding 10 ng/ml epidermal growth factor (EGF, Sigma-Aldrich, St Louis, MO, USA). Additionally, pharmacological inhibitors against key proteins on migration regulation are added to OA conditions: 2.5 µM PD153035 (Epidermal Growth Factor inhibitor, EGFRi), 50 µM PD098059 (Mitogen-activated protein kinase kinase inhibitor, MEKi) and 15 µM SP600125 (c-Jun N-terminal kinase inhibitor, JNKi). After a 24-hour incubation period, cells are fixed with 4% formaldehyde (Applichem GmbH, Darmstadt, Germany) in PBS (Biowest, Nuaillé, France) for 10 minutes. Finally, well plates are washed twice with PBS. Pictures are taken at 10X magnification using an optical microscope equipped with a digital camera (Motic Optic AE31, Motic Spain, Barcelona, Spain). To quantify cell migration, the areas of the gaps in the wounds are measured by ImageJ software. The initial cell-free surface (time 0 h) is subtracted from the endpoint cell-free surface (time 24 h) and plotted in a graph.

Cell-front migration assay, subcellular localization assay

Mv1Lu cells are grown until they reach confluence on round glass-coverslips in 10% FBS-EMEM medium. At this time, cells are washed and a 24h serum-starvation period is set by replacing the medium with FBS-free EMEM. After this, the epithelium is scratched using a razor blade, which produces an artificial wound with enough space to allow cells to migrate. The newly wound is set as a time 0 hours of the experiment and then 5 µM OA/DMSO or 12.5/3.125 µM/mM OA/HP-β-CD or are added to the medium. As parallel conditions, DMSO or HP-β-CD (3.125 mM) equivalent volumes are added as vehicle controls. After the selected times of incubation, glass-coverslips are fixed with 4% formaldehyde (Applichem GmbH, Darmstadt, Germany) in PBS (Biowest, Nuaillé, France) for 10 minutes and washed twice with PBS. After this, cells are permeabilized with 0,3% Triton X-100 (Sigma-Aldrich, St Louis, MO, USA) in PBS for 10 minutes. For immunostaining, a blocking is performed for 30 minutes at room temperature in PBS solution with 10% FBS, 5% skim milk (Beckton Dickinson, Franklin Lakes, NJ, USA), 0,3% bovine serum albumin (BSA, Sigma-Aldrich, St Louis, MO, USA) and 0,1% Triton

X-100. Then, cells are incubated 1 hour at room temperature with anti-paxillin or anti-phospho-c-Jun antibodies, diluted in blocking solution without skim milk. Proper fluorescent-labelled secondary antibodies (see Antibodies section) are co-incubated for 30 minutes with Alexa Fluor 594 conjugated phalloidin (Molecular Probes, Thermo Fisher Scientific, Waltham, MA, USA), and Hoechst 33258 (Fluka, Biochemika, Sigma-Aldrich, St Louis, MO, USA) to reveal actin cytoskeleton and nuclei respectively. Once samples are inmunostained, image acquisition is performed with a confocal microscope (LSM 510 META from ZEISS, Jena, Germany). The setting of images was performed using Zeiss Efficient Navigation (ZEN) interface software (ZEISS, Jena, Germany). When a wider view of the migration front is required, concretely in phospho-c-Jun staining (indicated in Figures), 4X3 linked fields are acquired by the "Tile scan" ZEN tool. Subsequently, tile scans fluorescent signals are converted to a linear mode and covered with a full data range using the Rainbow look up table (Rainbow LUT) in Image J software. In order to quantify phospho-c-Jun levels in immunofluorescence pictures, images are analyzed and quantified by Image J software. For this purpose, pictures in 8-bit three-channel format (Red, Green, Blue, RGB) were divided into three separate color channels (three pictures). By using blue channel picture (Hoechst staining), regions of interest (ROIs) are stablished to define each nucleus, creating as many ROIs masks as nuclei in the image. Then, by overlapping these masks onto the corresponding green channel picture (p-c-Jun staining), we calculate the green intensity value of each nucleus (ROI). Because of the large area covered in each picture (Tile scan), they are divided in three equal sectors (S1, S2 and S3), being S1 the outermost edge on the wound. Within each sector, the quantified signal of each nucleus is used as a replicate to obtain p-c-Jun intensity data in each of the conditions performed. For a better understanding, the relation of number of p-c-Jun positive nuclei between total nuclei number is calculated. For this purpose, a basal p-c-Jun intensity mean is calculated considering the control condition of the assays, set as a threshold. In this sense, nuclei with p-c-Jun intensity over the threshold are set as positive nuclei. On the other hand, "Z stack" ZEN feature is used when deep cytoskeleton structures observance is required, taking a proper number of pictures along the Z axis. Focal adhesion (FA) quantifications are performed as described in Horzum et al., 2014 by using CLAHE and Log3D macros for ImageJ {Horzum, 2014 #553}. Briefly, focal adhesions are quantified from paxillin stained acquired pictures. We used three different images for each condition. Specifically, cell filopodia are selected as regions of interest (ROIs) and the resulting areas (containing FAs) are considered for further analysis. A number of five filopodia are considered from each picture. Then, the number of FAs are calculated in each filopodia by using the previously mentioned macros. The obtained number is divided by the total filopodia area

to determine FAs density. In parallel, the size of each FA is measured using the macros mentioned above. Finally, FA average size is calculated for each treatment.

Western blot

Mv1Lu or MDA-MB-231 cells are seeded and allowed to reach 60% confluence in 10 cm diameter plates. At this time, culture medium containing 10% FBS is replaced by an FBS-free medium, incubating the cells for a 24-hours period. Serum-deprived cells are treated with either OA, OA/HP-β-CD, DMSO, HP-β-CD or 10 ng/ml EGF. After time incubations, cells are harvested, washed twice with ice-cold PBS and lysed with 20 mM TRIS pH 7.5, 150 mM NaCl, 1 mM EDTA, 1.2 mM MgCl2, 0.5%, Nonidet p-40, 1mM DTT, 25 mM NaF and 25 mM β-glycerophosphate supplemented with phosphatase inhibitors (I and II) and protease inhibitors (all from Sigma-Aldrich, St Louis, MO, USA). Total protein amount of all extracts is measured and normalized by Bradford assay (Sigma-Aldrich, St Louis, MO, USA). The extracts are analyzed by SDS-PAGE followed by Western blot (WB) using the indicated antibodies (see Antibodies section). Blots are revealed by using Horseradish peroxidase substrate (ECL) (GE Healthcare, GE, Little Chalfont, United Kingdom) and images are taken with a Chemidoc XRS1 (Bio-Rad, Hercules, Ca, USA). For protein quantification, Western pictures in 8-bit format are processed in ImageJ software. Subsequently, in all Western blot pictures, a lane is stablished for each of the samples. In each lane, the band is selected according to the specific size (kDa) of the protein of interest. For each total protein and their phosphorylated version, each band's intensity peak is plotted, and next, the area under the plot is measured by using "Wand (tracing) tool" of ImageJ to obtain the intensity value. In order to normalize, obtained intensity values are referred to obtained intensity values of either the unphosphorylated form of the protein (total) or a loading control protein such as β-actin, only if the unphosphorylated form is undetectable (non-available antibody for detecting the unphosphorylated form).

Antibodies

The following commercial primary antibodies are used: anti-phospho-ERK1/2, anti ERK1/2, anti-JNK1/2, anti-phospho-JNK1/2 and anti-phospho-c-Jun (all from Cell Signaling Technology, Danvers, MA, USA); anti-phospho-EGFR (Thermo Fisher Scientific, Rockford, IL, USA); anti-EGFR, anti-paxillin and anti-c-Jun (Santa Cruz Biotechnology, Heidelberg, Germany); and anti-β-actin (Sigma-Aldrich, St Louis, MO, USA). Secondary antibodies are anti-rabbit IgG Horseradish peroxidase linked F(ab')2 I

fragment (from donkey) (GE Healthcare, GE, Little Chalfont, United Kingdom), anti-mouse IgG_1 (BD Pharmingen, Beckton Dickinson, Franklin Lakes, NJ, USA); Alexa Fluor 488 conjugated anti-mouse (from donkey) (Thermo Fisher Scientific, Rockford, IL, USA).

Statistical analysis

All the collected data are analyzed using Graph Pad Prism 7 software. In every analysis, classic statistical parameters were calculated and statistical tests are performed with a 95% confidence interval, consequently, P-values lower than 0.05 are considered to be statistically significant. At the figure legends, the asterisks denote statistically significant difference between conditions (*p<0.05, **p<0.005, ***p<0.001 and ****p<0.0001). Data of intensity values, collected from Western blots, are analyzed by a One-way ANOVA test, comparing the mean of each condition with the mean of every other condition. Then, a Tukey's multiple comparisons test is performed.

Data of intensity values obtained from p-c-Jun nuclei quantifications in immunofluorescence pictures are analyzed by using two statistic tests: Two-way ANOVA test and One-way ANOVA test. Concretely, a Two-way ANOVA following Tukey's multiple comparison test is performed to compare the p-c-Jun intensity mean between sectors from different conditions (e.g. S1 DMSO versus S1 OA). On the other hand, a One-way ANOVA, following Tukey's multiple comparison test is performed to compare p-c-Jun intensity mean between sectors from the same condition (e. g. S1 DMSO versus S2 DMSO).

Results

Example 1.1: Analysis and quantification of OA by high-performance liquid chromatography (HPLC)

HPLC allows to detect and quantify OA in a solution on the basis of its absorbance at a specific wavelength (210 nm). Commercial OA from Sigma with a purity of 98% was used in this experiment. In order to obtain an adequate quantification of the OA /cyclodextrin complexes, a standard curve of the OA to be used is prepared. To do this, the HPLC equipment must be calibrated using a column specially designed for organic molecules and a mobile phase of acetonitrile, acetic acid and water. A solution of OA at a concentration of 0.5 mg/ml in methanol is then prepared in such a way that the HPLC equipment takes different volumes (punctures) of this solution in increasing order (**Table**

1). In this way the absorbance peaks of OA at 210 nm are recorded and their area is calculated, which is directly proportional to the volume of the spike. This provides a standard curve on which to base subsequent quantifications. Once the equation for the standard curve has been calculated, the amount of OA in the test solution can be calculated from the recorded absorbance of the OA (**Figure 1**).

Table 1. OA quantifications to produce the standard or calibration curve.

Injected µL	OA concentration mg/mL	Area (210nm)	Total µg
2	0.5	181	0.98
5	0.5	464.9	2.45
7	0.5	656.8	3.43
10	0.5	935.2	4.9
15	0.5	1451	7.35
20	0.5	1960.9	9.8
25	0.5	2489.1	12.25
30	0.5	2978.5	14.7

Oleanolic acid/cyclodextrin complexation

Beta- and gamma-cyclodextrins modified with hydroxypropyl groups (CD-HP-β and CD-HP-γ respectively) from Winplus International Limited are used for OA conjugation. In general, aqueous solutions of 50, 250 or 500 ml are prepared to which OA and cyclodextrins (CD-HP-β or CD-HP-γ) are added in a molar ratio of 0.2:50 (oleanolic acid:cyclodextrin). This molar ratio allows the encapsulation of one OA molecule for each cyclodextrin molecule, so that OA/CD complexes are formed in a 1:1 ratio. The OA/CD solutions are stirred for 24 hours at room temperature and protected from light. After 24 hours the solutions are sampled to determine the amount of encapsulated OA by extrapolation to the standard curve. **Table 2** shows representative data from one of the OA encapsulation batches performed with HP-β-CDs and HP-γ-CDs.

Table 2. Quantifications of OA in a solution with CDs after 24 hours of stirring.

CD	**CD g (50mL)**	**OA mg (50mL)**	**Liquid Complex Area**	**Liquid Complex Area (Avge)**	**mg/ml**	**Total mg. Liquid Complex**
CD-HP- β	3,85	5,0	314,4	315,3	0,08	3,92
			314,1			
			317,5			
CD	**CD g (50mL)**	**OA mg (50mL)**	**Liquid Complex Area**	**Liquid Complex Area (Avge)**	**mg/ml**	**Total mg. Liquid Complex**
CD-HP-γ	4,4	5,0	322,6	319,7	0,08	3,98
			319,9			
			316,6			

CDs with β- and γ-type hydroxypropyl (HP) groups gave similar OA loadings and encapsulation yields (between 80 and 100 %).

Example 1.2: Dehydration of OA/HP-β-CD complexes by freeze-drying and spray-drying methods

The OA/CDs solutions were divided into equal volumes to undergo two different dehydration processes: freeze-drying and spray-drying. For freeze-drying, the OA/CDs solutions were first subjected to lyophilization in a Christ Alpha 1-2 LD Plus freeze dryer under vacuum at a temperature of -48°C. On the other hand, the OA/CDs complexes were dried in a Spray-Dry Buchi B-290 at a temperature of 170ºC. In order to determine the efficiency of each of the two processes, the dehydration yield (RD), a percentage that indicates how many grams of CDs were recovered in the dehydrated powder relative to the initial grams of CDs weighed before OA encapsulation, was calculated. These data are presented in **Table 3**.

$$\mathrm{RD}\ (\%) = \frac{\text{solid complexes obtained (g)}}{\text{total solids in solution (g)}} \cdot 100$$

Table 3. Calculation of freeze-drying and Spray-Dry dehydration yields.

Freeze drying			
CD	Initial CD g	CD g powder after FD.	RD (%)
HP-β-CD	7,7	7,17	93,1
HP-γ-CD	8,8	8,03	91,3

Spray drying			
CD	Initial CD g	CD g powder after SD.	RD (%)
HP-β-CD	7,7	6,72	87,3
HP-γ-CD	8,8	6,23	73,29

As can be seen in **Table 3**, the dehydration yields obtained by Spray Dry were slightly lower than those obtained by Freeze drying. The speed of the Spray Dry treatment seems to affect the amount of OA/CDs powder recovered, but this small loss is acceptable as long as the encapsulated OA does not lose its effect on cell migration in subsequent in vitro tests on epithelial cells (see following sections) which is equally effective.

Example 1.3: Evaluation of OA concentration in the complexes and measurement of their stability

Once the solid (powdered) OA/CDs complexes have been obtained, the encapsulation yields of each type of cyclodextrin (EE) and the loading of active material (DL), i.e. OA, per gram of cyclodextrin must be calculated. To do this, the following calculations are carried out:

$$\text{EE}\ (\%) = \frac{\text{total compound encapsulated in solid complex (mg)}}{\text{total initial compound in solution (mg)}} \cdot 100$$

$$\text{DL}\ (\text{mg}\ g^{-1}) = \frac{\text{total compound encapsulated in solid complex (mg)}}{\text{total weight of solid complex (g)}}$$

Table 4 shows the encapsulation yields (EE) and OA loadings (DL) in different batches of OA/HP-β-CD and OA/HP-γ-CD complexes dehydrated by freeze-drying. As can be seen, the HP-γ and HP-β cyclodextrins showed very similar encapsulation performances, both being a priori suitable for encapsulating OA and producing preparations suitable for testing *in vitro* cell culture. The chemical conformation of cyclodextrins allow stability and protection of the encapsulated drug against adverse physical factors such as temperature. To evaluate this property, we focused on HP-β-type cyclodextrins and measurements were made on lyophilized OA/HP-β-CD

complexes stored at different temperatures, with the intention of measuring their stability over time (weeks from complex formation). All complexes were stored under light-protected conditions. The OA load (DL) of each of these complexes was then quantified, with the results shown in **Table 5**. The encapsulated OA loading (LD) data indicate that the OA milligrams per gram of cyclodextrin are hardly modified under the three temperature conditions, even up to 8 weeks after the preparation of the complexes. However, it would be necessary to further test these preparations preserved at different temperatures in functional wound assays on epithelial cells to confirm that despite the fact that no amount of OA is lost, its biological activity is also unaffected and it continues to exert the promoting effect on cell migration.

Table 4. Complexation performances of OA/HP-β-CD and OA/HP-γ-CD complexes obtained by freeze-drying and Spray Dry

		CD g	OA mg	Solid complexes area HPLC	Solid complexes mg	DL (mg/g)	DL (mg/g) expected	EE (%)
HP-β-CD	Spray drying	3,85	5,0	279,5	20,1	1,15	1,30	82,3
				249,5	21,0	0,99		
				261,5	20,3	1,07		
	Freeze drying	7,7	12	384	20,6	1,55	1,56	97,9
				373	20,4	1,52		
				391	21,4	1,52		
		CD g	OA mg	Solid complexes area HPLC	Solid complexes mg	DL (mg/g)	DL (mg/g) expected	EE (%)
HP- γ-CD	Spray drying	4,4	5,0	236,8	21,4	0,92	1,14	81,5
				236,0	21,6	0,91		
				234,9	20,4	0,96		
	Freeze drying	8,8	15	440,4	21,4	1,71	1,70	100
				444,6	21,6	1,71		
				417,8	20,4	1,70		

Table 5. Quantifications of freeze-dried OA/HP-β-CD complexes stored at -80°C, 4°C and room temperature protected from light.

Weeks after complexation (w)	ºC	Freeze dried complexes area HPLC	g freeze dried complexes	DL (mg/g)
0	20 ºC	489,0	21,3	1,11
	20 ºC	468,9	20,1	1,13
1 w	(-)80 ºC	527,5	22,0	1,16
	4 ºC	517,6	21,0	1,19
	20 ºC	415,2	19,0	1,06
2 w	(-)80 ºC	426,3	20,2	1,02
	4 ºC	467,4	21,7	1,04
	20 ºC	489,8	21,4	1,11
4 w	(-)80 ºC	514,0	21,9	1,14
	4 ºC	501,0	22,2	1,09
	20 ºC	505,0	21,9	1,12
8 w	(-)80 ºC	447,0	20,3	1,07
	4 ºC	431,2	19,6	1,07
	20 ºC	459,6	20,2	1,10

The freeze-dried OA/HP-CDs complexes, stored at room temperature, 4°C and -80°C, retained the stability of the encapsulated OA for two months, as the amount of OA was not affected by time and temperature.

Example 2.1: Wound healing scratch assays and protein expression analyses to test OA/CDs complexes activity

In functional scratch assays, OA/CDs complexes are tested for biological activity by quantifying cell migration. The epithelial cell lines Mv1Lu and MDA-MB-231 were used for this purpose. In both cases, cells are grown in culture to form an epithelium that is artificially wounded (time 0 h) and then treated with OA/CDs to determine the optimal concentration at which the greatest stimulatory effect on migration is achieved. A battery of assays was performed to test different concentrations of OA/CDs using both types of cyclodextrins: HP-β-CD and HP-γ-CD. **Figure 2** shows graphs of the cell migration values obtained with the OA/CDs treatments (migration percentage). In the assays shown, the already optimised concentrations of OA/CDs are indicated after testing different concentrations. In these assays, in addition to the OA/CDs conditions, a control with OA vehicleised with DMSO (OA/DMSO) was included, followed by controls with empty CDs and DMSO. The concentrations of OA/CDs complexes used are given in μM and refer to the concentration of encapsulated OA and are equivalent to the empty CD controls. An epidermal growth factor (EGF) condition was included as a positive control for cell migration.

Example 2.2: freeze-dried OA/HP-β-CD and OA/HP-γ-CD complexes in scratch assays with Mv1Lu cells

As can be seen in **Figure 2**, both OA complexes with HP-β and HP-γ cyclodextrins obtained by freeze-dry showed a very significant effect on cell migration at encapsulated OA concentrations of 12.5 μM and 62.5 μM, respectively. Both preparations showed cell migration values equal to those of OA/DMSO, which is difficult to handle due to its vehicleisation with DMSO. It is noteworthy that with the OA/CDs complexes, microscopy images showed a higher recruitment of moving cells, with the belt of migrating cells being wider than with OA/DMSO, which would suggest a more effective effect on wound closure. On the other hand, it should also be noted that HP-β-type cyclodextrins produced the effect on migration at lower concentrations of encapsulated OA than HP-γ-type cyclodextrins (12.5 μM vs. 62.5 μM), thus requiring less of the complex to achieve this effect. This is possibly due to the fact that OA is conjugated to HP-γ cyclodextrins with higher affinity (given their higher Kc), causing less OA to be released upon treatment.

Example 2.3: OA/HP-β-CD complexes dehydrated by freeze-drying and Spray Dry in scratch assays with Mv1Lu cells:

Similarly, following the same design as for the scratch assays, OA/HP-β-CD complexes obtained by spray drying were tested for comparison with those obtained by lyophilisation (**Figure 3**). It was observed that the complexes obtained by spray drying, despite having a lower dehydration yield than the lyophilized ones, also achieved a significant activity on cell migration compared to the controls. Furthermore, there were no significant differences in cell migration between the two types of preparation and the biological activity of the OA was very similar.

Example 2.4: In vitro assays with OA/CDs complexes; study of marker proteins involved in cell migration by immunostaining

The results of the wound assays were used to study the topographical and subcellular localisation of proteins involved in cell migration. This was done using immunostaining techniques, which allow a topographical measurement of what happens in the wound when OA/CD treatments are added, using specific fluorochrome-labelled antibodies and imaging by confocal microscopy. First, immunostaining for the transcription factor c-Jun, a key factor in cell migration, was performed. Specifically, an antibody against the active (phosphorylated) form of this factor (p-c-Jun) was used to test whether OA/CDs complexes promoted its expression and activation at the wound edges. In addition, co-immunostaining with Hoechst and phalloidin was performed to visualise the nuclei and actin cytoskeleton respectively, giving an idea of the location and structure of the wound (**Figure 4**). Immunostaining for p-c-Jun and analysis of the images showed that, as with OA/DMSO, OA/HP-β-CD complexes promote the up-regulation of this active form of c-Jun in cells at the edge of the wound. This factor is localised in the nuclei of the cells, where a higher number of p-c-Jun labelled nuclei could be observed than in the basal condition or in the vehicle controls (blank DMSO or CD). To confirm this result and complete this assay, the fluorescence of p-c-Jun (expression) present in the nuclei was quantified using ImageJ image analysis software (**Figure 5**).

Quantification of p-c-Jun fluorescence in the nuclei confirmed that it was much higher with the OA/CDs complexes treatment than with the control, as with the use of OA/DMSO in DMSO. Both OA/DMSO and encapsulated OA promoted the expression and activation of this factor to allow cell migration from the wound edges. However, it should be noted that the effect of the OA/CDs complexes, as seen in the scratch tests, is more effective than that obtained with OA/DMSO. This can be seen in **Figure 5b**, since in the condition with the OA/HP-β-CD complexes nuclei with high p-c-Jun fluorescence are recorded, a result that is reinforced in **Figure 5c**, where the ratio of activated nuclei to total nuclei

was much higher than with OA/DMSO. It is also interesting to note that the effect of OA/CDs complexes on p-c-Jun was higher in the S1 sectors, corresponding to the wound edges, and this effect was lower in the subsequent S2 and S3 sectors, further away from the edge, suggesting a gradient effect on p-c-Jun activation, which was maximal in the edge cells, which are usually found with a higher degree of motility.

On the other hand, the immunostaining technique also allowed us to study the cytoskeletal proteins paxillin and actin. Both proteins are associated and have the function of allowing the assembly and disassembly of the cellular architecture of focal adhesion complexes, which is very important during cell migration and allows cell movement. Their study therefore provides insight into the state of cell dynamics at the wound edge (**Figure 6**).

Paxillin is a protein that forms structures known as foci of adhesion (FAs). These structures anchor the cell to the extracellular matrix and increase in number and decrease in size as the cells move, resulting in a state of cellular dynamization. Therefore, if the encapsulated OA promotes cell migration, the epithelial cells must be in this high state of dynamization. By visualizing the adhesion foci with paxillin and quantifying them using image analysis in ImageJ, the degree of cell dynamization at the wound edge can be determined. To calculate this degree, the number of adhesion foci is divided by the area of each filopodia present in the cells, i.e. each projection generated by the cells to adhere to the substrate and migrate through the wound space, giving the density of foci per cell (FAs density). On the other hand, the area of each adhesion focus is also calculated to obtain the average size of all the foci. It can be seen that the OA/HP-β-CD complexes, as with OA/DMSO, produce a greater number of adhesion foci and, in addition, they are small foci, all with respect to the basal control and the vehicle control (**Figure 6**). It should be noted that no significant differences were found between OA/DMSO and encapsulated OA in the formation of these structures.

OA/HP-β-CD complexes promoted the remodeling of adhesion sites, as evidenced by the higher number of adhesion sites and their smaller size during migration promoted by OA/HP-β-CD complexes.

Example 2.5: Wound healing scratch assays in MDA-MB-231 cells with freeze dried OA/HP-β-CD complexes

To extrapolate previous results in other epithelial cell model we tested OA/HP-β-CD complexes in MDA-MB-231 cells. We tested several concentrations of OA/HP-β-CD complexes, where MDA-MB-231 cells showed significant cell migration compared to

basal (C) and vehicle control HP-β-CD conditions (**Figure 7a and b**). Similar migration percentages values were observed between OA/DMSO and all OA/HP-β-CD concentrations tested with no statistically significant differences reached. Nevertheless, there was a higher migration activity tendency within 17/4.25 μM/mM and 21/5.25 μM/mM OA/HP-β-CD concentration complexes. Furthermore, it was easy to notice that, in the case of OA/HP-β-CD, more cells could be found reaching wounded gap area than in OA/DMSO condition (**Figure 7a**).

Example 2.6: In vitro assays in MDA-MB-231 cells with freeze-dried OA/HP-β-CD complexes: key proteins related to cell migration analysis by Western blot

MDA-MB-231 cells are a suitable epithelial model for EGFR expression regulation studies. With the objective of deeply decipher the molecular mechanisms behind OA/HP-β-CD complexes effect on cell migration, we decided to set a whole study of key regulatory proteins involved in cell migration by using sub confluent. Cells were stimulated with 10 μM OA/DMSO and 21/5.25 μM/mM OA/HP-β-CD and the activation of different protein was evaluated. Mainly, the phosphorylation consequences of all proteins studied was milder when cells were stimulated with OA/HP-β-CD in comparison to its DMSO solubilized counterpart. To begin with, a p-EGFR stimulation was detected 2 hours after treatment with OA/HP-β-CD, later increasing at 3 and 4 hours, however, when compared to OA/DMSO the stimulation was softer (**Figure 8a and b**). When looking at a downstream EGFR kinase, p-ERK1/2, it was increased by OA/HP-β-CD treatment after 2 hours following the same trend that EGFR phosphorylation (**Figure 8a and b**). Interestingly, OA/HP-β-CD showed significantly lower intensity values at time 2 h, and it was kept higher for longer in time. Regarding p-JNK1/2, both OA/HP-β-CD and OA/DMSO induced stimulation stimulated this kinase at time 1 hours, however later in time dynamics were dissimilar. Interestingly, when blotting total c-Jun and active phosphorylated (p)-c-Jun forms we observed changes on both antigens in response to OA/HP-β-CD, an effect that is evident also in the case of OA/DMSO. In particular, in case of p-c-Jun, the treatment with OA/HP-β-CD showed a mild increase at time 2 h that was sustained up to 6 h. In contrast, OA/DMSO produced a stronger stimulation of p-c-Jun at time 1 hour, it was sustained in time up to 6 hours and exhibited higher values than cyclodextrin complexed OA. In any case, no increases on p-JNK1/2 and p-c-Jun regulatory proteins were observed with DMSO and HP-β-CD vehicle controls. Finally, total c-Jun levels were clearly increased by OA/HP-β-CD with 2 hours delay (3, 4 and 6 h) when compared to OA/DMSO, that stimulated c-Jun overexpression

at the early time of 1 h. The overexpression and activation of the above-mentioned proteins, in response to OA/HP-β-CD, imply their participation in the cell migration phenomenon promoted by cyclodextrin-complexed OA.

Example 2.7: Activity of the OA/HP-CD complexes without dehydration on cell migration Mv1Lu cell migration.

OA/CDs complexes need to be dehydrated due to its easier manipulation and addition to cell culture mediums. By contrast, using OA/CDs solutions directly added to the medium can produce osmolarity alterations and contaminations, consequently compromising cell viability and loosing OA activity. We tested liquid OA/HP-**γ**-CD complexes and freeze-dried OA/HP-**γ**-CD complexes in wound healing scratch assays by using Mv1Lu cells (**Figure 9**). As expected, liquid OA/HP-**γ**-CD complexes did not show any significant migration activity, since they had same migration percentages as control (C) condition or vehicle control with empty 0/12.5 µM/mM OA/HP-**γ**-CD. A concentration of 0.04 g/ml of the dehydrated complexes was used. Only dehydrated complexes have significant migration activity as indicated in previous assays.

CLAIMS

1. A process to complex oleanolic acid that comprises:

a) putting in contact oleanolic acid and at least one cyclodextrin in an aqueous mixture,

b) dehydrate the product obtained in the previous step

to obtain a dry powder comprising oleanolic acid/cyclodextrins complexes.

2. The process according to the preceding claim, wherein the cyclodextrin comprises at least one hydroxypropyl group.

3. The process according to the preceding claim, wherein the cyclodextrin is hydroxypropyl-β-cyclodextrin or hydroxypropyl-γ-cyclodextrin.

4. The process according to any of the preceding claims, wherein the ratio oleanolic acid/cyclodextrin in step a) is between approximately 1:100 to 1:400

5. The process according to any of the preceding claims, wherein oleanolic acid/cyclodextrin are put in contact in step a) for a time comprised between 5 h and 5 days, preferably, 10 h and 3 days, more preferably 15 h and 2 days.

6. The process according to any of the preceding claims, wherein the temperature in step a) is comprised 5ºC and 40ºC, preferably between 10ºC and 30ºC.

7. The process according to claims 5 and 6, wherein oleanolic acid/cyclodextrin are put in contact for a time comprised between 15 h and 2 days and a temperature comprised between 10ºC and 30ºC.

8. The process according to any of the preceding claims, wherein the dehydration is performed by freeze-drying, spray drying, vacuum stove and/or rotary evaporator.

9. The process according to the preceding claim, wherein the freeze-drying comprises subjecting the product of step a) to a temperature of less than -70 ºC for an appropriate time, and them under a vacuum, subject said product to a temperature comprised between -60ºC and -40ºC for at least 2 days to obtain a dry powder.

10. The process according to claim 9, wherein the spray drying comprises injecting the product of step a) into a circuit that sprays said product at a temperature between 110ºC and 210ºC and then cool it to a temperature between 40ºC and 90ºC to obtain a dry powder for a time between 10 min and 2 h.

11. A product obtained by the process according to any of the preceding claims 1 to 10.

12. A dry powder comprising a complex of oleanolic acid/cyclodextrin.

13. An aqueous mixture comprising the product of any of the preceding claims 11 or 12 with a concentration of at least 0.01 g/ml.

14. A product obtained by the process according to any of the preceding claims 1 to 10, a dry powder according to claim 12, and/or an aqueous mixture according to claim 13 for use in skin disorders.

15 A product for use, according to the preceding claim, wherein the skin disorders are selected from the group consisting of: wound healing, scarring, eczema, psoriasis, acne, rosacea, ichthyosis, vitiligo, urticaria and/or seborrheic dermatitis

ABSTRACT

PROCESS TO COMPLEX OLEANOLIC ACID WITH CYCLODEXTRINS AND PRODUCTS OBTAINED THEREOF

A process to complex oleanolic acid that comprises putting in contact oleanolic acid and at least one type of cyclodextrins in an aqueous mixture, dehydrate the product obtained in the previous step to obtain a solid powder comprising oleanolic acid/cyclodextrins complexes and the product obtained with said process, as well as its therapeutic use in skin disorders.

FIGURES

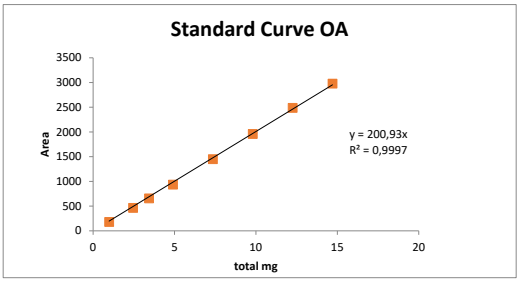

Fig.1

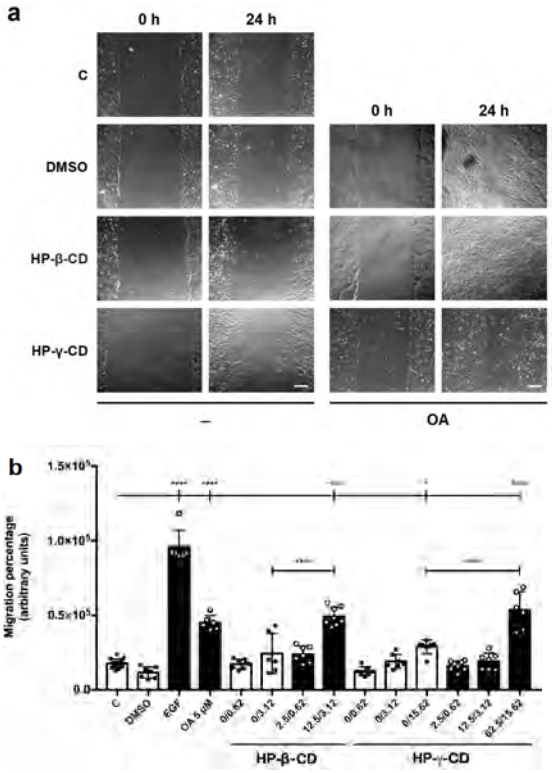

Fig. 2

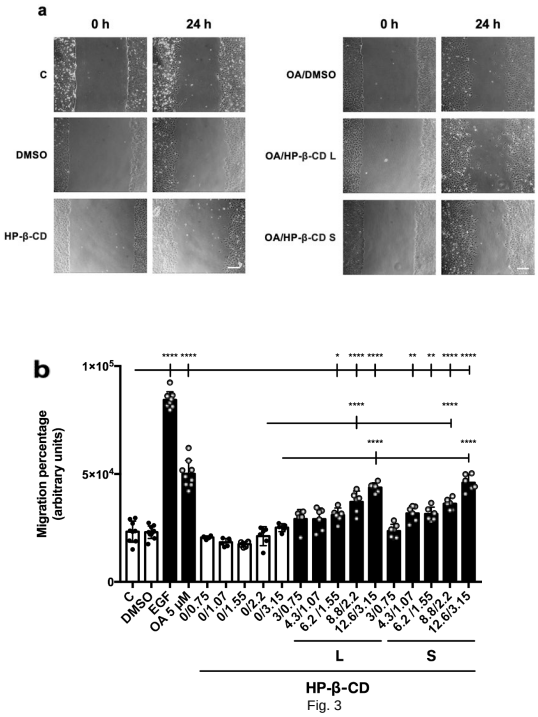

Fig. 3

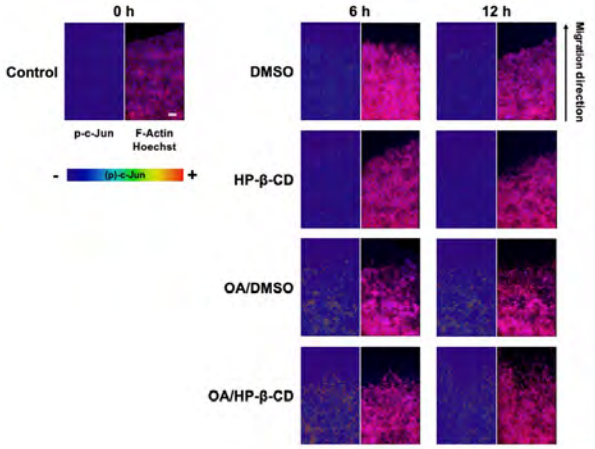

Fig. 4

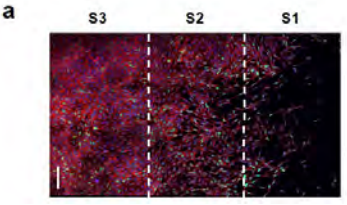

Fig. 5

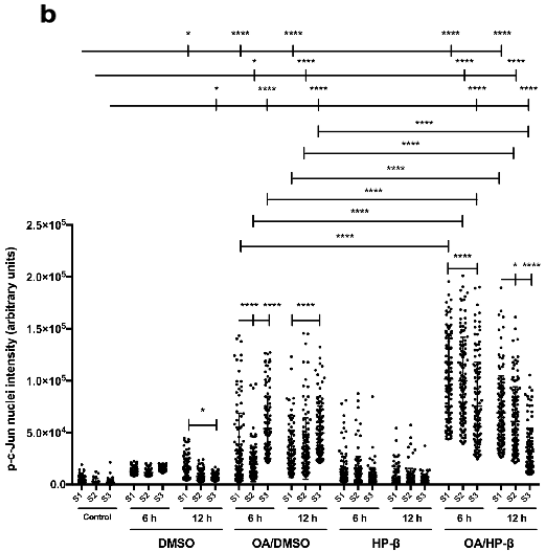

Fig. 5 (continuation)

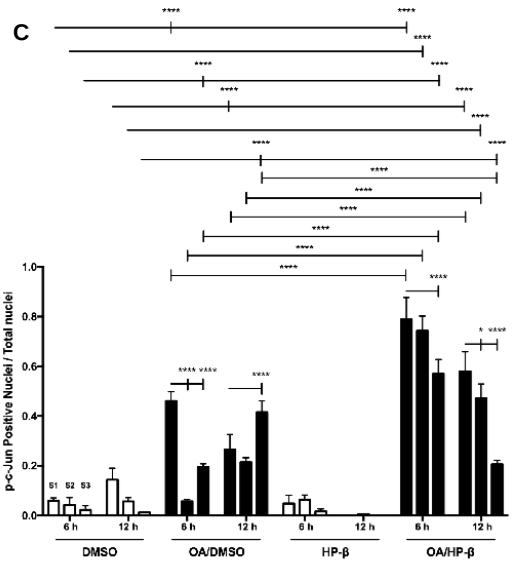

Fig. 5 (continuation)

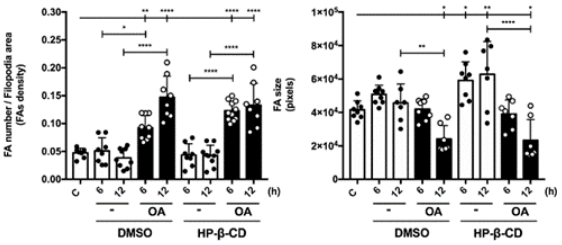

Fig. 6

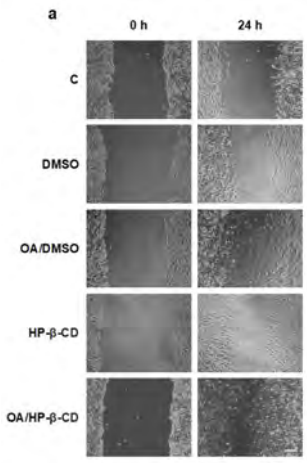

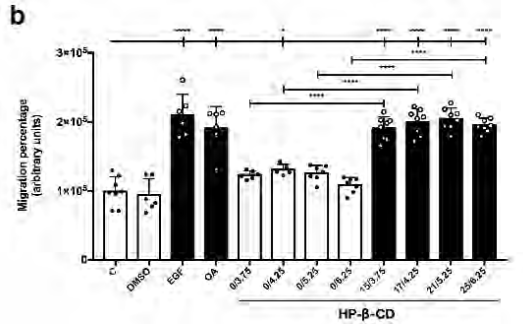

Fig. 7

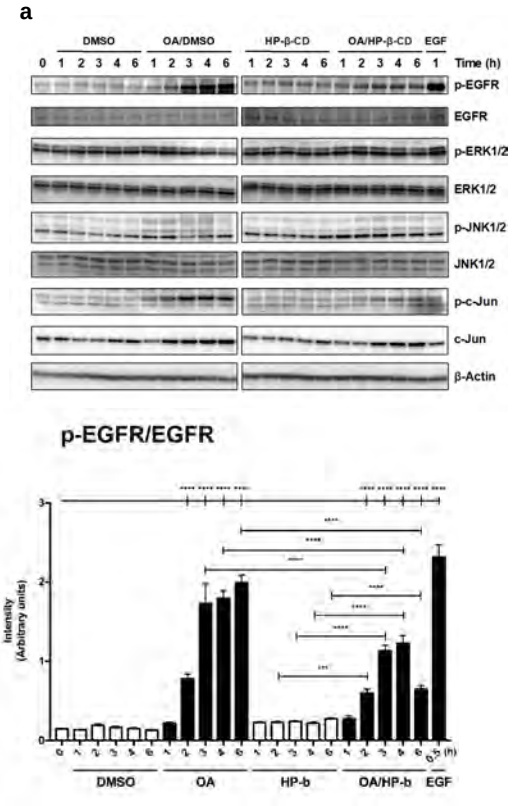

Fig. 8

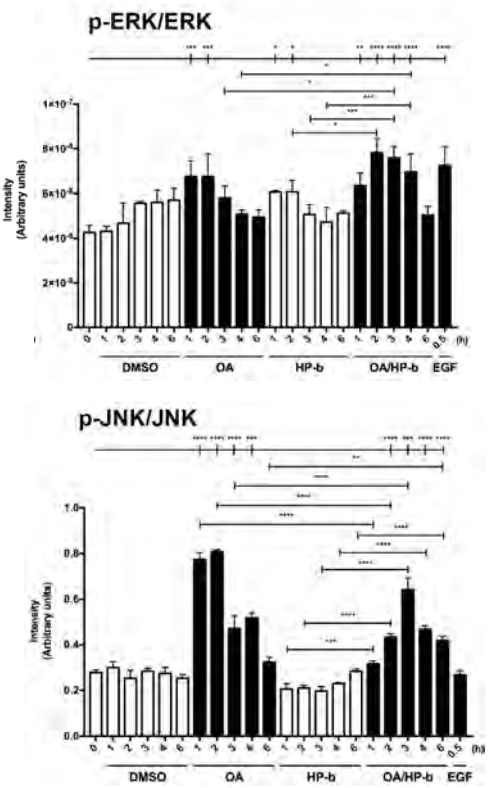

Fig. 8 (cont)

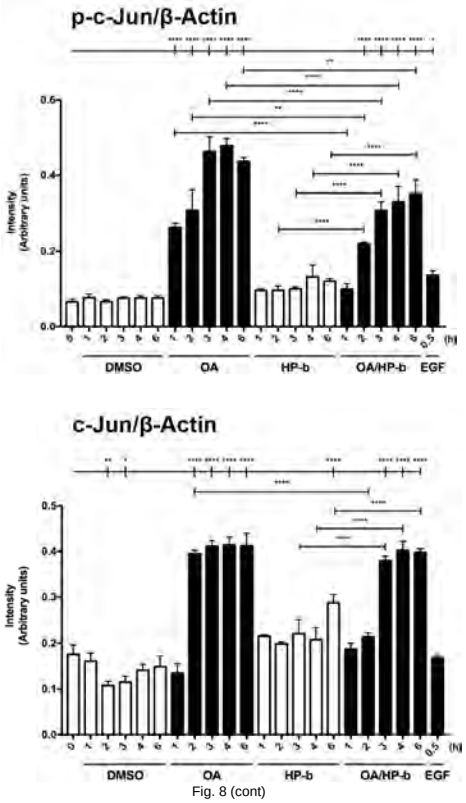

Fig. 8 (cont)

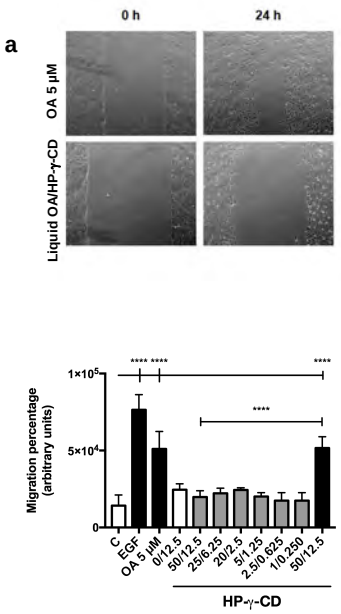

Fig. 9

Annex. 3. Scientific production derived from the thesis.

A. SCIENTIFIC ARTICLES

1. **Stelling-Férez J**, Gabaldón JA, Nicolás FJ. 2022. **Oleanolic acid stimulation of cell migration involves a biphasic signaling mechanism.** Scientific Reports. Nature Portfolio. Q2. IF: 4.6
2. **Stelling-Férez J**, Cappellacci I, Pandolfi A, Gabaldón JA, Pipino C, Nicolás FJ. 2023. **Oleanolic acid rescues critical features of umbilical vein endothelial cells permanently affected by hyperglycemia.** Frontiers in Endocrinology. Frontiers. Q1. IF: 5.2
3. **Stelling-Férez J**, López-Miranda S, Gabaldón JA, Nicolás FJ. 2023. **Oleanolic Acid Complexation with Cyclodextrins Improves Its Cell Bio-Availability and Biological Activities for Cell Migration**. International Journal of Molecular Sciences. MDPI. Q1. IF: 5.6

B. WORKS PRESENTED AT CONGRESSES

I. International congresses

1. IPLASS and COST SPRINT Action Joint Scientific Meeting (IPLASS). **Scientific Poster**. Oleanolic acid anti-inflammatory and pro-angiogenic effects on endothelial cells obtained from umbilical cord of gestational diabetes women. Venue: Brescia, Italy. Celebration date: 02-04/09/2022.
2. The Biochemistry Global Summit 2022 (IUBMB, FEBS and PABMB). **Scientific Poster**. Oleanolic acid (OA) encapsulation with cyclodextrins for its application in wound healing in vitro models. Venue: Lisbon, Portugal. Celebration date: 09-14/07/2022.
3. 6th World Congress 2021 Tissue Engineering and Regenerative Medicine International Society (TERMIS 2021). **Oral Communication**. Natural triterpenoid oleanolic acid and its complexation with cyclodextrins: cell migration effects and future

applications in wound healing. Venue: Maastricht, Netherlands. Celebration date: 15-19/11/2021.

II. National congresses

1. XX Congreso de la Sociedad Española de Biología Celular (SEBC). **Oral Communication**. Oleanolic acid anti-inflammatory and pro-angiogenic effects on endothelial cells obtained from umbilical cord of gestational diabetes women. Venue: Córdoba, Spain. Celebration date: 13-15/11/2023.
2. XX Congreso de la Sociedad Española de Biología Celular (SEBC). **Scientific Poster**. Oleanolic acid encapsulation with cyclodextrins for its application in wound healing in vitro models. Venue: Córdoba, Spain. Celebration date: 13-15/11/2023.
3. XXI Congreso de la Sociedad Española de Histología e Ingeniería Tisular (SEHIT) y VIII Congreso Iberoamericano de Histología. **Scientific Poster**. Oleanolic acid anti-inflammatory and pro-angiogenic effects on diabetic endothelial cells. Venue: Granada, Spain. Celebration date: 06-09/09/2022.
4. 43rd Annual Meeting of the Spanish Society of Biochemistry and Molecular Biology (SEBBM). **Scientific Poster**. Oleanolic acid as a potential molecule to treat wounds: molecular effects and its complexation with modified cyclodextrins. Venue: Barcelona, Spain. Celebration date: 19-22/07/2021.
5. IV Congreso Nacional de Jóvenes Investigadores en Biomedicina. **Scientific Poster**. Oleanolic acid and its complexation: effects on cell migration and applications in wound healing. Venue: Granada, Spain. Celebration date: 04-06/11/2020.
6. XVIII Congreso de la Sociedad Española de Biología Celular (SEBC). **Scientific Poster**. Oleanolic acid potentiates migration in Mv1Lu and MDA-MB 231 epithelial cell lines by promoting EGF receptor and MAP kinases activation. Venue: Badajoz, Spain. Celebration date: 15-18/09/2019.

7. 42nd Congress of the Spanish Society of Biochemistry and Molecular Biology (SEBBM). Scientific Poster. Oleanolic acid activates migration in Mv1Lu and MDA-MB-231 epithelial cells involving EGF receptor and MAP kinases activation. Venue: Madrid, Spain. Celebration date: 16-19/07/2019.

III. Symposiums

1. IX Jornadas de Investigación y Doctorado UCAM: Impacto Social de la Ciencia. **Oral Communication**. ¿La naturaleza es curativa? El ácido oleanólico tiene la respuesta. Venue: Murcia, Spain. Celebration date: 23/06/2023.
2. VIII Jornadas de Investigación y Doctorado UCAM: Ética en la Investigación Científica. **Oral Communication**. Oleanolic acid preliminary anti-inflammatory and pro-angiogenic effects on endothelial cells in vitro models HUVEC and GD-HUVEC. Venue: Murcia, Spain. Celebration date: 24/06/2022.
3. VI Jornadas Científicas IMIB-Arrixaca. **Scientific Poster**. Oleanolic acid stimulation of cell migration involves a complex biphasic mechanism. Venue: Murcia, Spain. Celebration date: 16/11/2021.
4. VII Jornadas de Investigación y Doctorado UCAM: ODS con Ciencia. Oral Communication. Novel oleanolic acid targets over wound healing. Venue: Murcia, Spain. Celebration Date: 25/06/2021.
5. V Jornadas Científicas IMIB-Arrixaca. **Oral Communication**. Natural triterpenoid oleanolic acid and its complexation with cyclodextrins: cell migration effects and future applications in wound healing. Venue: Murcia, Spain. Celebration date: 23/11/2020.
6. VI Jornadas de Investigación y Doctorado UCAM. **Oral Communication**. Oleanolic acid and its complexation: effects on cell migration. Venue: Murcia, Spain. Celebration date: 26/06/2020.
7. V Jornadas de Investigación y Doctorado UCAM: Ciencia sin Fronteras. **Oral Communication**. Triterpenic compounds as

promoters of cell migration and possible applications in wound healing. Venue: Murcia, Spain. Celebration date: 31/05/2019.

C. PATENTS AND INTELLECTUAL PROPERTY

Title of registered intellectual property: "Process to complex oleanolic acid with cyclodextrins and products obtained thereof". Inventors: Nicolás FJ, Stelling-Férez J, Gabaldón JA, López-Miranda S, Navarro S. Rights-holding entity: Fundación Universitaria San Antonio, Universidad Católica San Antonio (UCAM); Fundación para la Formación e Investigación Sanitarias (FFIS). European patent. Application number: EP23382932.4. Date of application for patent registration: 13/09/2023.

D. PARTICIPATION IN PROJECTS

1. Fibroin scaffold functionalized with perinatal cells for the treatment of chronic wounds and diabetic foot ulcers. Proyecto número PI21/01339. Instituto de Salud Carlos III. (2022-2024)

2. Modelizado del efecto epitelizante de la membrana amniótica en heridas crónicas. Proyecto número PI17/02164. Instituto de Salud Carlos III. Ministerio de Economía y Competitividad. (2018-2021).

3. International Network for Translating Research on Perinatal Derivatives into Therapeutic Approaches. Proyecto número CA17116. EU Framework Programme Horizon 2020. (2018-2020).

E. AWARDS

3rd Prize of 3 minutes thesis (3MT). Mejor Exposición de Tesis Doctoral en el Programa en Ciencias de la Salud, con la comunicación científica: ¿La naturaleza es curativa? El ácido oleanólico tiene la respuesta.

F. PH.D. STUDENT FUNDING

The PhD student was supported with a "Contrato Predoctoral para la Formación de Personal Investigador", from the Catholic University of Murcia (UCAM). Call 2018.